Bioengineering Approaches to Improve Islet Transplantation Outcomes for the Treatment of Type One Diabetes Mellitus

Dissertation

der Mathematisch-Naturwissenschaftlichen Fakultät

der Eberhard Karls Universität Tübingen

zur Erlangung des Grades eines

Doktors der Naturwissenschaften

(Dr. rer. nat.)

vorgelegt von

Abiramy Jeyagaran

aus Toronto, Kanada

Tübingen

2024

Gedruckt mit Genehmigung der Mathematisch-Naturwissenschaftlichen Fakultät der Eberhard Karls Universität Tübingen.

Tag der mündlichen Qualifikation:	30.01.2025
Dekan:	Prof. Dr. Thilo Stehle
1. Berichterstatter:	Prof. Dr. Katja Schenke-Layland
2. Berichterstatter:	Prof. Dr. Garry P. Duffy
3. Berichterstatter:	Prof. Dr. Antony Weiss

Table of Contents

Abstract

Type one diabetes mellitus is a chronic disease that results in the dysregulation of blood glucose levels. Current therapeutic approaches for patients with type one diabetes include continuous monitoring of blood glucose levels and self-administration of exogenous insulin. Islet or β-cell transplantation allows for insulin-independency and doesn't pose the risk of the patients under- or over-medicating themselves. With increasing studies understanding the human pancreas during development and as an adult, the field of islet transplantation has progressed greatly over the last decades with specific interest in the areas of enhancing donor islet survival, improving stem cell-derived β-cell differentiation protocols, and protecting islet transplants from the immune system. In this thesis, the different aspects of islet transplantation and cell monitoring modalities were addressed from a bioengineering perspective to improve transplant outcomes. We investigated the use of lentiviral forward programming protocols to improve the efficiency of β-cell differentiation, emphasizing the importance of recapitulating the temporal expression of the mature β-cell markers as in development. Further, to support the β-cells post-transplantation, we moved towards re-establishment of the human adult pancreatic environment using extracellular matrix proteins strongly associated with insulin-producing cells within the islets of Langerhans, decorin and nidogen-1. Interestingly, supplementation of these recombinantly-produced proteins to our immortalized β-cell line pseudo-islet model and isolated human donor islets improved glucose-responsiveness, and protected them under hypoxic conditions as experienced in a post-transplantation environment. Furthermore, decorin was observed to reduce the expression of fibrotic ECM proteins, suggesting a role in preventing fibrotic capsule formation surrounding the transplant which would otherwise render it ineffective. We also demonstrated the use of FLIM to non-invasively monitor the metabolic response of the β-cells to glucose stimulation and changes in oxygen levels in its environment in real-time. Altogether, this thesis highlights the importance of recapitulating the signals and cues β-cells experience *in vivo* to best improve islet transplantation outcomes.

Zusammenfassung

Typ-1-Diabetes mellitus ist eine chronische Erkrankung, die zur Beeinträchtigung der Blutzuckerregulation führt. Zu den derzeitigen Therapieansätzen für Patienten mit Typ-1-Diabetes gehören die regelmäßige Kontrolle des Blutzuckerspiegels sowie die Verabreichung von exogenem Insulin. Ein Alternative ist die Transplantation von Langerhans‘schen Inselzellen oder β-Zellen, um eine unabhängige endogene Blutzuckerregulation wiederherstellen und das Risiko von Unter- und Übermedikation von Patienten zu reduzieren. Mit wachsendem Verständnis über die Zusammensetzung der menschlichen Bauchspeicheldrüse während der Entwicklung und im Erwachsenenalter hat die Forschung im Bereich Transplantation von Spender-Inselzellen in den letzten Jahrzehnten große Fortschritte gemacht, insbesondere in Bezug auf die Verbesserung von Stammzelldifferenzierungsprotokollen zur Erweiterung von möglichen Stammzellresourcen und dem Schutz des Transplantats vor dem Immunsystem. In dieser Arbeit wurden die verschiedenen Aspekte der Inselzelltransplantation aus biotechnologischen Perspektiven betrachtet, um die Erfolgschancen von Transplantationen zu verbessern. Wir entwickelten und verwendeten lentiviral-basierte induzierte Differenzierungsprotokolle mit besonderem Augenmerk auf die zeitlich kontrollierte Expression von maturen β-Zellmarkern. Dieser Ansatz zielt darauf ab, die Effizienz von β-Zelldifferenzierung zu verbessern sowie die notwendige Differenzierungszeit zu verringern, um die Verfügbarkeit von β-Zellen für die Transplantation zu erhöhen. Um die β-Zellen nach der Transplantation zu unterstützen, haben wir die Nische der menschlichen adulten Bauchspeicheldrüse untersucht und mit Hilfe von extrazellulären Matrixproteinen wiederhergestellt, welche besonders stark mit den insulinproduzierenden Zellen in Langerhans-Inseln assoziiert sind, im Speziellen Decorin und Nidogen-1. Interessanterweise verbesserte die Zugabe dieser rekombinant hergestellten Proteine sowohl die Funktionalität und Glukoseempfindlichkeit von unserem immortalisierten β-Zelllinien-Pseudoinseln-Modell als auch von isolierten menschlichen Spenderinseln. Überdies schützte die Zugabe der Proteine die Zellen während hypoxischen Posttransplantationsbedingungen. Darüber hinaus wurde beobachtet, dass Decorin

die Expression von fibrotischen ECM-Proteinen reduziert, was auf eine Rolle bei der Verhinderung der Bildung einer fibrotischen Kapsel um das Transplantat herum hindeutet, eine besonders interessante Eigenschaft für die klinische Anwendung. Wir demonstrierten ebenfalls die Vorteile von FLIM zur nicht-invasiven Kontrolle der metabolischen Reaktion der β-Zellen auf Glukosestimulation durch Änderungen des Sauerstoffgehalts in ihrer Umgebung in Echtzeit. Insgesamt unterstreicht diese Arbeit die Wichtigkeit und Relevanznativer Signale sowie der extra- und intrazelluläre Kommunikation, um die Ergebnisse β-Zelldifferenzierung sowie das Überleben und die Funktionalität der Zellen nach der Inseltransplantation zu verbessern.

Abbreviations

ANOVA	analysis of variance
ATP	adenosine triphosphate
BM	basement membrane
COL	collagen
CTL	control
DCN	decorin
DM	diabetes mellitus
DNA	deoxyribonucleic acid
DOX	doxycycline
ECM	extracellular matrix
ER	endoplasmic reticulum
ESC	embryonic stem cell
FAD	flavin adenine dinucleotide
FBP1	fructose-1,6-bisphosphatase 1
FLIM	fluorescence lifetime imaging microscopy
FN	fibronectin
GAPDH	glyceraldehyde 3-phosphate dehydrogenase
GDF8	growth differentiation factor 8
GFP	green fluorescent protein
GLUT	glucose transporter
GO	gene ontology
GSGS	glucose-stimulated glucagon secretion
GSIS	glucose-stimulated insulin secretion
hESC	human embryonic stem cell
HIF1a	hypoxia-inducible factor 1 subunit alpha
HILO	human pancreatic islet-like organoid
hiPSC	human induced pluripotent stem cell
HLA	human leukocyte antigen
KDM3A	lysine demethylase 3A

KEGG	Kyoto Encyclopedia of Genes and Genomes
KLF4	krüppel-like factor 4
LN	laminin
LRP1	low density lipoprotein receptor-related protein-1
MAFA	MAF BZIP transcription factor A
MAFB	MAF BZIP transcription factor B
MCT	monocarboxylate transporter
NADH	nicotinamide adenine dinucleotide
NANOG	homeobox protein NANOG
NEUROD1	neurogenic differentiation-1
NGN3	neurogenin-3
NGS	next-generation sequence
NID1	nidogen-1
NKX6.1	homeobox protein Nkx-6.1
OCT4	octamer-binding transcription factor 4
PCK1	phosphoenolpyruvate carboxykinase 1
PD-L1	programmed death-ligand 1
PDX1	pancreatic and duodenal homeobox-1
PGK1	phosphoglycerate kinase-1
PSC	pluripotent stem cell
RNA	ribonucleic acid
RT-qPCR	quantitative reverse transcription polymerase chain reaction
SLC	solute carrier family
SOX2	sex determining region Y box-2
T1DM	type one diabetes mellitus
T2DM	type two diabetes mellitus
TGF-β	transforming growth factor-β
UCN3	urocortin-3
VEGF	vascular endothelial growth factor

List of Figures

List of Publications

[§] = authors contributed equally

[#] = authors contributed equally

1. Zbinden, A.[§], Carvajal, D.A.[§], Urbanczyk, M., Layland, S.L., Bosch, M., Fliri, S., Lu, C., **Jeyagaran, A.**, Loskill, P., Duffy, G.P., Schenke-Layland, K., Fluorescence Lifetime Metabolic Mapping of Hypoxia-induced Damage in Pancreatic Pseudo-islets, Journal of Biophotonics, 13(12), e202000375 (2020).
2. **Jeyagaran, A.[§]**, Lu, C.[§], Zbinden, A., Birkenfeld, A. L., Brucker, S. Y., Layland, S. L., Type 1 diabetes and engineering enhanced islet transplantation, Advanced Drug Delivery Reviews, 189, 114481 (2022).
3. Urbanczyk, M.[§], **Jeyagaran, A.[§]**, Zbinden, A., Lu, C., Marzi, J., Kuhlburger, L., Nahnsen, S., Layland, S.L., Duffy, G.P., Schenke-Layland, K., Decorin Improves Pancreatic β-cell Function and Regulates Extracellular Matrix Expression in vitro, Matrix Biology, 115, 160-183 (2023).
4. **Jeyagaran, A.**, Urbanczyk, M., Layland, S.L., Weise, F., Schenke-Layland, K., Forward programming of hiPSCs towards beta-like cells using Ngn3, Pdx1, and MafA, Scientific Reports, 14, 13608 (2024).
5. **Jeyagaran, A[§]**, Urbanczyk, M.[§], Carvajal-Berrio, D., Baldissera, T., Kaiser, P. D., Kuhlburger, L., Czemmel, S., Nahnsen, S., Duffy, G.P., Brucker, S.Y., Layland, S.L.[#], Schenke-Layland, K.[#], ECM Proteins Nidogen-1 and Decorin Restore Functionality of Human Islets of Langerhans upon Hypoxic Conditions, Advanced Healthcare Materials, 2403017 (2024).
6. Urbanczyk, M., Abuhelou, A., Koeninger, M., **Jeyagaran, A.**, Carvajal-Berrio, D., Kim, E., Marzi, J., Loskill, P., Layland, S.L., Schenke-Layland, K., Heterogeneity of endothelial cells impacts the functionality of human pancreatic in vitro models, Tissue Engineering Part A (2024).

Contribution

R = review

No.	1	2	3	4	5	6
Accepted for publication	Yes	Yes	Yes	Yes	Yes	Yes
Number of authors	11	6	10	5	12	10
Position of the candidate in the list of authors	8	1	2	1	1	4
Scientific ideas by candidate (%)	10	R	30	60	30	30
Data generation (%)	30	R	30	80	30	30
Interpretation and analysis by candidate (%)	10	R	30	80	30	30
Paper writing by candidate (%)	10	40	40	80	40	20

Chapter 1

Introduction

1. Introduction

1.1. Pancreas and Islets of Langerhans

The pancreas is a heterocrine organ consisting of both exocrine digestive glands and endocrine glands. The exocrine part makes up most of the pancreas consisting of acinar and pancreatic ductal epithelial cells. This exocrine gland is responsible for the production and secretion of digestive enzymes and bicarbonate into the duodenum to support digestion. The endocrine part of the pancreas is responsible for maintaining blood glucose homeostasis through the production and secretion of hormones into the bloodstream[1]. Cells of the endocrine pancreas are found in clusters called the islets of Langerhans of around 100 µm diameter[2]. The majority of the endocrine cells are insulin-producing β-cells (70-80%), followed by glucagon-producing α-cells (15-20%), somatostatin-producing δ-cells (5-10%), and pancreatic polypeptide cells (5-10%) that are involved in the maintenance of blood glucose levels[3,4]. In rodent islets, β- and α-cells appear as distinct masses; however, human islets show no clear organization of the cell types. The islets themselves are highly vascularized and innervated with nerve fibers to support the exchange of hormones, oxygen, and growth factors[5]. Dysfunction and/or death of the islets' cells, specifically β-cells, are the main cause for the onset and progression of diabetes mellitus[6].

1.1.1. β-cell Function and Maturation

β-cells are the insulin-producing cells of the endocrine pancreas responsible for the production and secretion of insulin during high glucose episodes. Differentiating from pancreatic progenitors, β-cells are initially considered immature due to the lack of functionality defined as glucose-responsive insulin secretion. Upon maturation, β-cells are able the sense the levels of glucose in the bloodstream and regulate their insulin production and secretion in response[7].

Comparisons of islet functionality between infants and adults showed increased basal insulin secretion in infants suggesting that the islets were only mature/functional after the first year[8–10]. Interestingly, key differences between immature and mature β-

cells in mice could be attributed to differential expression of transcription factors. Particularly increased RNA expression of *Nkx6.1*, *NeuroD1*, *Ucn3*, and *MafA*, and decreased expression of *MafB* in mature β-cells was found compared to immature β-cells[8–10]. While *Ucn3* expression levels showed the greatest difference between the immature and mature cells, exogenous expression of Ucn3 into immature β-cells was not sufficient to promote their maturation[11]. In human islets, expression of both MAFA and MAFB allowed for greater expression of genes involved in sensing of glucose and electrophysiological activity than those expressing only one of the two transcription factors[12]. The differences between these two studies in mice and humans emphasize the importance of studying human pancreatic tissues and development to best understand β-cell development and maturation.

Investigation on how mature β-cells sense and tune their response to glucose levels identified pathways involved in different steps of glucose metabolism. Normally, glucose enters the cells passively using glucose transporters (GLUT). While GLUT2 was initially identified as the primary transporter in rodents, GLUT1 and GLUT3 were found to be enriched in humans islets[13,14]; though investigation of genetic mutations in patients with neonatal DM demonstrated that 5% of these patients had a homozygous mutation in the gene encoding GLUT2[15]. Upon entering the cell, glucose is metabolized through the glycolytic pathway to produce energy / adenosine triphosphate (ATP) and eventually depolarize the cell membrane allowing for the exocytosis of insulin granules. Analysis of β-cells from adult rats with different metabolic rates identified differences in hexokinase phosphorylation of glucose in the first step of glycolysis[16]. Of the four mammalian hexokinases, hexokinase 4, with a low-affinity for glucose, is found in mature β-cells while hexokinases with a high-affinity for glucose are repressed[17–20]. The rodent β-cells with low metabolic rates showed similar hexokinase activity of mature β-cells, while those with high metabolic rates also showed high levels of hexokinase 1[16]. This suggested that the switch from hexokinase 1 to hexokinase 4 was important for the maturation of β-cells and the tight regulation of glucose levels. This was also observed *in vitro* where fetal rat islets initially expressed hexokinase 1, but with extended culture, they only expressed hexokinase 4, in line with the maturation of the β-cells[17]. Interestingly, similar observations were

made in mice where undernourished mice pups had increased hexokinase 1 activity due to the poor diet not supporting the maturation of β-cells[21,22]. Hexokinase activity is the first step of the glycolytic pathway and does not account for all the differences observed between immature and mature β-cells. In islet-like cell clusters from human fetal tissue, hexokinase 4 had similar Michaelis coefficients between human fetal islet clusters and human adult islets, while the maximal velocity of the enzyme was significantly lower in the fetal islet clusters. As expected, the maximal velocity of hexokinase 4 in the fetal islet clusters increased upon extended culture; however, this did not improve insulin secretion, suggesting that events downstream in the glycolytic pathway are also altered between the immature and mature β-cells[23]. β-cell maturation is a complex process especially for the generation of functional β-cells as each step of the glucose sensing and responding, as well as insulin production and secretion processes need to be tightly regulated.

1.2. Diabetes Mellitus

Diabetes mellitus (DM) is a chronic disease resulting in the dysregulation of blood glucose levels due to the body's inability to effectively produce or use insulin[24]. DM is classified into two categories: type 1 (T1DM) and type 2 (T2DM)[25,26]. T1DM results from the autoimmune attack and death of β-cells; while T2DM is caused by the inability of β-cells to produce insulin and/or other cells' ability to respond to insulin. Patients with DM suffer from hyperglycemic episodes that, when untreated, can lead to blindness, kidney failure, heart disease, stroke, coma, and possibly death. Studies have identified a few genetic predispositions of T1DM; however, there is no clear marker linked to the disease or its progression[27]. T2DM is a result of desensitization of the insulin receptors that could be attributed to genetic and lifestyle factors leading to insulin resistance[28]. Patients with DM rely on continuous monitoring of blood glucose levels and self-administration of exogenous insulin. This also comes with the risk of over- and/or under-administering the insulin resulting in poor blood glucose homeostasis[29]. Significant advances have been made in the development of glucose sensors and insulin pumps; however, this technology still lacks the innate glucose control at levels similar to the physiological activity of the pancreatic islets[30].

1.2.1. Islet Transplantation and the Edmonton Protocol

Pancreatic islet transplants from donor tissues hold great promise for T1DM treatment[31]. Islet isolation methods have been optimized to maximize the usable tissue obtained from donor pancreases. A couple of milestones in the islet transplantation process were the generation of the Ricordi chamber[32] and development of the Edmonton protocol[33]. Following enzymatic digestion, the pancreatic tissue is treated within the Ricordi chamber consisting of an isolation chamber with stainless steel balls for the mechanical disruption of the pancreatic tissue and a filtration chamber to separate the islets from the rest of the pancreatic tissue. Over the years, the Ricordi chamber has been modified to improve islet yield through the use of hooks to mechanically tear the tissue allowing for the reduction in enzymatic digestion time[34]. The Edmonton protocol improved the success rates of islets transplantation through optimization of the transplant site and changes to the post-transplantation treatment. Following islet isolation using the Ricordi chamber, islets were transfused into the patient through the portal vein of the liver[33,35] and implemented a steroid-free immunosuppressive regimen to protect the islets from the immune system. These changes allowed for the reduction of the adverse effects from the use of steroids as immunosuppressants[36], and for insulin-independency for up to a decade[37].

1.2.2. Limitations of Islet Transplantation

An obstacle that limits the applicability of islet transplantation for all patients with T1DM is the availability of islets. While many advances in islet isolation have allowed for increased procurement of healthy islets, it still does not allow for 100% isolation of the islets in a healthy state and further, transplanted islets are often lost in the initial weeks post-transplantation as a result of an immune reaction and unfavourable conditions. To meet the demand for the number of islet requires, on average, two donor pancreases are needed for one patient[34,38]. As such, other islet cell sources such as stem-cell derived insulin-producing cells are being heavily explored to meet the high demand for endocrine replacement therapy. Once enough islets are procured, they need to be protected and supported during the initial hypoxic conditions

and instant blood-mediated inflammatory reaction[39,40]. Islets are highly vascularized structures; however, this vasculature is lost during the isolation process and not re-established until the transplant site is vascularized by the host's system. This results in a hypoxic environment during which islets lose their functionality and eventually die, resulting in the failure of the transplant[41,42]. Incorporating accessory cells such as endothelial cells to quicken the vascularization process and/or oxygen-releasing molecules with the transplant has been shown to support islet function and transplant survival[6]. Many advancements in the field of encapsulation have been made to co-transplant accessory cells, extracellular matrix (ECM) proteins, and small molecules while also protecting the islets from the host's immune system; however, this also poses the limitation of inducing a foreign body response where excessive fibrogenesis and fibrotic tissue formation isolates the transplant from the host's system rendering it ineffective. As such, encapsulation devices made of polymers such as modified alginates or incorporation of molecules for regulation of fibrogenesis are being investigated to improve transplant outcomes[6]. Future studies on optimizing stem cell differentiation protocols to increase the availability of transplantable β-cells and how to best support the survival and function of the β-cells would be very beneficial to increase the efficacy of islet transplantation.

1.3. Stem cell-derived Insulin-producing Cells

Stem cells act as a renewable source of cells capable of differentiating into multiple cell types. When isolated from later stages of development, their potency to differentiate into specific cell types becomes restricted, where they have the greatest potency when derived from the pre-implantation embryo. These embryonic stem cells (ESCs) are considered pluripotent and can generate cells of all lineages. When derived from tissues of the fetus or adult, they are considered multipotent stem cells and are restricted in their differential potential to the germ layer from which the tissue originated[43]. Furthermore, adult somatic cells can also be reprogrammed back into pluripotent stem cells (PSCs). Human adult somatic cells can be reprogrammed into human induced pluripotent stem cells (hiPSCs) using the Yamanaka factors OCT4, KLF4, SOX2, and MYC. These hiPSCs obtain ESC-like characteristics, avoiding the

ethical concerns regarding the use of human ESCs (hESCs). Through extensive culture protocols, these stem cells can be directed to differentiate towards a specific cell type, resulting in generation of large numbers of cells for therapeutic purposes[44,45]. Over the past decade, many groups have studied the use of stem cells for the generation of glucose-responsive insulin-producing β-cells to be transplanted in patients with T1DM. The use of hiPSCs further overcomes the risk of immune rejection as the patient's own somatic cells can be used for the reprogramming into hiPSCs[46–48]; however, for the purpose of T1DM the insulin-producing cells would need to be protected as the disease is due to an autoimmune attack against the patient's β-cells.

1.3.1. Differentiation of Embryonic and Induced Pluripotent Stem Cells into β-cells

With increasing understanding of pancreatic development, the chemical and physical cues progenitor cells experience to become β-cells are also better understood[6]. Step-wise differentiation of hESCs and/or hiPSCs into definitive endoderm, primitive gut tube, pancreatic progenitors, endocrine progenitors, and finally β-cells proved to be effective in generating functional insulin-producing β-cells. Each stage is mimicked using various growth factors and cell culture platforms over the course of around two months[6,49] following which, the stem cell-derived β-cells are assessed for functionality using a glucose-stimulated insulin secretion (GSIS) assay. Similar differentiation protocols as hESCs have been used for hiPSCs though with slightly reduced efficiencies[50–55]. The discrepancies in differentiation efficiencies between hESCs and hiPSCs could be attributed to the epigenetic profiles of hiPSCs[56]. It must be noted that a protocol that works for one hESC or hiPSC line may not be effective for a cell line from a different donor, emphasizing the need to find optimal culture conditions for each cell type and cell line.

Many culture protocols from different labs are similar in terms of pathways targeted, some groups further optimized the protocols using specific molecules and cell culture systems used to produce glucose-responsive β-cells. Rezania, A., et al., (2014)[50] assessed specific signalling pathways defined in earlier studies and targeted the same pathways using different molecules. Exchanging the commonly used activin

A for GDF8 from the TGF-β-family increased the differentiation efficiency of the hESCs towards pancreatic progenitors. Furthermore, incorporation of vitamin C in the medium allowed for the expansion of the pancreatic progenitor population, increasing the number of cells that could finally be differentiated into β-cells. Interestingly, they also observed that switching the cell culture platform from a planar culture to an air-liquid interface culture later in the protocol allowed for the cells to obtain apical-basal polarity and a greater number of cells with β-cell-specific markers. Importantly, this improved the expression of insulin, and these cells were able to restore normoglycemia in diabetic mice.

Many groups have also investigated the importance of the physical structure of islets of Langerhans for the functionality of β-cells. Through addition of cell aggregation, dissociation, and reaggregation steps, Nair, G. G., et al., (2019)[57] were able to increase the differentiation efficiency of hESCs into mature β-cells to around 90%. Furthermore, they used hESCs engineered with GFP-tagged insulin to be able to sort out the GFP^{+ve} cells at the last stage to form aggregates which functioned similarly to mature human β-cells. Another study focusing on the regulation of cluster size also noted the importance of ensuring uniform differentiation throughout the cluster to obtain greater insulin production and glucose-responsiveness[51,58]. This group further achieved a larger β-cell population through sorting of the cells for the intracellular zinc content rather than an introduced tag. The zinc content of β-cells increase due to their role in the packing and secreting of insulin, allowing for increased zinc content to be used to select for β-cells[59]. Hogrebe, N. J., et al., (2020)[60] also focused on modulating the actin cytoskeleton to allow for cell polarization to support the maturation of the β-cells. This allowed for GSIS results similar to that of human islets and the restoration of normoglycemia in diabetic mice. These studies pointed out the importance of modulating cellular structure and organization to best support stem cell differentiation.

A key element that must be considered before the transplantation of hPSC-derived β-cells is its long-term functionality. The stem cell-derived cells must be able to maintain their glucose-responsiveness to continuous and multiple glucose challenges as mature β-cells do. Differentiated cells display β-cell markers and glucose-responsive insulin secretion; however, their functionality is still inferior to that of human islets. Extensive

analysis of hPSC-derived β-cells from previously published protocols and human islets identified key differences in glucose metabolism. While similar glucose-response and exocytotic machinery was present in the hPSC-derived β-cells and human islets, there was reduced mitochondrial activity in the hPSC-derived β-cells suggesting an immature state[61]. Interestingly, it was also observed that while stem cell-derived β-cells and human donor islets present similar glucose uptake levels and early glycolysis products, the stem cell-derived β-cells have reduced electron transport chain[62]. They were unable to replenish the glycolytic metabolites following the PGK1 and GAPDH reactions; however, when these metabolites were supplemented to the cells through the cell culture medium, the stem cell-derived β-cells functioned similarly to that of the donor islets[62,63]. Transcriptomic analysis also showed that engraftment of the hPSC-derived β-cells into mice allowed for the maturation of the cells[61,64]. These studies emphasized the importance of evaluating hPSC-derived β-cells at all levels, including transcriptomics, proteomics, and functionality, to improve current differentiation protocols and ensure sufficient long-term function of the cells. Further work into the reason behind the inhibition in the glycolysis of stem cell-derived β-cells and how this could be circumvented without exogenous supplementation is necessary to generate β-cells for therapeutic purposes.

1.3.2. Immune-evasive Stem Cells

T1DM is an autoimmune disease where the host's immune system targets and kills the insulin-producing β-cells. As such, transplanted β-cells would still be at risk of being targeted by the patient's immune system. A current strategy to protect the transplant is to encapsulate them in biomaterials and/or co-transplant cells that can modulate the immune system such as mesenchymal stromal cells[6]; however, an ideal situation would be to not need anything other than the transplant cells to reduce the invasiveness of the procedure. To this extent, scientists have engineered stem cell lines that are considered universal stem cells due to their lack of human leukocyte antigen (HLA) genes. These cells have the potential to be differentiated into any cell type for any patient without the risk of immune rejection. These cells do not stimulate T-cells or become targets of natural killer cells, and survive longer once transplanted[65–68]. When

HLA-deficient stem cells were differentiated towards insulin-producing cells and assessed for their immunogenicity, they showed reduced activation of natural killer cells compared to their wild-type counterparts[69]. Furthermore, they had longer viability and greater cell mass a month post-transplantation compared to the wild-type cells. Transplantation of β2M-deficient islets in the kidney capsule of diabetic mice showed increased efficacy and viability compared to wild-type islets[70]. A more recent study used hiPSCs overexpressing PD-L1, a suppressor of the adaptive immune system, to generate human islet-like organoids (HILOs) more representative of native islets[71]. Following differentiation of the hiPSCs into pancreatic endocrine progenitor cells and co-culture with human adipose-derived stem cells and human umbilical vein endothelial cells to form HILOs, the pancreatic progenitors differentiated further into mature β-cells with improved GSIS. When these HILOs were transplanted into immune-competent mice, they were able to evade the immune response and restore normoglycemia for a longer period compared to the wild-type cells. Another protein of interest to be overexpressed in universal stem cell lines is CD47, known for its “don’t eat me” signal to the immune system[72]. Unfortunately, its overexpression and signalling has been shown to downregulate insulin secretion[73], emphasizing the need to better understand how cellular interactions and signalling pathways can affect the cell’s metabolism.

Engineering of stem cells to evade the immune system are an attractive solution of cell replacement therapies for their off-the-shelf capabilities and especially for those with autoimmune disorders such as T1DM; however, they could be dangerous if the differentiation is not complete and the cells become tumourigenic post-transplantation[74]. Evading the immune system is also a characteristic of tumour growth and is a continuing obstacle in cancer therapy, and the generation of hypoimmunogenic stem cells for transplantation purposes further increases this risk if the cells become cancerous.

1.3.3. Transdifferentiation Protocols

Over the last decade, the differentiation protocols of stem cells into insulin-producing β-cells have been optimized in terms of timing of supplement

addition/exclusion, cell culture platforms, and culture period for each stage of differentiation[6,50,51,57–59,61,75,76]. The protocols, however, generate a heterogenous population of pancreatic cells and are not necessarily efficient for different stem cell lines. To address this limitation, overexpression of mature cell markers in cells to reprogram or transdifferentiate adult cells into β-cells have been studied. Investigation of murine pancreatic development identified multiple transcription factor combinations required for β-cells[77,78]. Interestingly, transcription factors Ngn3, Pdx1, and MafA were sufficient to transdifferentiate mouse[79] and rat[80,81] pancreatic exocrine tissues, and mouse liver tissues[82–84] to insulin-producing β-cells *in vivo* and restore normoglycemia in diabetic mice. Further, the differentiation efficiencies of mouse ESCs[85] and hiPSCs[86] into β-cells were also improved upon the exogenous expression of these three factors in a temporal manner. The temporal expression of these three factors aimed to better mimic their developmental expression patterns. Pdx1 expression specifies the pancreatic lineage, followed by Ngn3 expression to specify the pancreatic endocrine lineage during which Pdx1 is downregulated[87]. When Pdx1 is upregulated again, Ngn3 is downregulated, and MafA is activated, allowing for the maturation of the β-cells[78,88,89]. Saxena, P., et al. (2016)[86] engineered hiPSCs where the three genes are under promoters activated by different concentrations of vanillic acid. Following differentiation towards the pancreatic progenitor stage, they were able to control the expression of these three genes with the concentration of vanillic acid in then medium to drive the cells towards mature β-cells. Through the exogenous (over)expression of NGN3, PDX1, and MAFA, these studies were able to generate an increased number of glucose-responsive insulin-producing cells within a shorter timeline, suggesting this could be a potential approach for improving the differentiation efficiency of hiPSCs.

1.3.4. Assessing β-cell Function

Assessing β-cell function is an important step before their transplantation into patients. During the isolation, many islets are damaged such that they lose their functionality and initiate apoptosis or anoikis during the culture period[90,91]. With stem cell-derived β-cells, there is the risk that the cells do not mature in culture or dedifferentiate from the mature state such that they do not respond in a similar manner

to donor islets[61–63]. This requires regular assessments on how well the β-cells sense and respond to glucose levels. The most common and accepted method is to perform a GSIS assay to determine whether the cells are functional[92]. During this assay, the cells are incubated in a buffer solution with varying glucose concentrations and the amount of insulin they secrete is evaluated through the supernatant. This value is then normalized by the insulin content (the amount of insulin within the cells) to account for the actual number of β-cells measured as there is a heterogenous cell population in the culture (including the other endocrine cell types in the donor islets or cells that didn't differentiate towards the β-cell lineage from the stem cells); however, the cells need to be lysed to obtain the insulin content. This assay acts as an indirect quality control measure of the culture dish and reduces the number of cells available for transplant. While the functionality of the cells is directly measured, it does not provide insight into the dynamic metabolic processes which allows for distinguishing between immature and mature β-cells.

1.3.5. Non-invasive Monitoring of β-cell Function using Fluorescence Lifetime Imaging Microscopy

Fluorescence lifetime imaging microscopy (FLIM) allows for the analysis of live tissues' metabolic rates[93,94]. Nicotinamide adenine dinucleotide (NADH) and flavin adenine dinucleotide (FAD) are two autofluorescent coenzymes that play key roles during cellular respiratory and metabolic pathways including glycolysis and oxidative phosphorylation. Through sensing and metabolizing of glucose, β-cells undergo these metabolic pathways to generate ATP for energy, producing NADH and FAD, to produce and secrete insulin. The unbound and protein-bound states of these coenzymes provide further insight into the cell's metabolism. Unbound NADH is a product of glycolysis and the Krebs cycle, and has a shorter lifetime (NADH $\tau 1$) compared to its protein-bound form's lifetime (NADH $\tau 2$) that is observed at the electron transport chain during oxidative phosphorylation within the mitochondria[95]. Conversely, unbound FAD has a longer fluorescent lifetime (FAD $\tau 2$) compared to its protein-bound form's lifetime (FAD $\tau 1$) that is involved in the Krebs cycle and electron transport chain within the mitochondria[96]. Analysis of these values can allow for an

understanding of the cell's metabolic state and the dynamic switches between glycolysis and oxidative phosphorylation in a non-invasive manner, suggesting FLIM can be used to select for β-cells that can respond to glucose and use them for transplantation purposes.

1.4. Strategies to Support Islet Transplantation

During the islet isolation process, pancreatic tissue is digested mechanically and chemically using enzymes such as collagenases. This allows for the efficient isolation of the islets of Langerhans; however, it also separates these cells from their native ECM environment and other surrounding cell types including endothelial cells, fibroblasts, and pericytes[97]. Paracrine signalling from the ECM and surrounding cells is extremely important for the survival and function of β-cells[98]. To support islets post-transplantation, many research groups have studied and tried to recapitulate the islet niche and vasculature through co-culture/transplantation with native ECM proteins and supportive cell types[6].

1.4.1. Restoring the Pancreatic Islet Extracellular Matrix

The ECM acts as a supportive scaffold for cells throughout the body providing both biophysical and biochemical signalling cues, sequestering growth factors, and activating signalling pathways to maintain tissue homeostasis. Expectedly, the ECM composition of each tissue is unique to the tissue's function and location. The pancreatic ECM is composed largely of fibrous ECM proteins including collagen types I (COL1) and IV (COL4)[99], laminins (LN)[100,101], fibronectin (FN), and various proteoglycans[97,102,103]. Interestingly, human islets consist of a double BM rather than the usual single BM observed in the majority of other human tissues or rodent islets[101]. BMs are important for supporting the physical structure of the tissue as well as influencing cellular morphologies and activity. They are largely composed of LN interconnected with COL4 via nidogen (NID) complexes, and proteoglycans[103,104]. In the human islet, a BM sheath was observed surrounding the blood vessels within the islets along with a peri-islet BM and interstitial matrix around the islet, suggesting that the endocrine cells of the islets and the endothelial cells of the blood vessels are

exposed to separate BM compositions. Interestingly, this double BM could be differentiated through the presence and absence of specific laminin isoforms. The BM surrounding the blood vessels were composed of LN411 and LN511, while the BM surrounding the endocrine cells was composed of LN511[105]. Investigation of LN receptors within the islets identified presence of integrins α3 and β1, and the Lutheran glycoprotein basal cell adhesion molecule (BCAM) on both the endocrine and endothelial cells while integrin α6 was only observed on the endothelial cells. Analysis of the BM of islets post-isolation identified significant loss of LN α5, one of the three subunits of LN511, and proteoglycan content which was not restored upon culture[103]. COL4 was present at reduced levels post-isolation; however, it was disorganized and eventually completely lost during the culture period. The lack of ECM support can impair islet function and lead to anoikis[91,103,106,107].

To restore the ECM environment, many groups have studied the effects of co-culture and/or supplementation of specific ECM proteins with/to isolated islets[102]. Culturing isolated human islets on COL4- or LN-coated substrates allowed for increased survival[100,108–110] and functionality[110–115], increasing the yield of islets for transplantation. As expected, the co-culture with both COL4 and LN supported cell survival and function greater than with one of the two ECM proteins[112,116,117]. Furthermore, the ratio of the two proteins influenced cell behaviour. Culturing human islets with an 8:2 ratio of COL4 and LN111 had the greatest positive effects on islet architecture, survival, and function[117]. This emphasizes how appropriate amounts of ECM proteins are also important for the formation of a BM that would best support isolated human islets. While the lack of ECM support could result in dysregulated cell function, increased concentrations of ECM protein supplementation could also have adverse effects. The positive effects of COL4 on the human islets were dose-dependent[116] where in some cases it even disrupted gene transcription and secretion of insulin[118]. Furthermore, increased ECM deposition, that does not result in BM formation or strengthening, can also result in the formation of a fibrotic capsule which isolates the cells from the patient's system, such that the patient cannot use the transplant, highlighting the need to ensure that the exogenously provided ECM proteins are regulated.

1.4.2. Restoring the Pancreatic Islet Vasculature

Islets are highly vascularized structures that allow for the constant and rapid exchange of nutrients, oxygen, small molecules, glucose, and hormones such as insulin and glucagon to tightly regulate blood glucose levels. Unfortunately, the vascularization is lost during the islet isolation process, impacting cell viability and function post-transplantation[119]. Without an intact vascular system throughout the islets, they are subjected to hypoxic and nutrient-deficient environments post-transplantation until the patient's system undergoes neoangiogenesis into the transplant. This process can take up to a week during which many of the transplanted islets are lost, reducing the transplant efficacy[6]. Many groups have tried to enhance angiogenesis at the transplant site through hypoxic preconditioning, co-transplantation with vascular endothelial growth factors (VEGF), or endothelial cells[6]. Hypoxic preconditioning involves the culturing of islets in low oxygen conditions before they are transplanted. Through gradually regulating the oxygen levels in the culture system, the islets are used to the lower oxygen levels allowing for the restoration of insulin secretion[120,121]. Interestingly, such pre-treatments can also reduce inflammatory reactions post-transplantation while also promoting angiogenesis to the transplant site and mitigate oxidative stress[122]. Co-transplantation of islets with VEGF, a pro-angiogenic factor[123,124], has been shown to improve vascularization to the transplant site[125–129]. Furthermore, when transplanted with heparin and VEGF, instant blood-mediated inflammatory reaction was also reduced, improving transplant survival and function[130–133]. It must be noted that incorporation of VEGF without regulating the concentration and timing of its release poses the risk of angioma formation[134], where the co-transplantation of endothelial cells that can produce and secrete VEGF when needed is a safer alternative. Co-transplantation of endothelial cells of different origins, including aortic and umbilical vein, with islets were able to restore normoglycemia while reducing macrophage infiltration[135–139]. Interestingly, coating islets with endothelial cells before transplantation also improved angiogenesis and pro-longed the transplant's viability[140], where the ECM deposited by the endothelial cells further aided islet survival and function, particularly in post-transplantation settings[141]. Co-transplantation of islets with endothelial cells allowed for the increased

insulin levels in the blood due to the increased vasculature through the islets, further enabling the islets maintain their viability and structural integrity[142–145], though it must be noted that endothelial cells composition and function are unique depending on their vascular structure[146], suggesting pancreas-specific or at least microvascular endothelial cells would have the most beneficial effect on the islets. Incorporation of oxygenation molecules or endothelial cells could greatly improve islet transplantation outcomes through supporting the islets during the initial hypoxic conditions.

Chapter 2

Objective of the Thesis

2. Objective of the Thesis

The aim of this thesis is to investigate advanced bioengineering techniques to address and overcome the current limitations of islet transplantation. To this extent, we focused on improving the differentiation efficiency of hiPSCs into β-cells, supporting β-cell survival and functionality in a post-transplantation setting, and assessing the function of β-cells in a non-invasive manner.

In the first step, we investigated the use of lentiviral constructs to forward program hiPSCs into β-cells to improve differentiation efficiency. A limitation of current β-cell differentiation protocols is the generation of a heterogenous pancreatic cell population at the end of a two-month period. Furthermore, many of the β-cells from the protocol are considered immature due to their inability to demonstrate glucose-responsive insulin secretion. Through design and generation of lentiviral constructs for the inducible expression of three mature β-cell-specific markers, NGN3, PDX1, and MAFA, we attempted to forward program hiPSCs towards a homogeneous population of β-like cells in a shortened timeline of around two weeks. We further characterized these cells in relation to human fetal pancreas and human adult islets to understand the developmental stage of the stem cell-derived cells.

During islet isolation and hiPSC differentiation into β-cells, there is an absence of pancreatic ECM which plays a key role in β-cell survival and function. To understand which ECM proteins would best support the β-cells, we studied human pancreatic tissues and identified the proteoglycan decorin (DCN) to be highly co-localized with the insulin-producing β-cells. Furthermore, DCN is a known regulator of the ECM with potential to reduce the formation of a fibrotic capsule[147] in a post-transplantation setting. We investigated the effects of DCN on β-cell functionality and ECM deposition using an immortalized human β-cell line for its application as a co-transplant protein to improve transplantation success.

We further assessed β-cell metabolism and how it is affected by hypoxia, non-invasively, using FLIM. Current techniques to measure and monitor β-cell function restrict the use of the measured cell(s) for transplantation, requiring tests that do not reduce the number of islets available for transplantation. Using the immortalized

human β-cell line, we determined whether FLIM, a non-invasive method, was suitable to discriminate between glucose-responsive and unresponsive cells, and between healthy and hypoxia-induced apoptotic cells. With complementary techniques including GSIS assays, viability assays, and immunofluorescence staining, we assessed the use of FLIM as a screening tool to select functional β-cells for transplantation.

We built on our previous studies on the effects of BM protein NID1 and proteoglycan DCN on the β-cell line to further understand the influence of these ECM proteins on isolated human donor islets. Isolated human islets are composed of multiple pancreatic endocrine cell types and have undergone harsh treatments during the isolation process. It has been shown that the use of NID1 during the isolation of human islets improves the yield, particularly in a hypoxic setting[148]. To determine whether these ECM proteins are potential candidates for co-transplantation with the islets to support their survival and function in the hypoxic post-transplantation setting until the patient's system can support the transplant, we cultured isolated human islets in normoxic and hypoxic conditions with the recombinantly-produced ECM proteins. We assessed their survival and β-cell functionality at the end of the culture period using GSIS assays and FLIM.

Through these studies we aim to highlight the importance of supporting islet transplantation at the various stages from acquiring sufficient β-cells, recapitulation of their native niche, to assessing their long-term functionality. We address the importance of temporal expression of β-cell markers in hiPSCs for their maturation and function, as well as the significant impact re-establishment of the native ECM has in maintaining cell survival and function in a post-transplantation setting.

Chapter 3

Results & Discussion

The content is based on:

Zbinden, A.[§], Carvajal, D.A.[§], Urbanczyk, M., Layland, S.L., Bosch, M., Fliri, S., Lu, C., **Jeyagaran, A.**, Loskill, P., Duffy, G.P., Schenke-Layland, K., Fluorescence Lifetime Metabolic Mapping of Hypoxia-induced Damage in Pancreatic Pseudo-islets, Journal of Biophotonics, 13(12), e202000375 (2020).

Urbanczyk, M.[§], **Jeyagaran, A.[§]**, Zbinden, A., Lu, C., Marzi, J., Kuhlburger, L., Nahnsen, S., Layland, S.L., Duffy, G.P., Schenke-Layland, K., Decorin Improves Pancreatic β-cell Function and Regulates Extracellular Matrix Expression in vitro, Matrix Biology, 115, 160-183 (2023).

Jeyagaran, A., Urbanczyk, M., Layland, S.L., Weise, F., Schenke-Layland, K., Forward programming of hiPSCs towards beta-like cells using Ngn3, Pdx1, and MafA, Scientific Reports, 14, 13608 (2024).

Jeyagaran, A.[§], Urbanczyk, M.[§], Carvajal-Berrio, D., Baldissera, T., Kaiser, P. D., Kuhlburger, L., Czemmel, S., Nahnsen, S., Duffy, G. P., Layland, S.L.[#], Schenke-Layland, K.[#], ECM Proteins Nidogen-1 and Decorin Restore Functionality of Human Islets of Langerhans upon Hypoxic Conditions, Advanced Healthcare Materials, 2403017 (2024).

[§] = authors contributed equally

[#] = authors contributed equally

3. Results & Discussion

3.1. Forward programming of hiPSCs towards a beta-like state to improve differentiation efficiency and timeline

Transplantation of stem cell-derived β-cells is a promising therapeutic advancement in the treatment of T1DM; however, it is limited by the differentiation period of around two months with low differentiation efficiencies resulting in a heterogeneous population of pancreatic endocrine cells. Differentiation timelines and efficiencies have been improved for other cell types using lentiviral overexpression systems. Overexpression of cell-specific markers in hPSCs, have allowed researchers to forward program and direct the differentiation towards the desired cell type such as hepatocytes[149], hematoendothelial cells[150], neurons[151–153], skeletal myocytes[153], oligodendrocytes[153], megakaryocytes[154], microglia[155], and endothelial cells[156,157], suggesting a similar method could also be used for β-cells.

Three transcription factors, NGN3, PDX1, and MAFA, were identified as key markers of β-cells required for β-cell maturation and functionality[77,78]. Exogenous expression of these three markers in rodent pancreatic exocrine tissues[79–81], hepatocytes[82–84], and murine α-cells[158,159] were sufficient for the transdifferentiation into β-cells capable of restoring normoglycemia in diabetic models. To determine whether the expression of NGN3, PDX1, and MAFA can also drive the differentiation of hiPSCs into β-cells, we designed and produced a lentiviral construct for the inducible expression of NGN3, PDX1, and MAFA, such that upon the addition of doxycycline (DOX) to the medium, the markers of interest would be expressed. The constructs also allowed for antibiotic selection of successfully transduced cells to further support a homogenous population (Jeyagaran *et al.*, **Appendix 1**, Figure 1a,b). Successfully transduced hiPSCs were selected for using the appropriate antibiotic and then assessed for stem cell markers. The transduced hiPSCs were assessed through RT-qPCR for *OCT4*, *SOX2*, *NANOG*, and *KLF4*, relative to the un-transduced hiPSCs. The un-transduced and transduced hiPSCs had similar expression levels of the naïve stem cell markers at the gene (Jeyagaran *et al.*, **Appendix 1**, Figure 1c) and protein

levels (Jeyagaran *et al.*, **Appendix 1**, Figure 1e). RT-qPCR analysis for the markers of interest also showed that there were no significant differences in expression levels between the un-transduced and transduced hiPSCs (Jeyagaran *et al.*, **Appendix 1**, Fig. 1d), suggesting there was no premature expression of the markers of interest in the transduced hiPSCs.

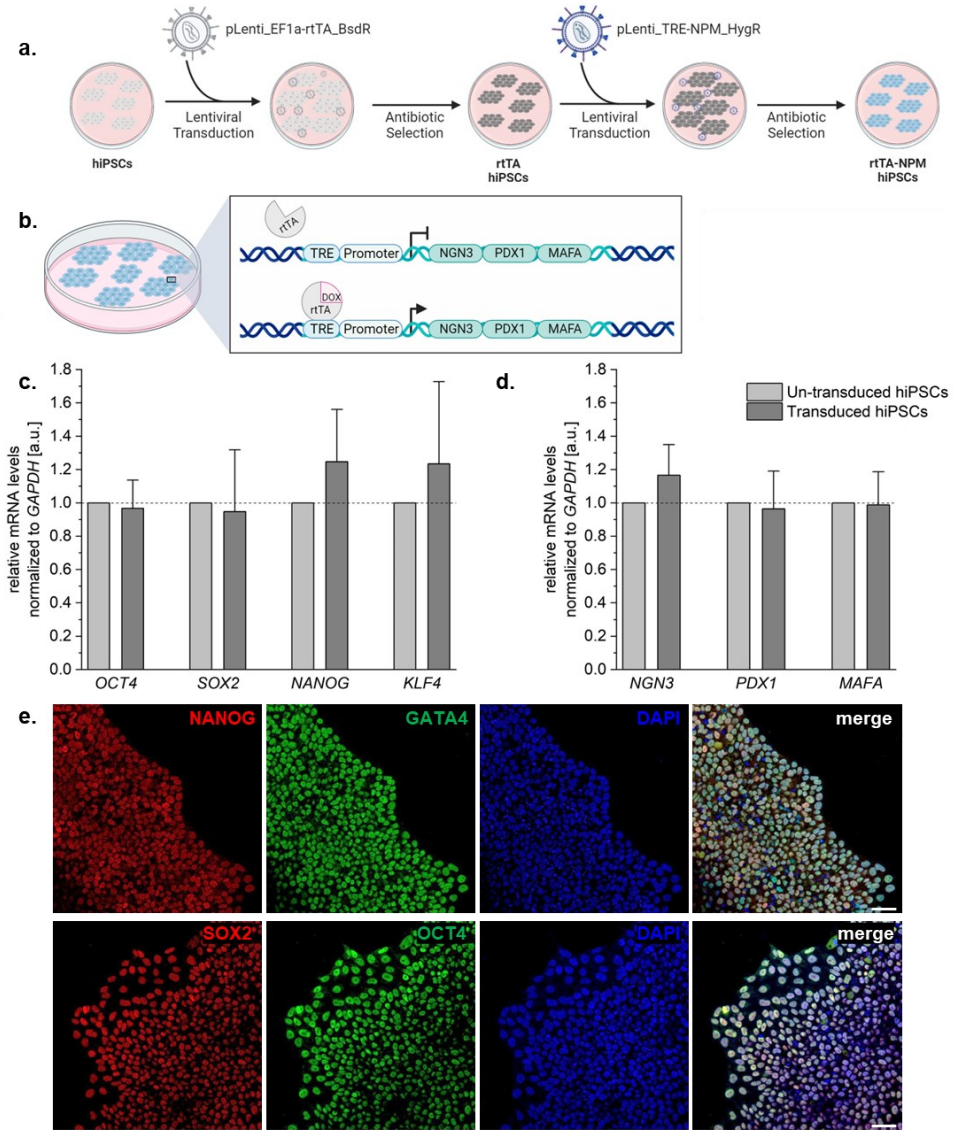

Figure 1: Introduction of inducible lentiviral construct into hiPSCs does not affect pluripotency marker expression. **a.** Schematic of how the rtTA-NPM hiPSCs were generated and **b.** induction of gene expression upon DOX treatment. Gene expression analysis for **c.** stem cell markers and **d.** markers of interest before DOX treatment relative to un-transduced hiPSCs (dashed line at 1), normalized to GAPDH levels. Error bars represent standard deviation. **e.** Immunofluorescence staining in transduced hiPSCs to confirm protein expression of the stem cell markers. Scale bar equals 50 µm. Schematics created with BioRender.com. Adapted from[160].

Transduced hiPSCs were cultured for five days in medium supporting pancreatic lineage specification with and without DOX to induce differentiation towards β-cells. Expectedly, the cells cultured with DOX had greater levels of the markers of interest compared to those cultured without DOX (Jeyagaran *et al.*, **Appendix 1**, Figure 2a). Interestingly, two other pancreatic lineage markers *NKX6.1* and *MAFB* were also upregulated upon five days of culture in the medium with and without DOX compared to day zero (Jeyagaran *et al.*, **Appendix 1**, Figure 2b). Furthermore, the cells cultured with DOX had significantly more expression of the proteins of interest in the nucleus compared to the cultures without DOX (Jeyagaran *et al.*, **Appendix 1**, Figure 2c-e); however, each marker was not expressed at the same level.

NGN3 and MAFA were observed in 88.4% (± 7.4%) and 98.9% (± 1.1%), respectively, of the cells cultured with DOX compared to 0.0% (± 0.0%) of the cells cultured without DOX. PDX1 was only observed in 29.8% (± 15.9%) of the cells cultured with DOX compared to 0.0% (± 0.0%) of the cells cultured without DOX. This could be attributed to varying numbers of the lentiviral construct in each cell or the position of PDX1 in the lentiviral construct. The positive selection of successfully transduced cells ensures that there is one copy, minimum, of the lentivirus is present in the cell, but not that it is equal in each cell[161] and could be addressed by adapting the design of the lentiviral construct to direct its integration into specific loci[153]. Also, it has been shown that in tri-cistronic constructs where three genes are in the same construct, there was greatest expression of the first gene, followed by the third gene, and the second gene had the weakest expression[162]. This is similar to our results where NGN3 and MAFA, the first and third genes in the construct, had the greatest expression levels and PDX1, the second gene in the construct, was poorly expressed. This could possibly be addressed by using separate lentiviral constructs for each marker of interest; however, this would also require multiple safe integration loci, and the risk of disrupting the genome with three lentiviral constructs could pose a problem in genetic integrity.

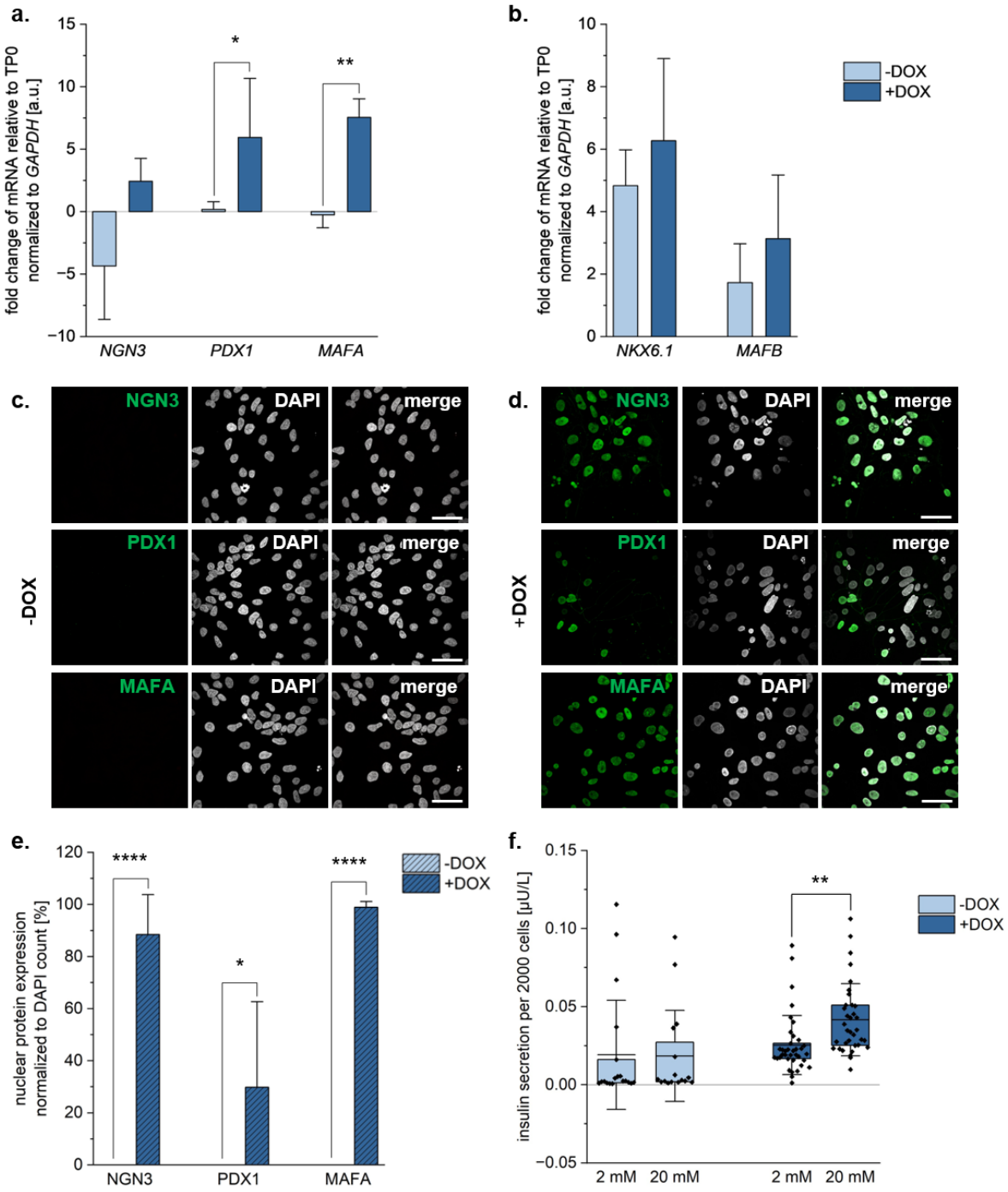

Figure 2: Markers of interest are upregulated after five days of monolayer culture with DOX. Gene expression analysis of **a.** markers of interest and **b.** pancreatic progenitor markers NKX6.1 and MAFB after five days of culture with and without DOX. Fold change relative to day zero (TP0) at the stem cell stage and normalized to GAPDH. Immunofluorescence staining for markers of interest in cells cultured for five days **c.** without and **d.** with DOX (scale bars equal 50 µm), and **e.** the quantification of the % nuclear protein expression of the markers of interest normalized to DAPI counts. **f.** Parallel GSIS results: amount of insulin secreted upon stimulation with 2 mM and 20 mM glucose normalized to cell count. Error bars represent standard deviation. Unpaired t-test, *p≤0.05, **p≤0.01, ****p≤0.0001. Adapted from[160].

Interestingly, when assessed for functionality using a parallel GSIS assay, the five-day cultures with DOX did show a functional β-cell response where they secreted significantly more insulin in response to increased glucose concentrations, unlike the cells cultured without DOX (Jeyagaran *et al.*, **Appendix 1**, Figure 2f). This suggests that the five-day DOX-treated cells already present similar functional characteristics to β-cells; however, the overall amount of insulin being secreted was extremely low. Human islets of Langerhans are found in clusters, and cell-cell contact has been shown to improve insulin secretion of β-cells[3], and so our five-day cultures were also aggregated into spheroids and cultured for another five days. The spheroids were then assessed for expression of the markers of interest and functionality. While all three genes had increased expression in the cells cultured for ten days with DOX compared to those without DOX (Jeyagaran *et al.*, **Appendix 1**, Figure 3a), at the protein level, only NGN3 and MAFA had significantly increased expression in the cells of spheroids cultured with DOX versus without DOX. Quantification of PDX1 expression demonstrated that it was completely lost at the end of the ten-day culture period with 0.0% (± 0.0%) of cells both with and without DOX (Jeyagaran *et al.*, **Appendix 1**, Figure 3b-d). As expected, the amount of insulin secreted was enhanced compared to the monolayer cultures. To determine whether the DOX-treatment supported glucose-responsive insulin secretion to multiple glucose challenges, a serial GSIS was performed. GSIS assays demonstrated that spheroids, both with and without DOX, secreted significantly more insulin in response to increased glucose concentrations (Jeyagaran *et al.*, **Appendix 1**, Figure 4a). Unfortunately, the DOX-treated cultures did not show functional responses to a serial GSIS (Jeyagaran *et al.*, **Appendix 1**, Figure 4b), and analysis of insulin production through C-peptide secretion revealed no significant differences in C-peptide secretion between the low and high glucose conditions (Jeyagaran *et al.*, **Appendix 1**, Figure 4c), suggesting that the cells are not necessarily producing insulin in response to the glucose, but are rather only secreting the insulin they already have. This also suggests that these cells are capable of glucose-responsive insulin secretion even if they are not yet producing it themselves.

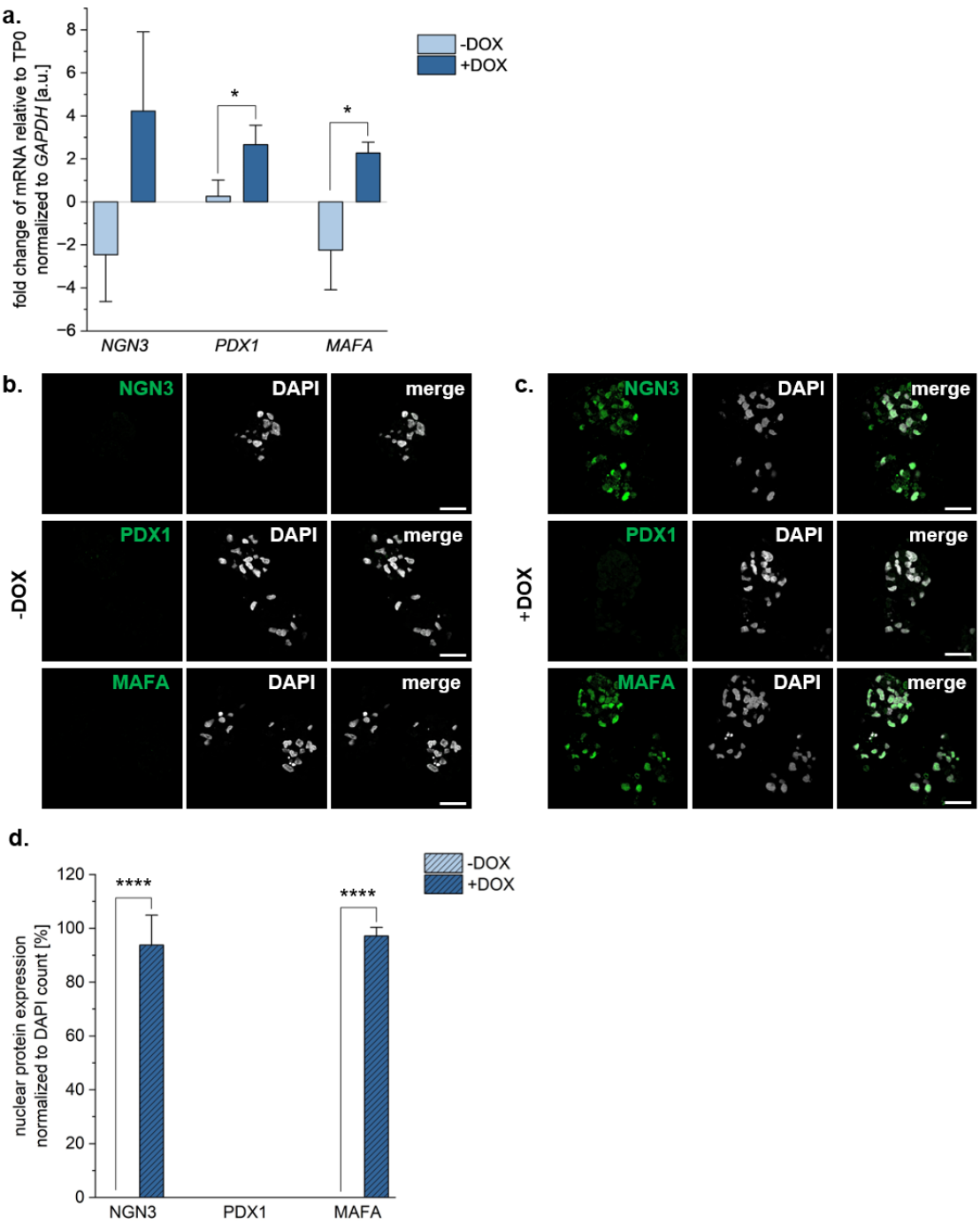

Figure 3: NGN3 and MAFA expression maintained upon ten days of 3D culture. a. Gene expression analysis of the markers of interest after ten days of culture with and without DOX. Fold change relative to day zero (TP0) at the stem cell stage and normalized to *GAPDH*. Immunofluorescence staining for markers of interest in cells cultured for ten days with the last five days as a 3D spheroid **b.** without and **c.** with DOX (scale bars equal 25 µm), and **d.** the quantification of the % nuclear protein expression of the markers of interest normalized to DAPI counts. Error bars represent standard deviation. Unpaired t-test, *p≤0.05, ****p≤0.0001. Adapted from[160].

The lack of PDX1 expression and minimal insulin production by these cells could be due to the cells' genetic background. The source of the cells reprogrammed into hiPSCs, in terms of organ origin and genetics, can influence and limit the differentiation potential of hiPSCs[56,163–165]. The hiPSC line used in our study was generated from fibroblasts[166] which are of the mesoderm lineage while the pancreas is of the endoderm lineage. As PDX1 is one of the earlier markers of pancreatic lineage specification, it may be targeted for degradation by the cell to avoid differentiating in that direction. The downregulation of PDX1 in our cells could be the result of the cell compensating for the forced expression patterns by the DOX treatment. Recently, another group successfully directed the differentiation of adult gut stem cells into glucose-responsive insulin-producing cells using similar lentiviral constructs for the same three markers of interest and similar culture conditions[167]. They adjusted the expression timing of the markers of interest where NGN3 was overexpressed for the first two days followed by continuous expression of PDX1 and MAFA for another two weeks. The differentiated cells produced levels of insulin similar to β-cells and were able to restore glucose homeostasis in diabetic mice for at least 100 days[167,168]. Gut stem cells are adult cells also of the endoderm lineage, and have been identified to also be hormone-secreting, including insulin in the fetus[169], posing the question whether such a cell source is required or changing the expression patterns of the three markers would have been sufficient for the successfully differentiation into β-cells. Tweaking the temporal expression of the three markers was found to be sufficient for the reprogramming of adult cells into glucose-responsive β-cells. Fontcuberta-PiSunyer, M., et al. (2023)[170] directly reprogrammed human fibroblasts into β-cells using a ten-day protocol similar to our approach. They used adenoviral constructs for the exogenous expression of NGN3, PDX1, and MAFA, followed by expression of PAX4 and NKX2.2 in the first week of culture as a monolayer. Following this, they aggregated the cells into spheroids for another week of culture to generate glucose-responsive insulin-producing cells. Huang, X., et al. (2023)[167] only induced expression of NGN3 for the first two days and then expressed PDX1 and MAFA, while Fontcuberta-PiSunyer, M., et al. (2023)[170] introduced adenoviral constructs for NGN3, PDX1, and MAFA together and separate constructs for PAX4 and NKX2.2 were introduced later in the culture, while we induced

the expression of NGN3, PDX1, and MAFA throughout the entire culture period. This suggested that the temporal expression of the markers of interest may be of more importance than the origin of the cells.

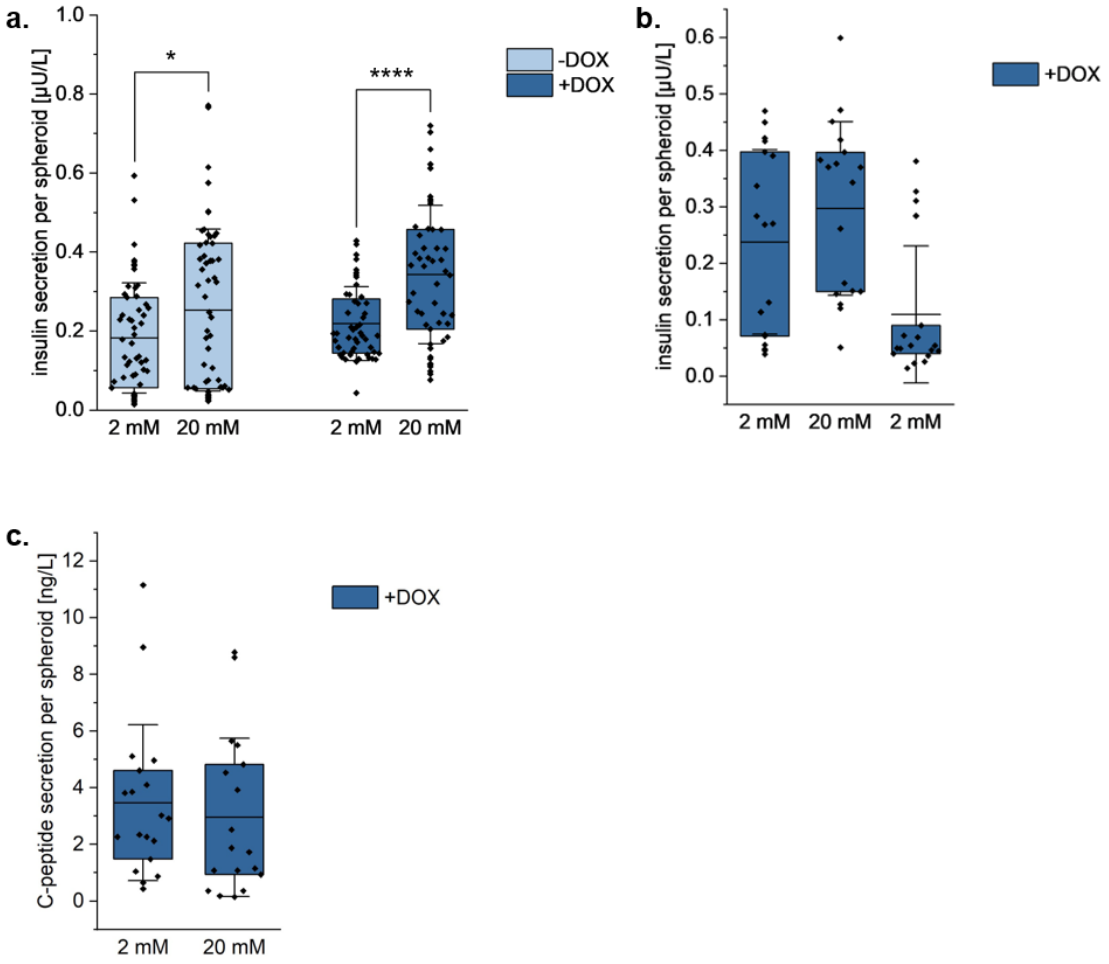

Figure 4: 3D spheroids show glucose-responsive insulin secretory behaviour. **a.** Parallel GSIS results: amount of insulin secreted by cells cultured with and without DOX upon stimulation with 2 mM and 20 mM glucose normalized to cell count. **b.** Serial GSIS results: amount of insulin secreted upon consecutive stimulation with 2 mM, 20 mM, and again 2 mM glucose normalized to cell count. **c.** Parallel GSIS results: amount of C-peptide secreted by cells cultured with DOX upon stimulation with 2 mM and 20 mM glucose normalized to cell count. Error bars represent standard deviation. Unpaired t-test, *p≤0.05, ****p≤0.0001. Adapted from[160].

Our ten-day spheroids cultured with DOX were positive for mature β-cell markers NGN3 and MAFA, and demonstrated glucose-responsive insulin secretion. To determine what stage in development these cells are representative of, we performed

immunofluorescence staining of human fetal tissues, human adult islets, and our spheroids cultured with and without DOX for pancreatic markers NKX6.1, PDX1, NGN3, MAFA, C-peptide, and insulin (Jeyagaran *et al.*, **Appendix 1**, Figure 5). The pancreatic cells of fetal tissues showed nuclear expression of NKX6.1 and PDX1 with limited C-peptide and insulin staining while the adult donor islets of Langerhans showed nuclear expression of NKX6.1 in the nucleus of cells that also showed cytoplasmic C-peptide expression. Unfortunately, the hiPSC-derived spheroids did not show any presence of NKX6.1 or C-peptide. Interestingly, in adult donor islets, PDX1 was observed to be both nuclear and cytoplasmic with some co-localization with insulin. In our DOX-treated hiPSC-derived spheroids, PDX1 was found to have puncta-like expression within the cytoplasm whereas this is absent in the spheroids without DOX. The fetal pancreatic tissues did not have any cells expressing NGN3 or MAFA. The adult donor islets showed both nuclear and cytoplasmic expression of NGN3 while it was only in the nucleus of the cells of the hiPSC-derived spheroids with DOX and absent in the spheroids cultured without DOX. MAFA was found in the nucleus of cells of the adult donor islets and all the cells of the hiPSC-derived spheroids with DOX, while it was absent in the hiPSC-derived spheroids without DOX. These results suggested that the hiPSC-derived spheroids cultured with DOX showed similar marker expression to that of adult donor pancreatic islets of Langerhans while being functionally similar to fetal tissues with its limited C-peptide presence. Further investigation into extending the culture conditions to support the functional maturity of these cells and incorporation of the temporal expression of the three markers of interest in hiPSCs has great potential in improving the availability of hiPSC-derived β-cells for therapeutic purposes.

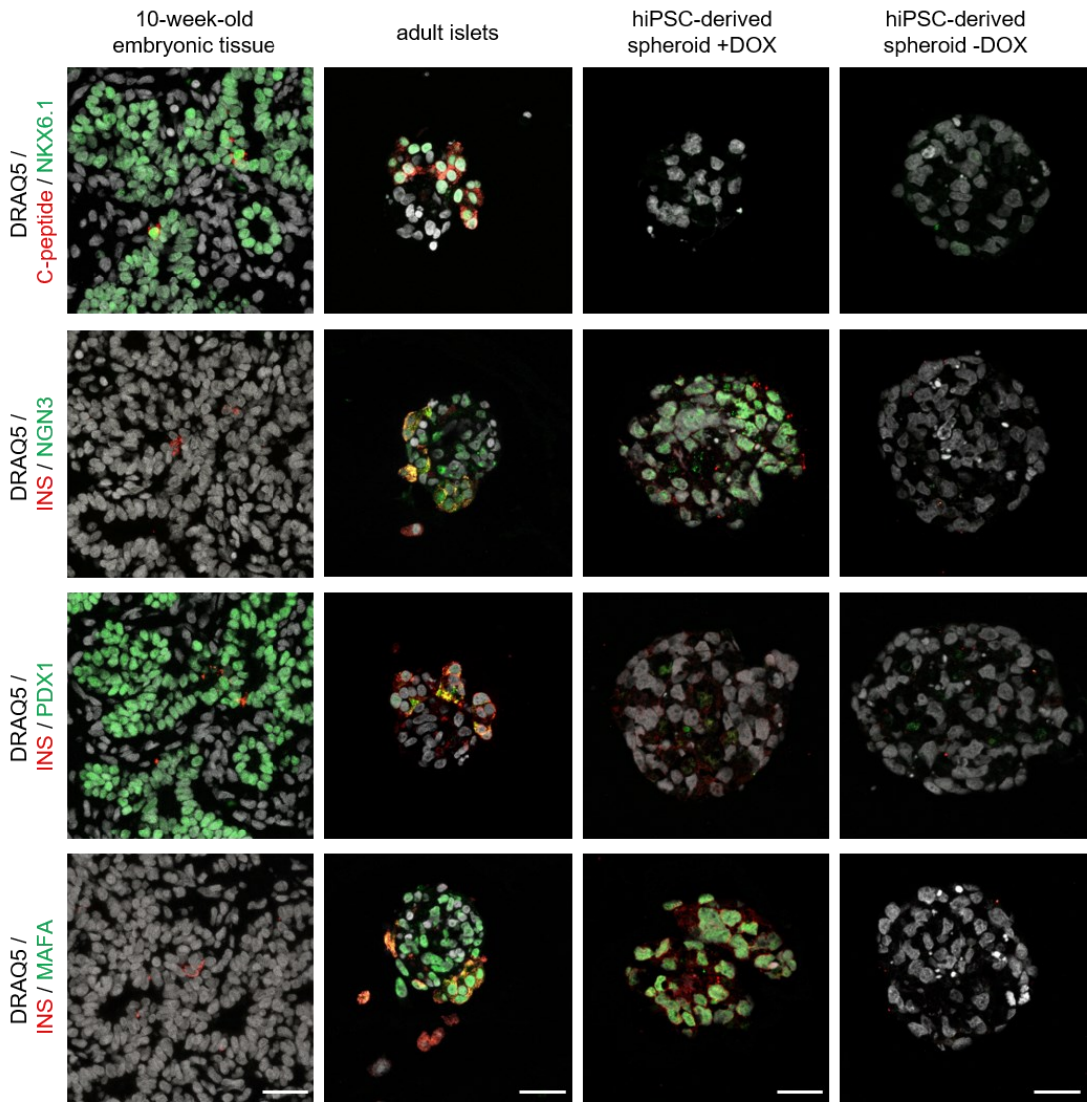

Figure 5: hiPSC-derived spheroids cultured with DOX present similar markers to adult donor islets but are functionally similar to embryonic tissue. 10-week-old embryo tissues, adult donor islets, and the hiPSC-derived spheroids cultured with and without DOX were assessed for protein expression of the markers of interest, NKX6.1, and the functionality markers C-peptide and insulin. Scale bars equal 25 µm. Adapted from[160].

3.2. Use of ECM protein decorin to improve human pancreatic β-cell function

Islet transplantation outcomes can be improved by supporting islet and/or β-cell survival post-transplantation. A large number of transplanted islets are lost as a result of poor oxygen and nutrient levels as revascularization of the transplant can take up to two weeks[171]. It was demonstrated that supplementation of ECM proteins can support islet survival and functionality[172–174], also in a post-transplantation setting[175];

however, this must be tightly regulated to ensure that the exogenously introduced ECM proteins such as COL1[90,176–182] or FN[90,110,115,180,181,183–186] do not drive pathogenesis. A potential risk is the formation of a fibrotic capsule as a result of the foreign body response where there is excessive deposition of COL1, COL3, and/or FN limiting the integration of the transplant into the patient's system, and therefore, its functionality and longevity[187–189]. This requires further investigation of methods to modulate the deposition of the ECM proteins and their network formation.

Investigation of BM and interstitial matrix proteins in human adult pancreatic tissues using immunofluorescence staining identified the small, leucine-rich proteoglycan DCN to be highly co-localized with the endocrine cells, particularly insulin (Urbanczyk & Jeyagaran *et al.*, **Appendix 2**, Figure 6a-f). Interestingly, a detailed observation of DCN and the different endocrine cells of human donor islets of Langerhans showed that DCN was significantly more co-localized with the insulin-producing β-cells rather than the glucagon-producing α-cells (Urbanczyk & Jeyagaran *et al.*, **Appendix 2**, Figure 6g-i). These results show that DCN is found in the native pancreatic endocrine environment, and as a known modulator of the ECM due to its regulation of collagen fibrillogenesis, it could be beneficial for reducing formation of the fibrotic capsule[147]. We hypothesized that DCN could be a candidate for co-transplantation with β-cells to support transplant survival and function. Using the immortalized human β-cell line, EndoC-βH3, aggregated into pseudo-islet structures, we determined whether DCN has a supportive role in β-cell function. We supplemented the pseudo-islets with recombinantly produced full-length human DCN[190] over a 72-hour culture period and then assessed their functionality and ECM expression. Immunofluorescence staining of DCN on the pseudo-islets in control and DCN-treated samples showed that the supplemented DCN attaches to the peripheral cells of the pseudo-islets (Urbanczyk & Jeyagaran *et al.*, **Appendix 2**, Figure 7a), and that this interaction is visible from 24 hours post-treatment (Urbanczyk & Jeyagaran *et al.*, **Appendix 2**, Figure 7b) as this is when there is significant increase in DCN presence on the treated pseudo-islets. Interestingly, serial GSIS assays demonstrated that β-cell functionality was improved upon DCN supplementation with significantly more insulin secreted at the increased glucose challenge compared to

the control (Urbanczyk & Jeyagaran *et al.*, **Appendix 2**, Figure 7c), which was also translated into a significantly greater GSIS index in the DCN-treated samples versus the control (Urbanczyk & Jeyagaran *et al.*, **Appendix 2**, Figure 7d). We were also interested in the known effect of DCN on fibrillogenesis and used IF staining to determine whether DCN had any effect on the fibrillar proteins FN and COL1. Interestingly, DCN-treatment significantly reduced the expression of FN (Urbanczyk & Jeyagaran *et al.*, **Appendix 2**, Figure 7e) and COL1 (Urbanczyk & Jeyagaran *et al.*, **Appendix 2**, Figure 7f) compared to the control in our pseudo-islet model.

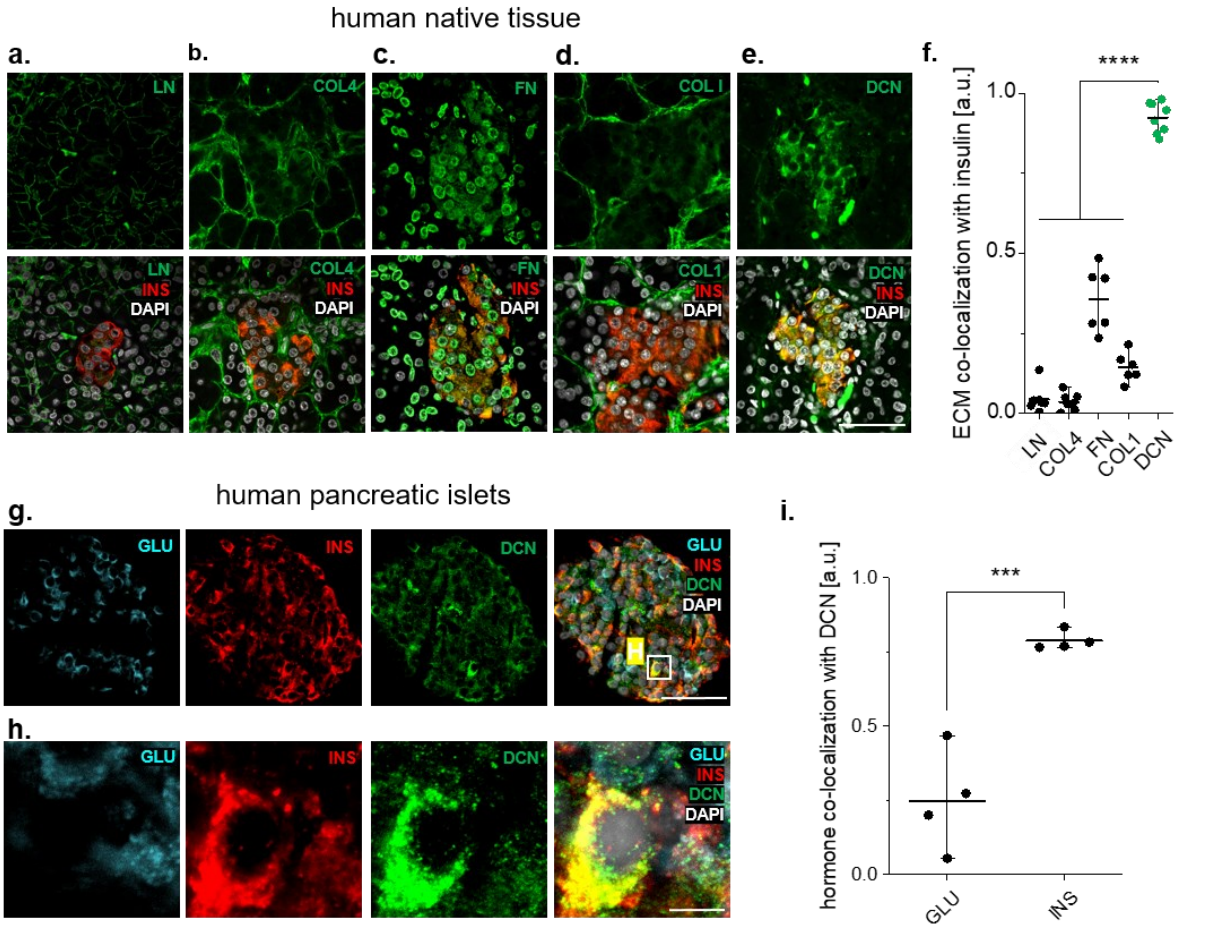

Figure 6: Decorin strongly co-localizes with insulin-producing β-cells in vivo and stimulates β-cells functionality in vitro. Expression patterns of **a.** LN, **b.** COL4, **c.** FN, **d.** COL1, and **e.** DCN in native pancreatic tissue. **f. C**o-localization study shows strong correlation between DCN and insulin-expressing β-cells in islets of Langerhans. One-way ANOVA, ****p≤0.0001. **g-h.** Expression patterns of glucagon (GLU), insulin (INS) and DCN in isolated human pancreatic islets. **i.** Co-localization study shows significantly higher correlation of DCN with insulin compared to glucagon. Unpaired t-test, ***p≤0.001. Scale bars equal 50 µm (**a-e, g**) and 5 µm (ROI **h**). Error bars represent standard deviation. Adapted from[191].

Previous studies also identified DCN in pancreatic tissues, with increased expression by pancreatic pericytes to further establish the islet BM[192]. It has been reported that DCN plays a role in glucose tolerance. Interestingly, DCN was found to be downregulated in the insulinoma mouse model where there was dysregulated production of insulin[193], and mice lacking DCN displayed poor glucose tolerance, lack of ECM organization, and increased inflammatory markers[194]. While the role of DCN in β-cell function is not well-known, these studies suggested that it does have an important effect in glucose-sensing and insulin secretion. Our results showed that DCN has a stimulatory effect on β-cell function upon high glucose challenges in our pseudo-islet model. Furthermore, our results where DCN-treatment downregulated expression of fibrotic proteins FN and COL1 is in line with previous work highlighting the positive role of DCN has in reducing scar tissue and inflammation[195–197]. These results support our hypothesis that DCN could support β-cells post-transplantation through stimulating β-cell function and reducing fibrotic capsule formation. We used next-generation sequencing (NGS) and Raman microspectroscopy to understand the changes occurring in the β-cells upon DCN-treatment. NGS identified 348 genes differentially expressed between the DCN-treated and control pseudo-islets; 84 of which were involved in pathways specified by the Kyoto Encyclopedia of Genes and Genomes (KEGG; Urbanczyk & Jeyagaran *et al.*, **Appendix 2**, Figure 8a). 51 of these genes were mapped to pathways related to β-cells (Urbanczyk & Jeyagaran *et al.*, **Appendix 2**, Figure 8b), but of great interest were those involved in glucose metabolism and insulin secretion. DCN-treatment resulted in the increased expression of genes involved in oxidative phosphorylation, particularly of the electron transport chain (Figure 8c,d), and endoplasmic reticulum (ER; Urbanczyk & Jeyagaran *et al.*, **Appendix 2**, Figure 8e,f). Oxidative phosphorylation is the final process of cellular respiration for the production of ATP[198], suggesting increased mitochondrial activity. This process is essential in β-cells to effectively metabolize the glucose and secrete appropriate levels of insulin[199,200]. Interestingly, purified mitochondria from glucose-responsive β-cells displayed significantly greater electron transport chain function than those from glucose-unresponsive β-cells[201]. Further, reduced oxidative phosphorylation and mitochondrial DNA was associated with T2DM[202]. These studies

support our results where DCN-treatment of the pseudo-islets could improve glucose-responsiveness through increased activation of oxidative phosphorylation pathways. The ER is responsible for the regulation of protein folding and transport to the correct cellular compartment[203]. Our NGS results identified an upregulation of genes involved in ER stress responses and vesicular trafficking.

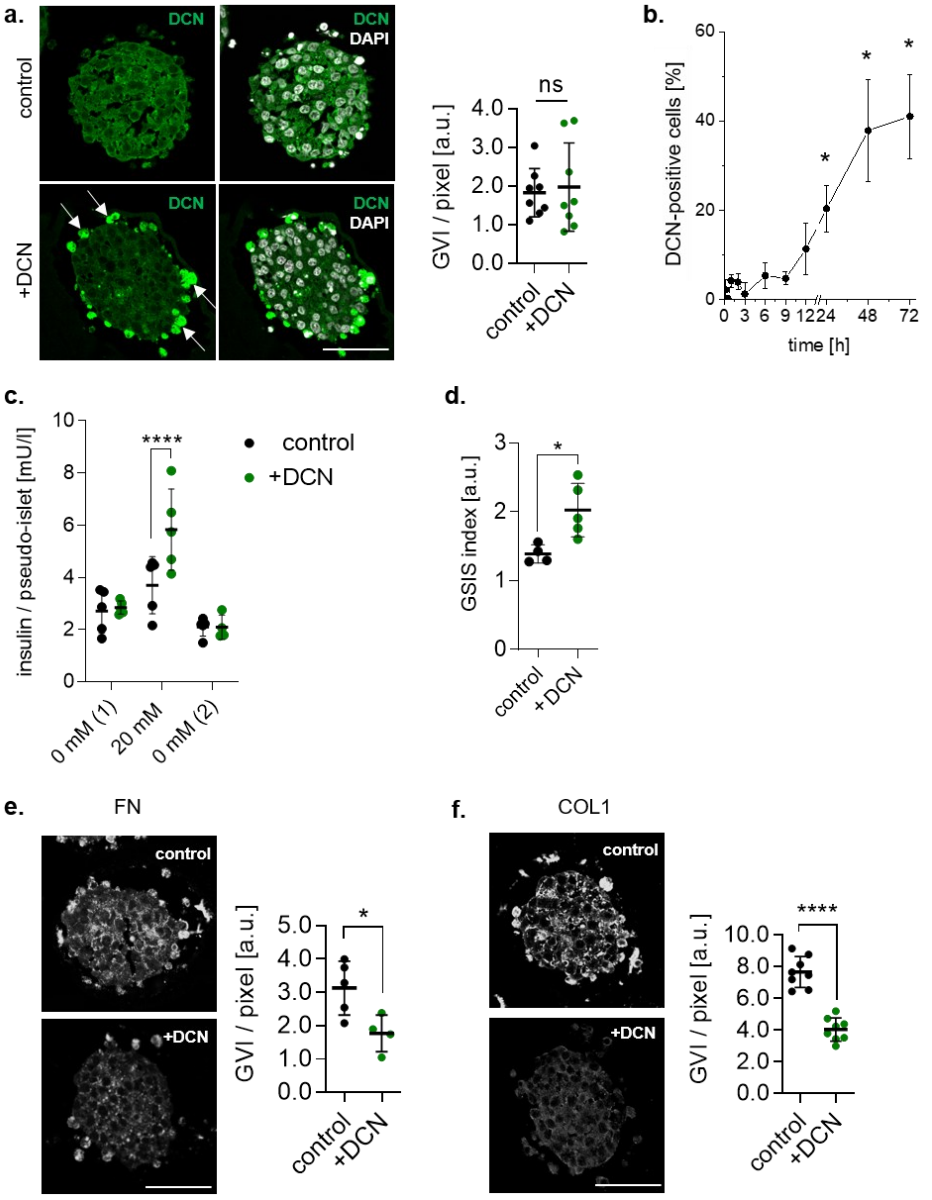

Figure 7: Decorin stimulates pseudo-islet functionality in suspension cultures and modulates ECM expression. **a.** Peripheral expression of DCN in the DCN-supplemented pseudo-islets (white arrows). Unpaired t-test. **b.** Time lapse of DCN-positive cells on the periphery of the pseudo-islets. One-way ANOVA, *p≤0.05. **c.** GSIS results and **d.** index of pseudo-islets treated with and without DCN. One-way ANOVA, ****p≤0.0001. Unpaired t-test, *p≤0.05. Immunofluorescence staining quantification of **e.** FN and **f.** COL1 upon DCN supplementation. Unpaired t-test, *p≤0.05, ****p≤0.0001. Scale bars equal 50 µm. Error bars represent standard deviation. Adapted from[191].

ER stress responses are observed in β-cells, particularly during glucose challenges, due to insulin production and secretory mechanisms[203–206]. Furthermore, it has been suggested that around 20% of proinsulin, the pre-cursor of insulin, is misfolded and degraded[207–209], which would also increase ER stress[210]. The greater expression of genes involved in vesicular trafficking observed in the DCN-treated samples could be explained by the increase in number of vesicles required for the increased insulin secretion at the high glucose conditions compared to the control samples. Interestingly, Raman microspectroscopy also identified the ER to be significantly different between the DCN-treated and control pseudo-islets (Figure 9a-d). In particular, Raman microspectroscopy identified differences in phosphatidylinositol (Urbanczyk & Jeyagaran *et al.*, **Appendix 2**, Figure 9e) which is also required for vesicle formation[211–213], and in line with previous studies that also observed greater phosphatidylinositol content in β-cells challenged with high glucose[214,215]. The NGS and Raman microspectroscopy results suggested that the increased β-cell functionality observed in the DCN-treated pseudo-islets could be attributed to increased mitochondrial activity for ATP, and increased ER activity for insulin production and secretion using vesicular transport. We further investigated the NGS data and literature for possible binding partners of DCN on β-cells and identified low density lipoprotein receptor-related protein 1 (LRP1). We found LRP1 to be significantly downregulated in the DCN-treated pseudo-islets at the gene (Urbanczyk & Jeyagaran *et al.*, **Appendix 2**, Figure 10a) and protein (Urbanczyk & Jeyagaran *et al.*, **Appendix 2**, Figure 10b,c) levels**.** LRP1 is an endocytic receptor found on many different cell types[216] that can bind ECM proteins[217,218] and growth factors[218], activating various pathways for cell homeostasis. In rodent islets, LRP1 was necessary for insulin secretion and lipid metabolism[219]. In addition, LRP1 has been shown to activate downstream TGF-β signalling cascades[220], which in turn can stimulate insulin secretion and survival of β-cells[221,222]. As an endocytic receptor, LRP1 is also involved in autophagic pathways suggesting that DCN-binding can induce internalization and downregulation of the receptor as shown by our results. Together, these results suggest that the increased insulin secretion observed in the

DCN-treated pseudo-islets during the glucose challenges could be potentially mediated through LRP1.

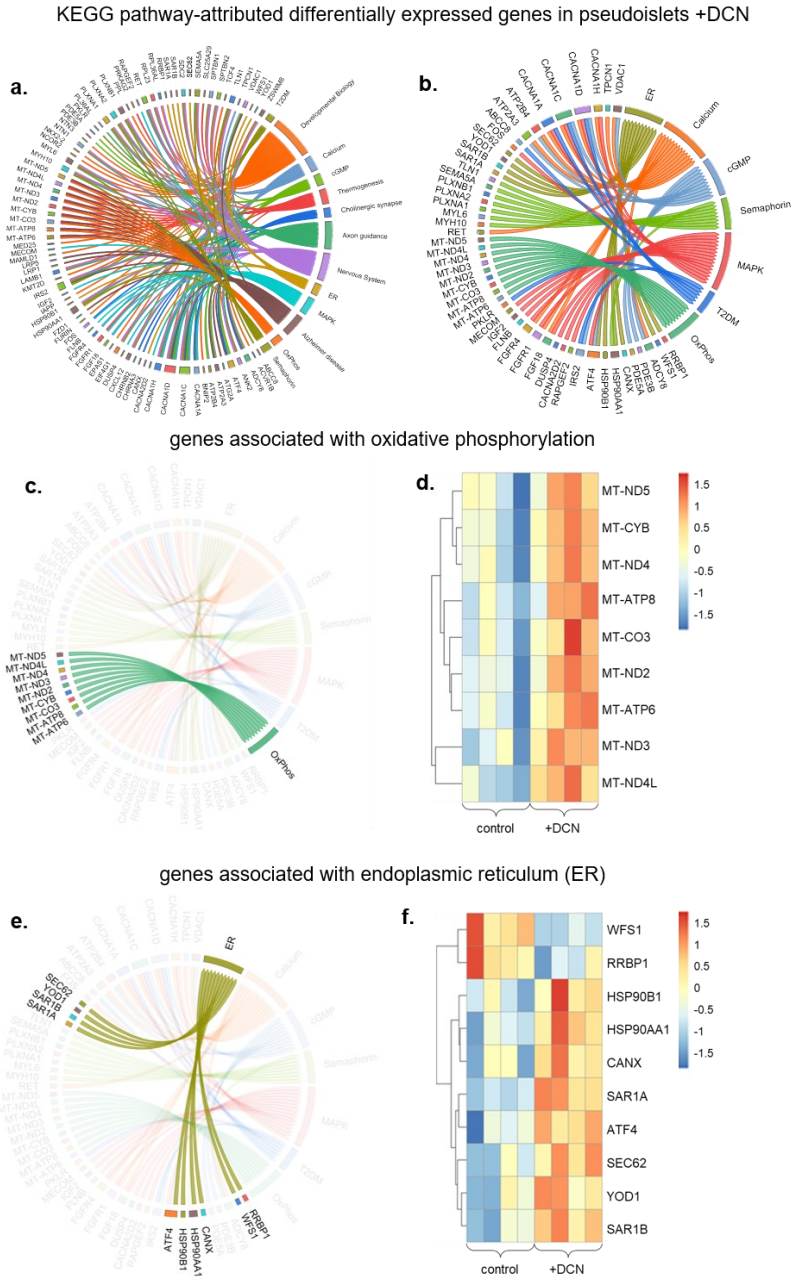

Figure 8: NGS identifies differentially expressed genes in pseudo-islets +DCN. RNA was harvested during high-glucose treatment of pseudo-islets to identify genes affected by DCN treatment during insulin secretion (n = 4). **a.** 84 differentially expressed genes have been matched to specific pathways using the KEGG database after DCN treatment. **b.** 51 of these 84 genes are β-cell related genes, which are involved in 7 different pathways and mechanisms. **c.** 9 genes related to oxidative phosphorylation were differentially expressed. **d.** All of these 9 genes were upregulated after DCN-treatment. **e.** 10 genes related to the endoplasmic reticulum were differentially expressed in DCN-treated β-cell pseudo-islets. **f.** 8 of these 10 genes were upregulated after DCN treatment. Genes were classified as differentially expressed with $p_{adjusted} \leq 0.05$. Adapted from[191].

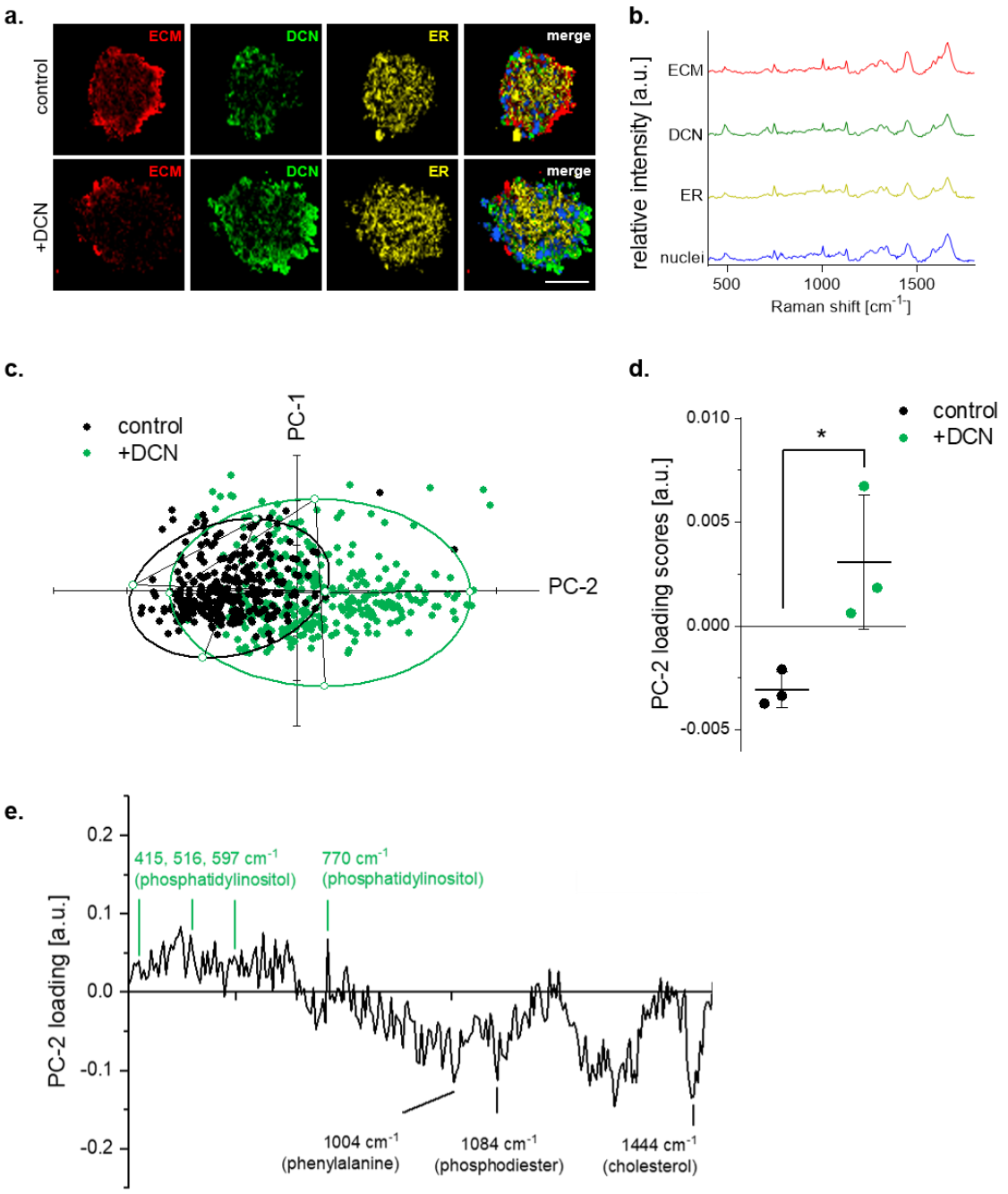

Figure 9: Raman imaging of live pseudo-islets. **a.** Application of Raman spectra for ECM, DCN and ER on live pseudo-islets +DCN and control. Scale bar equals 50 µm. **b.** Corresponding Raman spectra of ECM, DCN, ER and nuclei. **c.** PCA of the obtained ER component shows a separation via PC-2 between control pseudo-islets and pseudo-islets +DCN. **d.** Comparing the PC-2 loading scores of 100 spectra shows a significant difference between control and pseudo-islets +DCN. Unpaired t-test, *p≤0.05. **e.** Loading of PC-2 indicates an increase expression of phosphatidylinositol in pseudo-islets +DCN compared to control. Error bars represent standard deviation. Adapted from[191].

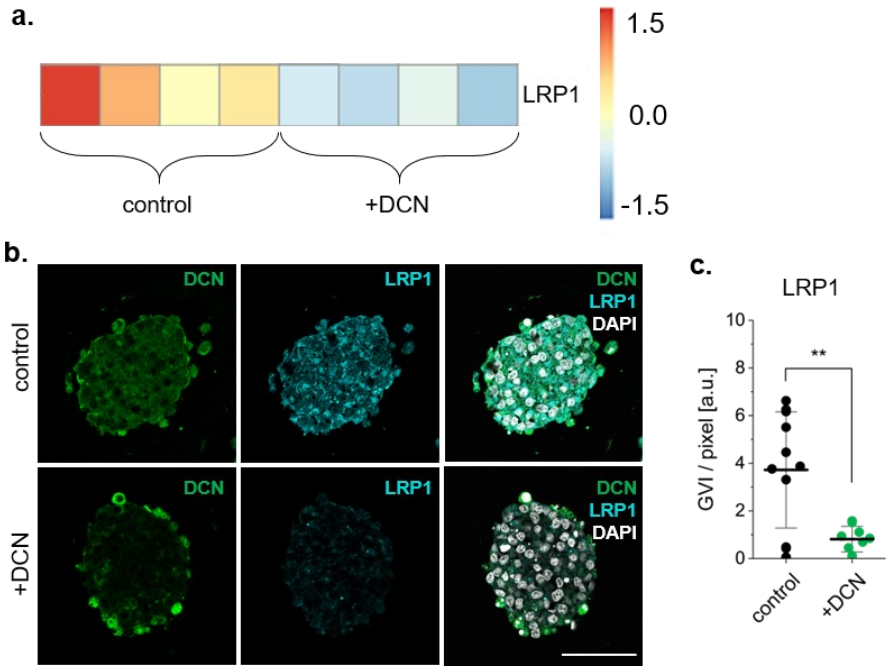

Figure 10: DCN-treatment significantly downregulates LRP1 expression in β-cell-composed pseudo-islets. **a.** NGS identifies RNA levels of LRP1 to be significantly downregulated after DCN-treatment. **b.** Immunofluorescence staining of control and DCN-treated pseudo-islets for DCN and LRP1. **c.** Quantification showed a significant decrease in LRP1 intensity in DCN-treated pseudo-islets. Unpaired t-test, **p≤0.01. Scale bar equals 50 µm. Error bars represent standard deviation. Adapted from[191].

3.3. Fluorescence lifetime imaging microscopy to assess the dynamics of β-cell metabolism

Islet functionality assessments are important to ensure transplanted islets are glucose-responsive and capable of withstanding multiple glucose challenges. Currently used techniques such as GSIS assays often require lysing of the tested β-cell for the insulin content, and the cells serves as a representative of the remainder of β-cells from the donor/differentiation protocol. This results in the reduction of transplantable β-cells available and does not provide information on the metabolic dynamics of the cells. Understanding of the metabolic equilibrium, particularly, in stem cell-derived β-cells, is important to determine the functional maturity of the cells and if they have the appropriate metabolic machinery to respond to multiple glucose challenges. FLIM allows for the imaging and quantifying of the metabolic shifts between glycolysis and oxidative phosphorylation non-invasively through the

autofluorescence of NADH and FAD. We hypothesized that FLIM can be used for the non-invasive and real-time imaging of the dynamic metabolic processes as β-cells respond to glucose stimulation and to changes in their environment conditions.

Using our pseudo-islet model from the immortalized human β-cell line, EndoC-βH3, we assessed the real-time metabolic changes in β-cells upon glucose stimulation through FLIM. β-cells were exposed to prolonged starvation periods at 0 mM glucose conditions (non-stimulated), or exposed to 0 mM glucose and then glucose-stimulated with 20 mM glucose. FLIM measurements were performed every 27 min to observe the changes in metabolic machinery in the β-cells. In the non-stimulated pseudo-islets, NADH τ1, the unbound form of NADH produced during glycolysis, increased over the first hour following which it began oscillating (Zbinden & Carvajal Berrio *et al.*, **Appendix 3**, Figure 11a), while NADH τ2, the bound form of NADH found at the electron transport chain during oxidative phosphorylation, steadily decreased (Zbinden & Carvajal Berrio *et al.*, **Appendix 3,** Figure 11c). Interestingly, in the glucose-stimulated pseudo-islets NADH τ1 decreased and began oscillating upon stimulation (Zbinden & Carvajal Berrio *et al.*, **Appendix 3**, Figure 11b), while NADH τ2 showed increases and peaks (Zbinden & Carvajal Berrio *et al.*, **Appendix 3**, Figure 11d). NADH α1 represents the respective contribution of NADH τ1, which increased over time in the non-stimulated pseudo-islets (Zbinden & Carvajal Berrio *et al.*, **Appendix 3**, Figure 11e) while it increased and oscillated upon glucose-stimulation (Zbinden & Carvajal Berrio *et al.*, **Appendix 3**, Figure 11f,i). Of particular importance is the optical oxidative ratio which represents the metabolic equilibrium between glycolysis and oxidative phosphorylation. The non-stimulated pseudo-islets demonstrated an increasing optical oxidative ratio over time (Zbinden & Carvajal Berrio *et al.*, **Appendix 3**, Figure 11g) while the glucose-stimulated pseudo-islets' ratio decreased upon glucose stimulation (Zbinden & Carvajal Berrio *et al.*, **Appendix 3**, Figure 11h). Upon glucose stimulation, glucose enters β-cells through GLUTs following which it enters glycolysis and oxidative phosphorylation pathways to produce ATP. This results in the closing of K^{+}-ATP channels and an influx of calcium ions. The oscillations in the intracellular calcium allows for the exocytosis of insulin[14,223]. The increasing NADH α1 or optical oxidative ratios in the non-stimulated pseudo-islets is

not expected as there is no increased stimulation through glucose, though this could be attributed to the cells using alternative energy-producing pathways such as glutaminolysis or fatty acid biosynthesis[224,225]. The reduction in the optical oxidative ratio observed upon glucose stimulation demonstrated that glucose stimulation initially increases glycolytic activity, and the oscillating NADH α1 suggest the β-cells are capable of sensing and responding to the increased glucose conditions

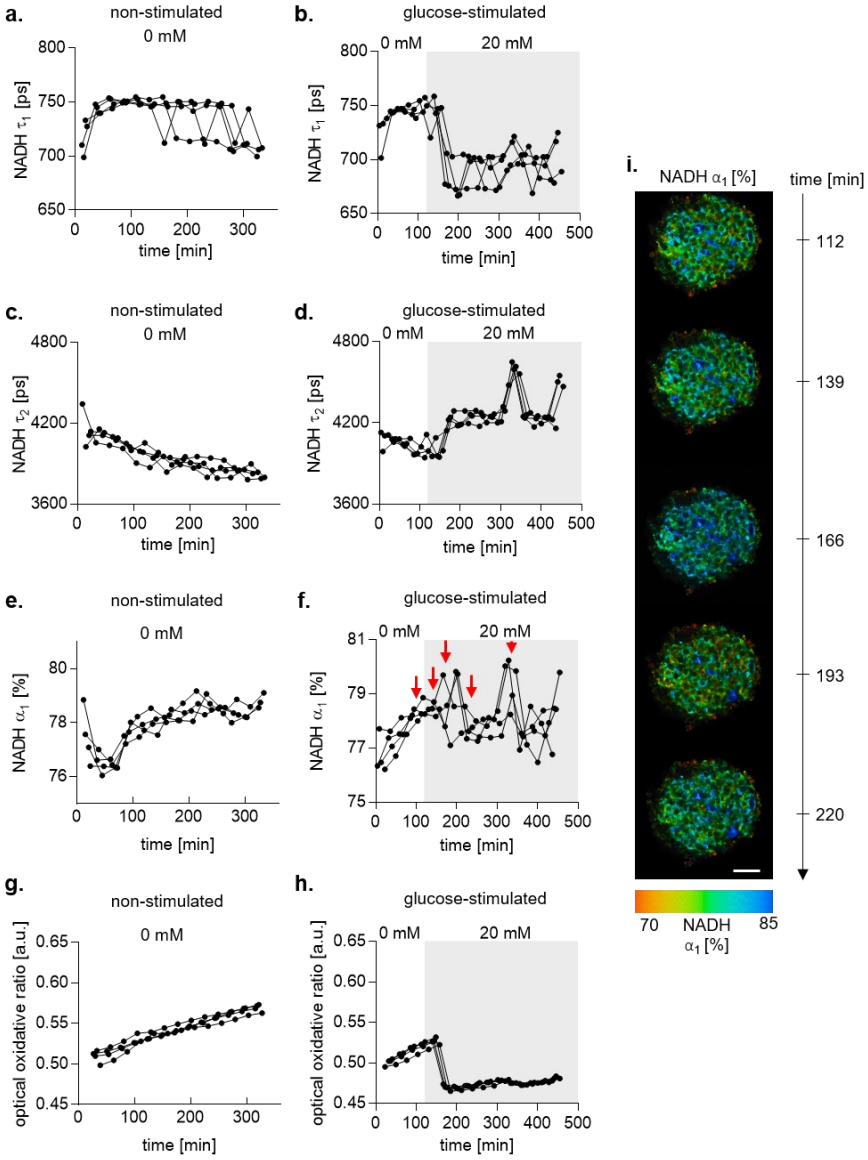

Figure 11: **In situ FLIM probes glucose-responsiveness of normoxic pseudo-islets in vitro.** FLIM analysis over time of non-stimulated pseudo-islets and glucose stimulation with 20 mM shows, **a-b.** NADH τ1, **c-d.** NADH τ2, **e-f.** NADH α1, and **g-h.** the optical oxidative ratio based on endogenous fluorescence of FAD/(FAD + NADH). **i.** Representative images of NADH α1 over time during glucose stimulation. Corresponding time points are shown with red arrows in **f.** Scale bar equals 50 µm. Adapted from[226].

3.3.1. Use of FLIM to identify hypoxia-induced cellular response in pseudo-islets

β-cell dysfunction as a result of hypoxic conditions during islet isolation and post-transplantation is a major limitation of transplant success[227]. To determine whether FLIM can also detect changes in β-cell metabolism in response to changes in oxygen levels, we cultured pseudo-islets in 1% oxygen and assessed them for hypoxia markers through immunofluorescence staining and metabolic changes through FLIM over time. Hypoxia-inducible factor 1α (HIF-1α) is expressed upon reduced oxygen concentrations to activate mechanisms to maintain oxygen homeostasis[228]. Accordingly, the pseudo-islets showed significantly increased HIF-1α expression after just an hour of hypoxic culture which continued to increase throughout the culture period (Zbinden & Carvajal Berrio *et al.*, **Appendix 3**, Figure 12a). HIF-1α expression can activate both cell repair and apoptotic pathways depending on the severity of hypoxia[229]. To determine whether an adaptive repair process or apoptotic pathway was activated we analysed the expression levels of VEGF which would be upregulated to increase blood vessel density for increased oxygen transport[228,230,231], and apoptotic marker cleaved caspase-3[232]. VEGF expression increased significantly over the first hour of hypoxic culture which then continually decreased over time (Zbinden & Carvajal Berrio *et al.*, **Appendix 3**, Figure 12b). Cleaved caspase-3 increased over the first 12 hours of hypoxia and remained significantly elevated through the culture period (Zbinden & Carvajal Berrio *et al.*, **Appendix 3**, Figure 12c), suggesting increased cell death upon extended periods of hypoxia. These results suggested that the pseudo-islets do sense the hypoxic environment and initially attempt to promote angiogenesis to overcome the low oxygen levels; however, upon extended periods of hypoxia, the cells initiate programmed cell death pathways. This was also demonstrated by multiphoton microscopy of endogenous NADH where the lack of NADH autofluorescence intensity in the core demonstrated a significantly larger ratio of lumen size upon 12 hours of hypoxia compared to the normoxic pseudo-islets (Zbinden & Carvajal Berrio *et al.*, **Appendix 3**, Figure 12d), indicative of a necrotic core.

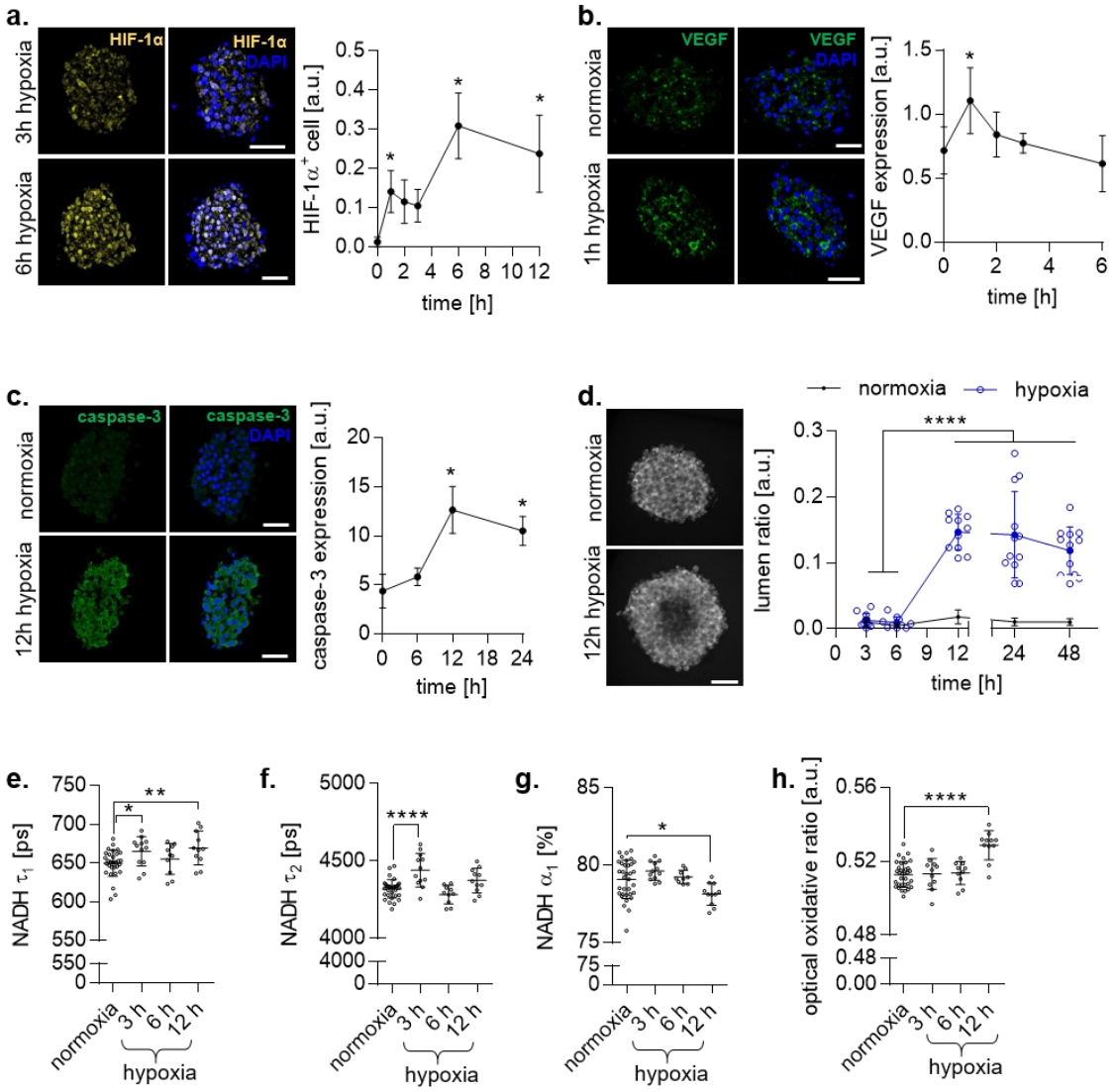

Figure 12: Hypoxia-induced cellular response in human pseudo-islets is detectable with FLIM. Immunofluorescence staining of **a.** HIF-1α, **b.** VEGF, and **c.** cleaved caspase-3 in pseudo-islets upon hypoxia and the corresponding quantifications. **d.** Multiphoton imaging and quantification of the lumen size of normoxic and hypoxic pseud-oislets over 12 hours. Time lapse FLIM analysis of hypoxic pseudo-islets showing **e.** NADH τ1, **f.** NADH τ2, **g.** NADH α1, and **h.** the optical oxidative ratio based on endogenous fluorescence of FAD/(FAD + NADH). Scale bars equal 50 µm. Error bars represent standard deviation. One-way ANOVA, *p≤0.05, **p≤0.01, ****p≤0.0001. Adapted from[226].

We used FLIM to observe changes in the cells' metabolism as they experience hypoxia and activate the adaptive and apoptotic pathways over 12 hours of hypoxic culture. There was a significant increase in NADH τ1 and τ2 in the first three hours of hypoxic culture (Zbinden & Carvajal Berrio *et al.*, **Appendix 3**, Figure 12e,f). The increase in the lifetime of the bound NADH indicates a change in the bound protein

and/or enzyme. As cells respond to the hypoxic environment, they are expected to increase their glycolytic activity compared to oxidative phosphorylation[233] and switch to anaerobic glycolysis which results in the production of lactate[234]. Lactate and pyruvate products from glycolysis both allow for the production of mitochondrial energy for the redox reactions of NADH[235] which could also attribute for the maintenance of the unbound NADH levels during the initial hypoxic culture period (Zbinden & Carvajal Berrio *et al.*, **Appendix 3**, Figure 12g). There was a significant decrease in NADH α1 and the optical oxidative ratio after 12 hours of hypoxia compared to the pseudo-islets cultured in normoxia (Zbinden & Carvajal Berrio *et al.*, **Appendix 3**, Figure 12g,h). The reduction in unbound NADH upon prolonged hypoxia culture suggests that the cells are undergoing apoptosis. This is in line with previous studies observing the metabolic changes in murine keratinocytes and cancer cells as they undergo apoptosis that demonstrated increased NADH τ2 and decreased NADH α1 upon initiation of apoptosis[236–239]. Furthermore, as cells undergo apoptosis, the mitochondrial membrane becomes permeabilized which can result in increased FAD in the cytosol which is reflected in the increased optical oxidative ratio[236,240–242]. Together these data demonstrated that FLIM can measure effects of hypoxic culture conditions in β-cells, and that NADH τ1 and τ2 can indicate hypoxia-induced apoptosis before the programmed cell death pathways are activated.

We further wanted to study the metabolic changes in pseudo-islets that have been cultured in hypoxia for 6 hours upon glucose stimulation. Control pseudo-islets cultured in normoxic conditions and showed a reduction in NADH τ1 upon glucose stimulation followed by a slight increase and plateau, while hypoxic pseudo-islets showed large fluctuations before and after glucose stimulation (Zbinden & Carvajal Berrio *et al.*, **Appendix 3**, Figure 13a). NADH τ2 values were similar for both normoxic and hypoxic pseudo-islets before glucose-stimulation and they had similar behaviour after glucose-stimulation where both groups showed increased NADH τ2 values; however, the hypoxic pseudo-islets had much higher levels of NADH τ2 (Zbinden & Carvajal Berrio *et al.*, **Appendix 3**, Figure 13b,e). While the control NADH α1 values increased during glucose stimulation, the NADH α1 values of the hypoxic pseudo-islets showed oscillatory behaviour before and after glucose stimulation, with only a

slight decrease in the overall values after stimulation (Zbinden & Carvajal Berrio *et al.*, **Appendix 3**, Figure 13c). Interestingly, the optical oxidative ratio was higher in the hypoxic pseudo-islets compared to the normoxic control, but they showed similar trends with a decrease in the ratio upon glucose stimulation (Zbinden & Carvajal Berrio *et al.*, **Appendix 3**, Figure 13c). The decrease in the ratio of the hypoxic pseudo-islets suggest that they are still glucose-responsive after 6 hours of hypoxic culture. The abnormal NADH τ1 and α1 patterns, as well as the increased NADH τ1 and α1 values, in the hypoxic pseudo-islets could be attributed to cellular stress as the cells undergo anaerobic glycolysis and eventually initiate apoptotic pathways. Together, we were able to show FLIM was capable of measuring changes in β-cell metabolism dynamics in response to glucose stimulation and hypoxic environments and can be used to determine the quality of a cell's functional capability before transplantation.

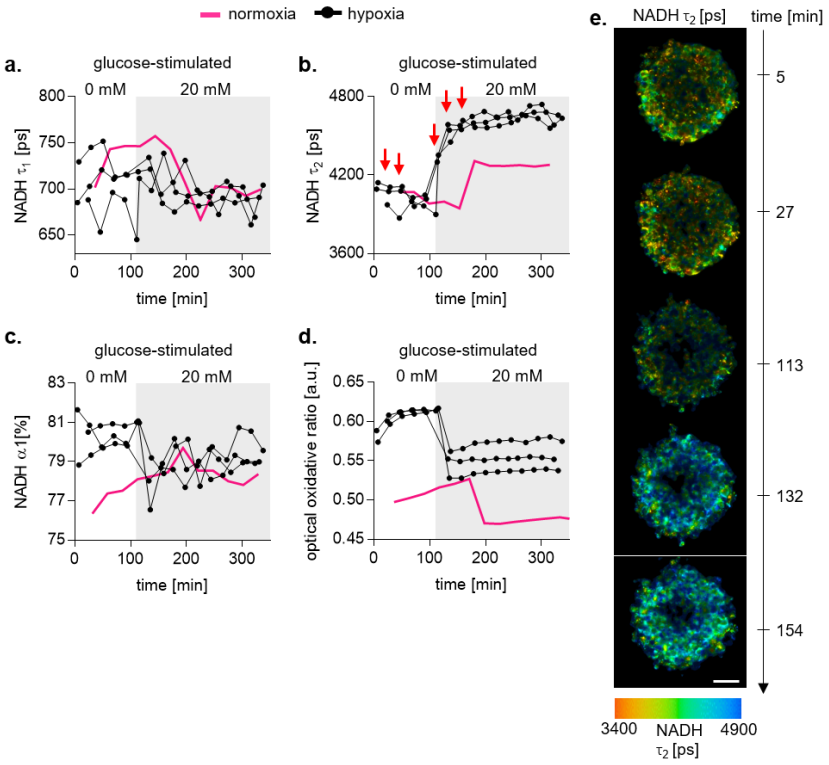

Figure 13: In situ FLIM monitors individual pseudo-islet glucose responses under hypoxic conditions for 6 hours. FLIM analysis of pseudo-islets in normoxia and hypoxia over time during glucose stimulation with 20 mM for **a.** NADH τ1, **b.** NADH τ2, **c.** NADH α1, and **d.** the optical oxidative ratio based on endogenous fluorescence of FAD/(FAD + NADH). Hypoxic pseudo-islets are shown in black and normoxic controls are shown in pink. **e.** Representative images of NADH τ_2 over time during glucose stimulation. Corresponding time points are highlighted with red arrows in **b.** Scale bar equals 50 µm. Adapted from[226].

3.4. ECM proteins Nidogen-1 and Decorin restore functionality of human islets of Langerhans upon hypoxic conditions

In this last chapter, we built on the previous studies of this thesis to support and non-invasively measure the functionality of isolated human donor islets of Langerhans in a hypoxic, post-transplantation setting. Re-establishment of the native ECM environment is crucial for the success of islet transplantation, particularly to support their viability in the initial hypoxic environment. We previously identified BM protein NID1 to support β-cell survival and functionality in hypoxic culture conditions, possibly through pro-survival pathways activated via its binding to integrin αvβ3 in our pseudo-islet model from the immortalized human β-cell line, EndoC-βH3[172]. Earlier in this thesis, we also demonstrated the positive effect DCN has on the pseudo-islets' functionality and ECM expression. To determine whether these ECM proteins can also support isolated human islets of Langerhans in a hypoxic post-transplantation setting, we cultured donor islets with NID1, DCN, or without either protein (control, CTL) for 72 hours and then assessed them for functionality and viability markers. In normoxic cultures, all treatment groups, CTL-, NID1-, and DCN-treated donor islets displayed glucose-responsive insulin secretion with a GSIS index above 1 (Jeyagaran & Urbanczyk *et al.*, **Appendix 4**, Figure 14a). Control donor islets cultured in hypoxia showed a dysfunctional response where they secreted significantly lower insulin at high glucose conditions and had a GSIS index below 1 (Jeyagaran & Urbanczyk *et al.*, **Appendix 4**, Figure 14b). Interestingly, donor islets cultured in hypoxia with either NID1 or DCN displayed glucose-responsive insulin secretion and a GSIS index above 1 (Jeyagaran & Urbanczyk *et al.*, **Appendix 4**, Figure 14b). In normoxia, 75% of donors showed functionality, which was increased to 83% upon NID1- or DCN-treatment (Jeyagaran & Urbanczyk *et al.*, **Appendix 4**, Figure 14c). Further, in hypoxia, only 45% of donors showed functionality, while NID1- or DCN-treatment increased this to 92% and 100%, respectively (Jeyagaran & Urbanczyk *et al.*, **Appendix 4**, Figure 14d). These results suggested that NID1- and DCN-treatment maintain β-cell functionality in normoxia and can restore functionality of islets from majority of the donors upon hypoxic conditions.

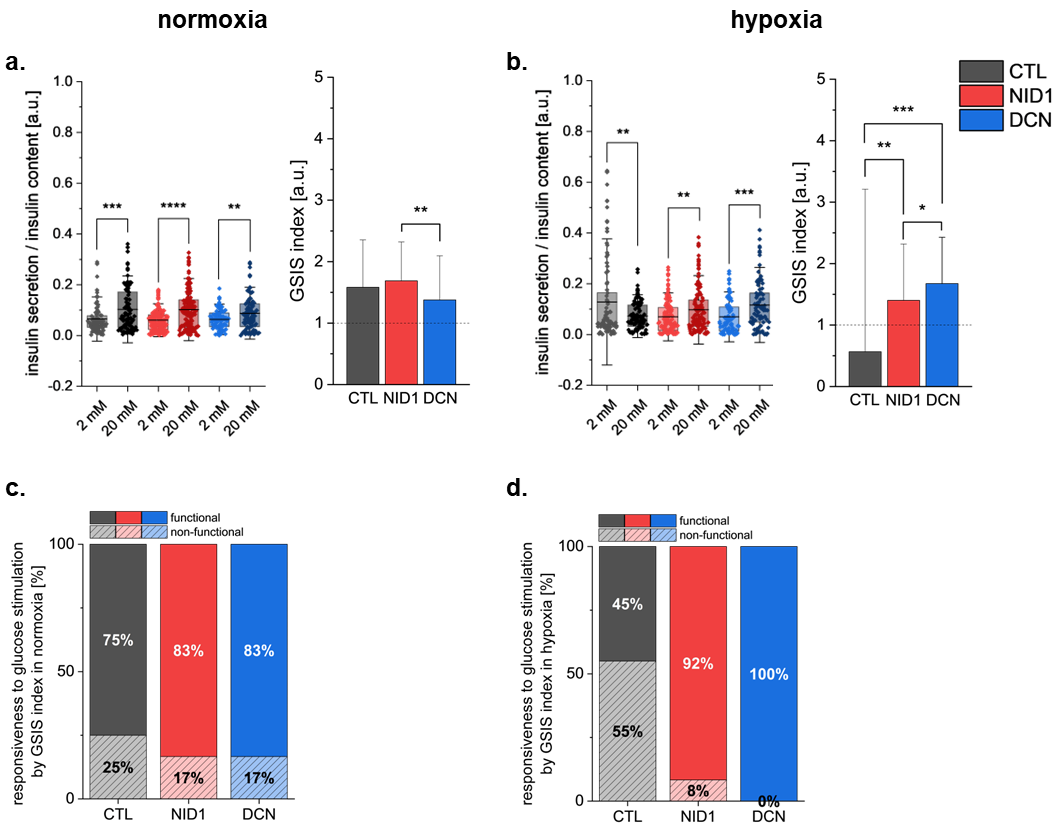

Figure 14: ECM protein treatment improves donor islet functionality in hypoxic conditions. GSIS assay results and index of donor islets treated with either PBS as control (CTL), NID1, or DCN in **a.** normoxic and **b.** hypoxic conditions. Insulin secretion normalized by insulin content of the donor islets.. GSIS index was determined by the fold change in insulin secretion between the 2 mM and 20 mM glucose challenges. Percentage of donors showing functional GSIS responses in **c.** normoxic and **d.** hypoxic conditions. A GSIS index < 1 is considered unresponsive and dysfunctional, and a GSIS index of 1 and above is considered functional. Error bars represent standard deviation. Unpaired t-test, *p≤0.05, **p≤0.01, ***p≤0.001, ****p≤0.0001.

To determine whether these effects were specific to the β-cells, we also performed glucose-stimulated glucagon secretion (GSGS) assays to determine the functionality of α-cells within the donor islets. We expected to observe reduced glucagon secretion in response to increased glucose concentrations and a GSGS index below 1. In both normoxia and hypoxia, none of the treatments showed significant differences in glucagon secretion in response to glucose (Jeyagaran & Urbanczyk *et al.*, **Appendix 4**, Figure 15a,b). Under normoxic conditions, NID1- and DCN-treated donor islets showed a GSGS index below 1 suggesting functional α-cells; however, this was not significantly different from the CTL donor islets (Jeyagaran & Urbanczyk *et al.*, **Appendix 4**, Figure 15a). In hypoxia, the CTL and DCN-treated donor islets had a

GSGS index below 1, while NID1-treated donor islets had a significantly higher GSGS index than the other two treatments (Jeyagaran & Urbanczyk *et al.*, **Appendix 4**, Figure 15b). The larger ranges of glucagon secretion in the hypoxic donor islets could be attributed to cell death and lysis resulting in the release of stored glucagon. These results suggested that the protective and supportive effects of NID1 and DCN in hypoxic conditions on human islets are specific to β-cells.

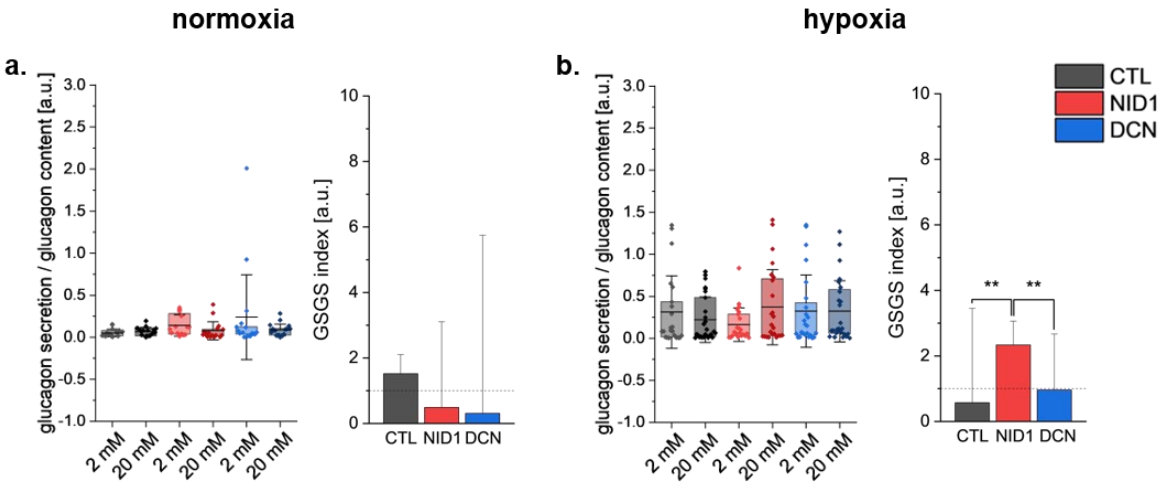

Figure 15: Glucagon secretion analysis of donor islets. Glucagon secretion normalized by glucagon content and fold change of glucagon secretion between low and high glucose in **a.** normoxic and **b.** hypoxic conditions. Error bars represent standard deviation. Unpaired t-test, **p≤0.01.

The increased functionality of the β-cells in hypoxic conditions upon protein treatment could be attributed to increased cell viability or increased metabolic activity. To determine whether the NID1- or DCN-treatments support β-cell functionality through protecting the cells from cell death in hypoxia, we performed IF staining for TUNEL to visualize DNA fragmentation events and cleaved caspase-3 to visualize apoptotic cells. In normoxia, there were no changes in the number of TUNEL^{+ve} cells between the treatment groups; though expectedly, there was a significant increase in TUNEL^{+ve} cells between the normoxic and hypoxic conditions (Jeyagaran & Urbanczyk *et al.*, **Appendix 4**, Fig. 16a,b). Interestingly, in hypoxia, NID1- and DCN-treatments resulted in a significant reduction in TUNEL^{+ve} cells (Jeyagaran & Urbanczyk *et al.*, **Appendix 4**, Figure 16a,b). Furthermore, cleaved caspase-3 staining revealed no significant differences between the culture conditions or

treatment groups (Jeyagaran & Urbanczyk *et al.*, **Appendix 4**, Figure 16c,d), implicating that the protein treatments do not affect caspase-3-mediated apoptosis. Together, these results suggest that NID1 and DCN protect the cells through either preventing DNA fragmentation or repairing DNA fragmentation upon hypoxia.

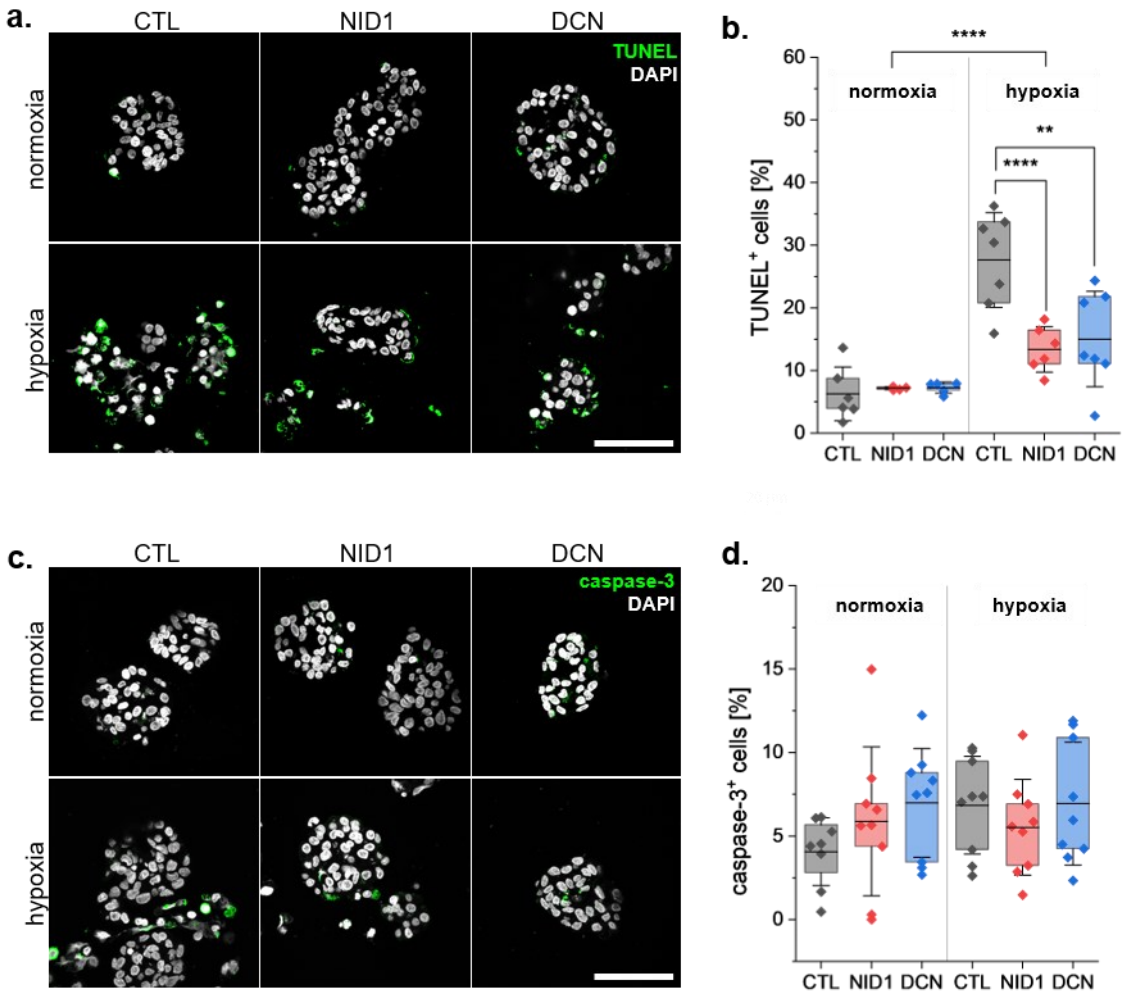

Figure 16: ECM protein treatment reduces DNA fragmentation events in hypoxic conditions. a. Representative images and **b.** quantification of TUNEL$^+$ cells to identify DNA fragmentation in donor islets under normoxic and hypoxic conditions. **c.** Representative images and **d.** quantification of caspase-3$^+$ cells to identify cells undergoing apoptosis in donor islets under normoxic and hypoxic conditions. Error bars represent standard deviation. Two-way ANOVA, **p≤0.01, ****p≤0.0001. Scale bars equal 50 µm.

To determine whether NID1 and DCN also influence the metabolism of the donor islets, we used FLIM to measure changes in the donor islets' metabolic equilibrium. Human donor islets contain lipofuscin bodies that accumulate in post-mitotic cells and

increase with age[243,244]. Unfortunately, these lipofuscin bodies are autofluorescent and interfere with the FLIM and analysis of the NADH lifetimes[244]. To subtract the high autofluorescence in the donor islets' FLIM images, we used previously published protocols[245,246] to objectively remove the lipofuscin effect from all samples. Following removal of the lipofuscin signal, we observed that the χ^2 fitting value was significantly improved allowing for a better understanding of the NADH lifetimes (Jeyagaran & Urbanczyk *et al.*, **Appendix 4**, Figure 17).

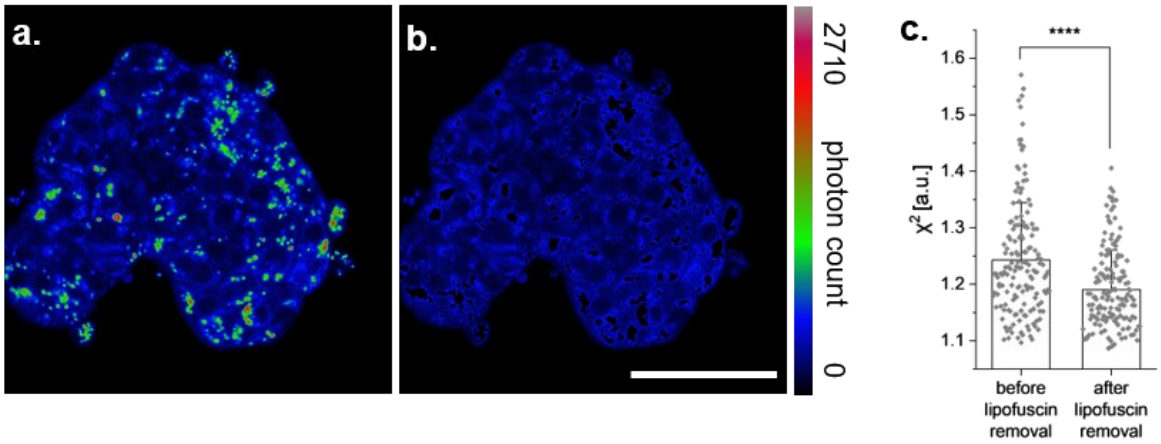

Figure 17: Lipofuscin removal improves χ^2 for FLIM. **a.** NADH before and **b.** after quartile outlier removal. Scale bar equals 50 µm. **c.** χ^2 fitting value is significantly reduced after lipofuscin outlier removal. Unpaired t-test, ****p≤0.0001.

Analysis of the FLIM images showed that both NADH τ1 and τ2 and FAD τ1 and τ2 values were significantly downregulated in the NID1-treated hypoxic donor islets compared to the CTL donor islets (Jeyagaran & Urbanczyk *et al.*, **Appendix 4**, Figure 18a-d), which was accompanied with a significant increase in NADH α1 values in the NID1 group (Jeyagaran & Urbanczyk *et al.*, **Appendix 4**, Figure 18e). In the previous study, we demonstrated that increased NADH τ1 and τ2 values could be indicative of apoptosis prior to activation of cleaved caspase-3 pathways (Figure 12). The decreased NADH τ1 and τ2 values and increased functionality imply that NID1-treatment under hypoxic conditions protect the donor islets and reduce cell death. NADH α1 values were significantly elevated in the hypoxic cultures compared to normoxic cultures (Jeyagaran & Urbanczyk *et al.*, **Appendix 4**, Figure 18e), and a

two-way ANOVA demonstrated a significant increase in NADH α1 between the normoxic and hypoxic conditions in both the NID1- and DCN-treatment groups.

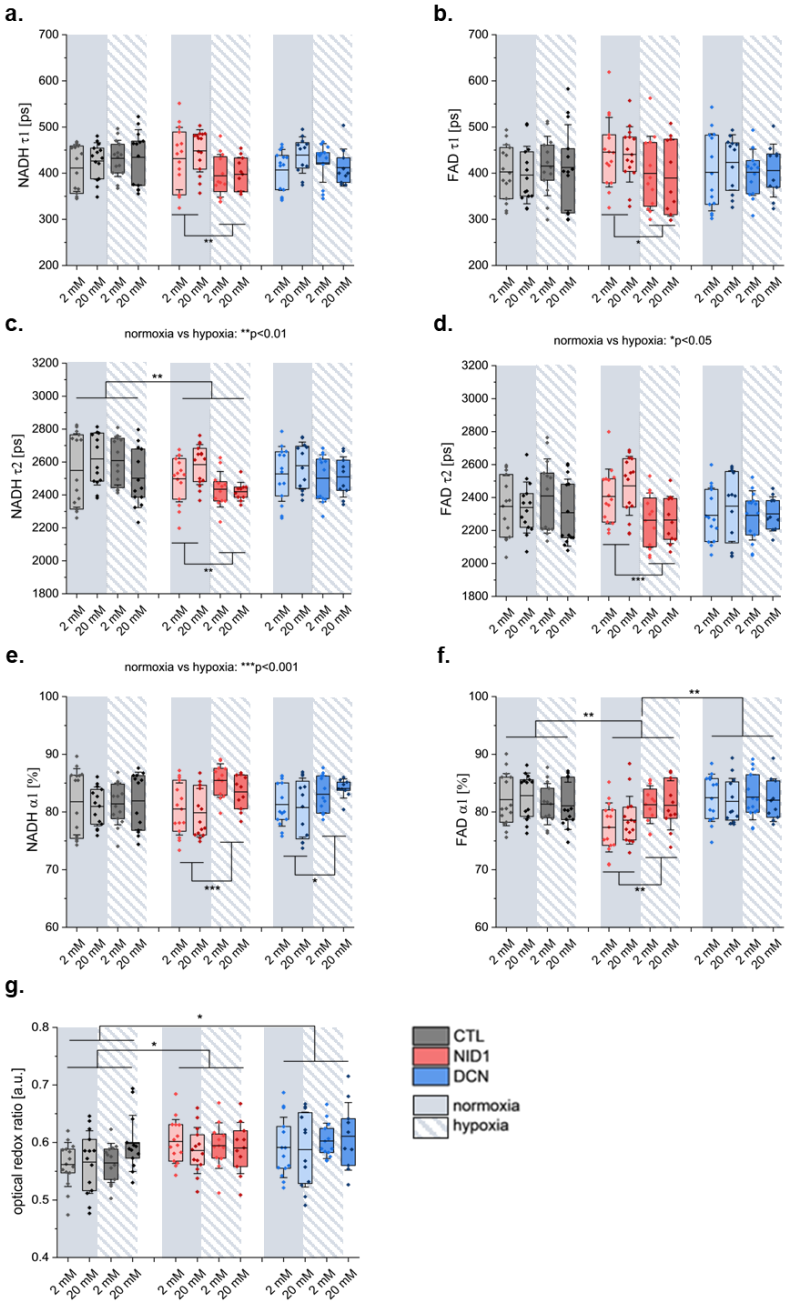

Figure 18: FLIM analysis demonstrate ECM protein-treatment shifts metabolism towards glycolysis under hypoxic conditions. FLIM image analysis of **a.** NADH τ1, **b.** FAD α1, **c.** NADH τ2, **d.** FAD τ2, **e.** NADH α1, **f.** FAD α1, and g**.** the optical redox ratio based on endogenous photon count of FAD / FAD+NADH in normoxia and hypoxia. Error bars represent standard deviation. Statistical significance above graphs: 3-way ANOVA, *p≤0.05, **p≤0.01. Statistical significance below graphs: Two-way ANOVA, *p≤0.05, **p≤0.01, ***p≤0.001.

These results suggest there is increased unbound NADH in the hypoxic donor islets, particularly those treated with either NID1 or DCN which could be attributed to increased glycolysis and pentose phosphate pathways generating NADH and NADPH to produce ATP as mentioned earlier. FAD α1 values of the NID1-treated donor islets were significantly lower than the control or DCN-treated donor islets, where a two-way ANOVA demonstrated a significant increase in FAD α1 between the normoxic and hypoxic conditions within the NID1-treated donor islets (Jeyagaran & Urbanczyk *et al.*, **Appendix 4**, Figure 18f). The reduction in the proportion of bound FAD, or the increase unbound FAD, could be attributed to increased FAD synthesis[247] to accommodate for the increased metabolic activity of the cells upon NID1-treatment which is reduced in the hypoxic environment due to the lack of electron transport chain activity. Interestingly, optical redox ratios showed no significant effects as a result of oxygen conditions, but both NID1- and DCN-treatments shows significantly increased ratios compared to the CTL (Jeyagaran & Urbanczyk *et al.*, **Appendix 4**, Figure 18g). This suggests the protein-treatments shift the metabolic activity towards increased oxidative phosphorylation which is also in line with our previous study where NGS analysis of DCN-treated pseudo-islets showed increased expression of genes involved in oxidative phosphorylation (Figure 8c-d). Unfortunately, none of the NADH or FAD parameters or optical redox ratio values, showed significant changes upon glucose stimulation (Jeyagaran & Urbanczyk *et al.*, **Appendix 4**, Figure 18). This could be attributed to the cellular composition of donor islets where the number of β-cells and their distribution within the donor islet would be heterogeneous. The lack of homogenous signal of the β-cells responding to glucose as we observed using the human β-cell line earlier in the thesis suggests that FLIM may not be sensitive enough to determine metabolic stimulation of one cell type in a heterogeneous population. Recently, other research groups have been able to segment islets into α- and β-cells post-FLIM measurements using IF staining for glucagon and insulin, respectively[245,246]. This post-processing allowed for identification of each cell type's metabolic dynamics which may have otherwise balanced each other out when looking at the islet. They were able to identify that while α-cells responded to increased insulin secretion with a shift towards increased NADH τ1, while β-cells showed a shift towards

increased NADH τ2, such that there was increased oxidative phosphorylation in the β-cells compared to the α-cells upon glucose stimulation[245,246]. Together, our results demonstrate that FLIM could discriminate metabolic changes in donor islets arising from changes in oxygen levels and supportive protein treatment in a non-invasive manner; however, the heterogenous cell composition of donor islets make it difficult to assess the functionality of β-cells without processing the donor islets further to determine the position of the β-cells within the islet and their availability to interact with glucose.

NGS analysis was performed to identify potential pathways NID1 and DCN could be supporting β-cell functionality upon hypoxic exposure. As there were no significant differences between the NID1- and DCN-treatments on β-cell function or viability, we analyzed differentially expressed genes in both NID-1 and DCN-treated donor islets under hypoxia compared to the normoxic control. 93 protein-coding genes were identified to be significantly differentially expressed (Jeyagaran & Urbanczyk *et al.*, **Appendix 4**, Figure 19a), 53 of which were mapped to the GO term metabolism (Jeyagaran & Urbanczyk *et al.*, **Appendix 4**, Figure 19b). Interestingly, there was a significant upregulation of solute carrier family 2 members 1 and 3 (*SLC2A1* and *SLC2A3*, respectively), solute carrier family 16 member 3 (*SLC16A3*), and lysine demethylase 3A (*KDM3A*) (Jeyagaran & Urbanczyk *et al.*, **Appendix 4**, Figure 19c, marked with arrows). *SLC2A1*, *SLC2A3*, and *SLC16A3* encode GLUT1, GLUT3, and monocarboxylate transporter 4 (MCT4), respectively. GLUT1 and GLUT 3 are glucose transporters in β-cells that play key roles in glucose-responsive insulin secretion due to their high affinity for glucose compared to GLUT2[248–250]. While rodent islets predominantly use GLUT2, human pancreatic islets use GLUT1[13,14,248]. Further, GLUT1 was shown to be upregulated by HIF1a in stress conditions such as hypoxia to meet the increased energy demands[251]. The upregulation of *SLC2A1* and *SLC2A3* in the protein-treated donor islets upon hypoxia would allow for increased transport of glucose into the cells to be used for glycolysis and ATP production. The upregulation of *SLC16A3* allows for increased clearance of lactate and glycolysis product pyruvate from the cells in the absence of the Krebs cycle and oxidation phosphorylation[252]. KDM3A plays key roles in cell cycle progression, particularly in DNA repair and

preventing apoptosis[253]. It has also been shown to support cell survival of myeloma cells in hypoxia through promoting glycolysis[254].

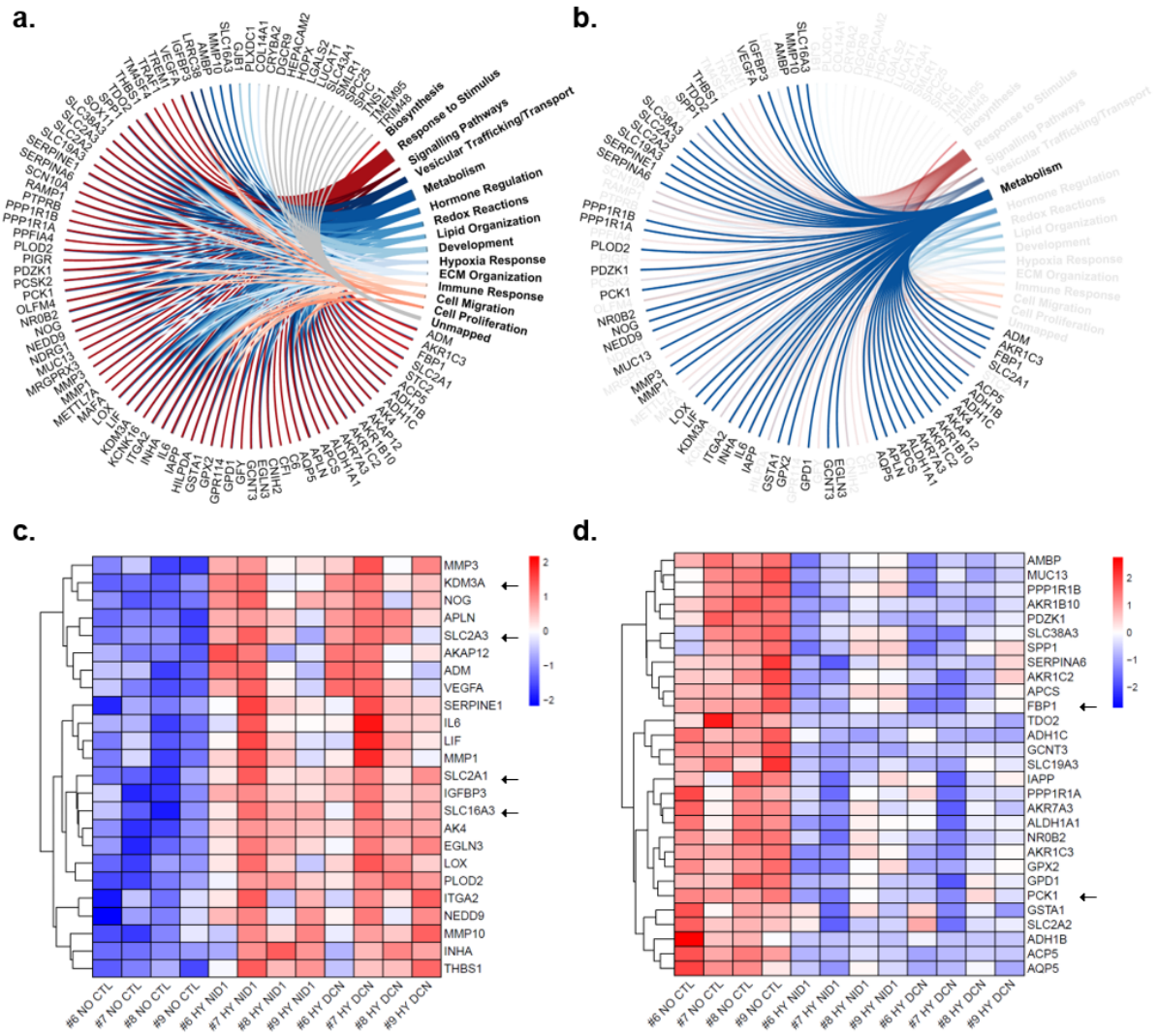

Figure 19: Genes involved in glycolysis differentially expressed in protein-treated donor islets under hypoxia. Differentially expressed genes of donor islets treated with the ECM proteins in hypoxia were compared to the normoxic control. **a.** 93 protein-coding genes differentially expressed only in the NID1- and DCN-treated hypoxic donor islets compared to normoxia were identified. **b.** GO term enrichment analysis mapped 53 of these genes to metabolic pathways, **c.** 24 of which were upregulated and **d.** 29 of which were downregulated. All genes are considered as significantly differentially expressed with a $p_{adjusted} \leq 0.05$.

This suggests that the protein-treatments upregulation of KDM3A in the donor islets plays both a pro-survival and functional role in the donor islets as well in hypoxia conditions. Interestingly, there was also a significant downregulation of gluconeogenic

enzymes fructose-1,6-bisphosphatase 1 (*FBP1*) and phosphoenolpyruvate carboxykinase 1 (*PCK1*) (Figure 19, marked with arrows). FBP1 and PCK1 are enzymes catalyzing rate-limiting gluconeogenic reactions, reversing glycolysis. They are important for the regulation of cell metabolism and cell cycle progression. FBP1 dephosphorylates fructose-1,6-bisphosphate into fructose-1-phosphate[255]. Fructose-1,6-bisphosphate is important for the biphasic insulin secretory behaviour of β-cells[256,257], emphasizing the need to maintain its levels without being dephosphorylated. Inhibition of FBP1 in murine β-cells resulted in increased insulin secretion and a higher GSIS index[258], while overexpression of FBP1 had the opposite effect[259]. PCK1 catalyzes the reversible conversion of the Krebs Cycle intermediate product oxaloacetate into phosphoenolpyruvate and carbon dioxide in the cytoplasm[260,261]. Overexpression of PCK1 in hepatic cancers suppressed glycolytic activity[262–264]. In our donor islets, both NID1- and DCN-treatment downregulated *FBP1* and *PCK1* under hypoxia, potentially as an energy-saving mechanism to maintain ATP levels and support glycolysis to ensure cell viability and function. Taken together, these results show that NID1- and DCN can support the viability and function of donor islets upon hypoxic exposure similar to the post-transplantation environment. Through improving DNA fragmentation events and supporting glycolytic pathways to produce ATP, NID1 and DCN are potential candidates for co-transplantation to support transplant survival and reduce the number of donor islets required for a transplant.

Chapter 4

Conclusion & Outlook

4. Conclusion & Outlook

Islet transplantation is a promising long-term solution for the treatment of T1DM, allowing for endogenous maintenance of blood glucose homeostasis; however, its' success is hindered by poor islet availability and survival. Current proposed solutions including stem cell-derived β-cells and encapsulation of β-cells/islets are also limited by the extended culture periods and the patient's immune responses isolating the transplant. In this thesis, we explored native pancreatic β-cell markers and their environment to advance bioengineering techniques to improve differentiation efficiency of hiPSCs into β-cells, support β-cell function in hypoxic post-transplantation settings, regulate fibrotic capsule formation post-transplantation, and non-invasively monitor β-cell function.

To address the extensive differentiation timelines of hiPSCs into β-cells and the heterogeneous population of cells that result at the end, we introduced lentiviral constructs for the inducible expression of three mature β-cell-specific markers, NGN3, PDX1, and MAFA in hiPSCs. We hypothesized that the expression of the mature β-cell markers along with medium that support pancreatic differentiation, we could forward program the hiPSCs into glucose-responsive insulin-producing β-cells in a shortened timeline of two weeks. We achieved expression of the three mature β-cell markers at the gene and protein level, as well as glucose-responsive insulin secretion just after five days of culture. Further 3D culture for a total of ten days showed gene expression of the markers of interest while PDX1 was lost at the protein level, possibly due to its position within the lentiviral construct. Insulin secretion in a parallel GSIS assay was maintained; however, insulin production and secretion upon consecutive glucose challenges was limited. Comparison to human fetal and adult donor tissues suggested that although the hiPSC-derived spheroids presented similar markers to adult insulin-producing cells, they were functionally representative of fetal tissues due to the limited insulin production. Interestingly, recent studies using lentiviral constructs for inducing the temporal expression of the same three markers achieved generation of glucose-responsive insulin-producing cells from adult (stem) cells[167,170]. This suggests that with the use of separate lentiviral constructs for each gene of interest to

allow for temporal control of their expression, and slight optimization to the culture timeline, we would be able to forward program hiPSCs into glucose-responsive insulin-producing cells as an alternative cell source for implantation.

The ECM plays a key role in the survival and specific functions of tissues and organs. Isolated islets and stem cell-derived β-cells lack the native pancreatic ECM niche. While many studies have assessed the effects of ECM proteins on β-cell functionality and survival, few studies have assessed how the ECM surrounding the transplant could be regulated. To this extent, we studied ECM protein expression in adult pancreatic tissues and identified DCN, known regulator of collagen fibrillogenesis, to be highly co-localized with β-cells within the islets of Langerhans. We hypothesized that DCN plays a role on β-cell survival and function, and its effect on the surrounding ECM would be beneficial in reducing fibrotic capsule formation that would otherwise render the transplant ineffective. *In vitro* studies demonstrated that DCN treatment of our human pseudo-islet model improved glucose-responsive insulin secretion. This was supported by NGS and Raman microspectroscopy data that identified upregulation of oxidative phosphorylation and vesicular trafficking pathways, as expected with increased glucose metabolism and insulin secretion. Furthermore, DCN-treatment reduced expression of fibrotic ECM proteins FN and COL1, suggesting DCN as a potential co-transplantation ECM protein to improve β-cell function and transplant efficacy through prevention of fibrotic capsule formation. Further studies investigating whether DCN can be used as an encapsulation material for islet transplantation and its long-term effects on ECM organization in an *in vivo* model would prove to be beneficial in improving transplant survival.

Assessment of β-cell responsiveness to consecutive glucose challenges is essential for a successful transplant. Mature β-cells can sense glucose and secrete appropriate amounts of insulin on continuous basis. Unfortunately, current β-cell functionality tests result in the loss of the assessed islet/β-cell, where the measurement is used as a representation of the remainder of the cell population from the donor/culture. In this thesis, we hypothesized that FLIM can non-invasively monitor β-cell function through detection of the autofluorescent metabolic coenzymes NADH and FAD. FLIM was capable of monitoring glucose-responsiveness in our

human pseudo-islet model in real-time. Interestingly, FLIM was also sensitive enough to detect changes in the mitochondrial environment suggesting cell death upon hypoxic culture before programmed cell death pathways were even activated. Along with GSIS results and cell viability assays, we were able to demonstrate that FLIM can be used to assess the functional capacity and viability of β-cells. The real-time information FLIM can provide in a non-invasive manner makes it a suitable screening tool to assess and select functional β-cells to be transplanted.

In the last step of this thesis, we built on our previous studies to determine the effects of ECM proteins NID1 and DCN on isolated human donor islets in a hypoxic, post-transplantation environment, and the suitability of using FLIM to assess their functionality. Isolated islets are more sensitive to the culture conditions and post-transplantation environment as it is not comparable to the *in vivo* environment prior to the isolation, making them more sensitive to the protein treatments and measurements than our immortalized human β-cell pseudo-islets. Interestingly, we observed that both NID1 and DCN specifically restore functionality of β-cells within the donor islets and reduce DNA fragmentation events in hypoxic conditions. Furthermore, FLIM analysis demonstrated that NID1 and DCN-treatment results in a metabolic shift in the donor islets towards glycolysis under hypoxic conditions; however, the heterogenous cell composition of the donor islets do not allow for a non-invasive measurement of changes in β-cell metabolism in response to glucose stimulation as observed in the pseudo-islet model. This was further supported by the NGS analysis identifying significant differential expression of key glucose transporters and gluconeogenic enzymes that support the increased glycolytic activity observed. Together, these results demonstrated that when co-transplanted with donor islets, NID1 and DCN can support donor islet functionality in a hypoxic, post-transplantation setting, possibly through preventing or repairing DNA fragmentation to support cell survival.

In summary, this thesis addresses multiple bioengineering approaches to improve islet transplant outcomes at different stages of the transplant process. From optimizing differentiation protocols to forward program hiPSCs into glucose-responsive insulin producing, to supporting β-cell functionality and viability in a hypoxic

environment, this dissertation highlights the importance of recapitulating the native pancreatic microenvironment to improve the success of islet transplantation. We demonstrated that the temporal expression of the mature β-cell markers and re-establishment of the pancreatic ECM is important for the generation and maintenance of long-term functional β-cells. Future studies optimizing the culture protocol for the forward programming of hiPSCs into insulin-producing cells, and assessing the effectiveness of NID1 and DCN *in vivo* hold great promise to improving transplantation efficacy for the treatment of T1DM.

References

1. Zhou, Q. & Melton, D. A. Pancreas regeneration. *Nature* **557,** 351–358 (2018).
2. Huang, H.-H., Harrington, S. & Stehno-Bittel, L. The Flaws and Future of Islet Volume Measurements. *Cell Transplant.* **27,** 1017–1026 (2018).
3. Islam, S. *The Islets of Langerhans*. *Adv. Exp. Med. Biol.* **654,** (Springer Netherlands, 2010).
4. Da Silva Xavier, G. The Cells of the Islets of Langerhans. *J. Clin. Med.* **7,** 54 (2018).
5. Koma, Y., Furuno, T., Hagiyama, M., Hamaguchi, K., Nakanishi, M., Masuda, M., Hirota, S., Yokozaki, H. & Ito, A. Cell Adhesion Molecule 1 Is a Novel Pancreatic–Islet Cell Adhesion Molecule That Mediates Nerve–Islet Cell Interactions. *Gastroenterology* **134,** 1544–1554 (2008).
6. Jeyagaran, A., Lu, C., Zbinden, A., Birkenfeld, A. L., Brucker, S. Y. & Layland, S. L. Type 1 diabetes and engineering enhanced islet transplantation. *Adv. Drug Deliv. Rev.* **189,** 114481 (2022).
7. STANESCU, D. E., LI, C., YANG, J., YAU, D. & STANLEY, C. A. Functional Maturation of Pancreatic ß Cells during Development. *Diabetes* **67,** A558 (2018).
8. Henquin, J.-C. & Nenquin, M. Dynamics and Regulation of Insulin Secretion in Pancreatic Islets from Normal Young Children. *PLoS One* **11,** e0165961 (2016).
9. Henquin, J. C. & Nenquin, M. Immaturity of insulin secretion by pancreatic islets isolated from one human neonate. *J. Diabetes Investig.* **9,** 270–273 (2018).
10. Kaestner, K. H., Campbell-Thompson, M., Dor, Y., Gill, R. G., Glaser, B., Kim, S. K., Sander, M., Stabler, C., Stewart, A. F. & Powers, A. C. What is a beta cell? - Chapter I in the Human Islet Research Network (HIRN) review series. *Mol. Metab.* **53,** 101323 (2021).
11. Blum, B., Hrvatin, S., Schuetz, C., Bonal, C., Rezania, A. & Melton, D. A. Functional beta-cell maturation is marked by an increased glucose threshold and by expression of urocortin 3. *Nat. Biotechnol.* **30,** 261–264 (2012).
12. Shrestha, S., Saunders, D. C., Walker, J. T., Camunas-Soler, J., Dai, X. Q., Haliyur, R., Aramandla, R., Poffenberger, G., Prasad, N., Bottino, R., Stein, R., Cartailler, J. P., Parker, S. C., MacDonald, P. E., Levy, S. E., Powers, A. C. & Brissova, M. Combinatorial transcription factor profiles predict mature and functional human islet alpha and beta cells. *JCI Insight* **6,** e151621 (2021).
13. De Vos, A., Heimberg, H., Quartier, E., Huypens, P., Bouwens, L., Pipeleers, D., Schuit K., F. A. & Schuit, F. Human and rat beta cells differ in glucose transporter but not in glucokinase gene expression. *J. Clin. Invest.* **96,** 2489–95 (1995).
14. McCulloch, L. J., van de Bunt, M., Braun, M., Frayn, K. N., Clark, A. & Gloyn, A. L. GLUT2 (SLC2A2) is not the principal glucose transporter in human pancreatic beta cells: Implications for understanding genetic association signals at this locus. *Mol. Genet. Metab.* **104,** 648–653 (2011).
15. Sansbury, F. H., Flanagan, S. E., Houghton, J. A. L., Shuixian Shen, F. L., Al-Senani, A. M. S., Habeb, A. M., Abdullah, M., Kariminejad, A., Ellard, S. & Hattersley, A. T. SLC2A2 mutations can cause neonatal diabetes, suggesting GLUT2 may have a role in human insulin secretion. *Diabetologia* **55,** 2381–2385 (2012).
16. Heimberg, H., De Vos, A., Vandercammen, A., Van Schaftingen, E., Pipeleers, D. & Schuit, F. Heterogeneity in glucose sensitivity among pancreatic β-cells is correlated to differences in glucose phosphorylation rather than glucose transport. *Eur. Mol. Biol. Organ.* **12,** 2873–2879 (1993).
17. Liu, J. S. E. & Hebrok, M. All mixed up- defining roles for β-cell subtypes in mature islets. *Genes Dev.* **31,** 228–240 (2017).
18. Liang, Y., Bonner-Weir, S., Wu, Y.-J., Berdanier, C. D., Berner, D. K., Efrat, S. & Matschinsky, F. M. In situ glucose uptake and glucokinase activity of pancreatic islets in diabetic and obese rodents. *J. Clin. Invest.* **93,** 2473–2481 (1994).
19. Matschinsky, F., Liang, Y., Kesavan, P., Wang, L., Froguel, P., Velho, G., Cohen, D., Permutt, M. A., Tanizawa, Y., Jetton, T. L., Niswender, K. & Magnuson, M. A. Glucokinase as pancreatic beta cell glucose sensor and diabetes gene. *J. Clin. Invest.* **92,** 2092–2098 (1993).
20. Shimzu, T., Parker, J. C., Najafi, H. & Matschinsky, F. M. Control of glucose metabolism in pancreatic beta-cells by glucokinase, hexokinase, and phosphofructokinase. Model study with cell lines derived from beta-cells. *Diabetes* **11,** 1524–1530 (1988).
21. Jimenez-Chillaron, J. C., Hernandez-Valencia, M., Reamer, C., Fisher, S., Joszi, A., Hirshman, M., Oge, A., Walrond, S., Przybyla, R., Boozer, C., Goodyear, L. D. & Patti, M.-E. β-cell secretory dysfunction in the pathogenesis of low birth weight–associated diabetes. *Diabetes* **54,** 702–711 (2005).
22. Schuit, F., Moens, K., Heimberg, H. & Pipeleers, D. Cellular origin of hexokinase in pancreatic islets. *J. Biol. Chem.* **274,** 32803–32809 (1999).
23. Tu, J. & Tuch, B. E. Expression of glucokinase in glucose-unresponsive human fetal pancreatic islet-like cell clusters. *J. Clin. Endocrinol. Metab.* **82,** 943–948 (1997).
24. Williams, R. & Colagiuri, S. *IDF Diabetes Atlas - Ninth Edition*. (2019). at <http://www.diabetesatlas.org>
25. Rogal, J., Zbinden, A., Schenke-Layland, K. & Loskill, P. Stem-cell based organ-on-a-chip models for diabetes research. *Adv. Drug Deliv. Rev.* **140,** 101–128 (2019).
26. Diagnosis and Classification of Diabetes Mellitus. *Diabetes Care* **37,** S81–S90 (2014).
27. Erlich, H., Valdes, A. M., Noble, J., Carlson, J. A., Varney, M., Concannon, P., Mychaleckyj, J. C., Todd, J. A., Bonella, P., Fear, A. L., Lavant, E., Louey, A., Moonsamy, P. & Type 1 Diabetes Genetics, C. HLA DR-DQ haplotypes and genotypes and type 1 diabetes risk: analysis of the type 1 diabetes genetics consortium families. *Diabetes* **57,** 1084–1092 (2008).
28. DeFronzo, R. A., Ferrannini, E., Groop, L., Henry, R. R., Herman, W. H., Holst, J. J., Hu, F. B., Kahn, C. R., Raz, I., Shulman, G. I., Simonson, D. C., Testa, M. A. & Weiss, R. Type 2 diabetes mellitus. *Nat. Rev. Dis. Prim.* **1,** 15019 (2015).
29. Weinstock, R. S., Xing, D., Maahs, D. M., Michels, A., Rickels, M. R., Peters, A. L., Bergenstal, R. M., Harris, B., Dubose,

S. N., Miller, K. M. & Beck, R. B. Severe hypoglycemia and diabetic ketoacidosis in adults with type 1 diabetes: results from the T1D Exchange clinic registry. *J. Clin. Endocrinol. Metab.* **98,** 3411–3419 (2013).
30. Berget, C., Messer, L. H. & Forlenza, G. P. A clinical overview of insulin pump therapy for the management of diabetes: Past, present, and future of intensive therapy. *Diabetes Spectr.* **32,** 194–204 (2019).
31. Robertson, R. P. Pancreas and islet transplantation in diabetes mellitus. *Wolters Kluwer* (2019).
32. Ricordi, C., Lacy, P. E., Finke, E. H., Olack, B. J. & Scharp, D. P. Automated method for isolation of human pancreatic islets. *Diabetes* **37,** 413–420 (1988).
33. Shapiro, A. M. J., Lakey, J. R. T., Ryan, E. A., Korbutt, G. S., Toth, E., Warnock, G. L., Kneteman, N. M., Rajotte, R. V & Shapiro, J. Islet transplantation in seven patients with type 1 diabetes mellitus using a glucocorticoid-free immunosuppressive regimen. *N. Engl. J. Med.* **343,** 230–238 (2000).
34. Gray, D. W., Sudhakaran, N., Titus, T. T., McShane, P. & Johnson, P. Development of a novel digestion chamber for human and porcine islet isolation. *Transplant. Proc.* **36,** 1135–1138 (2004).
35. Gamble, A., Pepper, A. R., Bruni, A. & Shapiro, A. M. J. The journey of islet cell transplantation and future development. *Islets* **10,** 80–94 (2018).
36. Aref, A., Sharma, A. & Halawa, A. Does steroid-free immunosuppression improve the outcome in kidney transplant recipients compared to conventional protocols? *World J. Transplant.* **11,** 99–113 (2021).
37. Brennan, D. C., Kopetskie, H. A., Sayre, P. H., Alejandro, R., Cagliero, E., Shapiro, A. M., Goldstein, J. S., DesMarais, M. R., Booher, S. & Bianchine, P. J. Long-Term Follow-Up of the Edmonton Protocol of Islet Transplantation in the United States. *Am. J. Transplant.* **16,** 509–517 (2015).
38. Shapiro, A. M., Pokrywczynska, M. & Ricordi, C. Clinical pancreatic islet transplantation. *Nat. Rev. Endocrinol.* **13,** 268–277 (2017).
39. Lammert, E., Gu, G., McLaughlin, M., Brown, D., Brekken, R., Murtaugh, L. C., Gerber, H. P., Ferrara, N. & Melton, D. A. Role of VEGF-A in vascularization of pancreatic islets. *Curr. Biol.* **13,** 1070–1074 (2003).
40. Barra, J. M. & Tse, H. M. Redox-Dependent Inflammation in Islet Transplantation Rejection. *Front. Endocrinol. (Lausanne).* **9,** (2018).
41. Komatsu, H., Kandeel, F. & Mullen, Y. Impact of Oxygen on Pancreatic Islet Survival. *Pancreas* **47,** 533–543 (2018).
42. Komatsu, H., Kang, D., Medrano, L., Barriga, A., Mendez, D., Rawson, J., Omori, K., Ferreri, K., Tai, Y. C., Kandeel, F. & Mullen, Y. Isolated human islets require hyperoxia to maintain islet mass, metabolism, and function. *Biochem. Biophys. Res. Commun.* **470,** 534–538 (2016).
43. Romito, A. & Cobellis, G. Pluripotent Stem Cells: Current Understanding and Future Directions. *Stem Cells Int.* **2016,** 9451492 (2015).
44. Johnston, P. V, Duckers, H. J., Raval, A. N., Cook, T. D. & Pepine, C. J. Not All Stem Cells Are Created Equal. *Circ. Res.* **123,** 944–946 (2018).
45. Forbes, S. & Rosenthal, N. Preparing the ground for tissue regeneration: from mechanism to therapy. *Nat. Med.* **20,** 857–869 (2014).
46. Takahashi, K., Tanabe, K., Ohnuki, M., Narita, M., Ichisaka, T., Tomoda, K. & Yamanaka, S. Induction of pluripotent stem cells from adult human fibroblasts by defined factors. *Cell* **131,** 861–872 (2007).
47. Nakagawa, M., Koyanagi, M., Tanabe, K., Takahashi, K., Ichisaka, T., Aoi, T., Okita, K., Mochiduki, Y., Takizawa, N. & Yamanaka, S. Generation of induced pluripotent stem cells without Myc from mouse and human fibroblasts. *Nat. Biotechnol.* **26,** 101–106 (2008).
48. Yu, J., Vodyanik, M. A., Smuga-Otto, K., Antosiewicz-Bourget, J., Frane, J. L., Tian, S., Nie, J., Jonsdottir, G. A., Ruotti, V., Stewart, R., Slukvin, I. I. & Thomson, J. A. Induced Pluripotent Stem Cell Lines Derived from Human Somatic Cells. *Science (80-.).* **318,** 1917–1920 (2007).
49. Mayhew, C. N. & Wells, J. M. Converting human pluripotent stem cells into beta-cells: recent advances and future challenges. *Curr. Opin. Organ Transplant.* **15,** 54–60 (2010).
50. Rezania, A., Bruin, J. E., Arora, P., Rubin, A., Batushansky, I., Asadi, A., O'Dwyer, S., Quiskamp, N., Mojibian, M., Albrecht, T., Yang, Y. H., Johnson, J. D. & Kieffer, T. J. Reversal of diabetes with insulin-producing cells derived in vitro from human pluripotent stem cells. *Nat. Biotechnol.* **32,** 1121–1133 (2014).
51. Pagliuca, F. W., Millman, J. R., Gürtler, M., Segel, M., Van Dervort, A., Ryu, J. H., Peterson, Q. P., Greiner, D. & Melton, D. A. Generation of Functional Human Pancreatic β Cells In Vitro. *Cell* **159,** 428–439 (2014).
52. Shahjalal, H. M., Shiraki, N., Sakano, D., Kikawa, K., Ogaki, S., Baba, H., Kume, K. & Kume, S. Generation of insulin-producing β-like cells from human iPS cells in a defined and completely xeno-free culture system. *J. Mol. Cell Biol.* **6,** 394–408 (2014).
53. Pellegrini, S., Manenti, F., Chimienti, R., Nano, R., Ottoboni, L., Ruffini, F., Martino, G., Ravassard, P., Piemonti, L. & Sordi, V. Differentiation of Sendai Virus-Reprogrammed iPSC into β Cells, Compared with Human Pancreatic Islets and Immortalized β Cell Line. *Cell Transplant.* **27,** 1548–1560 (2018).
54. Toyoda, T., Mae, S., Tanaka, H., Kondo, Y., Funato, M., Hosokawa, Y., Sudo, T., Kawaguchi, Y. & Osafune, K. Cell aggregation optimizes the differentiation of human ESCs and iPSCs into pancreatic bud-like progenitor cells. *Stem Cell Res.* **14,** 185–197 (2015).
55. Yabe, S. G., Fukuda, S., Nishida, J., Takeda, F., Nashiro, K. & Okochi, H. Induction of functional islet-like cells from human iPS cells by suspension culture. *Regen. Ther.* **10,** 69–76 (2019).
56. Kim, K., Doi, A., Wen, B., Ng, K., Zhao, R., Cahan, P., Kim, J., Aryee, M., Ji, H., Ehrlich, L., Yabuuchi, A., Takeuchi, A., Cunniff, K., Hongguang, H., Mckinney-Freeman, S., Naveiras, O., Yoon, T., Irizarry, R., Jung, N., Seita, J., Hanna, J., Murakami, P., Jaenisch, R., Weissleder, R., Orkin, S., Weissman, I., Feinberg, A. & Daley, G. Epigenetic memory in induced pluripotent stem cells. *Nature* **467,** 285–290 (2010).
57. Nair, G. G., Liu, J. S., Russ, H. A., Tran, S., Saxton, M. S., Chen, R., Juang, C., Li, M. L., Nguyen, V. Q., Giacometti, S., Puri, S., Xing, Y., Wang, Y., Szot, G. L., Oberholzer, J., Bhushan, A. & Hebrok, M. Recapitulating endocrine cell clustering in culture promotes maturation of human stem-cell-derived beta cells. *Nat. Cell Biol.* **21,** 263–274 (2019).
58. Velazco-Cruz, L., Song, J., Maxwell, K. G., Goedegebuure, M. M., Augsornworawat, P., Hogrebe, N. J. & Millman, J. R. Acquisition of dynamic function in human stem cell-derived beta cells. *Stem Cell Reports* **12,** 351–365 (2019).

59. Davis, J. C., Helman, A., Rivera-Feliciano, J., Langston, C. M., Engquist, E. N. & Melton, D. A. Live cell monitoring and enrichment of stem cell-derived β cells using intracellular zinc content as a population marker. *Curr. Protoc. Stem Cell Biol.* **51,** e99 (2019).
60. Hogrebe, N. J., Augsornworawat, P., Maxwell, K. G., Velazco-Cruz, L. & Millman, J. R. Targeting the cytoskeleton to direct pancreatic differentiation of human pluripotent stem cells. *Nat. Biotechnol.* **38,** 460–470 (2020).
61. Balboa, D., Barsby, T., Lithovius, V., Saarimäki-Vire, J., Omar-Hmeadi, M., Dyachok, O., Montaser, H., Lund, P. E., Yang, M., Ibrahim, H., Näätänen, A., Chandra, V., Vihinen, H., Jokitalo, E., Kvist, J., Ustinov, J., Nieminen, A. I., Kuuluvainen, E., Hietakangas, V., Katajisto, P., Lau, J., Carlsson, P. O., Barg, S., Tengholm, A., Otonkoski, T., Saarimaki-Vire, J., Omar-Hmeadi, M., Dyachok, O., Montaser, H., Lund, P. E., Yang, M., Ibrahim, H., Naatanen, A., Chandra, V., Vihinen, H., Jokitalo, E., Kvist, J., Ustinov, J., Nieminen, A. I., Kuuluvainen, E., Hietakangas, V., Katajisto, P., Lau, J., Carlsson, P. O., Barg, S., Tengholm, A. & Otonkoski, T. Functional, metabolic and transcriptional maturation of human pancreatic islets derived from stem cells. *Nat Biotechnol* **40,** 1042–1055 (2022).
62. Davis, J. C., Alves, T. C., Helman, A., Chen, J. C., Kenty, J. H., Cardone, R. L., Liu, D. R., Kibbey, R. G. & Melton, D. A. Glucose response by stem cell-derived beta cells in vitro is inhibited by a bottleneck in glycolysis. *Cell Rep.* **31,** 107623 (2020).
63. Kibbey, R. G., Pongratz, R. L., Romanelli, A. J., Wollheim, C. B., Cline, G. W. & Shulman, G. I. Mitochondrial GTP regulates glucose-stimulated insulin secretion. *Cell Metab.* **5,** 253–264 (2007).
64. Chmielowiec, J., Szlachcic, W. J., Yang, D., Scavuzzo, M. A., Wamble, K., Sarrion-Perdigones, A., Sabek, O. M., Venken, K. J. T. & Borowiak, M. Human pancreatic microenvironment promotes beta-cell differentiation via non-canonical WNT5A/JNK and BMP signaling. *Nat Commun* **13,** 1952 (2022).
65. Riolobos, L., Hirata, R. K., Turtle, C. J., Wang, P. R., Gornalusse, G. G., Zavajlevski, M., Riddell, S. R. & Russell, D. W. HLA engineering of human pluripotent stem cells. *Mol. Ther.* **21,** 1232–1241 (2013).
66. Norbnop, P., Ingrungruanglert, P., Israsena, N., Suphapeetiporn, K. & Shotelersuk, V. Generation and characterization of HLA-universal platelets derived from induced pluripotent stem cells. *Sci. Rep.* **10,** 8472 (2020).
67. Mattapally, S., Pawlik, K. M., Fast, V. G., Zumaquero, E., Lund, F. E., Randall, T. D., Townes, T. M. & Zhang, J. Human leukocyte antigen class I and II knockout human induced pluripotent stem cell-derived cells: universal donor for cell therapy. *J. Am. Heart Assoc.* **7,** e010239 (2018).
68. Han, X., Wang, M., Duan, S., Franco, P. J., Kenty, J. H., Hedrick, P., Xia, Y., Allen, A., Ferreira, L. M. R., Strominger, J. L., Melton, D. A., Meissner, T. B. & Cowan, C. A. Generation of hypoimmunogenic human pluripotent stem cells. *Proc. Natl. Acad. Sci. U. S. A.* **116,** 10441–10446 (2019).
69. Parent, A. V, Faleo, G., Chavez, J., Saxton, M., Berrios, D. I., Kerper, N. R., Tang, Q. & Hebrok, M. Selective deletion of human leukocyte antigens protects stem cell-derived islets from immune rejection. *Cell Rep.* **36,** 109538 (2021).
70. Prange, S., Zuckner, P., Jevnikar, A. M. & Singh, B. Transplanted MHC class I-deficient nonobese diabetic mouse islets are protected from autoimmune injury in diabetic nonobese recipients. *Transplantation* **71,** 982–985 (2001).
71. Yoshihara, E., O'Connor, C., Gasser, E., Wei, Z., Oh, T. G., Tseng, T. W., Wang, D., Cayabyab, F., Dai, Y., Yu, R. T., Liddle, C., Atkins, A. R., Downes, M. & Evans, R. M. Immune-evasive human islet-like organoids ameliorate diabetes. *Nature* **586,** 606–611 (2020).
72. Liu, X., Pu, Y., Cron, K., Deng, L., Kline, J., Frazier, W. A., Xu, H., Peng, H., Fu, Y. X. & Xu, M. M. CD47 blockade triggers T cell-mediated destruction of immunogenic tumors. *Nat. Med.* **21,** 1209–1215 (2015).
73. Ghimire, K., Kale, A., Li, J., Julovi, S. M., O'Connell, P., Grey, S. T., Hawthorne, W. J., Gunton, J. E. & Rogers, N. M. A metabolic role for CD47 in pancreatic β cell insulin secretion and islet transplant outcomes. *Sci. Transl. Med.* **15,** eadd2387 (2023).
74. Vinay, D. S., Ryan, E. P., Pawelec, G., Talib, W. H., Stagg, J., Elkord, E., Lichtor, T., Decker, W. K., Whelan, R. L., Shantha umara, H. M. C., Signori, E., Honoki, K., Georgakilas, A. G., Amin, A., Helferich, W. G., Boosani, C. S., Guha, G., Ciriolo, M. R., Chen, S., Mohammed, S. I., Azmi, A. S., Keith, W. N., Bilsland, A., Bhakta, D., Halicka, D., Fujii, H., Aquilano, K., Ashraf, S. S., Nowsheen, S., Yang, X., Choi, B. K. & Kwon, B. S. Immune evasion in cancer: Mechanistic basis and therapeutic strategies. *Semin. Cancer Biol.* **35,** S185–S198 (2015).
75. Liu, H., Li, R., Liao, H. K., Min, Z., Wang, C., Yu, Y., Shi, L., Dan, J., Hayek, A., Martinez Martinez, L., Nunez Delicado, E. & Izpisua Belmonte, J. C. Chemical combinations potentiate human pluripotent stem cell-derived 3D pancreatic progenitor clusters toward functional beta cells. *Nat. Commun.* **12,** 3330 (2021).
76. Chmielowiec, J. & Borowiak, M. In vitro differentiation and expansion of human pluripotent stem cell-derived pancreatic progenitors. *Rev. Diabet. Stud.* **11,** 19–34 (2014).
77. Zhou, Q., Law, A. C., Rajagopal, J., Anderson, W. J., Gray, P. A. & Melton, D. A. A Multipotent Progenitor Domain Guides Pancreatic Organogenesis. *Dev. Cell* **13,** 103–114 (2007).
78. Zhu, Y., Liu, Q., Zhou, Z. & Ikeda, Y. PDX1, Neurogenin-3, and MAFA: critical transcription regulators for beta cell development and regeneration. *Stem Cell Res. Ther.* **8,** 240 (2017).
79. Zhou, Q., Brown, J., Kanarek, A., Rajagopal, J. & Melton, D. A. In vivo reprogramming of adult pancreatic exocrine cells to beta-cells. *Nature* **455,** 627–632 (2008).
80. Akinci, E., Banga, A., Greder, L. V, Dutton, J. R. & Slack, J. M. Reprogramming of pancreatic exocrine cells towards a beta (beta) cell character using Pdx1, Ngn3 and MafA. *Biochem. J.* **442,** 539–550 (2012).
81. Koblas, T., Leontovyc, I., Loukotova, S., Kosinova, L. & Saudek, F. Reprogramming of Pancreatic Exocrine Cells AR42J Into Insulin-producing Cells Using mRNAs for Pdx1, Ngn3, and MafA Transcription Factors. *Mol. Ther. - Nucleic Acids* **5,** e320 (2016).
82. Banga, A., Akinci, E., Greder, L. V, Dutton, J. R. & Slack, J. M. In vivo reprogramming of Sox9+ cells in the liver to insulin-secreting ducts. *Proc. Natl. Acad. Sci. U. S. A.* **109,** 15336–15341 (2012).
83. Banga, A., Greder, L. V., Dutton, J. R. & Slack, J. M. W. Stable insulin secreting ducts formed by reprogramming of cells in the liver using a three gene cocktail and a PPAR agonist. *Gene Ther.* **21,** 19–27 (2014).
84. Akinci, E., Banga, A., Tungatt, K., Segal, J., Eberhard, D., Dutton, J. R. & Slack, J. M. Reprogramming of various cell types to a beta-like state by Pdx1, Ngn3 and MafA. *PLoS One* **8,** e82424 (2013).
85. Xu, H., Tsang, K. S., Chan, J. C. N., Yuan, P., Fan, R., Kaneto, H. & Xu, G. The combined expression of Pdx1 and

MafA with either Ngn3 or NeuroD improves the differentiation efficiency of mouse embryonic stem cells into insulin-producing cells. *Cell Transplant.* **22,** 147–158 (2013).
86. Saxena, P., Heng, B. C., Bai, P., Folcher, M., Zulewski, H. & Fussenegger, M. A programmable synthetic lineage-control network that differentiates human IPSCs into glucose-sensitive insulin-secreting beta-like cells. *Nat. Commun.* **7,** 11247 (2016).
87. Johansson, K. A., Dursun, U., Jordan, N., Gu, G., Beermann, F., Gradwohl, G. & Grapin-Botton, A. Temporal control of neurogenin3 activity in pancreas progenitors reveals competence windows for the generation of different endocrine cell types. *Dev. Cell* **12,** 457–465 (2007).
88. Schwitzgebel, V. M., Scheel, D. W., Conners, J. R., Kalamaras, J., Lee, J. E., Anderson, D. J., Sussel, L., Johnson, J. D. & German, M. S. Expression of neurogenin3 reveals an islet cell precursor population in the pancreas. *Development* **127,** 3533–3542 (2000).
89. Nishimura, W., Bonner-Weir, S. & Sharma, A. Expression of MafA in pancreatic progenitors is detrimental for pancreatic development. *Dev. Biol.* **333,** 108–120 (2009).
90. Weber, L. M., Hayda, K. N. & Anseth, K. S. Cell-matrix interactions improve β-cell survival and insulin secretion in three-dimensional culture. *Tissue Eng. - Part A* **14,** 1959–1968 (2008).
91. Thomas, F. T., Contreras, J. L., Bilbao, G., Ricordi, C., Curiel, D. & Thomas, J. M. Anoikis, extracellular matrix, and apoptosis factors in isolated cell transplantation. *Surgery* **126,** 299–304 (1999).
92. Deepa Maheshvare, M., Raha, S., König, M. & Pal, D. A pathway model of glucose-stimulated insulin secretion in the pancreatic β-cell. *Front. Endocrinol. (Lausanne).* **14,** (2023).
93. Kolenc, O. I. & Quinn, K. P. Evaluating cell metabolism through autofluorescence imaging of NAD(P)H and FAD. *Antioxidants Redox Signal.* **30,** 875–889 (2019).
94. Heikal, A. A. Intracellular coenzymes as natural biomarkers for metabolic activites and mitochondrial anomalies. *Biomark. Med.* **4,** 241–263 (2010).
95. Suhling, K., Hirvonen, L. M., Levitt, J. A., Chung, P.-H., Tregidgo, C., Le Marois, A., Rusakov, D. A., Zheng, K., Ameer-Beg, S., Poland, S., Coelho, S., Henderson, R. & Krstajic, N. Fluorescence lifetime imaging (FLIM): Basic concepts and some recent developments. *Med. Photonics* **27,** 3–40 (2015).
96. Kunz, W. S. & Kunz, W. Contribution of different enzymes to flavoprotein fluorescence of isolated rat liver mitochondria. *Biochim. Biophys. Acta - Gen. Subj.* **841,** 237–246 (1985).
97. Smink, A. M. & de Vos, P. Therapeutic strategies for modulating the extracellular matrix to improve pancreatic islet function and survival after transplantation. *Curr. Diab. Rep.* **18,** 39 (2018).
98. Hartig, S. M. & Cox, A. R. Paracrine signaling in islet function and survival. *J. Mol. Med.* **98,** 451–467 (2020).
99. Sakata, N., Yoshimatsu, G. & Koadma, S. The Roles of Collagen in Islet Transplantation. *OBM Transplant.* **4,** (2020).
100. Armanet, M., Wojtusciszyn, A., Morel, P., Parnaud, G., Rousselle, P., Sinigaglia, C. & Thierry Berney, D. B. Regulated laminin-332 expression in human islets of Langerhans. *FASEB J.* **23,** 4046–4055 (2009).
101. Virtanen, I., Banerjee, M., Palgi, J., Korsgren, O., Lukinius, A., Thornell, L.-E., Kikkawa, Y., Sekiguchi, K., Hukkanen, M., Konttinen, Y. T. & Otonkoski, T. Blood vessels of human islets of Langerhans are surrounded by a double basement membrane. *Diabetologia* **51,** 1181–1191 (2008).
102. Stendahl, J. C., Kaufman, D. B. & Stupp, S. I. Extracellular matrix in pancreatic islets: Relevance to scaffold design and transplantation. *Cell Transplant.* **18,** 1–12 (2009).
103. Cross, S. E., Vaughan, R. H., Willcox, A. J., McBride, A. J., Abraham, A. A., Han, B., Johnson, J. D., Maillard, E., Bateman, P. A., Ramracheya, R. D., Rorsman, P., Kadler, K. E., Dunne, M. J., Hughes, S. J. & Johnson, P. R. V. Key Matrix Proteins Within the Pancreatic Islet Basement Membrane Are Differentially Digested During Human Islet Isolation. *Am. J. Transplant.* **17,** 451–461 (2017).
104. Mats Paulsson. Basement Membrane Proteins: Structure, Assembly, and Cellular Interactions. *Crit. Rev. Biochem. Mol. Biol.* **27,** 93–127 (1992).
105. Otonkoski, T., Banerjee, M., Korsgren, O., Thornell, L.-E. & Virtanen, I. Unique basement membrane structure of human pancreatic islets: implications for β-cell growth and differentiation. *Diabetes, Obes. Metab.* **10,** 119–127 (2008).
106. Rosenberg, L., Wang, R., Paraskevas, S. & Maysinger, D. Structural and functional changes resulting from islet isolation lead to islet cell death. *Surgery* **126,** 0393–0398 (1999).
107. Thomas, F., Wu, J., Contreras, J. L., Smyth, C., Bilbao, G., He, J. & Thomas, J. A tripartite anoikis-like mechanism causes early isolated islet apoptosis. *Surgery* **130,** 333–338 (2001).
108. Sigmundsson, K., Ojala, J. R. M., Öhman, M. K., Österholm, A. M., Moreno-Moral, A., Domogatskaya, A., Chong, L. Y., Sun, Y., Chai, X., Steele, J. A. M., George, B., Patarroyo, M., Nilsson, A. S., Rodin, S., Ghosh, S., Stevens, M. M., Petretto, E. & Tryggvason, K. Culturing functional pancreatic islets on α5-laminins and curative transplantation to diabetic mice. *Matrix Biol.* **70,** 5–19 (2018).
109. Banerjee, M., Virtanen, I., Palgi, J., Korsgren, O. & Otonkoski, T. Proliferation and plasticity of human beta cells on physiologically occurring laminin isoforms. *Mol. Cell. Endocrinol.* **355,** 78–86 (2012).
110. Matsushima, H., Kuroki, T., Adachi, T., Kitasato, A., Ono, S., Tanaka, T., Hirabaru, M., Kuroshima, N., Hirayama, T., Sakai, Y., Soyama, A., Hidaka, M., Takatsuki, M., Kin, T., Shapiro, J. & Eguchi, S. Human Fibroblast Sheet Promotes Human Pancreatic Islet Survival and Function in Vitro. *Cell Transplant.* **25,** 1425–1588 (2016).
111. Kaido, T., Yebra, M., Cirulli, V. & Montgomery, A. M. Regulation of human β-cell adhesion, motility, and insulin secretion by collagen IV and its receptor α1β1. *J. Biol. Chem.* **279,** 53762–53769 (2004).
112. Llacua, L. A., Haan, B. J. de & Vos, P. de. Laminin and collagen IV inclusion in immunoisolating microcapsules reduces cytokine-mediated cell death in human pancreatic islets. *J. Tissue Eng. Regen. Med.* **12,** 460–467 (2018).
113. Pal, V., Wang, Y., Regeenes, R., Kilkenny, D. M. & Rocheleau, J. V. Laminin matrix regulates beta-cell FGFR5 expression to enhance glucose-stimulated metabolism. *Sci. Rep.* **12,** 1–15 (2022).
114. Nakashima, Y., Iguchi, H., Takakura, K., Nakamura, Y., Izumi, K., Koba, N., Haneda, S. & Tsukahara, M. Adhesion Characteristics of Human Pancreatic Islets, Duct Epithelial Cells, and Acinar Cells to a Polymer Scaffold. *Cell Transplant.* **31,** 1–15 (2022).
115. Fernández-Montes, R. D., Blasi, J., Busquets, J., Montanya, E. & Nacher, M. Fibronectin Enhances Soluble N-

ethylmaleimide-Sensitive Factor Attachment Protein Receptor Protein Expression in Cultured Human Islets. *Pancreas* **40,** 1153–1157 (2011).
116. Llacua, A., Haan, B. J. de, Smink, S. A. & Vos, P. de. Extracellular matrix components supporting human islet function in alginate-based immunoprotective microcapsules for treatment of diabetes. *J. Biomed. Mater. Res.* **104,** 1788–1796 (2016).
117. Hadavi, E., Leijten, J., Engelse, M., De Koning, E., Jonkheijm, P., Karperien, M. & Van Apeldoorn, A. Microwell scaffolds using collagen-IV and laminin-111 lead to improved insulin secretion of human islets. *Tissue Eng. - Part C Methods* **25,** 71–81 (2019).
118. Kaido, T., Yebra, M., Cirulli, V., Rhodes, C., Diaferia, G. & Montgomery, A. M. Impact of defined matrix interactions on insulin production by cultured human beta-cells: effect on insulin content, secretion, and gene transcription. *Diabetes* **55,** 2723–2729 (2006).
119. Bowers, D. T., Song, W., Wang, L.-H. L.-H. & Ma, M. Engineering the vasculature for islet transplantation. *Acta Biomater.* **95,** 131–151 (2019).
120. Lo, J. F., Wang, Y., Blake, A., Yu, G., Harvat, T. A., Jeon, H., Oberholzer, J. & Eddington, D. T. Islet preconditioning via multimodal microfluidic modulation of intermittent hypoxia. *Anal. Chem.* **84,** 1987–1993 (2012).
121. Ma, Z., Moruzzi, N., Catrina, S. B., Hals, I., Oberholzer, J., Grill, V. & Bjorklund, A. Preconditioning with associated blocking of Ca2+ inflow alleviates hypoxia-induced damage to pancreatic beta-cells. *PLoS One* **8,** e67498 (2013).
122. Dugbartey, G. J. Carbon Monoxide in Pancreatic Islet Transplantation: A New Therapeutic Alternative to Patients With Severe Type 1 Diabetes Mellitus. *Front. Pharmacol.* **12,** 750816 (2021).
123. Linn, T., Schneider, K., Hammes, H. P., Preissner, K. T., Brandhorst, H., Morgenstern, E., Kiefer, F. & Bretzel, R. G. Angiogenic capacity of endothelial cells in islets of Langerhans. *FASEB* **17,** 1–17 (2003).
124. Koch, S. & Claesson-welsh, L. Signal Transduction by Vascular Endothelial Growth Factor Receptors. *Cold Spring Harb Perspect Med.* **2,** a006502 (2012).
125. Weaver, J. D., Headen, D. M., Aquart, J., Johnson, C. T., Shea, L. D., Shirwan, H. & García, A. J. Vasculogenic hydrogel enhances islet survival, engraftment, and function in leading extrahepatic sites. *Sci. Adv.* **3,** e1700184 (2017).
126. Phelps, E. A., Templemann, K. L., Thulé, P. M. & García, A. J. Engineered VEGF-releasing PEG-MAL hydrogel for pancreatic islet vascularization. *Drug Deliv. Transl. Res.* **5,** 125–136 (2015).
127. Phelps, E. A., Headen, D. M., Taylor, W. R., Thule, P. M. & Garcia, A. J. Vasculogenic bio-synthetic hydrogel for enhancement of pancreatic islet engraftment and function in type 1 diabetes. *Biomaterials* **34,** 4602–4611 (2013).
128. Farina, M., Ballerini, A., Fraga, D. W., Nicolov, E., Hogan, M., Demarchi, D., Scaglione, F., Sabek, O. M., Horner, P., Thekkedath, U., Gaber, O. A. & Grattoni, A. 3D Printed Vascularized Device for Subcutaneous Transplantation of Human Islets. *Biotechnol. J.* **12,** 1700169 (2017).
129. Scheiner, K. C., Coulter, F., Maas-Bakker, R. F., Ghersi, G., Nguyen, T. T., Steendam, R., Duffy, G. P., Hennink, W. E., O'Cearbhaill, E. D. & Kok, R. J. Vascular endothelial growth factor (VEGF)-releasing microspheres based on poly(ε-caprolactone-PEG-ε-caprolactone)-b-poly(L-lactide) multi-block copolymers incorporated in a 3D-printed poly(dimethylsiloxane) (PDMS) cell macroencapsulation device. *J. Pharm. Sci.* **109,** 863–870 (2020).
130. Cabric, S., Sanchez, J., Lundgren, T., Foss, A., Felldin, M., Källen, R., Salmela, K., Tibell, A., Tufveson, G., Larsson, R., Korsgren, O. & Nilsson, B. Islet Surface Heparinization Prevents the Instant Blood-Mediated Inflammatory Reaction in Islet Transplantation. *Diabetes* **56,** 2008–2015 (2007).
131. Cabric, S., Sanchez, J., Johansson, U., Larsson, R., Nilsson, B., Korsgren, O. & Magnusson, P. U. Anchoring of vascular endothelial growth factor to surface-immobilized heparin on pancreatic islets: implications for stimulating islet angiogenesis. *Tissue Eng. Part A* **16,** 961–970 (2010).
132. Stendahl, J. C., Wang, L. J., Chow, L. W., Kaufman, D. B. & Stupp, S. I. Growth factor delivery from self-assembling nanofibers to facilitate islet transplantation. *Transplantation* **86,** 478–481 (2008).
133. Chow, L. W., Wang, L.-J., Kaufman, D. B. & Stupp, S. I. Self-assembling nanostructures to deliver angiogenic factors to pancreatic islets. *Biomaterials* **31,** 6154–6161 (2010).
134. Carmeliet, P. VEGF gene therapy: stimulating angiogenesis or angioma-genesis? *Nat. Med.* **6,** 1102–1103 (2000).
135. Song, H. J., Xue, W. J., Li, Y., Tian, X. H., Ding, X. M., Feng, X. S., Song, Y. & Tian, P. X. Prolongation of islet graft survival using concomitant transplantation of islets and vascular endothelial cells in diabetic rats. *Transplant. Proc.* **42,** 2662–2665 (2010).
136. Pan, X., Xue, W., Li, Y., Feng, X., Tian, X. & Ding, C. Islet graft survival and function: concomitant culture and transplantation with vascular endothelial cells in diabetic rats. *Transplantation* **92,** 1208–1214 (2011).
137. Johansson, U., Elgue, G., Nilsson, B. & Korsgren, O. Composite islet-endothelial cell grafts: a novel approach to counteract innate immunity in islet transplantation. *Am. J. Transplant.* **5,** 2632–2639 (2005).
138. Jung, H. S., Kim, M. J., Hong, S. H., Lee, Y. J., Kang, S., Lee, H., Chung, S. S., Park, J. S. & Park, K. S. The potential of endothelial colony-forming cells to improve early graft loss after intraportal islet transplantation. *Cell Transplant.* **23,** 273–283 (2014).
139. Zbinden, A., Urbanczyk, M., Layland, S. L., Becker, L., Marzi, J., Bosch, M., Loskill, P., Duffy, G. P. & Schenke-Layland, K. Collagen and endothelial cell coculture improves beta-cell functionality and rescues pancreatic extracellular matrix. *Tissue Eng. Part A* **27,** 977–991 (2020).
140. Hamlet, S. M., Vaquette, C., Shah, A., Hutmacher, D. W. & Ivanovski, S. 3-Dimensional functionalized polycaprolactone-hyaluronic acid hydrogel constructs for bone tissue engineering. *J. Clin. Periodontol.* **44,** 428–437 (2016).
141. Urbanczyk, M., Zbinden, A., Layland, S. L., Duffy, G. & Schenke-Layland, K. Controlled heterotypic pseudo-islet assembly of human β-cells and HUVECs using magnetic levitation. *Tissue Eng. Part A* **26,** 387–399 (2020).
142. Kang, S., Park, H. S., Jo, A., Hong, S. H., Lee, H. N., Lee, Y. Y., Park, J. S., Jung, H. S., Chung, S. S. & Park, K. S. Endothelial progenitor cell cotransplantation enhances islet engraftment by rapid revascularization. *Diabetes* **61,** 866–876 (2012).
143. Oh, B. J., Oh, S. H., Jin, S. M., Suh, S., Bae, J. C., Park, C.-G., Lee, M.-S., Lee, M.-K., Kim, J. H. & Kim, K.-W. Co-transplantation of bone marrow-derived endothelial progenitor cells improves revascularization and organization in islet grafts. *Am. J. Transplant.* **13,** 1429–1440 (2013).

144. Penko, D., Rojas-Canales, D., Mohanasundaram, D., Peiris, H. S., Sun, W. Y., Drogemuller, C. J., Keating, D. J., Coates, P. T., Bonder, C. S. & Jessup, C. F. Endothelial progenitor cells enhance islet engraftment, influence beta-cell function, and modulate islet connexin 36 expression. *Cell Transplant.* **24,** 37–48 (2015).
145. Barba-Gutierrez, D. A., Daneri-Navarro, A., Villagomez-Mendez, J. J., Kanamune, J., Robles-Murillo, A. K., Sanchez-Enriquez, S., Villafan-Bernal, J. R. & Rivas-Carrillo, J. D. Facilitated engraftment of isolated islets coated with expanded vascular endothelial cells for islet transplantation. *Transplant. Proc.* **48,** 669–672 (2016).
146. Urbanczyk, M., Zbinden, A. & Schenke-Layland, K. Organ-specific endothelial cell heterogenicity and its impact on regenerative medicine and biomedical engineering applications. *Adv. Drug Deliv. Rev.* **186,** 114323 (2022).
147. Neill, T., Schaefer, L. & Iozzo, R. V. Decorin - A Guardian from the Matrix. *Am. J. Pathol.* **181,** 380–387 (2012).
148. Brandhorst, D., Brandhorst, H., Layland, S. L., Acreman, S., Schenke-Layland, K. & Johnson, P. R. V. Basement membrane proteins improve human islet survival in hypoxia: Implications for islet inflammation. *Acta Biomater* **137,** 92–102 (2022).
149. Tomaz, R. A., Zacharis, E. D., Bachinger, F., Wurmser, A., Yamamoto, D., Petrus-Reurer, S., Morell, C. M., Dziedzicka, D., Wesley, B. T., Geti, I., Segeritz, C. P., de Brito, M. C., Chhatriwala, M., Ortmann, D., Saeb-Parsy, K. & Vallier, L. Generation of functional hepatocytes by forward programming with nuclear receptors. *Elife* **11,** 1–25 (2022).
150. Lange, L., Hoffmann, D., Schwarzer, A., Ha, T. C., Philipp, F., Lenz, D., Morgan, M. & Schambach, A. Inducible Forward Programming of Human Pluripotent Stem Cells to Hemato-endothelial Progenitor Cells with Hematopoietic Progenitor Potential. *Stem Cell Reports* **14,** 122–137 (2020).
151. Pang, Z. P., Yang, N., Vierbuchen, T., Ostermeier, A., Fuentes, D. R., Yang, T. Q., Citri, A., Sebastiano, V., Marro, S., Südhof, T. C. & Wernig, M. Induction of human neuronal cells by defined transcription factors. *NatureNature* **476,** 220–223 (2012).
152. Chanda, S., Ang, C. E., Davila, J., Pak, C., Mall, M., Lee, Q. Y., Ahlenius, H., Jung, S. W., Südhof, T. C. & Wernig, M. Generation of induced neuronal cells by the single reprogramming factor ASCL1. *Stem Cell Reports* **3,** 282–296 (2014).
153. Pawlowski, M., Ortmann, D., Bertero, A., Tavares, J. M., Pedersen, R. A., Vallier, L. & Kotter, M. R. N. Inducible and Deterministic Forward Programming of Human Pluripotent Stem Cells into Neurons, Skeletal Myocytes, and Oligodendrocytes. *Stem Cell Reports* **8,** 803–812 (2017).
154. Evans, A. L., Dalby, A., Foster, H. R., Howard, D., Waller, A. K., Taimoor, M., Lawrence, M., Mookerjee, S., Lehmann, M., Burton, A., Valdez, J., Thon, J., Italiano, J., Moreau, T. & Ghevaert, C. Transfer to the clinic: Refining forward programming of hPSCs to megakaryocytes for platelet production in bioreactors. *Blood Adv.* **5,** 1977–1990 (2021).
155. Speicher, A. M., Korn, L., Csatari, J., Gonzalez-Cano, L., Heming, M., Thomas, C., Schroeter, C. B., Schafflick, D., Li, X., Gola, L., Engler, A., Kaehne, T., Vallier, L., Meuth, S. G., Horste, G. M. zu, Kovac, S., Wiendl, H., Scholer, H. R. & Pawlowski, M. Deterministic programming of human pluripotent stem cells into microglia facilitates studying their role in health and disease. *Proc. Natl. Acad. Sci. U. S. A.* **119,** 1–11 (2022).
156. Wang, K., Lin, R. Z., Hong, X., Ng, A. H., Lee, C. N., Neumeyer, J., Wang, G., Wang, X., Ma, M., Pu, W. T., Church, G. M. & Melero-Martin, J. M. Robust differentiation of human pluripotent stem cells into endothelial cells via temporal modulation of ETV2 with modified mRNA. *Sci. Adv.* **6,** 1–15 (2020).
157. Li, J., Zhu, Y., Li, N., Wu, T., Zheng, X., Heng, B. chin, Zou, D. & Xu, J. Upregulation of ETV2 Expression Promotes Endothelial Differentiation of Human Dental Pulp Stem Cells. *Cell Transplant.* **30,** 1–11 (2021).
158. Matsuoka, T. A., Kawashima, S., Miyatsuka, T., Sasaki, S., Shimo, N., Katakami, N., Kawamori, D., Takebe, S., Herrera, P. L., Kaneto, H., Stein, R. & Shimomura, I. Mafa enables Pdx1 to effectively convert pancreatic islet progenitors and committed islet α-cells into β-cells in vivo. *Diabetes* **66,** 1293–1300 (2017).
159. Guo, P., Zhang, T., Lu, A., Shiota, C., Huard, M., Whitney, K. E. & Huard, J. Specific reprogramming of alpha cells to insulin-producing cells by short glucagon promoter-driven Pdx1 and MafA. *Mol. Ther. - Methods Clin. Dev.* **28,** 355–365 (2023).
160. Jeyagaran, A., Urbanczyk, M., Layland, S. L., Weise, F. & Schenke-Layland, K. Forward programming of hiPSCs towards beta-like cells using Ngn3, Pdx1, and MafA. *Sci. Rep.* **14,** 13608 (2024).
161. Santeramo, I., Bagnati, M., Harvey, E. J., Hassan, E., Surmacz-Cordle, B., Marshall, D. & Di Cerbo, V. Vector Copy Distribution at a Single-Cell Level Enhances Analytical Characterization of Gene-Modified Cell Therapies. *Mol. Ther. - Methods Clin. Dev.* **17,** 944–956 (2020).
162. Liu, Z., Chen, O., Wall, J. B. J., Zheng, M., Zhou, Y., Wang, L., Ruth Vaseghi, H., Qian, L. & Liu, J. Systematic comparison of 2A peptides for cloning multi-genes in a polycistronic vector. *Sci. Rep.* **7,** 2193 (2017).
163. Poetsch, M. S., Strano, A. & Guan, K. Human Induced Pluripotent Stem Cells: From Cell Origin, Genomic Stability, and Epigenetic Memory to Translational Medicine. *Stem Cells* **40,** 546–555 (2022).
164. Ohi, Y., Qin, H., Hong, C., Blouin, L., Polo, J. M., Guo, T., Qi, Z., Downey, S. L., Manos, P. D., Rossi, D. J., Yu, J., Hebrok, M., Hochedlinger, K., Costello, J. F., Song, J. S. & Ramalho-Santos, M. Incomplete DNA methylation underlies a transcriptional memory of somatic cells in human iPS cells. *Nat. Cell Biol.* **13,** 541–549 (2011).
165. Hu, S., Zhao, M. T., Jahanbani, F., Shao, N. Y., Lee, W. H., Chen, H., Snyder, M. P. & Wu, J. C. Effects of cellular origin on differentiation of human induced pluripotent stem cell-derived endothelial cells. *J. Clin. Invest.* **1,** 1–12 (2016).
166. Stock, R., Vogel, S., Mau-Holzmann, U. A., Kriebel, M., Wüst, R., Fallgatter, A. J. & Volkmer, H. Generation and characterization of human induced pluripotent stem cells lines from four patients diagnosed with schizophrenia and one healthy control. *Stem Cell Res.* **48,** 101961 (2020).
167. Huang, X., Gu, W., Zhang, J., Lan, Y., Colarusso, J. L., Li, S., Pertl, C., Lu, J., Kim, H., Zhu, J., Breault, D. T., Sévigny, J. & Zhou, Q. Stomach-derived human insulin-secreting organoids restore glucose homeostasis. *Nat. Cell Biol.* **25,** 778–786 (2023).
168. Ariyachet, C., Alessio Tovaglieri, Xiang, G., Lu, J., Shah, M. S., Richmond, C. A., Verbeke, C., Melton1, D. A., Stanger, B. Z., Mooney, D., Shivdasani, R. A., Mahony, S., Xia, Q., Breault, D. T. & Zhou, Q. Reprogrammed Stomach Tissue as a Renewable Source of Functional β Cells for Blood Glucose Regulation. *Cell Stem Cell* **176,** 139–148 (2017).
169. Egozi, A., Llivichuzhca-Loja, D., McCourt, B. T., Bahar Halpern, K., Farack, L., An, X., Wang, F., Chen, K., Konnikova, L. & Itzkovitz, S. Insulin is expressed by enteroendocrine cells during human fetal development. *Nat. Med.* **27,** 2104–2107 (2021).

170. Fontcuberta-PiSunyer, M., García-Alamán, A., Prades, È., Téllez, N., Alves-Figueiredo, H., Ramos-Rodríguez, M., Enrich, C., Fernandez-Ruiz, R., Cervantes, S., Clua, L., Ramón-Azcón, J., Broca, C., Wojtusciszyn, A., Montserrat, N., Pasquali, L., Novials, A., Servitja, J. M., Vidal, J., Gomis, R. & Gasa, R. Direct reprogramming of human fibroblasts into insulin-producing cells using transcription factors. *Commun. Biol.* **6,** 1–15 (2023).
171. Del Toro-Arreola, A., Robles-Murillo, A. K., Daneri-Navarro, A. & Rivas-Carrillo, J. D. The role of endothelial cells on islet function and revascularization after islet transplantation. *Organogenesis* **12,** 28–32 (2016).
172. Zbinden, A., Layland, S. L., Urbanczyk, M., Carvajal Berrio, D. A., Marzi, J., Zauner, M., Hammerschmidt, A., Brauchle, E. M., Sudrow, K., Fink, S., Templin, M., Liebscher, S., Klein, G., Deb, A., Duffy, G. P., Crooks, G. M., Eble, J. A., Mikkola, H. K. A., Nsair, A., Seifert, M. & Schenke-Layland, K. Nidogen-1 Mitigates Ischemia and Promotes Tissue Survival and Regeneration. *Adv. Sci.* **8,** 2002500 (2021).
173. Crisóstomo, J., Pereira, A. M., Bidarra, S. J., Gonçalves, A. C., Granja, P. L., Coelho, J. F. J., Barrias, C. C. & Seiça, R. ECM-enriched alginate hydrogels for bioartificial pancreas: an ideal niche to improve insulin secretion and diabetic glucose profile. *J. Appl. Biomater. Funct. Mater.* **17,** 2280800019848923 (2019).
174. Cheng, J., Raghunath, M., Whitelock, J. & Poole-Warren, L. Matrix components and scaffolds for sustained islet function. *Tissue Eng. Part B, Rev.* **17,** 235–247 (2011).
175. Brandhorst, D. & Et al. Recombinant Nidogen-1 Significantly Improves Survival of Hypoxic Human Islets. *J. Nuff. Dep. Surg. Sci.* **1,** (2020).
176. Nagata, N., Gu, Y., Hori, H., Balamurugan, A. N., Touma, M., Kawakami, Y., Wang, W., Baba, T. T., Satake, A., Nozawa, M., Tabata, Y. & Inoue, K. Evaluation of Insulin Secretion of Isolated Rat IsletsCultured in Extracellular Matrix. *Cell Transplant.* **10,** 447–451 (2001).
177. Pinkse, G. G. M., Bouwman, W. P., Jiawan-lalai, R., Terpstra, O. T., Bruijn, J. A. & Heer, E. De. Integrin Signaling via RGD Peptides and Anti-B1 Antibodies Confers Resistance to Apoptosis in Islets of Langerhans. *Diabetes* **55,** 312–317 (2006).
178. Krishnamurthy, M., Li, J., Al-Masri, M. & Wang, R. Expression and function of αβ1 integrins in pancretic beta (INS-1) cells. *J. Cell Commun. Signal.* **2,** 67–79 (2008).
179. Stephens, C. H., Orr, K. S., Acton, A. J., Tersey, S. A., Mirmira, R. G., Considine, R. V. & Voytik-Harbin, S. L. In situ type I oligomeric collagen macroencapsulation promotes islet longevity and function in vitro and in vivo. *Am. J. Physiol. - Endocrinol. Metab.* **315,** E425–E734 (2018).
180. Liu, J., Liu, S., Chen, Y., Zhao, X., Lu, Y. & Cheng, J. Functionalized self-assembling peptide improves INS-1 β-cell function and proliferation via the integrin/FAK/ERK/cyclin pathway. *Int. J. Nanomedicine* **10,** 3519–3531 (2015).
181. Sojoodi, M., Farrokhi, A., Moradmand, A. & Baharvand, H. Enhanced maintenance of rat islets of Langerhans on laminin-coatedelectrospun nanofibrillar matrix in vitro. *Cell Biol. Int.* **37,** 370–379 (2013).
182. Jalili, R. B., Rezakhanlou, A. M., Hosseini-Tabatbaei, A., Ao, Z., Warnock, G. L., Ghahary, A., Hosseini-Tabatabaei, A., Ao, Z., Warnock, G. L. & Ghahary, A. Fibroblast populated collagen matrix promotes islet survival and reduces the number of islets required for diabetes reversal. *J. Cell. Physiol.* **226,** 1813–1819 (2011).
183. Salvay, D. M., Rives, C. B., Zhang, X., Chen, F., Kaufman, D. B., Lowe, W. L., Shea, L. D., Lowe Jr., W. L., Shea, L. D., Lowe, W. L., Shea, L. D., Jr, W. L. L. & Shea, L. D. Extracellular Matrix Protein-Coated Scaffolds Promote the Reversal of Diabetes After Extrahepatic Islet Transplantation. *Transplantation* **85,** 1456–1464 (2008).
184. Atchison, N. A., Fan, W., Papas, K. K., Hering, B. J., Tsapatsis, M. & Kokkoli, E. Binding of the fibronectin-mimetic peptide, PR_b, to α5β1 on pig islet cells increases fibronectin production and facilitates internalization of PR_b functionalized liposomes. *Langmuir* **26,** 14081–14088 (2010).
185. Kuehn, C., Dubiel, E. A., Sabra, G. & Vermette, P. Culturing INS-1 cells on CDPGYIGSR-, RGD- and fibronectin surfaces improves insulin secretion and cell proliferation. *Acta Biomater.* **8,** 619–626 (2012).
186. Hamamoto, Y., Fujimoto, S., Inada, A., Takehiro, M., Nabe, K., Shimono, D., Kajikawa, M., Fujita, J., Yamada, Y. & Seino, Y. Beneficial effect of pretreatment of islets with fibronectin on glucose tolerance after islet transplantation. *Horm. Metab. Res.* **35,** 460–465 (2003).
187. Wynn, T. A. & Ramalingam, T. R. Mechanisms of fibrosis: therapeutic translation for fibrotic disease. *Nat. Med.* **18,** 1028–40 (2012).
188. Ricard-Blum, S., Baffet, G. & Théret, N. Molecular and tissue alterations of collagens in fibrosis. *Matrix Biol.* **68–69,** 122–149 (2018).
189. Menke, A. & Adler, G. TGFbeta-induced Fibrogenesis of the Pancreas. *Int. J. Gastrointest. Cancer* **31,** 41–46 (2002).
190. Hinderer, S., Sudrow, K., Schneider, M., Holeiter, M., Layland, S. L., Seifert, M. & Schenke-Layland, K. Surface functionalization of electrospun scaffolds using recombinant human decorin attracts circulating endothelial progenitor cells. *Sci. Rep.* **8,** 110 (2018).
191. Urbanczyk, M., Jeyagaran, A., Zbinden, A., Lu, C. en, Marzi, J., Kuhlburger, L., Nahnsen, S., Layland, S. L., Duffy, G. & Schenke-Layland, K. Decorin improves human pancreatic β-cell function and regulates ECM expression in vitro. *Matrix Biol.* **115,** 160–183 (2023).
192. Sakhneny, L., Epshtein, A. & Landsman, L. Pericytes contribute to the islet basement membranes to promote beta-cell gene expression. *Sci. Rep.* **11,** 2378 (2021).
193. Naba, A., Clauser, K. R., Mani, D. R., Carr, S. A. & Hynes, R. O. Quantitative proteomic profiling of the extracellular matrix of pancreatic islets during the angiogenic switch and insulinoma progression. *Sci. Rep.* **7,** 40495 (2017).
194. Svärd, J., Røst, T. H., Sommervoll, C. E. N., Haugen, C., Gudbrandsen, O. A., Mellgren, A. E., Rødahl, E., Fernø, J., Dankel, S. N., Sagen, J. V. & Mellgren, G. Absence of the proteoglycan decorin reduces glucose tolerance in overfed male mice. *Sci. Rep.* **9,** 4614 (2019).
195. Border, W. A., Noble, N. A., Yamamoto, T., Harper, J. R., Yamaguchi, Y. u, Pierschbacher, M. D. & Ruoslahti, E. Natural inhibitor of transforming growth factor-beta protects against scarring in experimental kidney disease. *Nature* **360,** 361–4 (1992).
196. Schaefer, L., Macakova, K., Raslik, I., Micegova, M., Gröne, H.-J., Schönherr, E., Robenek, H., Echtermeyer, F. G., Grässel, S., Bruckner, P., Schaefer, R. M., Iozzo, R. V. & Kresse, H. Absence of Decorin Adversely Influences Tubulointerstitial Fibrosis of the Obstructed Kidney by Enhanced Apoptosis and Increased Inflammatory Reaction. *Am.*

J. Pathol. **160,** 1181–1191 (2002).
197. Groeneveld, T. W. L., Oroszlán, M., Owens, R. T., Faber-Krol, M. C., Bakker, A. C., Arlaud, G. J., McQuillan, D. J., Kishore, U., Daha, M. R. & Roos, A. Interactions of the Extracellular Matrix Proteoglycans Decorin and Biglycan with C1q and Collectins. *J. Immunol.* **175,** 4715–4723 (2005).
198. Nolfi-Donegan, D., Braganza, A. & Shiva, S. Mitochondrial electron transport chain: Oxidative phosphorylation, oxidant production, and methods of measurement. *Redox Biol.* **37,** 101674 (2020).
199. Wiederkehr, A. & Wollheim, C. B. Minireview: implication of mitochondria in insulin secretion and action. *Endocrinology* **147,** 2643–2649 (2006).
200. Kaufman, B. A., Li, C. & Soleimanpour, S. A. Mitochondrial regulation of β-cell function: maintaining the momentum for insulin release. *Mol Asp. Med* **42,** 91–104 (2015).
201. Malmgreh, S., Nicholls, D. G., Taneera, J., Bacos, K., Koeck, T., Tamaddon, A., Wibom, R., Groop, L., Ling, C., Mulder, H. & Sharoyko, V. V. Tight coupling between glucose and mitochondrial metabolism in clonal β-cells is required for robust insulin secretion. *J. Biol. Chem.* **284,** 32395–32404 (2009).
202. Ritov, V. B., Menshikova, E. V., He, J., Ferrell, R. E., Goodpaster, B. H. & Kelley, D. E. Deficiency of subsarcolemmal mitochondria in obesity and type 2 diabetes. *Diabetes* **54,** 8–14 (2005).
203. Shrestha, N., Reinert, R. B. & Qi, L. Endoplasmic Reticulum Protein Quality Control in β Cells. *Semin. Cell Dev. Biol.* **103,** 59–67 (2020).
204. Yamaguchi, S., Ishihara, H., Yamada, T., Tamura, A., Usui, M., Tominaga, R., Munakata, Y., Satake, C., Katagiri, H., Tashiro, F., Aburatani, H., Tsukiyama-Kohara, K., Miyazaki, J., Sonenberg, N. & Oka, Y. ATF4-Mediated Induction of 4E-BP1 Contributes to Pancreatic β Cell Survival under Endoplasmic Reticulum Stress. *Cell Metab.* **7,** 269–276 (2008).
205. Fonseca, S. G., Gromada, J. & Urano, F. Endoplasmic reticulum stress and pancreatic β-cell death. *Trends Endocrinol. Metab.* **22,** 266–274 (2011).
206. Rabhi, N., Salas, E., Froguel, P. & Annicotte, J. S. Role of the unfolded protein response in β cell compensation and failure during diabetes. *J. Diabetes Res.* **2014,** 795171 (2014).
207. Wang, J., Chen, Y., Yuan, Q., Tang, W., Zhang, X. & Osei, K. Control of Precursor Maturation and Disposal Is an Early Regulative Mechanism in the Normal Insulin Production of Pancreatic β-Cells. *PLoS One* **6,** e19446 (2011).
208. Sun, J., Cui, J., He, Q., Chen, Z., Arvan, P. & Liu, M. Proinsulin misfolding and endoplasmic reticulum stress during the development and progression of diabetes☆. *Mol. Aspects Med.* **42,** 105–118 (2015).
209. Liu, M., Li, Y., Cavener, D. & Arvan, P. Proinsulin Disulfide Maturation and Misfolding in the Endoplasmic Reticulum. *J. Biol. Chem.* **280,** 13209–13212 (2005).
210. El Ouaamari, A., Zhou, J.-Y., Liew, C. W., Shirakawa, J., Dirice, E., Gedeon, N., Kahraman, S., De Jesus, D. F., Bhatt, S., Kim, J.-S., Clauss, T. R. W., Camp, D. G., Smith, R. D., Qian, W.-J. & Kulkarni, R. N. Compensatory Islet Response to Insulin Resistance Revealed by Quantitative Proteomics. *J. Proteome Res.* **14,** 3111–3122 (2015).
211. Cockcroft, S. & Carvou, N. Biochemical and biological functions of class I phosphatidylinositol transfer proteins. *Biochim. Biophys. Acta - Mol. Cell Biol. Lipids* **1771,** 677–691 (2007).
212. Blunsom, N. J. & Cockcroft, S. Phosphatidylinositol synthesis at the endoplasmic reticulum. *Biochim. Biophys. Acta - Mol. Cell Biol. Lipids* **1865,** 158471 (2020).
213. Mayinger, P. Phosphoinositides and vesicular membrane traffic. *Biochim. Biophys. Acta - Mol. Cell Biol. Lipids* **1821,** 1104–1113 (2012).
214. MacDonald, M. J., Ade, L., Ntambi, J. M., Ansari, I. U. H. & Stoker, S. W. Characterization of phospholipids in insulin secretory granules and mitochondria in pancreatic beta cells and their changes with glucose stimulation. *J. Biol. Chem.* **290,** 11075–11092 (2015).
215. Zbinden, A., Marzi, J., Schlünder, K., Probst, C., Urbanczyk, M., Black, S., Brauchle, E. M., Layland, S. L., Kraushaar, U., Duffy, G., Schenke-Layland, K. & Loskill, P. Non-invasive marker-independent high content analysis of a microphysiological human pancreas-on-a-chip model. *Matrix Biol.* **85–86,** 205–220 (2020).
216. Hofmann, S. M., Zhou, L., Perez-Tilve, D., Greer, T., Grant, E., Wancata, L., Thomas, A., Pfluger, P. T., Basford, J. E., Gilham, D., Herz, J., Tschöp, M. H. & Hui, D. Y. Adipocyte LDL receptor-related protein-1 expression modulates postprandial lipid transport and glucose homeostasis in mice. *J. Clin. Invest.* **117,** 3271–3282 (2007).
217. Salicioni, A. M., Mizelle, K. S., Loukinova, E., Mikhailenko, I., Strickland, D. K. & Gonias, S. L. The low density lipoprotein receptor-related protein mediates fibronectin catabolism and inhibits fibronectin accumulation on cell surfaces. *J. Biol. Chem.* **277,** 16160–16166 (2002).
218. Brandan, E., Retamal, C., Cabello-Verrugio, C. & Marzolo, M.-P. The Low Density Lipoprotein Receptor-related Protein Functions as an Endocytic Receptor for Decorin. *J. Biol. Chem.* **281,** 31562–31571 (2006).
219. Ye, R., Gordillo, R., Shao, M., Onodera, T., Chen, Z., Chen, S., Lin, X., SoRelle, J. A., Li, X., Tang, M., Keller, M. P., Kuliawat, R., Attie, A. D., Gupta, R. K., Holland, W. L., Beutler, B., Herz, J. & Scherer, P. E. Intracellular lipid metabolism impairs β cell compensation during diet-induced obesity. *J. Clin. Invest.* **128,** 1178–1189 (2018).
220. Shian Huang, S., M. Leal, S., Chen, C.-L., Liu, I.-H. & San Huang, J. Identification of insulin receptor substrate proteins as key molecules for the TβR-V/LRP-1-mediated growth inhibitory signaling cascade in epithelial and myeloid cells. *FASEB J.* **18,** 1719–1721 (2004).
221. Sjoholm, A. & Hellerstrom, C. TGF-beta stimulates insulin secretion and blocks mitogenic response of pancreatic beta-cells to glucose. *Am. J. Physiol. Physiol.* **260,** C1046–C1051 (1991).
222. Lee, J. H., Lee, J. H. & Rane, S. G. TGF-β Signaling in Pancreatic Islet β Cell Development and Function. *Endocrinol. (United States)* **162,** 1–10 (2021).
223. Bergsten, P. Slow and fast oscillations of cytoplasmic Ca2+ in pancreatic islets correspond to pulsatile insulin release. *Am. J. Physiol. Metab.* **268,** E282–E287 (1995).
224. Varone, A., Xylas, J., Quinn, K. P., Pouli, D., Sridharan, G., McLaughlin-Drubin, M. E., Alonzo, C., Lee, K., Münger, K. & Georgakoudi, I. Endogenous Two-Photon Fluorescence Imaging Elucidates Metabolic Changes Related to Enhanced Glycolysis and Glutamine Consumption in Precancerous Epithelial Tissues. *Cancer Res.* **74,** 3067–3075 (2014).
225. Mullarky, E. & Cantley, L. C. in *Innov. Med.* 3–23 (Springer Japan, 2015). doi:10.1007/978-4-431-55651-0_1
226. Zbinden, A., Carvajal Berrio, D. A., Urbanczyk, M., Layland, S. L., Bosch, M., Fliri, S., Lu, C. en, Jeyagaran, A., Loskill,

P., Duffy, G. P. & Schenke-Layland, K. Fluorescence lifetime metabolic mapping of hypoxia-induced damage in pancreatic pseudo-islets. *J. Biophotonics* **13,** 1–13 (2020).
227. Dionne, K. E., Colton, C. K. & Yarmush, M. L. Effect of hypoxia on insulin secretion by isolated rat and canine islets of Langerhans. *Diabetes* **42,** 12–21 (1993).
228. Semenza, G. L. Signal transduction to hypoxia-inducible factor 1. *Biochem. Pharmacol.* **64,** 993–998 (2002).
229. Piret, J. P., Mottet, D., Raes, M. & Michiels, C. Is HIF-1α a pro- or an anti-apoptotic protein? *Biochem. Pharmacol.* **64,** 889–892 (2002).
230. D'Hoker, J., De Leu, N., Heremans, Y., Baeyens, L., Minami, K., Ying, C., Lavens, A., Chintinne, M., Stangé, G., Magenheim, J., Swisa, A., Martens, G., Pipeleers, D., van de Casteele, M., Seino, S., Keshet, E., Dor, Y. & Heimberg, H. Conditional Hypovascularization and Hypoxia in Islets Do Not Overtly Influence Adult β-Cell Mass or Function. *Diabetes* **62,** 4165–4173 (2013).
231. Sankar, K. S., Altamentova, S. M. & Rocheleau, J. V. Hypoxia induction in cultured pancreatic islets enhances endothelial cell morphology and survival while maintaining beta-cell function. *PLoS One* **14,** e0222424 (2019).
232. Greijer, A. E. & van der Wall, E. The role of hypoxia inducible factor 1 (HIF-1) in hypoxia induced apoptosis: Figure 1. *J. Clin. Pathol.* **57,** 1009–1014 (2004).
233. Skala, M. C., Riching, K. M., Gendron-Fitzpatrick, A., Eickhoff, J., Eliceiri, K. W., White, J. G. & Ramanujam, N. In vivo multiphoton microscopy of NADH and FAD redox states, fluorescence lifetimes, and cellular morphology in precancerous epithelia. *PNAS* **104,** 19494–19499 (2007).
234. Lum, J. J., Bui, T., Gruber, M., Gordan, J. D., DeBerardinis, R. J., Covello, K. L., Simon, M. C. & Thompson, C. B. The transcription factor HIF-1α plays a critical role in the growth factor-dependent regulation of both aerobic and anaerobic glycolysis. *Genes Dev.* **21,** 1037–1049 (2007).
235. Rabinowitz, J. D. & Enerbäck, S. Lactate: the ugly duckling of energy metabolism. *Nat. Metab.* **2,** 566–571 (2020).
236. Bower, A. J., Marjanovic, M., Zhao, Y., Li, J., Chaney, E. J. & Boppart, S. A. Label-free in vivo cellular-level detection and imaging of apoptosis. *J. Biophotonics* **10,** 143–150 (2017).
237. Wang, H.-W., Gukassyan, V., Chen, C.-T., Wei, Y.-H., Guo, H.-W., Yu, J.-S. & Kao, F.-J. Differentiation of apoptosis from necrosis by dynamic changes of reduced nicotinamide adenine dinucleotide fluorescence lifetime in live cells. *J. Biomed. Opt.* **13,** 054011 (2008).
238. Zhao, Y., Marjanovic, M., Chaney, E. J., Graf, B. W., Mahmassani, Z., Boppart, M. D. & Boppart, S. A. Longitudinal label-free tracking of cell death dynamics in living engineered human skin tissue with a multimodal microscope. *Biomed. Opt. Express* **5,** 3699 (2014).
239. Bower, A. J., Sorrells, J. E., Li, J., Marjanovic, M., Barkalifa, R. & Boppart, S. A. Tracking metabolic dynamics of apoptosis with high-speed two-photon fluorescence lifetime imaging microscopy. *Biomed. Opt. Express* **10,** 6408–6421 (2019).
240. Tait, S. W. G. & Green, D. R. Mitochondria and cell death: Outer membrane permeabilization and beyond. *Nat. Rev. Mol. Cell Biol.* **11,** 621–632 (2010).
241. Rogers, C., Erkes, D. A., Nardone, A., Aplin, A. E., Fernandes-Alnemri, T. & Alnemri, E. S. Gasdermin pores permeabilize mitochondria to augment caspase-3 activation during apoptosis and inflammasome activation. *Nat. Commun.* **10,** 1689 (2019).
242. Levitt, J. M., Baldwin, A., Papadakis, A., Puri, S., Xylas, J., Münger, K. & Georgakoudi, I. Intrinsic fluorescence and redox changes associated with apoptosis of primary human epithelial cells. *J. Biomed. Opt.* **11,** 064012 (2006).
243. Cnop, M., Hughes, S. J., Igoillo-Esteve, M., Hoppa, M. B., Sayyed, F., Van De Laar, L., Gunter, J. H., De Koning, E. J. P., Walls, G. V., Gray, D. W. G., Johnson., P. R. V., Hansen., B. C., Morris, J. F., Pipeleers-Marichal, M., Cnop, I. & Clark, A. The long lifespan and low turnover of human islet beta cells estimated by mathematical modeling of lipofuscin accumulation. *Diabetologia* **53,** 321–330 (2010).
244. Di Guardo, G. Lipofuscin, lipofuscin-like pigments and autofluorescence. *Eur. J. Histochem.* **59,** (2015).
245. Azzarello, F., Pesce, L., De Lorenzi, V., Ferri, G., Tesi, M., Del Guerra, S., Marchetti, P. & Cardarelli, F. Single-cell imaging of α and β cell metabolic response to glucose in living human Langerhans islets. *Commun. Biol.* **5,** 1232 (2022).
246. Wang, Z., Gurlo, T., Matveyenko, A. V., Elashoff, D., Wang, P., Rosenberger, M., Junge, J. A., Stevens, R. C., White, K. L., Fraser, S. E. & Butler, P. C. Live-cell imaging of glucose-induced metabolic coupling of β and α cell metabolism in health and type 2 diabetes. *Commun. Biol.* **4,** 594 (2021).
247. Barile, M., Anna Giancaspero, T., Brizio, C., Panebianco, C., Indiveri, C., Galluccio, M., Vergani, L., Eberini, I. & Gianazza, E. Biosynthesis of Flavin Cofactors in Man: Implications in Health and Disease. *Curr. Pharm. Des.* **19,** 2649–2675 (2013).
248. Berger, C. & Zdzieblo, D. Glucose transporters in pancreatic islets. *Pflugers Arch.* **472,** 1249–1272 (2020).
249. Pingitore, A., Ruz-Maldonado, I., Liu, B., Huang, G. C., Choudhary, P. & Persaud, S. J. Dynamic Profiling of Insulin Secretion and ATP Generation in Isolated Human and Mouse Islets Reveals Differential Glucose Sensitivity. *Cell. Physiol. Biochem.* **44,** 1352–1359 (2017).
250. Chen, J.-Q. & Russo, J. Dysregulation of glucose transport, glycolysis, TCA cycle and glutaminolysis by oncogenes and tumor suppressors in cancer cells. *Biochim. Biophys. Acta - Rev. Cancer* **1826,** 370–384 (2012).
251. Zehetner, J., Danzer, C., Collins, S., Eckhardt, K., Gerber, P. A., Ballschmieter, P., Galvanovskis, J., Shimomura, K., Ashcroft, F. M., Thorens, B., Rorsman, P. & Krek, W. pVHL is a regulator of glucose metabolism and insulin secretion in pancreatic β cells. *Genes Dev.* **22,** 3135–3146 (2008).
252. Puri, S., Cano, D. A. & Hebrok, M. A Role for von Hippel-Lindau Protein in Pancreatic β-Cell Function. *Diabetes* **58,** 433–441 (2009).
253. Baker, M., Petasny, M., Taqatqa, N., Bentata, M., Kay, G., Engal, E., Nevo, Y., Siam, A., Dahan, S. & Salton, M. KDM3A regulates alternative splicing of cell-cycle genes following DNA damage. *RNA* **27,** 1353–1362 (2021).
254. Ikeda, S., Kitadate, A., Abe, F., Takahashi, N. & Tagawa, H. Hypoxia-inducible KDM3A addiction in multiple myeloma. *Blood Adv.* **2,** 323–334 (2018).
255. Westermeier, F., Holyoak, T., Asenjo, J. L., Gatica, R., Nualart, F., Burbulis, I. & Bertinat, R. Gluconeogenic Enzymes in β-Cells: Pharmacological Targets for Improving Insulin Secretion. *Trends Endocrinol. Metab.* **30,** 520–531 (2019).

256. Merrins, M. J., Van Dyke, A. R., Mapp, A. K., Rizzo, M. A. & Satin, L. S. Direct Measurements of Oscillatory Glycolysis in Pancreatic Islet β-Cells Using Novel Fluorescence Resonance Energy Transfer (FRET) Biosensors for Pyruvate Kinase M2 Activity. *J. Biol. Chem.* **288,** 33312–33322 (2013).
257. Yáñez, A. J., Bertinat, R., Spichiger, C., Carcamo, J. G., de los Angeles García, M., Concha, I. I., Nualart, F. & Slebe, J. C. Novel expression of liver FBPase in Langerhans islets of human and rat pancreas. *J. Cell. Physiol.* **205,** 19–24 (2005).
258. Zhang, Y., Xie, Z., Zhou, G., Zhang, H., Lu, J. & Zhang, W. J. Fructose-1,6-Bisphosphatase Regulates Glucose-Stimulated Insulin Secretion of Mouse Pancreatic β-Cells. *Endocrinology* **151,** 4688–4695 (2010).
259. Kebede, M., Favaloro, J., Gunton, J. E., Laybutt, D. R., Shaw, M., Wong, N., Fam, B. C., Aston-Mourney, K., Rantzau, C., Zulli, A., Proietto, J. & Andrikopoulos, S. Fructose-1,6-Bisphosphatase Overexpression in Pancreatic β-Cells Results in Reduced Insulin Secretion. *Diabetes* **57,** 1887–1895 (2008).
260. Yang, J., Kalhan, S. C. & Hanson, R. W. What is the metabolic role of phosphoenolpyruvate carboxykinase? *J. Biol. Chem.* **284,** 27025–9 (2009).
261. Yu, S., Meng, S., Xiang, M. & Ma, H. Phosphoenolpyruvate carboxykinase in cell metabolism: Roles and mechanisms beyond gluconeogenesis. *Mol. Metab.* **53,** 101257 (2021).
262. Xiang, J., Wang, K. & Tang, N. PCK1 dysregulation in cancer: Metabolic reprogramming, oncogenic activation, and therapeutic opportunities. *Genes Dis.* **10,** 101–112 (2023).
263. Xiang, J., Zhang, Y., Tuo, L., Liu, R., Gou, D., Liang, L., Chen, C., Xia, J., Tang, N. & Wang, K. Transcriptomic changes associated with PCK1 overexpression in hepatocellular carcinoma cells detected by RNA-seq. *Genes Dis.* **7,** 150–159 (2020).
264. Tang, Y., Zhang, Y., Wang, C., Sun, Z., Li, L., Cheng, S. & Zhou, W. Overexpression of PCK1 Gene Antagonizes Hepatocellular Carcinoma Through the Activation of Gluconeogenesis and Suppression of Glycolysis Pathways. *Cell. Physiol. Biochem.* **47,** 344–355 (2018).

Acknowledgements

I am grateful to have so many wonderful people in my life that supported me and my goals over the past few years. Firstly, I am extremely thankful for my supervisor, Prof. Dr. Katja Schenke-Layland, whose expertise and motivation allowed for my growth as a scientist. This thesis would not have been possible without her constant support, patience, and trust in me. I would also like to thank Shannon Lee Layland for his continuous moral support and reassurance, particularly during my moments of self-doubt and confusion. I would like to express my gratitude to Frank Weise for his patience and encouragement as he guided me at the beginning of my PhD while I navigated new experimental techniques and life in Germany.

I don't know if I can thank the Schenke-Layland Lab enough for their encouragement and strength. They very quickly and easily became my family here with everyone looking out for each other and sharing so many memorable moments both in and out of the lab. In particular, I would like to thank Daniel Carvajal-Berrio for his microscopy expertise and instant facetious comments to lighten the mood. I would like to thank Simone Liebscher for her expert opinion and assistance with immunofluorescence staining, especially when it felt like no antibody would work. I would also like to thank Dr. Julia Marzi, Dr. Chuan-En Lu, and Dr. Lucas Becker for constructive scientific discussions throughout my PhD. A special thanks to Julia Alber, Emanuel Behling, Teresa Baldissera, Sasha Mariianats, and Sema Demir for all the laughter, sarcasm, and moral support these past few years. I cannot thank you all enough for helping resolve the experiments that failed and celebrating the experiments that worked as if it were your own. I would also like to thank Diana Holzer for her help with all the administrative work and making sure everything ran smoothly.

I would like to thank my family, Amma, Appa, Archana, Polo, and Max, for always supporting my decisions and encouraging me to trust my gut. I could not have had this kind of curiosity or the confidence to pursue it without your backing. Last but not least, I would like to express my gratitude to the donors and their families who allowed us to improve our understanding of islet function and biology, and made this thesis possible.

Declaration

Ich erkläre hiermit, dass ich die zur Promotion eingereichte Arbeit mit dem Titel *“Bioengineering approaches to improve islet transplantation outcomes for the treatment of type one diabetes mellitus*” selbstständig verfasst, nur die angegebenen Quellen und Hilfsmittel benutzt und wörtlich oder inhaltlich übernommene Zitate also solche gekennzeichnet habe. Ich erkläre, dass die Richtlinien zur Sicherung guter wissenschaftlicher Praxis der Universität Tübingen beachtet wurden. Ich versichere an Eides statt, dass diese Angaben wahr sind und dass ich nichts verschwiegen habe. Mir ist bekannt, dass die falsche Angabe einer Versicherung an Eides statt mit Freiheitsstrafe bis zu drei Jahren oder mit Geldstrafe bestraft wird.

Tübingen, 23.09.2024

Appendices

Appendix I

www.nature.com/scientificreports

scientific reports

Check for updates

OPEN

Forward programming of hiPSCs towards beta-like cells using Ngn3, Pdx1, and MafA

Abiramy Jeyagaran[1], Max Urbanczyk[1], Shannon L. Layland[1,2], Frank Weise[3] & Katja Schenke-Layland[1,3]✉

Transplantation of stem cell-derived β-cells is a promising therapeutic advancement in the treatment of type 1 diabetes mellitus. A current limitation of this approach is the long differentiation timeline that generates a heterogeneous population of pancreatic endocrine cells. To address this limitation, an inducible lentiviral overexpression system of mature β-cell markers was introduced into human induced-pluripotent stem cells (hiPSCs). Following the selection of the successfully transduced hiPSCs, the cells were treated with doxycycline in the pancreatic progenitor induction medium to support their transition toward the pancreatic lineage. Cells cultured with doxycycline presented the markers of interest, NGN3, PDX1, and MAFA, after five days of culture, and glucose-stimulated insulin secretion assays demonstrated that the cells were glucose-responsive in a monolayer culture. When cultured as a spheroid, the markers of interest and insulin secretion in a static glucose-stimulated insulin secretion assay were maintained; however, insulin secretion upon consecutive glucose challenges was limited. Comparison to human fetal and adult donor tissues identified that although the hiPSC-derived spheroids present similar markers to adult insulin-producing cells, they are functionally representative of fetal development. Together, these results suggest that with optimization of the temporal expression of these markers, forward programming of hiPSCs towards insulin-producing cells could be a possible alternative for islet transplantation.

Pancreatic islets of Langerhans are the functional cells of the endocrine pancreas responsible for the maintenance of blood glucose homeostasis[1,2]. In type 1 diabetes, the β-cells, the insulin-producing cells, are lost as a result of an autoimmune attack, leading to the dysregulation of blood glucose levels[3,4]. Continuous monitoring of blood glucose levels and administration of appropriate levels of exogenous insulin is the gold standard treatment for many patients suffering from diabetes; however, there remains the risk of over- and/or under-administering the amount of insulin which calls for more endogenous maintenance of blood glucose such as islet transplantation[5]. There have been numerous advances in islet transplantation approaches in recent years to treat patients with type 1 diabetes including protecting transplanted cells from the host's immune system and utilizing new sources of β-cells to be transplanted[6]. Of great interest are stem cell-derived β-cells that can act as a continuous source of β-cells for the high demand of endocrine replacement therapy.

Recent advances in studying pancreatic development has improved our understanding of what biochemical and biophysical cues are required to signal stem cells to differentiate towards β-cells[6]. Stage-based differentiation using consecutive incorporation and exclusion of growth factors and / or signalling molecules have been successful in differentiating human embryonic stem cells (hESCs) and human induced pluripotent stem cells (hiPSCs) into glucose-responsive insulin-producing β-cells[7,8]. Through the years, there have been updates to the differentiation protocol where similar culture medium recipes are used with slight changes in timing and concentration of certain growth factors, or cell culture platforms (2-dimensional (2D) vs. 3-dimensional (3D))[9–16]. Along with selection of cells presenting pancreatic progenitor markers at the different stages of differentiation, these protocols have been improved to achieve increased differentiation efficiency of stem cells into β-cells over a month-long period, where they could be further matured in vivo in mice or in vitro through 3D cultures in bioreactors[16,17]. This maturation process and expression of maturation markers are extremely important for the glucose-responsive behaviour of β-cells; however, it is time-consuming and can result in a heterogeneous cell

[1]Institute of Biomedical Engineering, Department for Medical Technologies and Regenerative Medicine, Eberhard Karls University Tübingen, 72076 Tübingen, Germany. [2]Department of Women's Health, Eberhard Karls University, 72076 Tübingen, Germany. [3]NMI Natural and Medical Sciences Institute at the University Tübingen, 72770 Reutlingen, Germany. ✉email: katja.schenke-layland@uni-tuebingen.de

population. Interestingly, overexpression of mature cell markers has also been used to direct human pluripotent stem cells (hPSCs) towards a desired lineage. Through overexpression of cell-specific markers in hPSCs, researchers have essentially reprogrammed or directed the differentiation of multiple cell types including hepatocytes[18], hematoendothelial cells[19], neurons[20–22], skeletal myocytes[22], oligodendrocytes[22], megakaryocytes[23], microglia[24], and endothelial cells[25,26]. This suggests that similar methods can be used to improve the differentiation efficiency of hiPSCs into β-cells.

Extensive investigation of pancreas development in mice allowed for the identification of different combinations of transcription factor expression required for the specification of various pancreatic cells[27,28]. Interestingly, the adenoviral transfection of three specific transcription factors, NGN3, PDX1, and MAFA were sufficient to reprogram mouse[29] and rat[30,31] pancreatic exocrine tissues to insulin-producing β-cells in vivo. Furthermore, this was shown to be sufficient in preventing hyperglycemic episodes in diabetic mice. A similar approach was also successful in reprogramming murine hepatocytes such that they expressed the three markers as well as insulin and were capable of restoring glucose homeostasis in diabetic mice[32–34]. Interestingly, expression of PDX1 and MAFA in murine α-cells was also found to be sufficient to reprogram them into insulin-producing β-cells *in vivo*[35,36]. The expression of these three genes has also been shown to improve differentiation efficiency of mouse ESCs[37] and hiPSCs[38] when introduced at the pancreatic progenitor stage of the differentiation protocol in a temporal manner. These studies showed the exogenous expression of NGN3, PDX1, and MAFA were sufficient to reprogram adult pancreatic and hepatic cells into glucose-responsive insulin-producing β-cells. In this study, we investigated whether the expression of NGN3, PDX1, and MAFA in hiPSCs could drive the differentiation of the cells towards the pancreatic lineage within a two-week period. We aimed to determine whether this induced expression of the mature markers can activate and regulate the endogenous expression of the pancreatic and mature β-cell markers. We generated inducible lentiviral constructs for the expression of NGN3, PDX1, and MAFA, to be introduced into hiPSCs and induced the cells in medium supporting pancreatic lineage differentiation with factors known to support β-cell differentiation. Our markers of interest along with two other pancreatic progenitor markers, *NKX6.1* and *MAFB*, were upregulated upon five days of induction. Static glucose-stimulated insulin secretion assays demonstrated that the cells were glucose responsive to levels similar to previously published protocols; however, the upregulation of the gene expression was not directly translated into protein expression upon extended culture periods and endogenous insulin production was not observed. These results demonstrate that the overexpression of the three β-cell markers in hiPSCs over a ten-day culture period is not sufficient for the generation of pancreatic cells. The forward-programming of hiPSCs into mature functional β-cells would be a significant step towards the scaling and commercialization of insulin-secreting cells for transplantation into patients suffering from diabetes. This work serves as a tool to better understand the importance of temporal expression patterns of these three genes and how the inducible lentiviral construct could be optimized to fine-tune their expression to support development towards the pancreatic lineage.

Methods

Generation of inducible lentiviral constructs

For the inducible expression of our markers of interest, two lentiviral constructs were generated. The first lentiviral construct, pLenti_EF1a-rtTA_BsdR was generated as follows: The sequence for EF1a-rtTA, flanked with *att*B1 and *att*B2 sites, was synthesized and subsequently shuttled into a pDONR221 backbone through ThermoFisher, yielding an entry vector. Gateway Cloning was then used between this construct and pLenti6.3_V5-DEST_promoterless_mcs_BsdR conferring Blasticidin resistance to generate pLenti_EF1a-rtTA_BsdR.

The second lentiviral construct, pLenti_TRE-NPM_HygR, was generated as follows: The markers of interest, *NGN3* (GenBank ID 50,674), *PDX1* (GenBank ID 3651), and *MAFA* (GenBank ID 389,692) were designed downstream of the TRE3G promoter. Multicistronic expression of the markers of interest was achieved using the self-cleaving 2A-peptides T2A and P2A. This sequence was synthesized through ThermoFisher within a pENTR221 backbone and recombined with pLenti6.3_V5-DEST_promoterless_mcs_HygR conferring HygromycinB resistance to generate pLenti_TRE-NPM_HygR. Final construct maps (Supp.Fig. 1a,c) and detailed cloning information are available upon request.

Lentivirus production and transduction

The lentiviruses were produced separately using human embryonic kidney 293 T cells. Cells were cultured in DMEM + GlutaMax (Gibco, 31,966–021), 10% FCS (Gibco, 10,270–106), 1% NEAA (Gibco, 11,140–035), 1% L-Glutamine (Gibco, 25,030–024) and 1% Pen/Strep (Gibco, 15,140,122). At 80% confluency, the cells were transfected overnight with the lentiviral constructs along with Lipofectamine 2000 Reagent (Invitrogen, 11,668–500) and Ready-to-use Lentiviral Packaging Plasmid Mix (Cellecta, CPCP2KA) in OptiMEM + GlutaMax (Gibco, 51,985–026), 5% FCS, and 1% Pen/Strep. Medium was changed the next day, and viruses were harvested each day for the next two days and stored at − 80 C. The virus was then centrifuged at 19,600 rpm at 4 °C for 80 min. Supernatant was removed and 100 µL of DPBS + 1% BSA was pipetted on top of the pellet. The tube was then sealed with parafilm and incubated at 4 °C overnight before the pellet was resuspended, and aliquoted. The lentiviral titre was determined using a p24 ELISA.

hiPSCs[39] were maintained on Matrigel (Corning, 356,231)-coated dishes in mTesR + (StemCell Technologies, 100–1130) medium supplemented with 1% Pen/Strep, and 50.0 µg/mL Normocin (InvivoGen, ant-nr-1). hiPSC were transduced using the EF1a-rtTA_BsdR lentivirus, and successful recombinants were selected for using 1.0 µg/mL of Blasticidin S HCl (Gibco, A1113902) for five days, now referred to as rtTA-hiPSCs. Subsequently, rtTA-hiPSCs were transduced using the TRE-NPM_HygR lentivirus, and successful recombinants were selected for using 25.0 µg/mL of HygromycinB (Gibco, 10,687,010) for six days, now referred to as rtTA-NPM hiPSCs. The

rtTA-NPM hiPSCs were maintained on Matrigel-coated dishes in mTesR + medium supplemented with 1.0 µg/mL Blasticidin, 25.0 µg/mL HygromycinB, 1% Pen/Strep, and 50.0 µg/mL Normocin.

Doxycycline induction towards the pancreatic lineage

To begin the induction towards the pancreatic lineage, rtTA-NPM hiPSCs were cultured in medium supporting β-cell differentiation[14] with and without 1.0 µg/mL doxycycline hyclate (Sigma Aldrich, D9891-1G). The medium recipe is as follows: MCDB131 (Cellgro, 15–100-CV), 3.6 mg/mL D-(+)-Glucose (Sigma, G7528), 1.75 mg/mL $NaHCO_3$ (Sigma, S5761), 20.0 mg/mL FAF-BSA (Sigma, A9576), 1% Glutamax (LifeTech, 35,050–061), 0.5% ITS-X (Invitrogen, 51,500,056), 0.25 mM Vitamin C (Sigma, A4544), 100 nM Retinoic Acid (Sigma, R2625), 1.0 µM T3 (EMD Millipore, 64,245), 20.0 ng/mL Betacellulin (Peprotech, 100–50), 10.0 µM Y27632 (Abcam, ab120129), 0.25 µM Sant1 (Sigma S4572), 10.0 µg/mL Heparin (Sigma H3149), 10.0 µM Alk5 II (Axxora ALX-270–445), 1.0 µM XXI (EMD Millipore 565,790), 1% Pen/Strep, and 50.0 µg/mL Normocin.

During the induction, cells were cultured for five days as a monolayer with daily medium changes. At the end of the five days, 3D spheroids were generated by creating a single cell suspension of the cultures and seeding 2000 cells / well in a 96-well u-bottom plate (Greiner Bio-One, 650,101). The spheroids were cultured for five more days without further medium changes for a total culture period of ten days. All results presented are from at least three separate inductions.

RNA extraction and RT-qPCR

The Qiagen RNeasy Mini Kit (Qiagen, 74,101) was used for RNA extraction of samples and DNase (Promega, M6101) treatment was performed according to manufacturer's protocol. cDNA synthesis was performed using M-MuLV Reverse Transcriptase (New England Biolabs, M0253S), and qPCR was run using the Universal PCR Master Mix (Applied Biosystems, 4,304,449). The list of primers used can be found in Supplementary Table 1. Ready-to-use mixtures of primers and probes (Gene Expression Assays, Thermo Fisher, 4,331,182) were used unless otherwise specified. Gene expression was normalized to the housekeeper gene *GAPDH*. Relative mRNA levels (2^ΔΔCt) of the transduced rtTA-NPM hiPSCs were determined in relation to the un-transduced hiPSCs which was represented with a value of 1. Fold change of mRNA levels (ΔΔCt) of the cells cultured with and without DOX were determined in relation to that of the rtTA-NPM hiPSCs at the start with a timepoint 0 (TP0).

Ethical statement for the study of human tissue

Studies with human fetal tissue and human adult donor islets were conducted with approval from the Ethics Committee at the Medical Faculty of the Eberhard Karls University Tübingen and at the University Hospital in Tübingen in accordance with the ICH-GCP guidelines (IRB #406/2011BO1 and #290/2016BO1). Human islets for research were provided by the Alberta Diabetes Institute IsletCore at the University of Alberta in Edmonton (www.bcell.org/adi-isletcore). Islet isolation was approved by the Human Research Ethics Board at the University of Alberta (Pro00013094). All donors' families gave informed consent for the use of pancreatic tissue in research.

Human donor islet culture and static GSIS

Healthy human donor islets were purchased from the Alberta Diabetes Institute IsletCore (Alberta, Canada). Individual donor islets were handpicked into wells of 96well U-bottom non-adherent well plates (Greiner Bio-One, 650,101) and cultured for three days to recover from shipping conditions in CMRL1066 without Glutamine (Gibco, 21,530–027), 0.5% FAF-BSA (Sigma Aldrich, A9576), 1 g/L glucose (Gibco, A24940-01), 4 mM Glutamax (Gibco, 35,050–061), 1% Pen/Strep (Gibco, 15,070–063), and 100 µg/mL Normocin (InvivoGen, ant-nr-1).

For the static GSIS assays, donor islets were incubated for one hour in β-Krebs with 2 mM glucose. Donor islets were then incubated in β-Krebs buffer with either 2 mM glucose or 20 mM glucose for another hour, following which the supernatant was collected and stored at -20 °C. The donor islets were lysed with acid ethanol overnight at 4 °C, collected, and stored at -20 °C for insulin content analysis. The levels of insulin secreted by the donor islets and the insulin content within the donor islets were analyzed using the human insulin ELISA kit (Mercodia, 10–1132-01). The GSIS index was calculated by dividing each samples' insulin secretion during 20 mM glucose by 2 mM glucose.

Immunofluorescence (IF) staining and quantification

Following the five-day monolayer culture, cells were prepared for IF staining of the markers of interest. Cells were washed twice with PBS, fixed in 4% PFA for 20 min at room temperature (RT), permeabilized with 1% Triton-X for 30 min at RT, blocked with Goat Block for 30 min at RT, and incubated with the primary antibody overnight at 4 °C (see Supplementary Table 2 for list of antibodies used). Cells were washed and first incubated with the secondary antibody for 30 min at RT in the dark, and then with 2 µg/ml of 4′,6-Diamidin-2-phenylindole (DAPI) solution for 10 min at RT in the dark. Samples were mounted with Prolong Gold Antifade Mountant (Thermo Fisher Scientific, P36930) and imaged using the laser scanning microscope 780 (Carl Zeiss GmbH, Jena, Germany).

The 10-day spheroids, adult donor islets (from the McDonald Laboratory, Alberta, Canada), and 10-week-old fetal tissues (from the University of Tübingen, Tübingen, Germany) were prepared for IF staining, as previously described[40]. Briefly, samples were washed with PBS, fixed in 4% PFA, and embedded in paraffin with a Shandon Citadel 1000 (Thermo Fisher Scientific, Waltham, MA, USA). Samples were sectioned into 3 µm sections (Microtome RM2145, Leica, Nussloch, Germany), and deparaffinized with xylene, graded ethanol (100–50%), and VE-water. Antigen retrieval was performed using both Tris–EDTA (pH 9.0) and Citrate (pH 6.0) buffers. Primary antibody incubation was performed overnight at 4 °C, followed by secondary antibody incubation for 30 min at RT in the dark, with either DAPI solution for 10 min or DRAQ5 (ThermoFisher, 62,251) for 30 min

at RT in the dark for nuclear staining. Samples were treated with the Vector® TrueVIEW® Autofluorescence Quenching Kit (Vector Labs, SP-8400) for 1 min at RT before mounting with Prolong Gold Antifade Mountant. Images were obtained using the laser scanning microscope 780. Positive nuclear staining of the markers of interest was manually counted and normalized per DAPI or DRAQ5 nuclear count. Gray value intensity (GVI) was determined per channel for each image, subtracted by the value for the negative control, and then normalized per DAPI or DRAQ5 nuclear count.

Glucose-stimulated insulin secretion (GSIS) assays

GSIS assays were performed in β-Krebs buffer (recipe can be found in Supplementary Table 3) supplemented with glucose. Cells were washed with PBS and synchronized in β-Krebs buffer with 2 mM glucose (low glucose condition) for one hour in the incubator. Following the synchronization step, cells were either incubated in β-Krebs buffer with either 2 mM glucose or 20 mM glucose (high glucose condition) for one hour in the incubator for the static GSIS assays. For dynamic GSIS assays, the spheroids were incubated in β-Krebs buffer with either 2 mM glucose for an hour followed by buffer with 20 mM glucose for one hour, and then again in buffer with 2 mM glucose for an hour in the incubator. Supernatant was then collected at the end of each incubation and stored at -20 °C overnight before performing either an insulin ELISA (Mercodia, 10–1132-01) or C-peptide ELISA (Mercodia, 10–1141-01). Cells were then trypsinized and counted for normalization of insulin secretion per cell count or per spheroid size.

Statistics

Data presented is collected from at least three separate induction experiments where the data is presented as mean ± standard deviation (s.d.). Outliers were identified with Grubb's test ($p \leq 0.05$). Unpaired t-tests were used to analyze statistical differences between groups.

Results

hiPSCs maintain their stem cell characteristics following transduction of inducible lentiviral constructs

Following generation of the two lentiviral constructs and transduction of hiPSCs (Fig. 1a,b), successful recombinants were selected for through antibiotic treatments of Blasticidin and Hygromycin B using pre-determined concentrations from the antibiotic kill curves on these cells (Supp.Fig. 1b,d,e). The transduced hiPSCs were then assessed to ensure their naïveness through RT-qPCR of *OCT4*, *SOX2*, *NANOG*, and *KLF4*. All genes were normalized to *GAPDH* and assessed relative to the expression levels of the un-transduced hiPSCs. The rtTA-NPM hiPSCs had similar expression levels of the naïve stem cell markers to the un-transduced hiPSCs (Fig. 1c; unpaired t-test, n = 3, *OCT4*: $p = 0.7514$; *SOX2*: $p = 0.8178$; *NANOG*: $p = 0.2464$; *KLF4*: $p = 04{,}572$), which was also observed through IF staining for these markers in the rtTA-NPM hiPSCs (Fig. 1e). We also wanted to ensure that the markers of interest, *NGN3*, *PDX1*, and *MAFA* were not prematurely expressed in the absence of doxycycline (DOX). RT-qPCR analysis of these genes showed that there were no significant differences in expression levels between the un-transduced and transduced hiPSCs, suggesting there is no premature expression of the markers of interest at the hiPSC stage (Fig. 1d; unpaired t-test, n = 3, *NGN3*: $p = 0.1945$; *PDX1*: $p = 0.7954$; *MAFA*: $p = 0.9229$). Further, the *rtTA* gene, whose protein product is needed for the inducible expression of the gene expression system was significantly upregulated in our rtTA-NPM hiPSCs compared to the un-transduced hiPSCs (Supp.Fig. 2a) as expected.

Markers of interest are upregulated at the gene and protein levels upon five days of DOX-treatment

Upon culture in medium supporting pancreatic lineage specification for five days, cells cultured with DOX express greater levels of the markers of interest compared to those cultured without DOX relative to timepoint zero (TP0) when cells were still in their stem cell state (Fig. 2a), where *PDX1* and *MAFA* gene expression levels were significantly increased in cells cultured with DOX than those cultured without DOX (unpaired t-test, n = 3, *PDX1*: $p = 0.042$; *MAFA*: $p = 0.002$). Interestingly, two other pancreatic lineage markers *NKX6.1* and *MAFB* were also upregulated upon five days of culture in the medium with and without DOX compared to day zero (Fig. 2b). The markers of interest were also present at the protein level in the nucleus of significantly more cells in the DOX-treated cultures than in the cultures without DOX (Fig. 2c–e). NGN3 was observed in 88.4% (± 7.4%) of the cells cultured with DOX compared to 0.0% (± 0.0%) of the cells cultured without DOX (unpaired t-test, $n \geq 9$, $p = 3.352{*}10^{-14}$). PDX1 was observed in 29.8% (± 15.9%) of the cells compared to 0.0% (± 0.0%) of the cells cultured without DOX (unpaired t-test, $n \geq 9$, $p = 0.013$). MAFA was observed in 98.9% (± 1.1%) of the cells cultured with DOX compared to 0.0% (± 0.0%) of the cells cultured without DOX (unpaired t-test, $n \geq 9$, $p = 1.380{*}10^{-33}$). Interestingly, markers NGN3 and PDX1 were also observed at the cell membranes and so GVI analysis was also performed to account for the expression of the proteins outside of the nucleus. Similar trends were observed when looking at the GVI of the marker expression where the cultures without DOX had expression patterns similar to the negative control and the DOX-treated cultures had significantly greater GVI expression for all markers (Supp. Fig. 2b). To determine whether the cells show functional responses to glucose, static glucose-stimulated insulin secretion (GSIS) assays were performed. While the cultures without DOX did not show a functional response to glucose stimulation (2 mM: 0.019 µU/L ± 0.033 µU/L (2 mM) vs. 0.018 µU/L ± 0.028 µU/L (20 mM), unpaired t-test, $n \geq 16$, $p = 0.9479$), the five-day cultures with DOX did secrete significantly more insulin at the 20 mM glucose condition than at the 2 mM glucose (Fig. 2f; 0.025 µU/L ± 0.017 µU/L (2 mM) vs. 0.042 µU/L ± 0.023 µU/L (20 mM), unpaired t-test, $n \geq 16$, $p = 0.0014$).

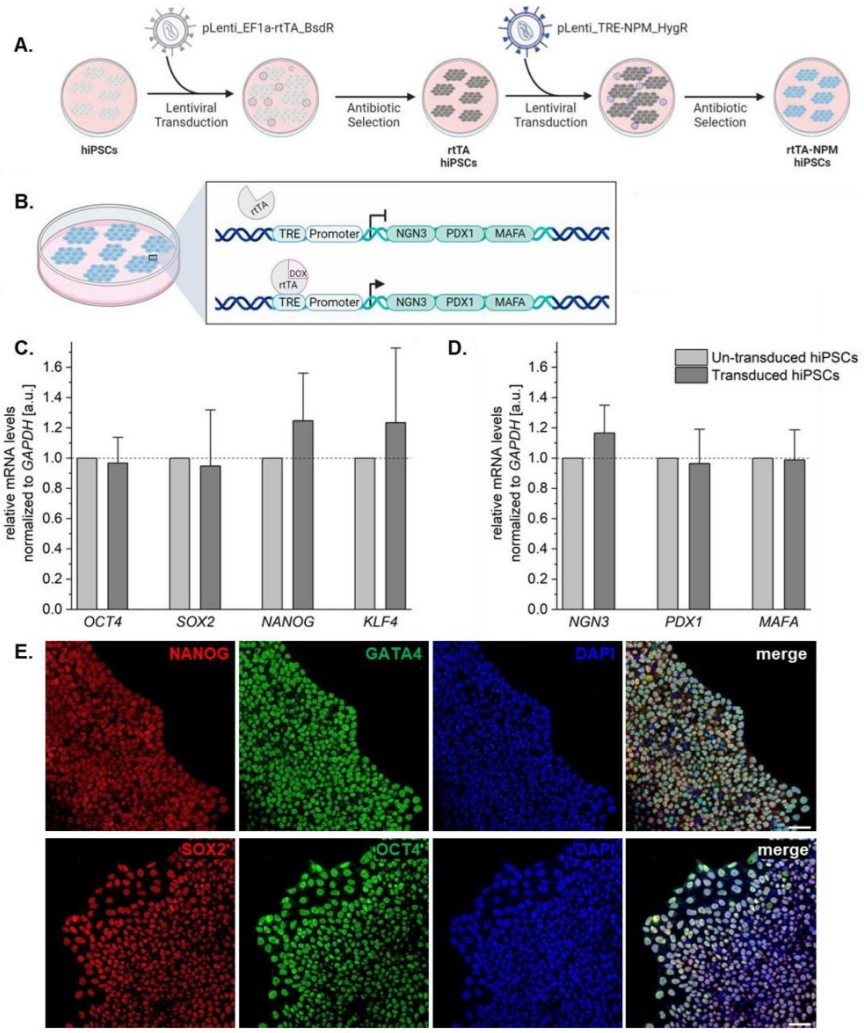

Figure 1. Introduction of inducible lentiviral construct into hiPSCs does not affect pluripotency marker expression. (**A**) Schematic of how the rtTA-NPM hiPSCs were generated and (**B**) how DOX treatment would activate transcription of the markers of interest. Gene expression analysis of transduced hiPSCs for (**C**) stem cell markers and (**D**) markers of interest before DOX treatment relative to un-transduced hiPSCs (dashed line at 1), normalized to GAPDH levels. Unpaired t-test (N = 3). Error bars represent standard deviation. (**E**) IF staining in transduced hiPSCs to confirm stem cell marker expression at the protein level. Scale bar equals 50 µm. Schematics created with BioRender.com.

Extended culture as a 3D spheroid maintains NGN3 and MAFA expression, and improves glucose-responsive insulin secretory behaviour

As human islets of Langerhans are found in clusters, and cell–cell contact has been shown to improve insulin secretion of β-cells [1], at day five of culture, the cells were aggregated into spheroids of 2000 cells each and cultured for another five days. At the end of the ten-day culture, NGN3 and MAFA remained to be expressed significantly greater in the cells of spheroids cultured with DOX versus without DOX (Fig. 3a–c: unpaired t-test, $n \geq 9$, NGN3: 0.0% ± 0.0%, s.d. (-DOX) vs. 93.8% ± 5.3% (+ DOX), $p = 3.976^{*}10^{-17}$; MAFA: 0.0% ± 0.0% (-DOX)

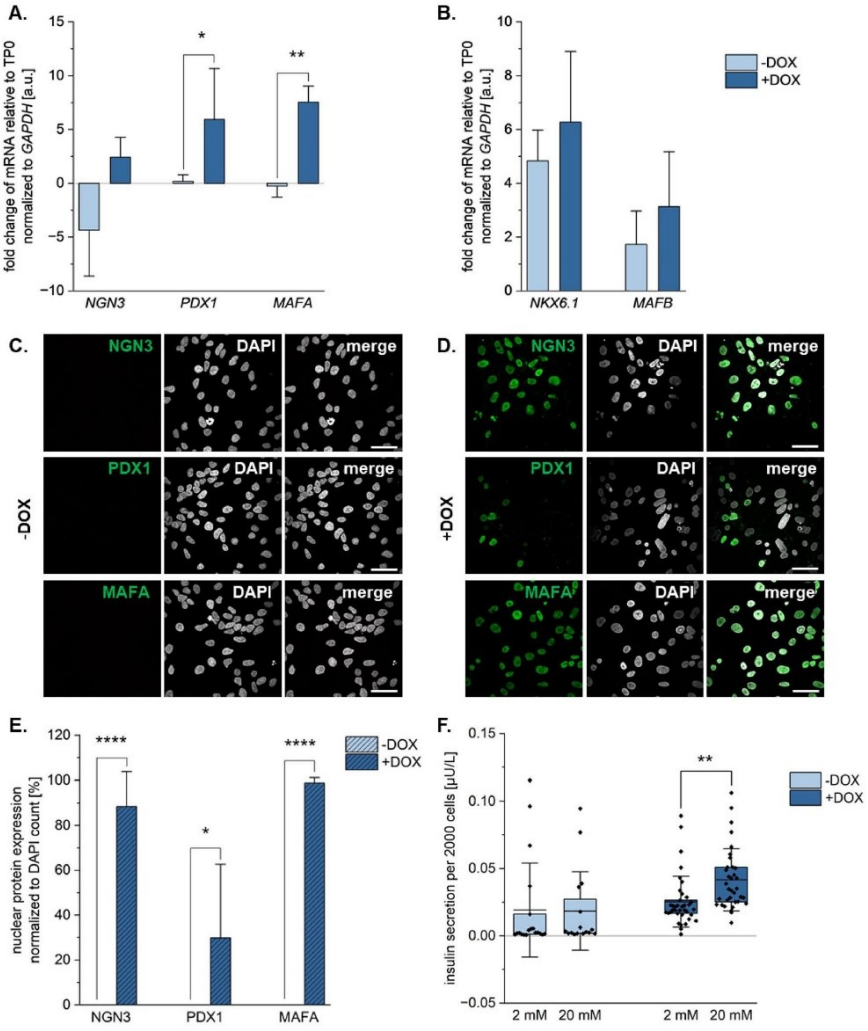

Figure 2. Markers of interest are upregulated at the gene and protein level upon five days of DOX treatment as a monolayer. Gene expression analysis of (**A**) markers of interest and (**B**) pancreatic progenitor markers Nkx6.1 and MafB after 5 days of culture with and without DOX. All values normalized to GAPDH and relative to timepoint 0 (TP0) at the stem cell stage. IF staining for markers of interest in cells cultured for five days (**C**) without and (**D**) with DOX. (**E**) Quantification of the % nuclear protein expression of the markers of interest, normalized to DAPI counts. Scale bar equals 50 µm. (**F**) Amount of insulin secreted upon stimulation with 2 mM and 20 mM glucose, normalized to cell count, during the static GSIS. Unpaired t-test ($N = 3$, $n \geq 9$), * $p \leq 0.05$, ** $p \leq 0.01$, **** $p \leq 0.0001$. Error bars represent standard deviation.

vs. 97.2% ± 1.5% (+DOX), $p = 1.815*10^{-32}$). Unexpectedly, in the DOX-treated cultures, nuclear expression of PDX1 was lost at the end of the ten-day culture period with 0.0% (± 0.0%) of cells both with and without DOX (Fig. 3a–c), though gene expression was observed after ten days of culture (Supp.Fig. 3a). To determine whether this could be attributed to differential localization, expression of the proteins through GVI analysis of the IF staining was performed. Again, similar trends were observed where there was a significant increase in NGN3 and MAFA expression in the DOX-treated versus without DOX cultures; however, no significant differences were observed in expression of PDX1 (Supp.Fig. 3b). Static GSIS assays demonstrated that spheroids cultured either

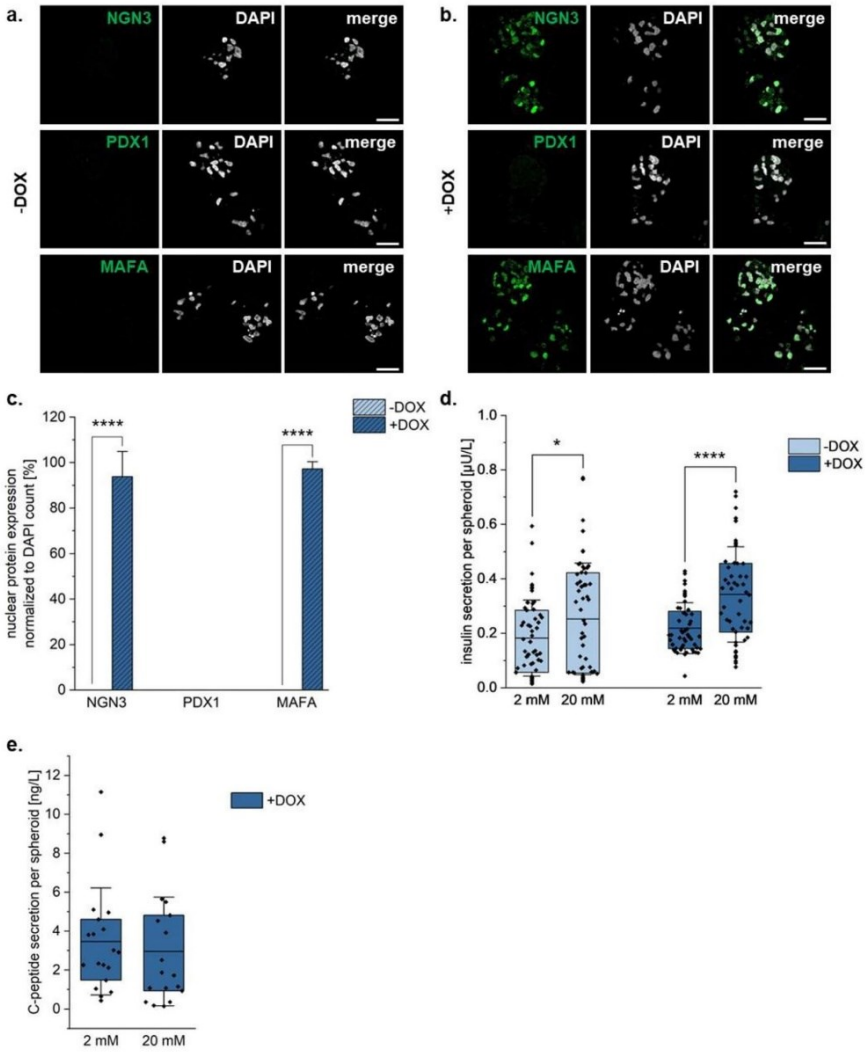

Figure 3. NGN3 and MAFA expression maintained upon ten days of culture as a 3D spheroid. IF staining for markers of interest in cells cultured for ten days with the last five days as a 3D spheroid (**A**) without and (**B**) with DOX. (**C**) Quantification of the % nuclear protein expression of the markers of interest, normalized to DAPI counts. Scale bar equals 25 µm. (**D**) Amount of insulin secreted by cells cultured with DOX upon stimulation with 2 mM and 20 mM glucose, normalized to cell count, during the static GSIS. (**E**) Amount of C-peptide secreted by cells cultured with DOX upon stimulation with 2 mM and 20 mM glucose, normalized to cell count. Unpaired t-test (N = 3, n ≥ 9), * $p \leq 0.05$, **** $p \leq 0.0001$. Error bars represent standard deviation.

with or without DOX secreted significantly more insulin to the increased glucose treatment (Fig. 3d: unpaired t-test, n ≥ 18, -DOX: 0.18 µU/L ± 0.07 µU/L (2 mM) vs. 0.25 µU/L ± 0.10 µU/L (20 mM), $p = 0.0342$; + DOX: 0.22 µU/L ± 0.05 µU/L (2 mM) vs. 0.34 µU/L ± 0.09 µU/L (20 mM), $p = 1.776*10^{-5}$). Unfortunately, the DOX-treated cultures did not show functional responses to multiple glucose stimulations in a dynamic GSIS (Supp.Fig. 3b). C-peptide secretion analysis of the DOX-treated spheroids showed no significant differences in C-peptide secretion between the low and high glucose conditions (Fig. 3e, unpaired t-test, n ≥ 18, + DOX: 3.47 ng/L ± 2.68 ng/L (2 mM) vs. 2.96 ng/L ± 2.71 ng/L (20 mM), $p = 0.5759$). This suggested that the majority of the insulins being

secreted at both the five-day monolayer culture and at the ten-day spheroid timepoint is likely uptake of insulin from the medium rather than insulin that the cells produce.

To determine how these cells compare to human fetal tissues and human adult islets, IF staining for the markers of interest was performed (Fig. 4). The pancreatic progenitor marker NKX6.1 was observed in the nucleus of the pancreatic cells in the fetal tissues with a limited number of cells showing insulin production through the C-peptide staining. Within the adult donor islets of Langerhans, NKX6.1 was observed in the nucleus of cells that also showed cytoplasmic C-peptide expression. The hiPSC-derived spheroids, both with and without DOX, did not show any presence of NKX6.1 or C-peptide. In 10-week-old fetal tissue, PDX1 was expressed in the nucleus of cells of the pancreas with a limited number of cells also showing cytoplasmic insulin staining. In adult donor islets, PDX1 can be observed to be both nuclear and cytoplasmic with some co-localization with insulin. In our DOX-treated hiPSC-derived spheroids, PDX1 was found to have puncta-like expression within the cytoplasm whereas this is absent in the spheroids without DOX. NGN3 and MAFA were absent in the fetal pancreatic tissues and the hiPSC-derived spheroids without DOX. In adult donor islets, NGN3 was present both in the nucleus and cytoplasm of some cells where it colocalized with the insulin expression. In the hiPSC-derived spheroids with DOX, NGN3 was present in the nucleus of most cells while absent in spheroids cultured without DOX. MAFA was found in the nucleus of cells of the adult donor islets and all the cells of the hiPSC-derived spheroids with DOX, while it was absent in the hiPSC-derived spheroids without DOX. The donor islets assessed

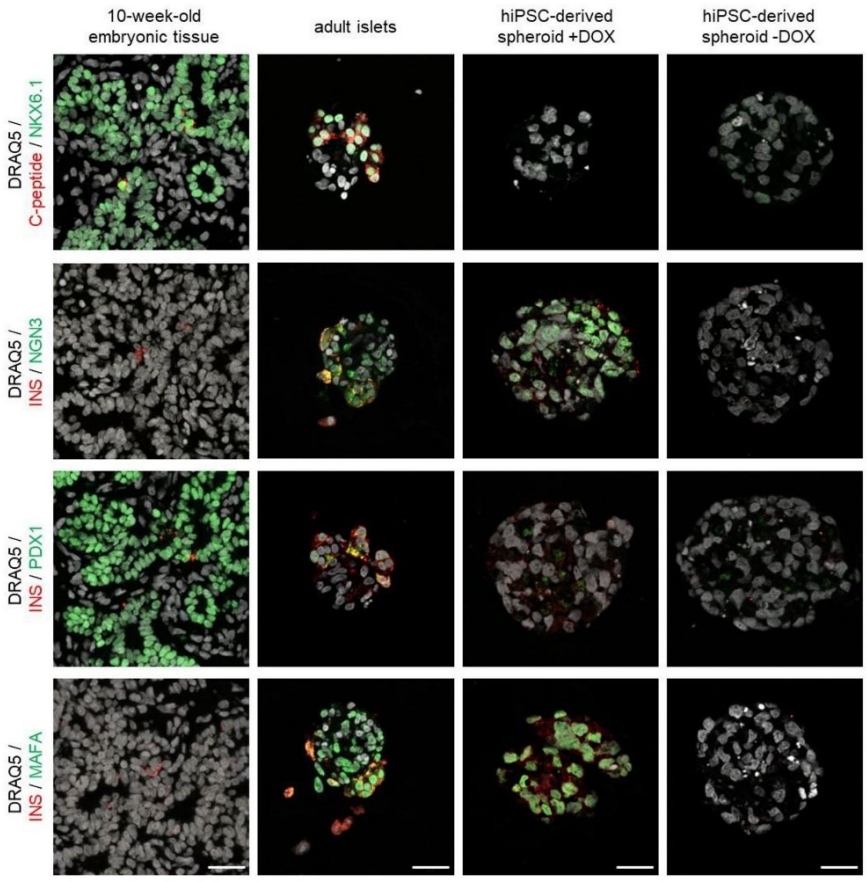

Figure 4. hiPSC-derived spheroids cultured with DOX present similar markers to adult donor islets but are functionally similar to embryonic tissue. 10-week-old embryo tissues, adult donor islets, and the hiPSC-derived spheroids cultured with and without DOX were assessed for protein expression of the three markers of interest (NGN3, PDX1, MAFA), NKX6.1, and the functionality markers C-peptide and insulin (INS). Scale bar equals 25 µm.

were from healthy donors; however, it must be noted that they did not show a functional GSIS response in our culture conditions (Supp.Fig. 4). This could be attributed to donor variability and/or the heterogeneous composition of the donor islets and needs to be considered when assessing the expression patterns of the β-cell markers.

Discussion

Stem cell-derived β-cells possess great potential to improve efficacy of islet transplantations by overcoming issues regarding immune rejection and availability[6]. Increasing understanding of pancreatic development and the required markers in model organisms and, recently, in human embryos has progressed the field of stem cell-derived β-cells greatly. The developmental process was recapitulated in vitro using hPSCs and chemical signaling through incorporation of various growth factors, supplements, and / or inhibitors in the cell culture medium. Regular changes to the media recipe allowed for the differentiation of the cells towards the pancreatic lineage and eventually to β-cells[6]; however, this process can require up to two months to generate a heterogenous population of pancreatic cells[16]. Past studies have shown that transcription factor overexpression in stem / progenitor cells can result in the differentiation into the desired cell type in a time-effective manner. To address the extended duration and low numbers of differentiated cells from classical differentiation protocols, we transduced hiPSCs with lentiviral constructs that allow for the inducible overexpression of β-cell markers. In this study, we generated hiPSCs with lentiviral constructs for the inducible overexpression of β-cell markers NGN3, PDX1, and MAFA to potentially reduce the required differentiation time and increase the number of mature β-cells produced. Interestingly, the cells cultured with DOX expressed the markers of interest and showed glucose-responsive insulin secretion after five days. When the cells were cultured for a further five days as a 3D spheroid, the expression of NGN3 and MAFA were maintained; however, PDX1 expression was lost. Further assessment of insulin production through C-peptide analysis showed that the cells were not producing insulin themselves, and were rather secreting insulin taken up from the medium. When comparing the hiPSC-derived DOX-treated spheroids to human 10-week-old fetal and adult pancreatic tissues, we found that these cells are still quite immature and require more cues and culture time to differentiate towards the pancreatic lineage. Together, these results demonstrated that the simultaneous overexpression of NGN3, PDX1, and MAFA is not sufficient for the forward programming of hiPSCs towards the pancreatic lineage within a ten-day period.

It has been well observed that the source of the cells used for generation of the hiPSCs, in terms of organ origin and donor's genetic background, can contribute to the differentiation potential of hiPSCs. During the reprogramming process of somatic cells to hiPSCs, the epigenetic landscape is not necessarily completely remodelled[41–44]. which then influences the lineage towards which the hiPSCs would more readily differentiate. Comparison of gene expression profiles of original somatic cells, the corresponding hiPSC line, and embryonic stem cells showed that genes expressed in the somatic cells were repressed in the corresponding hiPSC line though were found at much lower levels in the ESCs. This suggested that the hiPSCs retained the hypomethylation of the somatic genes, maintaining some of the initial transcriptional landscape[43–45]. The retention of epigenetic landscapes/memory of hiPSCs of the somatic cells they were derived from also explains the discrepancy between hESCs and hiPSCs[41,42] and/or alteration of metabolic pathways during the reprogramming of somatic cells into hiPSCs[46,47]. Interestingly, it has also been observed that donor-specific differences to have a greater effect on differentiation potential over the tissue of origin[48] and passage number[49]. Interestingly, a recent study overexpressing the same three transcription factors in adult gut stem cells had promising results following just three weeks of culture[50]. Using similar expression constructs to overexpress NGN3 for the first two days followed by continuous expression of PDX1 and MAFA, Huang et al.[50] were able to successfully differentiate adult gut stem cells into glucose-responsive insulin-producing cells similar to β-cells and were able to restore glucose homeostasis in diabetic mice for at least 100 days[50,51]. Fontcuberta-PiSunyer, et al.[52] directly reprogrammed human fibroblasts into glucose-responsive β-cells using a similar ten-day protocol with adenoviral constructs for the exogenous expression of NGN3, PDX1, and MAFA, followed by expression of PAX4 and NKX2.2 in the first week of culture. Both these studies used similar lentiviral constructs and culture conditions as in our study, where they performed monolayer cultures in the first week and then spheroid formation. A key difference from these two protocols compared to ours is the timing of expressing the markers of interest. Rather than expression of all three markers continuously for the entire culture period, Huang et al.[50] only induced expression of NGN3 for the first two days and then expressed PDX1 and MAFA, while Fontcuberta-PiSunyer et al.[52] introduced adenoviral constructs for NGN3, PDX1, and MAFA together and separate constructs for PAX4 and NKX2.2 were introduced later in the culture. This suggests that the continuous expression of these markers in our hiPSCs could have resulted in overload of cellular machinery for the continuous protein production. After five days of culture with DOX, NGN3 and MAFA were observed throughout the culture period while PDX1 was lost which could explain the lack of insulin production and glucose-responsive functionality. The loss of PDX1 expression could be a possible mechanism of compensation which could also be attributed to the gene's position within the lentiviral construct and the vector copy number.

The lentiviral construct design and integration could also have posed an effect on the expression levels of our markers of interest. Following titration of the lentivirus using a p24 ELISA, the virus was transduced into the cells and positively selected for through antibiotic treatment; however, the number of lentiviral constructs introduced into each cell was not controlled for. The positive selection through the antibiotic treatment ensures that there is at least one copy of the integrated into its genome but not that it is equal in each cell[53]. There have been many developments in the field of lentiviral gene therapy especially considering the design of the lentiviral construct including creating only one inducible lentiviral construct with all the necessary components[54,55], and / or directing the integration of the construct(s) into specific loci such that only one copy is integrated per cell[22]. Adapting the lentiviral design to only have one copy per cell could overcome the issue of PDX1 being lost at the protein level upon longer culture. This could possibly avoid protein compensation[56] where the cell maintains

homeostasis after protein translation and targets proteins to degradation rather than controlling the transcription. Through downregulation of PDX1, the cell prevents differentiation towards the pancreatic lineage; however, as NGN3 and MAFA are maintained, this raises the question whether the position of PDX1 in the lentiviral construct, in the middle of the three markers of interest, would be an issue. The T2A and P2A self-cleaving peptides are widely used for multi-cistronic expression constructs[57–59]. It has been shown that in tri-cistronic constructs similar to ours, there was greatest expression of the first gene, followed by the third gene, and weakest expression of the second gene[60]. This is in line with our results on day five where NGN3 and MAFA, our first and third genes in the construct were present in around 88% and 98% of the cells, respectively, while PDX1, the second gene in the construct, was only present in around 30% of the cells. Introducing separate lentiviral constructs for each gene could be a possible solution; however, the risk of disrupting the genome with three lentiviral constructs could pose a problem in genetic integrity. The constructs for the inducible overexpression of each gene would have to be carefully designed and introduced to the cells to ensure successful integration and reprogramming without negatively impacting the genome.

Recent success of studies[50,52] using similar lentiviral constructs and culture conditions to reprogram adult (stem) cells into glucose-responsive insulin-producing β-cells provide hope that a few adaptations to our protocol can also achieve such results. Future studies looking to direct the differentiation of hiPSCs towards β-cells should use separate lentiviral constructs with different induction factors for each marker of interest to allow for the most efficient expression of the markers of interest and control over their temporal expression patterns. Multiple hiPSC donors and tissue origins should also be studied to determine whether one tissue or donor is more readily differentiated towards the pancreatic lineage. When considering the use of hiPSC lines, many studies look at somatic cells that are most efficiently reprogrammed; however, it has also been shown that hiPSCs from somatic cells that were more resistant to being reprogrammed may be more effectively differentiated due to their epigenetic memory[61]. Further investigation into extending the culture conditions with the temporal expression of these three genes in hiPSCs has potential in dramatically improving the availability of hiPSC-derived β-cells for therapeutic purposes.

Received: 24 November 2023; Accepted: 7 June 2024
Published online: 13 June 2024

References

1. Islam, S. *The Islets Of Langerhans* (Advances in Experimental Medicine and Biology, Springer, Cham, 2010).
2. Xavier, G. The cells of the islets of langerhans. *J. Clin. Med.* **7**, 54 (2018).
3. Berget, C., Messer, L. H. & Forlenza, G. P. A clinical overview of insulin pump therapy for the management of diabetes: Past, present, and future of intensive therapy. *Diabetes Spectr.* **32**, 194–204 (2019).
4. Weinstock, R. S. *et al.* Severe hypoglycemia and diabetic ketoacidosis in adults with type 1 diabetes: Results from the T1D Exchange clinic registry. *J. Clin. Endocrinol. Metab.* **98**, 3411–3419 (2013).
5. Robertson, R. P. Pancreas and islet transplantation in diabetes mellitus. *Wolters Kluwer* (2019).
6. Jeyagaran, A. *et al.* Type 1 diabetes and engineering enhanced islet transplantation. *Adv. Drug Deliv. Rev.* **189**, 114481 (2022).
7. Mayhew, C. N. & Wells, J. M. Converting human pluripotent stem cells into beta-cells: Recent advances and future challenges. *Curr. Opin. Organ Transplant.* **15**, 54–60 (2010).
8. Maxwell, K. G. & Millman, J. R. Applications of iPSC-derived beta cells from patients with diabetes. *Cell reports. Med.* **2**, 100238 (2021).
9. Rezania, A. *et al.* Reversal of diabetes with insulin-producing cells derived in vitro from human pluripotent stem cells. *Nat. Biotechnol.* **32**, 1121–1133 (2014).
10. Liu, H. *et al.* Chemical combinations potentiate human pluripotent stem cell-derived 3D pancreatic progenitor clusters toward functional beta cells. *Nat. Commun.* **12**, 3330 (2021).
11. Chmielowiec, J. & Borowiak, M. In vitro differentiation and expansion of human pluripotent stem cell-derived pancreatic progenitors. *Rev. Diabet. Stud.* **11**, 19–34 (2014).
12. Nair, G. G. *et al.* Recapitulating endocrine cell clustering in culture promotes maturation of human stem-cell-derived beta cells. *Nat. Cell Biol.* **21**, 263–274 (2019).
13. Velazco-Cruz, L. *et al.* Acquisition of dynamic function in human stem cell-derived beta cells. *Stem Cell Rep.* **12**, 351–365 (2019).
14. Pagliuca, F. W. *et al.* Generation of functional human pancreatic β cells in vitro. *Cell* **159**, 428–439 (2014).
15. Davis, J. C. *et al.* Live cell monitoring and enrichment of stem cell-derived β cells using intracellular zinc content as a population marker. *Curr. Protoc. Stem Cell Biol.* **51**, e99 (2019).
16. Balboa, D. *et al.* Functional, metabolic and transcriptional maturation of human pancreatic islets derived from stem cells. *Nat Biotechnol* **40**, 1042–1055 (2022).
17. Fantuzzi, F. *et al.* In depth functional characterization of human induced pluripotent stem cell-derived beta cells in vitro and in vivo. *Front. Cell Dev. Biol.* https://doi.org/10.3389/fcell.2022.967765 (2022).
18. Tomaz, R. A. *et al.* Generation of functional hepatocytes by forward programming with nuclear receptors. *Elife* **11**, 1–25 (2022).
19. Lange, L. *et al.* Inducible forward programming of human pluripotent stem cells to hemato-endothelial progenitor cells with hematopoietic progenitor potential. *Stem Cell Rep.* **14**, 122–137 (2020).
20. Pang, Z. P. *et al.* Induction of human neuronal cells by defined transcription factors. *NatureNature* **476**, 220–223 (2012).
21. Chanda, S. *et al.* Generation of induced neuronal cells by the single reprogramming factor ASCL1. *Stem Cell Rep.* **3**, 282–296 (2014).
22. Pawlowski, M. *et al.* Inducible and deterministic forward programming of human pluripotent stem cells into neurons, skeletal myocytes, and oligodendrocytes. *Stem Cell Rep.* **8**, 803–812 (2017).
23. Evans, A. L. *et al.* Transfer to the clinic: Refining forward programming of hPSCs to megakaryocytes for platelet production in bioreactors. *Blood Adv.* **5**, 1977–1990 (2021).
24. Speicher, A. M. *et al.* Deterministic programming of human pluripotent stem cells into microglia facilitates studying their role in health and disease. *Proc. Natl. Acad. Sci. U. S. A.* **119**, 1–11 (2022).
25. Wang, K. *et al.* Robust differentiation of human pluripotent stem cells into endothelial cells via temporal modulation of ETV2 with modified mRNA. *Sci. Adv.* **6**, 1–15 (2020).
26. Li, J. *et al.* Upregulation of ETV2 expression promotes endothelial differentiation of human dental pulp stem cells. *Cell Transplant.* **30**, 1–11 (2021).

27. Zhou, Q. *et al.* A multipotent progenitor domain guides pancreatic organogenesis. *Dev. Cell* **13**, 103–114 (2007).
28. Zhu, Y., Liu, Q., Zhou, Z. & Ikeda, Y. PDX1, Neurogenin-3, and MAFA: critical transcription regulators for beta cell development and regeneration. *Stem Cell Res. Ther.* **8**, 240 (2017).
29. Zhou, Q., Brown, J., Kanarek, A., Rajagopal, J. & Melton, D. A. In vivo reprogramming of adult pancreatic exocrine cells to beta-cells. *Nature* **455**, 627–632 (2008).
30. Akinci, E., Banga, A., Greder, L. V., Dutton, J. R. & Slack, J. M. Reprogramming of pancreatic exocrine cells towards a beta (beta) cell character using Pdx1, Ngn3 and MafA. *Biochem. J.* **442**, 539–550 (2012).
31. Koblas, T., Leontovyc, I., Loukotova, S., Kosinova, L. & Saudek, F. Reprogramming of pancreatic exocrine cells AR42J into insulin-producing cells using mRNAs for Pdx1, Ngn3, and MafA transcription factors. *Mol. Ther. - Nucleic Acids* **5**, e320 (2016).
32. Banga, A., Akinci, E., Greder, L. V., Dutton, J. R. & Slack, J. M. In vivo reprogramming of Sox9+ cells in the liver to insulin-secreting ducts. *Proc. Natl. Acad. Sci. U. S. A.* **109**, 15336–15341 (2012).
33. Banga, A., Greder, L. V., Dutton, J. R. & Slack, J. M. W. Stable insulin secreting ducts formed by reprogramming of cells in the liver using a three gene cocktail and a PPAR agonist. *Gene Ther.* **21**, 19–27 (2014).
34. Akinci, E. *et al.* Reprogramming of various cell types to a beta-like state by Pdx1, Ngn3 and MafA. *PLoS One* **8**, e82424 (2013).
35. Matsuoka, T. A. *et al.* Mafa enables Pdx1 to effectively convert pancreatic islet progenitors and committed islet α-cells into β-cells in vivo. *Diabetes* **66**, 1293–1300 (2017).
36. Guo, P. *et al.* Specific reprogramming of alpha cells to insulin-producing cells by short glucagon promoter-driven Pdx1 and MafA. *Mol. Ther. - Methods Clin. Dev.* **28**, 355–365 (2023).
37. Xu, H. *et al.* The combined expression of Pdx1 and MafA with either Ngn3 or NeuroD improves the differentiation efficiency of mouse embryonic stem cells into insulin-producing cells. *Cell Transplant.* **22**, 147–158 (2013).
38. Saxena, P. *et al.* A programmable synthetic lineage-control network that differentiates human IPSCs into glucose-sensitive insulin-secreting beta-like cells. *Nat. Commun.* **7**, 11247 (2016).
39. Stock, R. *et al.* Generation and characterization of human induced pluripotent stem cells lines from four patients diagnosed with schizophrenia and one healthy control. *Stem Cell Res.* **48**, 101961 (2020).
40. Urbanczyk, M. *et al.* Decorin improves human pancreatic β-cell function and regulates ECM expression in vitro. *Matrix Biol.* **115**, 160–183 (2023).
41. Poetsch, M. S., Strano, A. & Guan, K. Human induced pluripotent stem cells: from cell origin, genomic stability, and epigenetic memory to translational medicine. *Stem Cells* **40**, 546–555 (2022).
42. Kim, K. *et al.* Epigenetic memory in induced pluripotent stem cells. *Nature* **467**, 285–290 (2010).
43. Ohi, Y. *et al.* Incomplete DNA methylation underlies a transcriptional memory of somatic cells in human iPS cells. *Nat. Cell Biol.* **13**, 541–549 (2011).
44. Hu, S. *et al.* Effects of cellular origin on differentiation of human induced pluripotent stem cell-derived endothelial cells. *J. Clin. Invest.* **1**, 1–12 (2016).
45. Chlebanowska, P. *et al.* Origin of the induced pluripotent stem cells affects their differentiation into dopaminergic neurons. *Int. J. Mol. Sci.* **21**, 1–23 (2020).
46. Davis, J. C. *et al.* Glucose response by stem cell-derived beta cells in vitro is inhibited by a bottleneck in glycolysis. *Cell Rep.* **31**, 107623 (2020).
47. Jasra, I. T., Cuesta-gomez, N., Verhoeff, K. & Shapiro, A. M. J. Mitochondrial regulation in human pluripotent stem cells during reprogramming and b cell differentiation. *Front. Endocrinol. (Lausanne)* **14**, 1–17 (2023).
48. Kyttälä, A. *et al.* Genetic variability overrides the impact of parental cell type and determines iPSC differentiation potential. *Stem Cell Rep.* **6**, 200–212 (2016).
49. Kilpinen, H. *et al.* Common genetic variation drives molecular heterogeneity in human iPSCs. *Nature* **546**, 370 (2017).
50. Huang, X. *et al.* Stomach-derived human insulin-secreting organoids restore glucose homeostasis. *Nat. Cell Biol.* **25**, 778–786 (2023).
51. Ariyachet, C. *et al.* Reprogrammed stomach tissue as a renewable source of functional β cells for blood glucose regulation. *Cell Stem Cell* **176**, 139–148 (2017).
52. Fontcuberta-PiSunyer, M. *et al.* Direct reprogramming of human fibroblasts into insulin-producing cells using transcription factors. *Commun. Biol.* **6**, 1–15 (2023).
53. Santeramo, I. *et al.* Vector copy distribution at a single-cell level enhances analytical characterization of gene-modified cell therapies. *Mol. Ther. - Methods Clin. Dev.* **17**, 944–956 (2020).
54. Zimmermann, K. *et al.* Design and characterization of an "all-in-one" lentiviral vector system combining constitutive anti-G. *Cancers Basel.* **12**, 375 (2020).
55. Ortinski, P. I., O'Donovan, B., Dong, X. & Kantor, B. Integrase-deficient lentiviral vector as an all-in-one platform for highly efficient CRISPR/Cas9-mediated gene editing. *Mol. Ther. - Methods Clin. Dev.* **5**, 153–164 (2017).
56. Ishikawa, K., Makanae, K., Iwasaki, S., Ingolia, N. T. & Moriya, H. Post-translational dosage compensation buffers genetic perturbations to stoichiometry of protein complexes. *PLoS Genet.* **13**, 1–22 (2017).
57. Daniels, R. W., Rossano, A. J., Macleod, G. T. & Ganetzky, B. Expression of Multiple Transgenes from a Single Construct Using Viral 2A Peptides in Drosophila. *Expert Opin. Biol. Therapy* **9**, e100637 (2014).
58. Szymczak, A. L. & Vignali, D. A. A. Development of 2A peptide-based strategies in the design of multicistronic vectors. *Expert Opin. Biol. Ther.* **5**, 627–638 (2005).
59. Luke, G. A., Escuin, H., Felipe, P. D. & Ryan, M. D. 2A to the fore – research, technology and applications 2A to the fore – research, technology and applications. *Biotechnol. Genet. Eng. Rev.* **26**, 223–260 (2009).
60. Liu, Z., Chen, O., Wall, J. B. J., Zheng, M. & Zhou, Y. Systematic comparison of 2A peptides for cloning multi-genes in a polycistronic vector. *Sci. Rep.* https://doi.org/10.1038/s41598-017-02460-2 (2017).
61. Wang, L. *et al.* Retinal cell type DNA methylation and histone modifications predict reprogramming efficiency and retinogenesis in 3D organoid cultures. *Cell Rep.* **11**, 509–533 (2018).

Acknowledgements

We thank Prof. Hansjürgen Volkmer (NMI Reutlingen, Germany) for providing us the hiPSCs. We like to thank Prof. Hanna K.A. Mikkola (UCLA, USA) and Prof. Garry P. Duffy (National University of Ireland, Galway) for the helpful discussions. Human islets for research were provided by the Alberta Diabetes Institute IsletCore at the University of Alberta in Edmonton (www.bcell.org/adi-isletcore) with the assistance of the Human Organ Procurement and Exchange (HOPE) program, Trillium Gift of Life Network (TGLN), and other Canadian organ procurement organizations.

Author contributions

A.J., S.L.L., F.W. and K.S-L. designed the experiments. A.J. performed experiments, and A.J. and M.U. analyzed data. A.J., S.L.L., F.W. and K.S-L wrote the manuscript. The main data supporting the findings of this study are

available within the article and its supplementary information. The raw data generated in this study are available from the corresponding author upon request.

Funding

Open Access funding enabled and organized by Projekt DEAL. This work was financially supported by the European Union (H2020-ITN 766181, DELIVER to K.S.-L.), and the Ministry of Science, Research and the Arts of Baden-Württemberg (33–729.55–3/214 and SI-BW 01222–91 to K.S.-L.) and the Deutsche Forschungsgemeinschaft (INST 2388/33-1 to K.S.-L).

Competing interests

The authors declare no competing interests.

Additional information

Supplementary Information The online version contains supplementary material available at https://doi.org/10.1038/s41598-024-64346-4.

Correspondence and requests for materials should be addressed to K.S.-L.

Reprints and permissions information is available at www.nature.com/reprints.

Publisher's note Springer Nature remains neutral with regard to jurisdictional claims in published maps and institutional affiliations.

Appendix II

Decorin improves human pancreatic β-cell function and regulates ECM expression *in vitro*

Max Urbanczyk [a,§], Abiramy Jeyagaran [a,b,§], Aline Zbinden [a,c], Chuan-en Lu [a], Julia Marzi [a,b,d], Laurence Kuhlburger [e,f], Sven Nahnsen [e,f], Shannon L. Layland [a,g], Garry Duffy [h,i] and Katja Schenke-Layland [a,b,d]

a - Institute of Biomedical Engineering, *Department for Medical Technologies and Regenerative Medicine, Eberhard Karls University Tübingen, Silcherstr. 7/1, Tübingen 72076, Germany*
b - NMI Natural and Medical Sciences Institute at the University of Tübingen, *Reutlingen, Germany*
c - Department of Immunology, *Leiden University Medical Center, Leiden, ZA 2333, the Netherlands*
d - Cluster of Excellence iFIT (EXC 2180) "Image-Guided and Functionally Instructed Tumor Therapies", *Eberhard Karls University Tübingen, Tübingen, Germany*
e - Quantitative Biology Center (QBiC), *Eberhard Karls University of Tübingen, Tübingen, Germany*
f - Biomedical Data Science, *Department of Computer Science, Eberhard Karls University Tübingen, Tübingen, Germany*
g - Department of Women's Health, *Eberhard Karls University Tübingen, Tübingen, Germany*
h - Discipline of Anatomy and the Regenerative Medicine Institute, *School of Medicine, College of Medicine Nursing and Health Sciences, National University of Ireland Galway, Ireland*
i - Science Foundation Ireland (SFI) Centre for Research in Advanced Materials for Biomedical Engineering (AMBER), *Trinity College Dublin & National University of Ireland Galway, Galway, Ireland*

Corresponding author. *katja.schenke-layland@uni-tuebingen.de.*
https://doi.org/10.1016/j.matbio.2022.12.005

Abstract

Transplantation of islets of Langerhans is a promising alternative treatment strategy in severe cases of type 1 diabetes mellitus; however, the success rate is limited by the survival rate of the cells post-transplantation. Restoration of the native pancreatic niche during transplantation potentially can help to improve cell viability and function. Here, we assessed for the first time the regulatory role of the small leucine-rich proteoglycan decorin (DCN) in insulin secretion in human β-cells, and its impact on pancreatic extracellular matrix (ECM) protein expression *in vitro*. In depth analyses utilizing next-generation sequencing as well as Raman microspectroscopy and Raman imaging identified pathways related to glucose metabolism to be upregulated in DCN-treated cells, including oxidative phosphorylation within the mitochondria as well as proteins and lipids of the endoplasmic reticulum. We further showed the effectiveness of DCN in a transplantation setting by treating collagen type 1-encapsulated β-cell-containing pseudo-islets with DCN. Taken together, in this study, we demonstrate the potential of DCN to improve the function of insulin-secreting β-cells while reducing the expression of ECM proteins affiliated with fibrotic capsule formation, making DCN a highly promising therapeutic agent for islet transplantation.

Introduction

Diabetes mellitus (DM) is a metabolic disease where the internal glycemic control is disrupted by the autoimmune destruction of insulin-producing β-cells (Type 1 DM) or the inefficient use of insulin (Type 2 DM) in response to glucose. Ten percent of the adult population suffers from DM and the numbers are predicted to increase from the current 537 million patients to 783 million by 2045. Type 1 DM accounts for 5−10% of the total number of patients and they mostly rely on exogenous insulin injections to control their glucose levels [1]. The use of pancreatic organ or islets of Langerhans

transplantation is an alternative treatment strategy for DM patients repeatedly suffering from severe hypoglycemia. The islets of Langerhans are the endocrine units of the pancreas responsible for controlling blood glucose levels. They contain β-cells, which are the glucose-responsive insulin-producing cells. Islet transplantation has been shown to improve glucose control and lead to insulin independency for up to 5 years [2]; however, its efficacy is limited by the loss of approximately 50% of donor islets post-transplantation, due to multiple factors such as hypoxia at the transplant site and immune system reactions [3]. During islet isolation, the human pancreas is mechanically and enzymatically digested to separate the endocrine and exocrine tissues, which results in the destruction of the vascularization and the loss of crucial extracellular matrix (ECM) proteins [4]. Following transplantation into the host's body, revascularization of the graft can take up to 14 days when no supporting intervention is used [5]. During this period, the islets are subjected to decreased oxygen and nutrient supply. The native ECM facilitates cell-cell contacts and controls several cellular processes, including cell proliferation, survival, and tissue-specific functions [6]. The removal of the essential islet ECM further diminishes the success rate of islet transplantation [7]. There are several different approaches to improve the survival rate of isolated islets post-transplantation, such as encapsulation in carrier materials [8–10], co-culture with supporting cells [7,11–13], or the supplementation of pancreatic ECM proteins [14–16], which has already been shown to improve cell survival and functionality post-isolation [17]; however, implantation still causes the formation of a fibrotic capsule composed of the fibril-forming proteins such as collagen type 1 (COLI), collagen type 3 (COLIII), and fibronectin (FN) [18–20], which hinders the functional integration of the transplant in the host's system. To improve the survival of isolated islets post-transplantation, supportive strategies need to address (1) the reestablishment of the pancreatic islet niche to improve islet survival as well as (2) the reduction of a fibrotic capsule formation to improve integration of the islets into the recipient's system.

The goal of this study was to identify potential ECM candidates that could improve the outcome of islet transplantation. We identified decorin (DCN) as target of interest and studied the impact of DCN on the function and endogenous ECM expression of human β-cells using the conditionally immortalized human β-cell line EndoC-βH3. We show that DCN-treatment significantly improved insulin secretion upon glucose challenge while ECM proteins affiliated with fibrosis were significantly downregulated. Utilizing Raman microspectroscopy and Raman imaging as well as next-generation sequencing (NGS), we further monitored the impact of DCN on mitochondrial activity and the endoplasmic reticulum (ER). To evaluate its potential as a treatment option in a carrier material for β-cell or islet transplantation, we incorporated DCN in a COLI carrier material and confirmed the improved functionality effects observed in suspension. Taken together, our results show for the first time the positive effects of DCN on improved insulin secretion in β-cells through modulation of mitochondrial activity as well as protein folding and vesicle formation processes. Additionally, we show that DCN can reduce the expression of ECM proteins affiliated with fibrotic capsule formation. Both properties make DCN a strong candidate for use in islet transplantation to support islet survival and potentially improve graft integration into the host's system.

Methods

Pseudo-islet assembly & culture

The human EndoC-βH3 β-cell line was cultured following the manufacturer's instructions (Human Cell Design, Toulouse, France). Pseudo-islets were formed as previously described [21]. Briefly, aggregates of 1000 β-cells were formed in U-bottom non-adherent well plates (Greiner Bio-One, Frickenhausen, Germany) over a period of five days under standard culture conditions (37 °C, 5% CO_2, 20% O_2). Culture media Optiβ1 and Optiβ2 (Human Cell Design) were supplemented with recombinantly-produced DCN at 50 μg/ml, and cells were cultured in these media for two days and four days after seeding. PBS supplementation was used as control. The DCN used in this study has been characterized previously [22,23]. Briefly, plasmids for the expression of recombinant human DCN were introduced into Chinese hamster ovary cells under good laboratory practices followed by protein purification using fast protein liquid chromatography-controlled immobilized metal affinity chromatography as described before in detail [22]. The molecular weight of the purified recombinantly-produced human DCN was determined to be between 51 and 64 kDa. Deglycosylation resulted in a shift towards a lower protein size, showing that the recombinantly-produced human DCN is initially present in its glycosylated form. Co-immunoprecipitation also showed its potential to specifically bind transforming growth factor β1 [22].

For COLI gel encapsulation, 120 pseudo-islets were grouped per well. Pseudo-islets were encapsulated in COLI with a concentration of 6.0 mg/ml as previously described and according to the manufacturer's instructions (Fraunhofer IGB, Stuttgart,

Germany) [8] [24]. The encapsulated pseudo-islets were cultured in a total volume of 250 μl for three days with DCN at 50 μg/ml or PBS (control).

Pseudo-islet and pancreatic tissue preparation for histological analysis

After culture, pseudo-islets were prepared for histological analysis as previously described [8]. Briefly, pseudo-islets were washed with PBS, fixed in 4% PFA and embedded in paraffin with a Shandon Citadel 1000 (Thermo Fisher Scientific, Waltham, MA, USA) according to the manufacturer's protocol. Pseudo-islets were cut in 3 μm sections (Microtom RM2145, Leica, Nussloch, Germany), deparaffinized with xylene, graded ethanol (100%–50%) and VE-water. Adult human pancreatic tissue was purchased from Novus Biologicals (NBP2–30,191, Novus Biological, Bio-Techne GmbH, Wiesbaden, Germany), which was treated by the same protocol that was used for the pseudo-islets.

Immunofluorescence (IF) staining

Antigen retrieval procedures for IF staining as well as primary and secondary antibodies are listed in Suppl. Table S1. Two different DCN antibodies were used to exclude possible staining artefacts. Sections were incubated for 10 min with 4′,6-Daimidin-2-phenylindol solution at 2 μg/ml (DAPI, Sigma-Aldrich, Schnelldorf, Germany) and mounted with Prolong Gold Antifade Mountant (Thermo Fisher Scientific). Images were obtained using a laser scanning microscope 780 (Carl Zeiss GmbH, Jena, Germany).

COLI gel E-modulus evaluation

Elastic modulus of the COLI gels was tested using a BOSE Electroforce 3000 (TA Instruments, New Castle, USA). The elastic modulus was calculated by means of Eq. (1).

$$E = \frac{\sigma(\varepsilon)}{\varepsilon} = \frac{(F/A)}{(\Delta L/L_0)} \quad (1)$$

The gel's surface area A was uniformly determined as 30 mm^2 and the total height L_0 was measured specifically for each gel. The elastic modulus was obtained by plotting the tensile stress against strain using Microsoft Excel (Microsoft Corporation, 2021. Microsoft Excel Version 2111, retrieved from https://office.microsoft.com/excel) where the slope of the graph's regression line displayed the elastic modulus.

Glucose-stimulated insulin secretion (GSIS) assays

GSIS assays were performed as previously described [7,21]. Briefly, pseudo-islets from suspension and COLI gel cultures were starved overnight in Optiβ2 medium (Univercell Biosolutions). Afterwards, pseudo-islets from suspension cultures were grouped, washed with 0.1% BSA (A-9576, Sigma-Aldrich) in β-Krebs (KREBS-BSA, human cell design) and incubated for 1 h in KREBS-BSA. After synchronization, pseudo-islets from suspension cultures were subsequently incubated for 1 hour each in basal KREBS-BSA, KREBS-BSA containing 20 mM glucose (A2494001, Thermo Fisher Scientific), and basal KREBS-BSA again. After each incubation, the supernatant was removed and stored at −20 °C until further analysis. The insulin content was analyzed using an ultrasensitive human insulin ELISA kit (10–1132–01, Mercodia, Uppsala, Sweden). For GSIS assays in COLI gels, all incubation times were tripled. The GSIS index was calculated by dividing each samples' insulin secretion during high-glucose treatment at 20 mM glucose by the insulin secretion at 0 mM glucose stimulation (1). For pseudo-islets in COLI gels, the mean ± SD of the insulin secretion during high-glucose treatment at 20 mM glucose was divided by the mean ± SD of the insulin secretion during 0 mM glucose stimulation while applying the propagation of error.

RNA isolation and NGS

To isolate RNA from pseudo-islets under glucose stimulation, pseudo-islets were washed five times using cold PBS after 30 min incubation with KREBS-BSA containing 20 mM glucose. Pseudo-islets were grouped as 180 per sample before RNA isolation was performed following the RNEasy micro kit protocol (74,004, Qiagen, Hilden, Germany). Briefly, grouped pseudo-islets were lysed in 250 μl RPE buffer containing 1% β-mercaptoethanol (M7522, Sigma-Aldrich) and frozen at −80 °C before further processing. On the day of the RNA isolation, vials were thawed, mixed with 250 μL of 70% ethanol and spun down at 15,000 × g for 15 s. Following discarding of the flowthrough, samples were washed with 350 μL RW1 and spun down at 15,000 × g for 15 s. After discarding the flowthrough, samples were washed with 500 μL RPE buffer at 15,000 × g for 15 s. Afterwards, samples were washed twice with 80% ethanol at 15,000 × g for 2 min. Samples were then spun down at 15,000 × g for 5 min with open lids to dry the membrane. All samples were resuspended in 14 μl RNAse-free water to elute the RNA and spun down at 15,000 × g for 7 min. The RNA content was quantified using the infinite M2000 Proplate reader with the NanoQuant Plate (Tecan,

Männedorf, Switzerland). All samples were stored at −80 °C until the NGS.

RNA quality was assessed with an Agilent Fragment analyzer (Agilent) and samples with RNA integrity number > 7 were selected for library construction on the automated workstation Biomek i7 (Beckman). 100 ng of total RNA was subjected to polyA enrichment using the NEBNext Poly(A) mRNA Magnetic Isolation Module (NEB). cDNA libraries were constructed using the resulting mRNA and the NEBNext Ultra II Directional RNA Library Prep Kit (NEB). Library molarity was determined by measuring the library size (approximately 400 bp) using the Fragment Analyzer with the High NGS Fragment 1−6000 bp assay (Agilent) and the library concentration (approximately 10 ng/μl) using the Infinite 200Pro (Tecan) and the Quant-iT HS Assay Kit (Thermo Fisher Scientific). The libraries were denaturated, diluted to 270 pM, and sequenced as paired-end 100 bp reads on an Illumina NovaSeq6000 (Illumina, San Diego, CA, USA) with a sequencing depth of approximately 40 million clusters per sample. Library preparation and sequencing procedures were performed by the same individual at the Quantitative Biology Center (QBiC) Tübingen, and a design aimed to minimize technical batch effects was chosen. Read quality of RNA-seq data in fastq files was assessed using ngs-bits (V2020_09−39) to identify sequencing cycles with low average quality, adaptor contamination, or repetitive sequences from PCR amplification. Data management and bioinformatic analysis were performed at QBiC Tübingen, Germany. A Nextflow-based nf-core pipeline nf-core/rnaseq (version 1.4.2; https://github.com/nf-core/rnaseq, accessed on 21 January 2021) was used for the RNA-seq bioinformatic analysis. As part of this workflow, FastQC (version v0.11.8) was used to determine the quality of the FASTQ files [25]. Subsequently, adapter trimming was conducted with Trim Galore (version 0.6.4) [26]. STAR aligner (version 2.6.1, [27]) was used to map the reads that passed quality control against GRCh37. RNA-seq data quality control was performed with RSeQC (version 3.0.1) [28] and read counting of the features (*e.g.*, genes) with featureCounts (version 1.6.4) [29]. An aggregation of the quality control for the RNA-seq analysis was performed with MultiQC (version 1.7; http://multiqc.info/, accessed on 21 January 2021) [30]. The analysis of the differential gene expression was performed in R language (version 3.5.1) using DESeq2 (version 1.22) through the Nextflow-based workflow qbic-pipelines/rnadeseq (https://github.com/qbic-pipelines/rnadeseq, accessed on 21 January 2021, version 1.3.2). Genes were considered differentially expressed when the Benjamini−Hochberg multiple testing adjusted p-value [31] was smaller than 0.05 ($p_{adj} \leq 0.05$). Multiple testing correction helped to reduce the number of false positives (not real DE genes). In the case of a threshold of 0.05, the proportion of false discoveries in the selected group of DE genes was controlled to be less than the threshold value—in this case, 5%. Final reports were produced using the R package rmarkdown (version 2.1) with the knitr (version 1.28) and DT (version 0.13) R packages. The sample similarity heatmaps were created using the edgeR (version 3.26.5) R package. Both KEGG and REACTOME databases were used for pathway analysis [32,33]. All differentially expressed genes were included, and enrichment was calculated using Fisher's exact test ($p \leq 0.05$).

Raman microspectroscopy and Raman imaging

A Raman microspectroscope (WiTec alpha 300 R, Ulm, Germany) with a charge-coupled device (CCD) camera (WiTec GmbH, Ulm, Germany) was utilized to analyze the pseudo-islets. A green laser (532 nm) with a grating of 600 g/mm, set to a laser power of 50 mW, and a 63x objective (W Plan-Apochromat 63x/1.0 M27, Carl Zeiss GmbH) was employed. Sections of the paraffin-embedded pseudo-islet samples were kept in PBS after deparaffinization and during the measurements. DCN reference spectra were obtained from pseudo-islets that were IF-stained for DCN. IF microscopy was used to locate DCN-positive areas before Raman measurements. The DCN spectrum was then extracted as the reference for further analyses. To obtain the reference spectrum of ER, ER-Tracker™ Green (E34251, Thermo Fisher Scientific) was used on EndoC-βH3 cells for Raman microscope navigation. The fluorescence signal from the ER was detected on the Raman heatmap (Suppl. Fig. S3). The ER spectrum was acquired by averaging the spectra of the fluorescence areas for the use of true component analysis (TCA) assessments. Unstained sections of pseudo-islets were scanned at an integration time of 0.05 s/spectrum and pixel resolution was set to either 0.5 × 0.5 μm or 1 × 1 μm to generate the spectral maps. For *in situ* scanning of living pseudo-islets in suspension culture, an organ-on-chip device was used as described earlier [21]. Briefly, pseudo-islets were loaded in flow traps by means of hydrostatic pressure. By applying a constant flow rate of 50 μl/h the pseudo-islets were kept immobilized. For imaging, the inverted Raman setup with a 60x objective (Carl Zeiss GmbH, Jena, Germany) was employed. The green laser of 50 mW with an integration time of 0.5 s/spectrum with pixel resolutions of 2 × 2 μm was used. The spectral data pre-processing and analysis was conducted on the Project Five 5.2 software (WiTec GmbH). The protocol is as follows: firstly, every spectrum was cropped from the range of 200 to 3000 cm^{-1} wavenumbers. Secondly, the artefacts caused by the cosmic rays were eliminated. Lastly, the graph background was then subtracted and the normalization of the area for each spectrum was performed. TCA was

utilized to generate the images with the signal intensity distribution representing all specific components of interest (DCN, ECM, ER). Principal component analysis (PCA) was employed to assess variations of molecular shifts as previously described [21]. PCA analysis was performed using the software Unscrambler X (CAMO Software AS, Oslo, Norway). PC scores and loadings plots were used to identify and interpret differences in the molecular composition of the three components.

Image analysis

For IF semi-quantification of pancreatic tissues, a minimum of five islets from a total of 5 different tissue sections were imaged. Co-localization analysis was performed *via* a self-written macro in Microsoft Excel (Microsoft Corporation). Briefly, the pixels of the red channel displaying insulin were compared to the pixels of the green channel displaying ECM proteins. The pixels were counted as co-localized if both pixels exceeded a defined threshold. Co-localization was normalized by the number of pixels of the ECM protein channel exceeding the threshold.

DCN-stained sections of DCN-treated and control samples were given randomly chosen encrypted file names and were counted by three unbiased observers. Cells were counted as DCN-positive if they expressed a clear DCN- and DAPI-positive staining. DCN-positive cells were categorized as periphery if they were present within the first two cell layers of the section viewed from outside to inside. All other DCN-positive cells were categorized as pseudo-islet core.

Semi-quantitative gray value intensity (GVI) analysis of IF-stained sections and Raman TCA was performed using ImageJ V 1.52p. For IF images, the region of interest (ROI) was chosen to include all DAPI-positive cells and copied into the channel to analyze. The obtained GVI was normalized by the area of the ROI. For Raman images, ROI for semi-quantification was chosen to include all nuclei-spectrum-positive pixels of the Raman TCA and copied to the channel for the components of interest (ECM, DCN and ER). The obtained GVI was normalized by the area of the ROI.

DCN direct labeling

For conjugation and purification of DCN, the Fluoro-spin 490 protein labeling & purification kit (MK-D0125-Z010.0−001, emp BIOTECH GmbH, Berlin, Germany) with DYOMICS DY-490 Fluorophore was used according to the manufacturer's instructions. Briefly, the required dye volume was calculated using the given Eq. (2:)

$$V_{dye} = \frac{(C_{protein,\ initial} * V_{protein} * 1000)}{C_{activated\ dye\ solution} * MW_{protein}} * MR \qquad (2)$$

The activated dye was gently mixed with protein solution and incubated for 5 min at RT. For purification, the dye-protein-mixture was pipetted onto a washing gel and centrifuged at 1000 x g for 2 min. The purified protein conjugate was collected, and the absorbance was measured at 280 nm and 493 nm. To verify the degree of labeling and calculate the final concentration of the labeled DCN, Eqs. (3), (4) and (5) were used.

$$\varepsilon = \frac{A_{280}}{C_{protein,\ initial} * b} \qquad (3)$$

$$C_{protein,\ conjugated} = \frac{A_{280} - (A_{493} * K) * DF}{\varepsilon} * MW \qquad (4)$$

$$D = \frac{A_{493} * DF}{6300 * C_{protein,\ conjugated}} * MW \qquad (5)$$

The description of the values and all values used and calculated can be found in Suppl. Table S2.

Results

DCN co-localizes with insulin in human pancreatic islets

To identify potential ECM proteins as treatment candidates to support β-cell functionality post-transplantation, IF staining was used on native human pancreatic tissue focusing on basement membrane (BM) proteins such as laminins (LAM) and collagen type 4 (COLIV), the fibrillar ECM proteins FN and COLI, as well as DCN (Fig. 1A-E). Co-localization studies showed a significantly higher ratio of co-localized DCN-positive and insulin (INS)-positive pixels within the native pancreatic tissue when compared with the other ECM proteins (Fig. 1F; LAM: 0.04 ± 0.04; COLIV: 0.03 ± 0.02; FN: 0.36 ± 0.09; COLI: 0.19 ± 0.13 *vs* DCN: 0.91 ± 0.04; $n \geq 6$, ****$p < 0.0001$). Further co-localization studies showed a significantly higher correlation of DCN with INS when compared with glucagon (GLU) (Fig. 1G, H; Fig 1I; GLU: 0.25 ± 0.15 *vs* INS: 0.79 ± 0.03; $n = 4$, ***$p < 0.001$), indicating a potentially important role of DCN in connection with the insulin-secreting β-cells within the islets of Langerhans.

DCN binds to the β-cells in pseudo-islets and improves insulin secretion in suspension

To test the hypothesis that DCN has a potential impact on the functionality of β-cells in the human pancreas, the human β-cell line EndoC-βH3 was aggregated into pseudo-islets and treated with in-house produced human recombinant full-length DCN (+DCN) [22]. Upon glucose stimulation with

20 mM glucose, pseudo-islets treated with 50 μg/ml DCN (pseudo-islets +DCN) secreted significantly more insulin compared with the control and other concentrations of DCN (Fig. 2A; control 3.70 ± 0.98 mU/l; 10 μg/ml DCN 3.66 ± 0.25 mU/l; 30 μg/ml DCN 3.66 ± 0.11 mU/l; 50 μg/ml DCN 5.83 ± 1.39 mU/l at 20 mM glucose; $n \geq 4$, $^{**}p < 0.01$, $^{****}p < 0.0001$) accompanied with a significant increase in the glucose-stimulated insulin secretion (GSIS) index (control: 1.38 ± 0.11 control; 10 μg/ml DCN 1.97 ± 0.31; 30 μg/ml DCN 1.80 ± 0.48; 50 μg/ml DCN 2.03 ± 0.35; $n \geq 4$, $^{*}p < 0.05$). IF staining for DCN of control pseudo-islets and pseudo-islets +DCN did not exhibit differences in GVI per pixel (Fig. 2B, 1.84 ± 0.58 control *vs* 1.98 ± 1.07 +DCN; $n = 8$, $p = 0.76$); however, structural variances were seen. In control pseudo-islets, DCN was homogenously expressed throughout the entire pseudo-islet, while pseudo-islets +DCN showed DCN-positive cells in the outer layer of the pseudo-islets (Fig. 2B, white arrows). This pattern was observed as early as 24 h after DCN-treatment (Fig. 2C, Suppl. Fig S1 A, B). The interaction of DCN in the periphery of the pseudo-islet was further confirmed using directly labeled DCN (Suppl. Fig. S1 C). Live tracking of the pseudo-islets +DCN showed that DCN directly attaches to the periphery of the pseudo-islets as early as 3 h post-treatment. Further analysis of the ECM composition of control pseudo-islets and pseudo-islets +DCN revealed a significant decrease of both fibrillar ECM proteins FN (Fig. 2D, 3.12 ± 0.72 control *vs* 1.76 ± 0.48 +DCN; $n \geq 4$, $^{*}p < 0.05$) and COLI (Fig. 2E, 7.66 ± 0.91 control *vs* 4.60 ± 1.44 +DCN; $n = 8$, $^{****}p < 0.0001$) after DCN-treatment. In contrast, DCN did not have a significant effect on the expression of E-cadherin (Suppl. Fig. 2A, 3.05 ± 0.47 control *vs* 3.29 ± 0.46 +DCN; $n \geq 4$, $p = 0.46$), INS (Suppl. Fig. 2B,

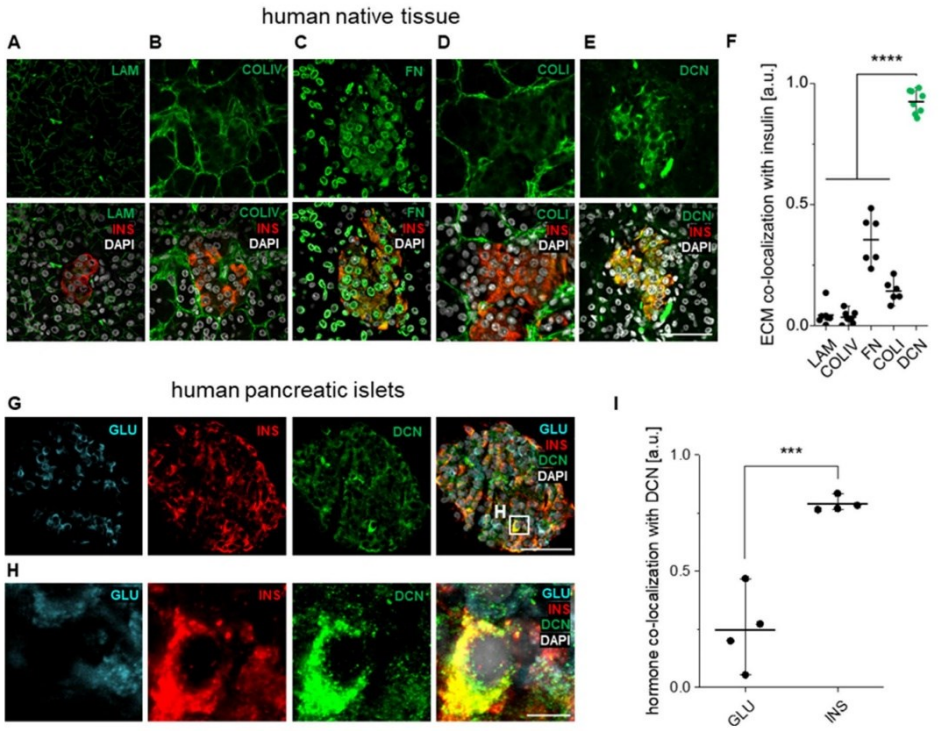

Fig. 1. DCN co-localizes with insulin-producing β-cells *in vivo*. Expression patterns of (A) LAM, (B) COLIV, (C) FN, (D) COLI, and (E) DCN in native pancreatic tissue. (F) Co-localization study shows strong correlation between DCN and insulin-expressing β-cells in islets of Langerhans. One-way ANOVA with Tukey's multiple comparison test ($n \geq 6$) $^{****}p < 0.0001$. (G, H) Expression patterns of GLU, INS, and DCN in isolated human pancreatic islets. (I) Co-localization study shows significantly higher correlation of DCN with INS compared to GLU. Unpaired *t*-test ($n = 4$) $^{***}p < 0.001$. Scale bars equal 50 μm (A-E, G) and 5 μm (H).

3.55 ± 1.66 control *vs* 3.84 ± 0.81 +DCN; $n \geq 4$, $p = 0.71$), or the BM proteins LAM (Suppl. Fig. 2C, 2.02 ± 1.13 control *vs* 2.70 ± 0.46 +DCN; $n = 7$, $p = 0.52$) and COLIV (Suppl. Fig. 2D, 3.08 ± 0.65 control *vs* 3.49 ± 1.06 +DCN; $n = 8$, $p = 0.18$). These results show for the first time the stimulatory effect of DCN-treatment on the insulin secretion of β-cells. Furthermore, DCN-treatment reduced the expression of fibrosis-affiliated ECM proteins under suspension culture conditions.

NGS reveals significant impact of DCN-treatment on mitochondria and ER and suggests lipoprotein receptor–related protein 1 as potential binding partner

NGS was performed to investigate the effects of DCN-treatment on the overall gene expression of pseudo-islets upon the glucose challenge. RNA was isolated after 30 min of high-glucose treatment at 20 mM glucose. In total, DCN-treatment led to a total of 348 differentially expressed genes, 84 of which were associated with a KEGG pathway (Fig. 3A). Fifty-one of these 84 genes were β-cell-related and classified to pathway networks related to ER, calcium-signaling, cyclic guanosine monophosphate (cGMP), semaphorin, mitogen-activated protein kinase (MAPK), Type 2 DM, and oxidative phosphorylation (OxPhos) (Fig. 3B). Of special interest were the genes related to OxPhos (Fig. 3C, D) and ER (Fig. 3E, F). In the OxPhos network, all genes that were differentially expressed were related to the electron transport chain and were significantly upregulated in pseudo-islets +DCN (Fig. 3D). This indicates an increased mitochondrial activity in the DCN-treated cells after high-glucose treatment at

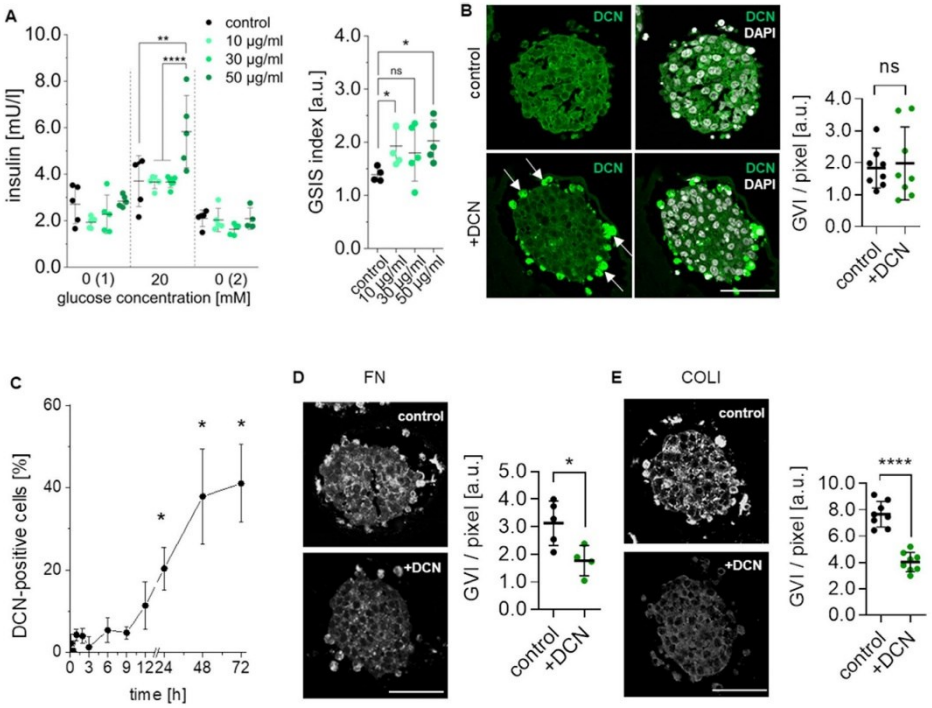

Fig. 2. DCN stimulates pseudo-islet functionality in suspension cultures and modulates ECM expression. (A) DCN treatment *in vitro* with 50 µg/ml significantly stimulates functionality of pseudo-islets. Two-way ANOVA with Tukey's multiple comparison test ($n \geq 4$), $^{**}p < 0.01$, $^{****}p < 0.0001$. Unpaired t-tests ($n \geq 4$), $^{*}p < 0.05$. (B) DCN-treatment resulted in strong expression of DCN in cells on the outside of the pseudo-islets (white arrows) with no difference in overall GVI per pixel ($n = 8$). Unpaired *t*-test. (C) DCN-positive cells on the periphery of the pseudo-islets are seen as early as 24 h after DCN treatment. One-way ANOVA with Tukey's multiple comparison ($n \geq 6$), $^{*}p < 0.05$. Quantification of (D) FN ($n \geq 4$) and (E) COLI ($n = 8$) IF staining shows a significant decrease for both ECM proteins upon DCN treatment. Unpaired *t*-test, $^{*}p < 0.05$, $^{****}p < 0.0001$. Scale bars equal 50 µm.

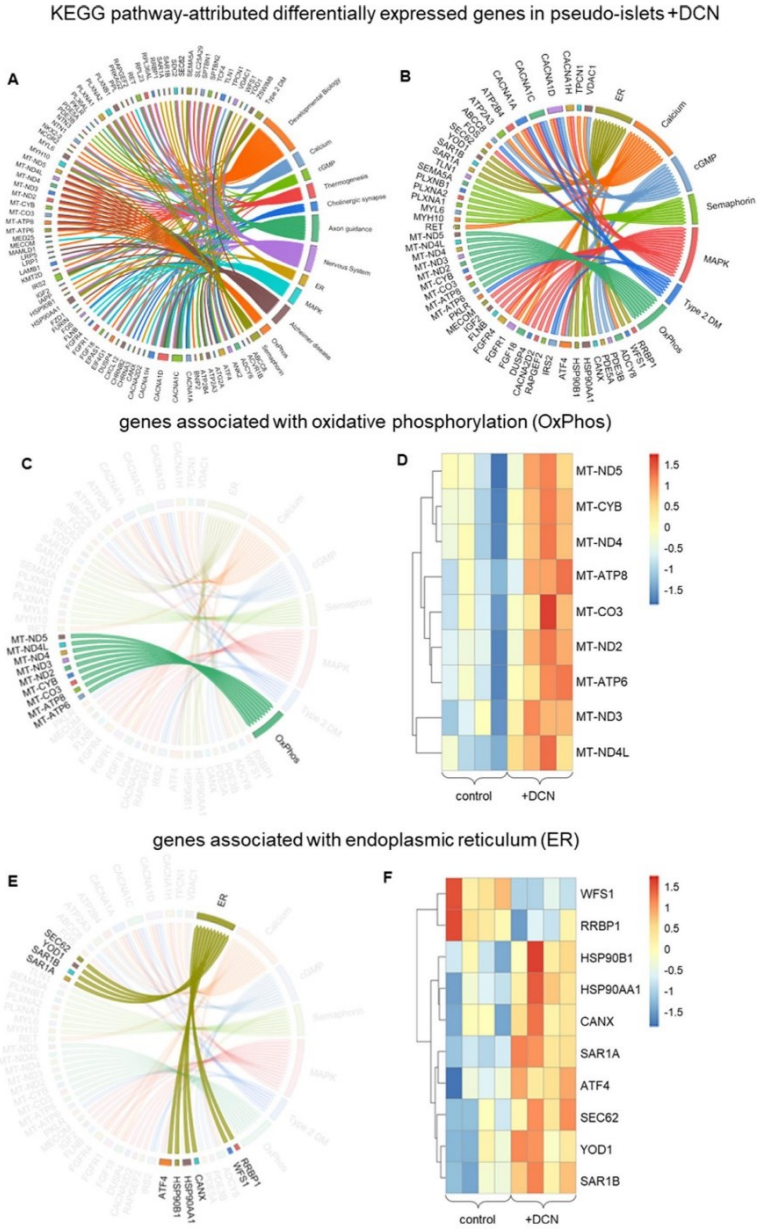

Fig. 3. NGS identifies differentially expressed genes in pseudo-islets +DCN. RNA was harvested immediately after high-glucose treatment of the pseudo-islets to identify genes affected by the DCN-treatment during insulin secretion (n = 4). (A) Eighty-four differentially expressed genes were matched to specific pathways using the KEGG database after

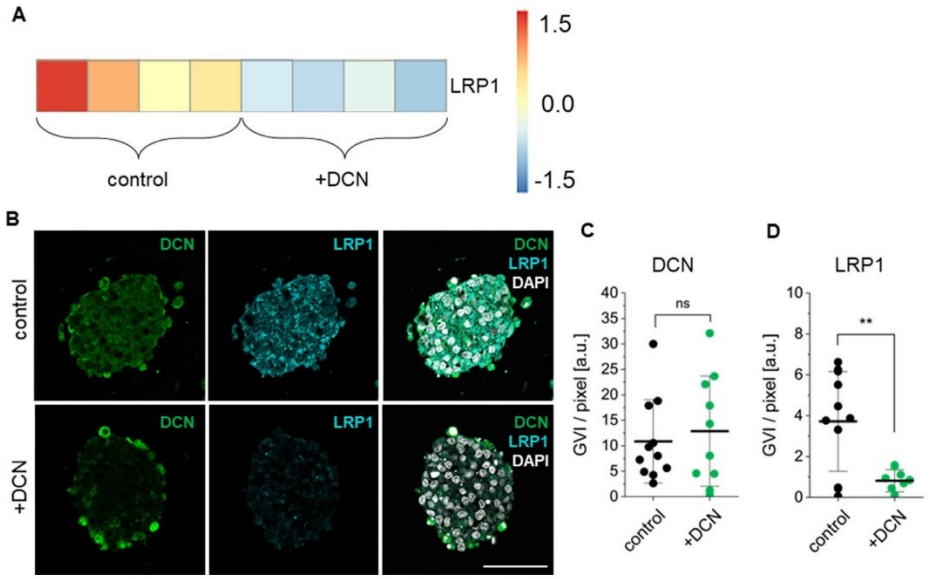

Fig. 4. DCN-treatment significantly downregulates LRP1 expression in β-cell-composed pseudo-islets. (A) NGS identifies RNA levels of LRP1 to be significantly downregulated after DCN-treatment ($n = 4$). (B) IF staining of control and DCN-treated pseudo-islets for DCN and LRP1 demonstrated the characteristic expression of DCN-positive cells at the periphery of the pseudo-islets. IF quantification showed (C) no difference in DCN intensity and (D) a significant decrease in LRP1 intensity in DCN-treated pseudo-islets ($n \geq 9$). Unpaired t-tests, $^{**}p < 0.01$. Scale bar equals 50 μm.

20 mM glucose. In the ER network, 8 of 10 genes were significantly upregulated after DCN-treatment (Fig. 3F). Among other tasks, the ER in β-cells is responsible for the folding and transport of proteins, such as insulin. Detailed NGS results are available in the data repository.

Furthermore, the list of differentially expressed genes was screened for potential binding partners of DCN. Interestingly, the RNA levels of the endocytic receptor low−density lipoprotein receptor−related protein 1 (LRP1) were significantly downregulated in DCN-treated pseudo-islets ($\log_2$ fold change −0.12, ** $p < 0.01$) (Fig. 4A, Suppl. Table S3). IF staining for LRP1 was performed to investigate whether the significant decrease in RNA levels was translated to the protein level (Fig. 4B). IF staining evaluation showed the characteristic DCN deposition at the periphery of the pseudo-islets with no change in overall GVI per pixel (Fig. 4C; 10.87 ± 7.83 control *vs* 12.87 ± 10.26 +DCN, $p = 0.64$). LRP1 intensity significantly decreased upon DCN-treatment (Fig. 4D; 3.72 ± 2.33 control *vs* 0.81 ± 0.51 +DCN, ** $p < 0.01$) in line with the NGS data, suggesting an LRP1-mediated interaction between the supplemented DCN and the β-cell-composed pseudo-islets.

Raman imaging confirms changes in the endoplasmic reticulum of DCN-treated pseudo-islets

Raman imaging was employed to further identify potential biochemical changes in the DCN-treated pseudo-islets with special focus on the ER. The acquired Raman data were analyzed using TCA as well as PCA. TCA is a quantitative Raman image analysis method that provides unique insight into the spatial distribution of pixels with specific spectral characteristics, which can be used to locate different components within a sample or tissue. In contrast, PCA is a more qualitative analysis method that gives further insight into differences of the overall

DCN treatment. (B) Fifty-one of these 84 genes are β-cell-related genes that have roles in 7 different pathways and mechanisms. (C) 9 genes related to OxPhos were differentially expressed. (D) All of these 9 genes were upregulated after DCN-treatment. (E) 10 genes related to the endoplasmic reticulum were differentially expressed in pseudo-islets +DCN. (F) 8 of these 10 genes were upregulated after DCN-treatment. Genes were classified as differentially expressed with $p_{adjusted} < 0.05$.

molecular composition between samples and tissues [21]. TCA was performed to localize three major components of interest within the control pseudo-islets and pseudo-islets +DCN, namely the general ECM component as well as the specific components for DCN and the ER (Fig. 5A, B). The spectrum for the general ECM component was obtained as described earlier [8]. The spectra for the DCN and the ER components were obtained by measuring cellular areas positively stained for DCN

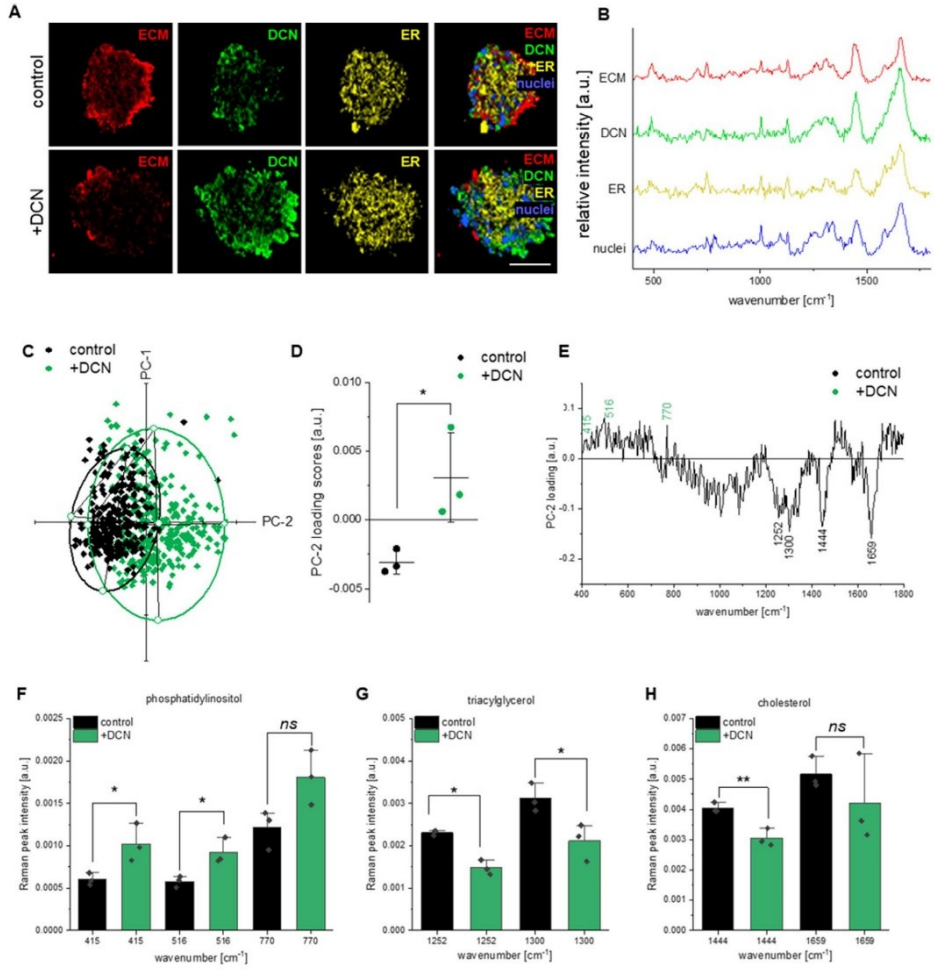

Fig. 5. Raman imaging of live pseudo-islets supplemented with 20 mM glucose. (A) Application of Raman spectra for ECM, DCN, and ER on live control pseudo-islets and pseudo-islets +DCN. Scale bar equals 50 μm. (B) Corresponding representative Raman spectra of ECM, DCN, ER, and nuclei. (C) PCA of the obtained ER component shows a separation *via* PC-2 between control pseudo-islets and pseudo-islets +DCN. (D) Comparing the PC-2 loading scores of 100 spectra shows a significant difference between control and pseudo-islets +DCN ($n = 3$). Unpaired *t*-test, $*p < 0.05$. (E) Loading of PC-2 indicates an increased expression of PI (peaks at 415, 516, and 770 cm^{-1}) in pseudo-islets +DCN compared with the control cultures while control pseudo-islets showed an increased presence of TAG (peaks at 1252 and 1300 cm^{-1}) and cholesterol (peaks at 1444 and 1659 cm^{-1}). After DCN-treatment, (F) PI levels are increased in pseudo-islets, whereas levels of (G) TAG and (H) cholesterol are decreased ($n = 3$). Unpaired t-tests, $*p < 0.05$, $**p < 0.01$.

and ER, respectively (Suppl. Fig. S3). We defined the ER spectrum by averaging Raman spectra obtained from pixels that stained positively for the ER tracker. The resulting ER spectrum showed characteristic peaks (750, 1001, 1128, 1303, 1446 and 1606 cm^{-1} (Suppl. Fig. S3 F) for protein-rich regions similar to those described by Prats Mateu et al. [34]. It should be mentioned that especially the peak at 750 cm^{-1} is usually described for cytochrome-c, a protein of the mitochondrial membrane, indicating contributions of other cell organelles to this ER spectrum [35]. The TCA false color images of the three components did not show differences in GVI per pixel (Suppl. Fig. S4, B (ECM): 0.32 ± 0.05 control *vs* 0.38 ± 0.10 +DCN; $n = 3$, $p = 0.49$; E (DCN): 0.45 ± 0.15 control *vs* 0.33 ± 0.03 +DCN; $n = 3$, $p = 0.35$; H (ER): 0.49 ± 0.05 control *vs* 0.43 ± 0.06 +DCN; $n = 3$, $p = 0.28$). Evaluation by component-positive area (Suppl. Fig. S4, C (ECM): 65.55 ± 8.97% control *vs* 70.04 ± 14.00% +DCN; $n = 3$, $p = 0.72$; F (DCN-positive area): 45.47 ± 8.64% control *vs* 45.45 ± 4.84% +DCN; $n = 3$, $p = 1.00$; I (ER): 74.00 ± 1.62% control *vs* 74.32 ± 8.60% +DCN; $n = 3$, $p = 0.96$) between control and DCN-treatment samples did not show any significant differences; however, PCA, which gives insights about the biochemical composition of the ER component, showed a separation between control pseudo-islets and pseudo-islets +DCN (Fig. 5C), with a significant difference between the mean PC-2 loading scores (Fig. 5D: −0.003 ± 0.0007 control *vs* 0.003 ± 0.003 +DCN; $n = 3$, $^{*}p < 0.05$). As the mean PC-2 loading score is positive for pseudo-islets +DCN (Fig. 5D), the changes after DCN-treatment can be attributed to positive peaks in the PC-2 loading plot indicating an increase in phosphatidylinositol (PI) (415, 516, and 770 cm^{-1}) (Fig. 5E). In contrast, control pseudo-islets with a negative mean PC-2 loading score (Fig. 5D) were characterized by negative peaks for triacylglycerol (TAG) (1252 and 1300 cm^{-1}) and cholesterol (1444 and 1659 cm^{-1}) (Fig. 5E). Peak intensity analysis of the ER Raman spectra of control pseudo-islets and pseudo-islets +DCN, which gives a quantitative result about the levels of the different components, indicated significant differences between both groups (Fig. 5F-H, Suppl. Fig. S5 G;). While PI levels were significantly upregulated after DCN-treatment (Fig. 5F; 415 cm^{-1}: 0.00060 ± 0.00006 control *vs* 0.0010 ± 0.0002 +DCN, $^{*}p < 0.05$; 516 cm^{-1}: 0.0006 ± 0.0001 control *vs* 0.0009 ± 0.0001 +DCN, $^{*}p < 0.05$; 770 cm^{-1}: 0.0012 ± 0.0002 control *vs* 0.0018 ± 0.0003 +DCN, $p = 0.06$), TAG (Fig. 5G; 1252 cm^{-1}: 0.00231± 0.0001 control *vs* 0.0015 ± 0.0001 +DCN, $^{*}p < 0.05$; 1300 cm^{-1}: 0.0031 ± 0.0003 control *vs* 0.0021 ± 0.0004 +DCN, $^{*}p < 0.05$) and cholesterol (Fig. 5H; 1444 cm^{-1}: 0.0041 ± 0.0001 control *vs* 0.00305 ± 0.0002 +DCN, $^{**}p < 0.01$; 1659 cm^{-1}: 0.0052 ± 0.0004 control *vs* 0.0042 ± 0.0012 +DCN, $p = 0.34$; 770 cm^{-1}: 0.0012 ± 0.00019 control *vs* 0.0018 ± 0.0027 +DCN, $p = 0.06$) levels were significantly downregulated after DCN-treatment. PCA of the ECM component (Suppl. Fig. S5 A-C, B (PC-1): −0.0007 ± 0.003 control *vs* 0.001 ± 0.007 +DCN; $n = 3$, $p = 0.77$; C (PC-2): −0.0006 ± 0.002 control *vs* 0.0007 ± 0.0009 +DCN; $n = 3$, $p = 0.47$) and the DCN component (Suppl. Fig. S5 D-F, E (PC-1): −0.002 ± 0.003 control *vs* 0.003 ± 0.004 +DCN; $n = 3$, $p = 0.25$; F (PC-2): 0.002 ± 0.002 control *vs* −0.002 ± 0.002 +DCN; $n = 3$, $p = 0.08$) did not show a significant separation between both groups. A detailed description of the peaks and their assignments can be found in Suppl. Table S4.

COLI and DCN mimic features of the native pancreatic environment in support of pseudo-islets *in vitro*

To determine whether DCN has similar effects in a biomaterial suitable for islet transplantation, pseudo-islets were encapsulated within a clinical grade, good manufacturing practice (GMP)-approved COLI gel [24] as a carrier material and treated with DCN. To investigate the structural distribution of the native fibrillar collagen network within the islets of Langerhans *in vivo*, we performed IF staining of human native pancreatic tissue (Fig. 6A, B). We were able to mimic the observed pattern by encapsulating our pseudo-islets in a COLI hydrogel (Fig. 6C, D). Evaluation of the stiffness of a pure COLI gel and a COLI gel with pseudo-islets showed a significant difference of the elastic modulus for both groups (Fig. 6E, 3.1 ± 0.24 COLI gel *vs* 4.1 ± 0.23 COLI gel with pseudo-islets, $n \geq 4$, $^{***}p < 0.001$); however, both groups lied within the stiffness range of pancreatic tissue reported in the literature [36–38]. IF staining for DCN of control pseudo-islets and pseudo-islets +DCN in the COLI gel showed that DCN in control pseudo-islets was homogeneously distributed, whereas DCN-treated pseudo-islets in the gel showed a DCN-positive layer of cells in the periphery of the pseudo-islets (Fig. 6F, white arrows). Overall, there were no significant differences of GVI per pixel between both groups (1.84 ± 1.52 control *vs* 1.80 ± 0.88 +DCN, $n \geq 12$, $p = 0.95$). This result is comparable to the results obtained in pseudo-islets treated with DCN in suspension. We further confirmed this observation by employing Raman imaging on fixed control pseudo-islets and fixed pseudo-islets +DCN in the COLI gel (Fig. 6G, Suppl. Fig. S6 B). We conducted TCA on the same three main components (ECM, DCN, and ER) and evaluated the component-positive area as described earlier for pseudo-islets in suspension. TCA false color images displayed a significant decrease of the component-positive area for

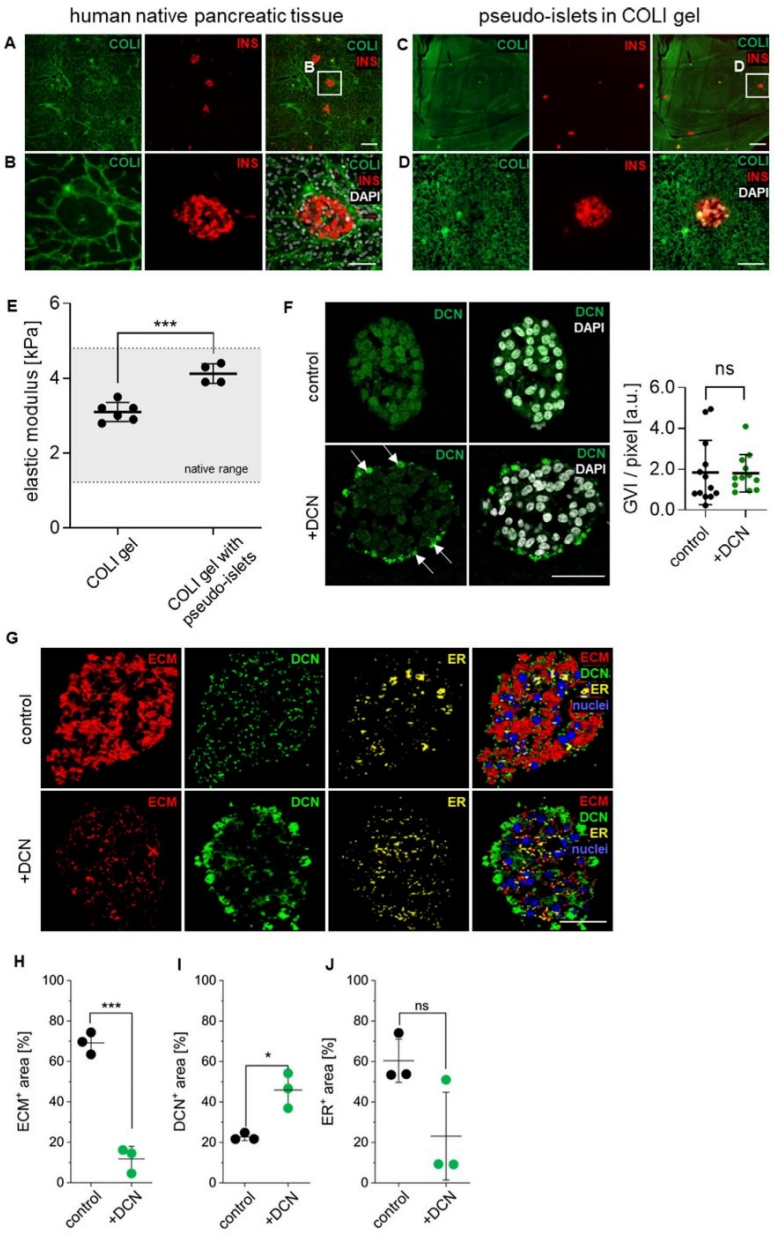

Fig. 6. Structural evaluation of control pseudo-islets and pseudo-islets +DCN in COLI gel. (A, B) Distribution of islets of Langerhans in native pancreatic tissue surrounded by a COLI matrix. (C, D) Pseudo-islets in a COLI gel recreates native distribution of islets of Langerhans *in vivo*. Scale bars equal 200 μm (A, C) and 50 μm (B, D). (E) Evaluation of the elastic

ECM within pseudo-islets +DCN (Fig. 6H, 69.16 ± 4.45% control *vs* 11.77 ± 5.12% +DCN, $n = 3$, ***$p < 0.001$). The component-positive area for DCN was significantly higher in pseudo-islets +DCN compared with the control (Fig 6I, 22.72 ± 1.48% control *vs* 45.89 ± 7.07% +DCN, $n = 3$, *$p < 0.05$). The ER component showed no difference between both groups (Fig. 6J, 60.38 ± 9.67% control *vs* 23.11 ± 19.67% +DCN, $n = 3$, $p = 0.07$). The GVI per pixel of the ECM component was significantly decreased in the DCN-treated pseudo-islets (Suppl. Fig. S6 B, C, 0.95 ± 0.04 control *vs* 0.83 ± 0.03 +DCN, $n = 3$, *$p < 0.05$), confirming the results of the component-positive area evaluation. GVI per pixel of the DCN component (Suppl. Fig. S6 D, E, 0.56 ± 0.02 control *vs* 0.61 ± 0.03 +DCN, $n = 3$, $p = 0.09$) and the ER component (Suppl. Fig. S6 G, H, 0.40 ± 0.09 control *vs* 0.51 ± 0.17 +DCN, $n = 3$, $p = 0.45$) showed no significant difference between both groups; however, the numbers followed a similar trend as the component-positive area evaluation. PCA of the components ECM and DCN did not show a separation between both groups (Suppl. Fig. S7 A-F, B (ECM, PC-1), 0.0019 ± 0.0016 control *vs* −0.0019 ± 0.0015 +DCN, $n = 3$, $p = 0.07$; C (ECM, PC-2), −0.0001 ± 0.0014 control *vs* 0.0001 ± 0.0006 +DCN, $n = 3$, $p = 0.85$; E (DCN, PC-1), 0.0019 ± 0.0030 control *vs* −0.0019 ± 0.0032 +DCN, $n = 3$, $p = 0.29$; F (DCN, PC-2), 0.0011 ± 0.0016 control *vs* −0.0014 ± 0.0035 +DCN, $n = 3$, $p = 0.42$). Interestingly, PCA of the ER component (Suppl. Fig. S7 G) showed a significant difference between control pseudo-islets and pseudo-islets +DCN attributed to PC-1 (Suppl. Fig S7 H, −0.0017 ± 0.0021 control *vs* 0.0027 ± 0.0036 +DCN, $n = 3$, $p = 0.21$), while PC-2 was not significantly different (Suppl. Fig S7 I, 0.0043 ± 0.0016 control *vs* −0.0042 ± 0.0031 +DCN, $n = 3$, *$p < 0.05$). Differences between both groups were attributed to cholesterol (1442 and 1602 cm^{-1}) as well as TAG (1249 and 1300 cm^{-1}) (Suppl. Fig. S7 J, K). After DCN-treatment, cholesterol peaks at 1442 cm^{-1} were significantly upregulated, whereas cholesterol peaks at 1662 cm^{-1} were significantly downregulated (Suppl. Fig. S7 L; 1442 cm^{-1}: 0.0036 ± 0.0001 control *vs* 0.0045 ± 0.0004 +DCN, *$p < 0.05$; 1662 cm^{-1}: 0.0058 ± 0.0001 control *vs* 0.0038 ± 0.0001 +DCN, **** $p < 0.0001$), indicating structural differences of cholesterol, such as *cis* or Z-confirmation found in fatty acids, rather than quantitative differences [39]. Interestingly, the decrease in TAG due to the DCN-treatment was preserved in the COLI gel cultures, represented by a significant decrease in the peak intensity at 1249 cm^{-1}. The peak at 1300 cm^{-1} did not show a statistically significant decrease (Suppl. Fig. S7 M; 1249 cm^{-1}: 0.0026 ± 0.0001 control *vs* 0.0017 ± 0.00007 +DCN, **$p < 0.01$; 1300 cm^{-1}: 0.0026 ± 0.0001 control *vs* 0.0026 ± 0.0003 +DCN, $p = 0.87$). Overall, the observed effects of the DCN-treatment on β-cell-containing pseudo-islets in suspension could be recapitulated in an encapsulation environment, especially regarding the DCN-binding to the periphery of the pseudo-islets as well as the rearrangement of the expressed ECM. These results suggest the suitability of COLI as a potential carrier material to use DCN in an islet transplantation environment.

DCN improves insulin secretion and impacts ECM patterns of β-cell-containing pseudo-islets embedded in a COLI gel

After confirming that the interaction of DCN and pseudo-islets in the COLI gel were comparable to the parameters observed in suspension, the effects of DCN on pseudo-islet function in the COLI gel were investigated. Upon glucose challenge, pseudo-islets +DCN secreted significantly more insulin when compared with the control group (Fig. 7A, 50.19 ± 6.68 mU/l control *vs* 61.53 ± 24.15 mU/l +DCN at 0 mM glucose; $n \geq 7$, $p = 0.20$; 98.82 ± 12.86 mU/l control *vs* 119.41 ± 14.57 mU/l +DCN at 20 mM glucose; $n \geq 8$, *$p < 0.05$); however, the glucose-stimulated insulin secretion (GSIS) index was not affected (Fig. 7B, 1.97 ± 0.09 control *vs* 1.94 ± 0.21 +DCN; $n \geq 7$, $p = 0.75$). IF staining for both INS (Fig. 7C, 3.88 ± 1.03 control *vs* 7.13 ± 3.17 +DCN; $n \geq 8$, **$p < 0.01$) and E-cadherin (Fig. 7D, 4.06 ± 0.99 control *vs* 6.75 ± 2.38 +DCN; $n \geq 8$, **$p < 0.01$) showed a significant increase in pseudo-islets +DCN compared with the control samples, supporting the results from the GSIS assay. Interestingly, evaluation of the impact of DCN on the pseudo-islet ECM showed that DCN-treatment significantly decreased COLI (Fig. 7E, 2.27 ± 0.61 control *vs* 0.98 ± 2.38 +DCN; $n \geq 9$, ****$p < 0.0001$) and LAM contents (Fig. 7F, 11.40 ± 1.77 control *vs* 5.78 ± 1.89 +DCN; $n = 10$,

modulus of pure COLI gel and COLI gel loaded with pseudo-islets in comparison to the elastic modulus of the of native pancreatic tissue according to literature shown in gray ($n \geq 4$). (F) Pseudo-islets in COLI gel +DCN show DCN-positive cells on the outside of the pseudo-islets with no difference in overall GVI per pixel ($n \geq 12$). (G) Raman images of unstained sections of control pseudo-islets and pseudo-islets +DCN in COLI gel presenting the components for ECM, DCN, ER, and the merged image including the nuclei component. Scale bar equals 50 μm. Area percentage analysis of (H) ECM component ($n = 3$), (I) DCN component ($n = 3$) and (J) ER component ($n = 3$) confirms the presence of DCN on the outside of the pseudo-islets and show an overall decrease in ECM content in pseudo-islets in COLI gel +DCN compared to control. Unpaired *t*-test, *$p < 0.05$, ***$p < 0.001$.

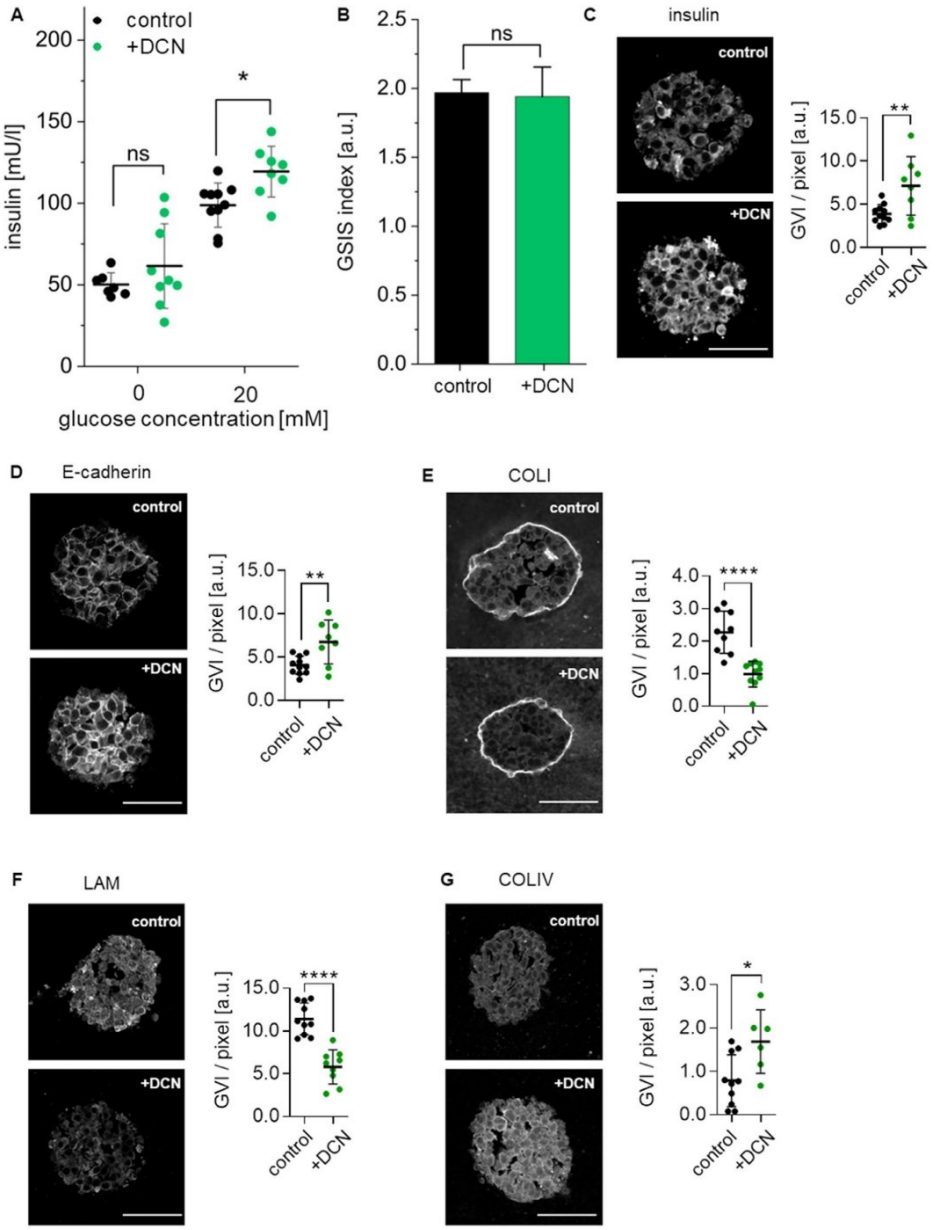

Fig. 7. Functionality and ECM assessment of control pseudo-islets and pseudo-islets +DCN in COLI gel. (A) Pseudo-islets in COLI gel +DCN show a significantly increased insulin secretion after high-glucose treatment when compared to the control ($n \geq 7$). One-way ANOVA with Fisher's multiple comparison, *$p < 0.05$. (B) GSIS index of pseudo-islets

$^{****}p < 0.0001$). In contrast, COLIV intensity was significantly increased after DCN-treatment compared with the control samples (Fig. 7G, 0.79 ± 0.57 control *vs* 1.69 ± 0.67 +DCN; $n \geq 6$, $^{*}p < 0.05$). DCN-treatment of pseudo-islets in the COLI gel did not influence the expression intensity of FN (Suppl. Fig S8, 2.51 ± 1.11 control *vs* 2.66 ± 1.29 +DCN; $n \geq 13$, $p = 0.76$).

Discussion

Research in the field of islet transplantation has progressed immensely over the last decade; however, clinical translation of the findings has been rather slow. The treatment and encapsulation of islets within materials based on native ECM proteins has been shown to support cell survival and function in transplantation settings [16]. In this study, we identified DCN to be highly co-localized with insulin-producing β-cells in human pancreatic tissues. We identified that DCN-treatment increased the glucose-responsiveness of our *in vitro* pseudo-islet model. DCN-treatment also reduced the expression of FN and COLI, ECM proteins affiliated with fibrosis. Further analysis using next-generation sequencing and Raman microspectroscopy identified changes in mitochondrial activity and ER because of the DCN-treatment. When the pseudo-islets were encapsulated within a clinically approved COLI gel, the positive effects of DCN-treatment on glucose-responsiveness and ECM expression were maintained, suggesting that the advantages of DCN-treatment are translatable to a transplantation setting.

DCN is a class I small leucine-rich proteoglycan (SLRP) involved in the regulation of multiple cellular processes including cell growth, proliferation, and migration [40]. In particular, it has been investigated for its anti-tumorigenic effects through antagonizing key receptor tyrosine kinase pathways involved in cancer progression and sequestering of growth factors within the ECM [40]. These properties were achieved through its role in preventing fibrillogenesis of fibrillar proteins such as COLI, as well as tumor-suppression *via* p53 signaling [41]. Within the pancreas, DCN is highly expressed by pancreatic pericytes forming the interstitial matrix and islet BM to support β-cells [42]. In the mouse model of insulinoma, where there is an excess production of insulin by β-cells, DCN was significantly downregulated [43]. In our study, DCN-treatment increased the glucose-responsiveness of the pseudo-islets. While little work has been done in understanding the role of this proteoglycan in the environment of a pancreatic islet, it is known that DCN plays a role in glucose tolerance. Mice lacking DCN had impaired glucose tolerance, which was associated with reduced ECM organization and increased activation of the complement cascades, promoting inflammation [44]. Interestingly, these effects of glucose intolerance and inflammation in DCN knockout mice could be attributed to the increased expression of histidase, a protein that degrades histidine. The amino acid histidine has been shown to ameliorate insulin resistance, inflammation, and oxidative stress when supplemented [45–47]. The protective effect of DCN in terms of modulating inflammation can be further advantageous in a transplantation setting. In response to a transplanted graft, the host's immune system attempts to repair the damaged tissue and limit the interaction with the foreign material at the transplant site. This results in the transplanted device becoming enclosed within a dense layer of inflammatory cells and connective tissue [48]. During this process, the ECM is remodeled to support the regeneration of the tissue resulting in the deposition of ECM proteins such as FN and the fibrillar COLI [49], which ultimately isolates the transplanted device from the host's system, rendering the transplant ineffective. Interestingly, in our study, DCN-treatment significantly downregulated the presence of ECM proteins FN and COLI, in line with past research that identified DCN as a modulator of scar tissue formation and reduced inflammatory responses [50–52]. These observations were recapitulated in our *in vitro* model in which the pseudo-islets were encapsulated within a COLI carrier gel. Similar to our suspension cultures, DCN treatment of the encapsulated pseudo-islets improved the glucose response and modulated the presence of COLI. While FN was not significantly affected by the DCN treatment in the gel as it did in suspension, LAM were significantly downregulated and COLIV was significantly upregulated upon DCN treatment.

Taken together our functional data of the pseudo-islets and the regulation of ECM presence, DCN-treatment has the potential to support islet transplantation by improving islet functionality and supporting graft survival post-transplantation through modulation of fibrotic tissue formation. It must be noted that DCN is an SLRP that shares similar structural and functional properties with other SLRPs including biglycan (also a class I SLRP), as well as lumican and fibromodulin of the class II SLRPs [53–55]. The different SLRPs have been shown to play key roles in collagen fibrillogenesis and ECM remodeling [56], as well as in cell signal transduction pathways

+DCN in COLI gel shows no significant difference compared with the control. Pseudo-islets +DCN in COLI gel show significantly increased expression of INS ($n \geq 8$) (C), E-cadherin ($n \geq 8$) (D), and the BM protein COLIV ($n \geq 6$) (G). In contrast, DCN-treatment significantly decreases the expression of COLI ($n \geq 9$) (E) and LAM ($n \geq 9$) (F). Unpaired *t*-test, $^{**}p < 0.01$, $^{****}p < 0.0001$. Scale bars equal 50 μm.

through binding of surface receptors including Toll-like receptor, vascular endothelial growth factor receptor (VEGFR), epidermal growth factor receptor (EGFR), LRPs, and insulin-like growth factor receptor [53,55]. Future studies exploring the effects of different SLRPs on β-cell function are necessary in order to better understand both glucose metabolism and the various effects of SLRPs. To investigate potential cellular processes through which the DCN-treatment improves insulin secretion in β-cells, pseudo-islets challenged with a high glucose concentration were used for NGS analysis. In our DCN-treated pseudo-islets, NGS results identified genes associated with the mitochondrial electron transport chain and the ER to be differentially expressed. The electron transport chain is the final step of cellular respiration in the mitochondria for the production of ATP through OxPhos [57], and is essential for the appropriate secretion of insulin by β-cells [58,59]. An upregulation of genes involved in the protein complexes of the electron transport chain was observed in the DCN-treated samples. This supports our observations of increased insulin secretion in the DCN samples, where greater levels of ATP are required for the highly metabolic processes of insulin production and secretion. Mitochondria isolated from β-cells revealed a significant decrease in electron transport activity in the glucose-unresponsive cells when compared with glucose-responsive cells [60]. Further, it has been shown that reduced electron transport chain activity, expression, and mitochondrial DNA can be associated with increased insulin resistance and Type 2 DM [61], supporting our finding of high metabolic activity of β-cells after DCN-treatment. Interestingly, previous studies have shown DCN to depolarize mitochondrial membranes, which results in mitochondrial fragmentation through its binding to VEGFR2 [62]. β-cells are metabolism-heavy cells that exhibit hyperpolarization of the mitochondrial membrane potential to respond to high glucose concentrations [63,64], which corresponds with increased insulin secretion [65,66]. It is possible that DCN has a similar effect of depolarizing the mitochondrial membrane potential in β-cells during glucose challenges. This allows for increased polarization events to improve cell functionality as we had observed with the increased insulin secretion. Future studies investigating DCN's effect on β-cell mitochondrial function would prove to be beneficial in understanding DCN's role in supporting β-cell functionality during periods of stress.

The ER is responsible for precise protein synthesis and trafficking to the necessary cellular compartments. Cells undergo ER stress when there is an accumulation of misfolded proteins at which point they activate response pathways including ER-associated degradation (ERAD) and the unfolded protein response (UPR). Through these pathways, they degrade misfolded proteins and increase the presence of molecular chaperones required for proper protein folding. β-cells experience high levels of ER stress due to the secretion of insulin upon a glucose challenge [67–70]. The increased amount of secretory proteins (in this case insulin) and proteins involved in the trafficking of said proteins allows for a greater number of proteins that can be misfolded, increasing ER stress [71]. It has been suggested that approximately 20% of proinsulin is misfolded [72–74], at which point the protein is degraded. Studies have also shown that this high requirement of the ER can also be the cause of β-cell dysfunction and loss, leading to the progression of Type 2 DM [75–77]. Our NGS data showed that the ER proteins Wolframin ER transmembrane glycoprotein (WFS1) and Ribosome Binding Protein 1 (RRBP1) were downregulated in the DCN-treated samples. WFS1 is a calcium (Ca^{2+}) channel protein that allows Ca^{2+} to enter the ER [78], which is found primarily within the β-cells of the pancreatic islets [79]. Ca^{2+} plays a key role in both protein folding and insulin secretion, where ER stress is known to lead to a decrease in Ca^{2+} within the ER [80,81]. The reduced WFS1 at the ER can increase Ca^{2+} oscillations within the cytosol, increasing the amount of Ca^{2+} being secreted as a result of the DCN-treatment. There have been conflicting studies indicating the role of WFS1 in the cellular response to ER stress. Within the pancreatic islet, WFS1 expression at the mRNA and protein levels were increased following drug-induced ER stress [79]. It has also been shown that the loss of WFS1 can lead to ER stress and β-cell dysfunction [82], where mutations in the WFS1 gene, associated with Wolfram syndrome, also leads to the onset and progression of Type 2 DM [83]. Additionally, we observed a downregulation of RRBP1. RRBP1 is involved in the interaction of the ribosomes with the ER to support protein translation and transport, where the knockdown of this protein resulted in ER stress [84]; however, a genomic and proteomic study in murine islets showed that RRBP1 was upregulated in mice with Type 2 DM, suggesting it may have a role in β-cell dysfunction [85].

NGS identified further genes associated with ER stress including heat shock proteins (HSPs), ATF4, and YOD1 to be upregulated in the DCN-treated samples. HSP90A is an indicator of cellular stress, particularly in response to inflammation [86], and it is also associated with the onset of Type 1 DM [87]. ATF4 is a transcription factor that plays a key role in response to ER stress, through activation of 4E-BP1 expression [68,88]. The upregulation of the HSPs and ATF4 in the DCN-treated samples can be in response to the cellular stress caused by the increased demand for protein production and trafficking within the ER to maintain homeostasis. YOD1 is a deubiquitinase involved in ERAD for the degradation and removal of lysosomes [89]. Its upregulation in the DCN-treated samples implies its

necessity for both the processing of autophagocytosed DCN and quality control of the increased amount of protein (insulin) produced and trafficked.

NGS analyses showed an upregulation of genes involved in protein and vesicular trafficking including CANX, SAR1A, SEC62, and SAR1B, potentially due to the increased release of insulin in the secretory vesicles. CANX is a Ca^{2+}-binding protein involved in the processing and the quality control of protein folding within the ER. SAR1A, SEC62, and SAR1B play a role in vesicular trafficking of proteins from the ER to the golgi apparatus in preparation for secretion. The upregulation of such genes is in line with our observations of increased insulin secretion in the DCN-treated samples. An impaired transport of (pro) insulin between the two organelles can result in β-cell failure, lipotoxicity, and DM [90–93], where in MIN6 cells, a murine pancreatic insulinoma β-cell line, a mutant for Sar1A was unable to achieve proper folding of proinsulin, resulting in ER stress and β-cell failure [94,95]. The upregulation of SAR1A suggests DCN-treatment improves insulin secretion through upregulation of proteins that support the folding of insulin. Experiments evaluating the presence of trafficking and extracellular vesicles for the transport of insulin to be secreted and/or degraded would provide greater insight in to how DCN supports β-cell function and insulin secretion.

Interestingly, Raman microspectroscopy also identified the ER component to be significantly affected in the DCN-treated samples with emphasis on PI. PIs are the precursor to the many variations of phosphoinositides that are involved in a variety of cellular processes including vesicular trafficking, engulfment, ion channel regulation, and intracellular signaling [96–98]. As such, the increased presence of PI can be attributed to the need for increased numbers of vesicles for insulin secretion. Past studies observing phospholipid presence during glucose-stimulated insulin secretion also identified an increase in PI when there is increased insulin secretion at high glucose concentrations [21,99]. Apart from an increase in PI, Raman microspectroscopy and Raman imaging highlighted the decrease in TAG in DCN-treated samples. Sánchez-Archidona et al. identified TAGs as potential regulators of insulin secretion and insulin signaling pathways [100]. They observed that reduced TAG content led to an increase in insulin secretion by increased K_{ATP}-channel expression. Furthermore, β-cells secrete lipase, a lipoprotein involved in the release of free fatty acids from TAG that increases basal insulin secretion [101]. The addition of DCN in our study might have shifted the balance towards higher free fatty acid uptake by β-cells, resulting in an increased insulin secretion and reduced levels of TAG in the DCN-treated samples. One limitation of our Raman imaging data, especially in regard to the data obtained from the fixed pseudo-islets +DCN in COLI, is the use of paraffin-embedded samples. Although deparaffinization is one crucial step in the pre-Raman imaging processing propotcol, paraffin generates a strong Raman signal in the range from 1000 to 1500 cm^{-1}, which is an area of interest especially for lipids and proteins. Hence, some features, especially regarding PI, TAG, and cholesterol that were observable during our *in situ* Raman imaging of living non-processed pseudo-islets, were potentially not identifiable in the COLI gel samples in this study.

The increased stress experienced by β-cells and the corresponding pathways identified by our NGS results also suggests autophagy to be involved in the maintenance of β-cell homeostasis [93,102,103]. It has been reported that impairments in autophagy are observed in mice with Type 1 DM [104]. In addition to the aforementioned UPR, autophagy also plays a key role in responding to ER stress [105] by protecting β-cells from apoptosis [106]. However, it has also been reported that inhibition of autophagy allows for increased insulin secretion as reservoirs of insulin and pro-insulin are maintained and not degraded [107]. These findings highlight the importance of maintaining the balance between cell survival and function. Previous studies have shown that DCN is an autophagy-inducing proteoglycan [108]. DCN-binding to EGFR initiated internalization of the receptor through caveolae for degradation [109], contributing to the downregulation of the receptor [110]. DCN was also shown to stimulate autophagy of VEGFR2 via AMPK signaling [62,111], eventually resulting in reduced cell migration, supporting DCN's role as a tumor suppressor. This process of autophagy was observed to occur through expression and recruitment of paternally expressed gene 3 (Peg3), Beclin1, and microtubule-associated protein light chain 3 (MAPLC3A) [62]. LC3 has also been suggested to be involved in the autophagy within β-cells for the degradation of proinsulin [107]. While VEGFRs or the genes involved in the autophagic process were not identified in our NGS study, another microtubule-associated protein, MAP1A, autophagy related 2a (ATG2a) and the previously mentioned YOD1 were differentially expressed between our control and DCN-treated pseudo-islets, suggesting a possible autophagic pathway being involved in the β-cells. Interestingly, in a study where fibroblasts were cultured without serum to stimulate autophagy, there was increased expression of both DCN and ATF4 [112]. Our NGS data also identified an increased expression of ATF4 in the DCN-treated pseudo-islets, suggesting a similar mechanism may be present in the β-cells. Evaluation of the presence of endosomes and lysosomes in DCN-treated β-cells would help clarify the increased lipid content that we had observed in the Raman microspectroscopy and NGS results. This would further aid in determining whether DCN has

similar autophagy-inducing properties in β-cells and would provide meaningful insight into how it contributes to maintaining β-cell homeostasis.

Our NGS data also identified potential binding receptors for DCN. Of interest is the significant downregulation of LRP1 in the DCN-treated samples. The endocytic receptor binds ECM proteins [113], including DCN [114], and growth factors [115] such as transforming growth factor β (TGFβ) [116], influencing glucose metabolism and lipid turnover [117]. LRP1 plays a key role in murine islets in terms of maintaining cell homeostasis of lipid metabolism and insulin secretion, particularly in obese mice [118]. When LRP1 was deleted, reduced insulin secretion and increased lipid content was observed [117]. Furthermore, studies have shown that activation of TGFβ pathways through LRP1 [114,119] has a stimulatory effect on β-cells' insulin secretion and survival [120,121], which is in line with our results. In addition, LRP1 has been shown to be involved in similar autophagic pathways as described earlier [122,123], suggesting that DCN induces a similar autophagic effect of LRP1 upon binding. This observation is also supported by our data where there was a significant downregulation of LRP1 at both the gene and protein level after DCN treatment. The interaction between DCN and LRP1 and LRP1's ability to stimulate insulin secretion make LRP1 a potential mediator of DCN's effect on β-cells. Future studies investigating DCN binding to LRP1 to initiate autophagocytosis and activate pathways to both modulate the ECM and stimulate insulin secretion in β-cells would need to be performed.

Conclusion

In this study, we demonstrated the beneficial effect of DCN on the insulin production of human β-cells. DCN-treatment improved glucose-stimulated insulin secretion of β-cells in pseudo-islets cultured in suspension, with an increased expression of genes involved in mitochondrial activity as well as protein folding and vesicle formation. Additionally, we showed that ECM expression patterns within pseudo-islets were significantly impacted by DCN treatment. Interestingly, expression of ECM proteins affiliated with the formation of fibrotic capsules were significantly downregulated in the DCN-treated samples. Our findings have potential implications for the design of improved islet transplantation strategies since we showed that DCN-treatment can potentially address two major hurdles: (1) help to regenerate lost or inadequately expressed ECM of isolated islets of Langerhans [17], and (2) prevent the formation of a fibrotic capsule that commonly forms around an implant. Furthermore, increased insulin production and secretion in response to glucose is a burdensome process for the cell. DCN-treated samples were able to activate response pathways within the ER and mitochondria to cope with the increased cellular stress. Taken together, we propose that DCN-treatment of islet transplants can potentially support β-cell survival and increase function post-transplantation.

Author contributions

M.U. and A.J. contributed equally to this work. M. U., A.J., A.Z., S.N., S.L.L. and K.S-L. designed the experiments and wrote the manuscript. M.U., A.J., A.Z., C.L., S.N., S.L.L. and J.M. performed experiments and analyzed data. L.K. analyzed data. G.D. gave conceptual advice. The main data supporting the findings of this study are available within the article and its supplementary information. The raw data generated in this study are available from the corresponding author upon request.

Funding sources

This work was financially supported by the European Union (H2020-NMP10-2014-645991-2, DRIVE; H2020-ITN 766181, DELIVER; both to G.P. D. and K.S.-L.), the International Foundation for Ethical Research and the Swiss National Science Foundation (both to A.Z.), the State Ministry of Science, Research and the Arts of Baden-Württemberg (33-729.55-3/214 and SI-BW 01222-91 to K.S.-L.), the Deutsche Forschungsgemeinschaft (INST 2388/64-1 to K.S.-L.), and the State Ministry for Economic Affairs, Labour and Tourism of Baden-Württemberg (3-4332.62-NMI/65 to K.S.-L.).

Data Availability

Data will be made available on request.

Declaration of Competing Interests

The authors declare that they have no known competing financial interests or personal relationships that could have appeared to influence the work reported in this paper.

Acknowledgements

We thank Prof. Peter Loskill (University Tübingen, NMI Reutlingen) for providing the organ-on-chip device, and Mariella Bosch (University Tübingen) for her technical support. NGS methods were performed with the support of the DFG-funded NGS Competence Center Tübingen (INST 37/1049-1).

Supplementary materials

Supplementary material associated with this article can be found, in the online version, at doi:10.1016/j.matbio.2022.12.005.

Received 21 September 2022;
Received in revised form 23 December 2022;
Accepted 29 December 2022
Available online 30 December 2022

Keywords:
Decorin;
Pancreatic β-cells;
Diabetes mellitus *in vitro* model;
Next-generation sequencing;
Raman microspectroscopy;
Extracellular matrix remodeling

Abbreviations:
DM, diabetes mellitus; ECM, extracellular matrix; COLI, collagen type 1; COLIII, collagen type 3; FN, fibronectin; DCN, decorin; NGS, next-generation sequencing; ER, endoplasmic reticulum; IF, immunofluorescence; GSIS, glucose-stimulated insulin secretion; QBiC, Quantitative Biology Center; TCA, true component analysis; PCA, principal component analysis; GVI, gray value intensity; ROI, region of interest; BM, basement membrane; LAM, laminins; COLIV, collagen type 4; INS, insulin; GLU, glucagon; cGMP, cyclic guanosine monophosphate; MAPK, mitogen-activated protein kinase; OxPhos, oxidative phosphorylation; LRP1, lipoprotein receptor–related protein 1; PI, phosphatidylinositol; TAG, triacylglycerol; GMP, good manufacturing practice; SLRP, small leucine-rich proteoglycan; VEGFR, vascular endothelial growth factor receptor; EGFR, epidermal growth factor receptor; ATP, adenosine triphosphate; ERAD, endoplasmic reticulum associated degradation; UPR, unfolded protein response; WFS1, Wolframin ER transmembrane glycoprotein; RRBP1, Ribosome Binding Protein 1; HSP, heat shock protein

[§]Authors contributed equally.

References

[1] E.J. Boyko, D.J. Magliano, S. Karuranga, L. Piemonti, P. Riley, P. Saeedi, H. Sun, eds., IDF diabetes atlas, 10th ed., 2021.

[2] B.J. Hering, W.R. Clarke, N.D. Bridges, T.L. Eggerman, R. Alejandro, M.D. Bellin, K. Chaloner, C.W. Czarniecki, J.S. Goldstein, L.G. Hunsicker, D.B. Kaufman, O. Korsgren, C.P. Larsen, X. Luo, J.F. Markmann, A. Naji, J. Oberholzer, A.M. Posselt, M.R. Rickels, C. Ricordi, M.A. Robien, P.A. Senior, A.M. James Shapiro, P.G. Stock, N.A. Turgeon, Phase 3 trial of transplantation of human islets in type 1 diabetes complicated by severe hypoglycemia, Diabetes Care 39 (2016) 1230–1240, doi: 10.2337/dc15-1988.

[3] Q. Zhou, D.A. Melton, Pancreas regeneration, Nature 557 (2018) 351–358, doi: 10.1038/s41586-018-0088-0.

[4] A.M.J. Shapiro, J.R.T. Lakey, E.A. Ryan, G.S. Korbutt, E. Toth, G.L. Warnock, N.M. Kneteman, R.V. Rajotte, J. Shapiro, Islet transplantation in seven patients with type 1 diabetes mellitus using a glucocorticoid-free immunosuppressive regimen, N. Engl. J. Med. 343 (2000) 230–238, doi: 10.1056/NEJM200007273430401.

[5] A. Del Toro-Arreola, A.K. Robles-Murillo, A. Daneri-Navarro, J.D. Rivas-Carrillo, The role of endothelial cells on islet function and revascularization after islet transplantation, Organogenesis 12 (2016) 28–32, doi: 10.1080/15476278.2016.1165378.

[6] M. Urbanczyk, S.L. Layland, K. Schenke-Layland, The role of extracellular matrix in biomechanics and its impact on bioengineering of cells and 3D tissues, Matrix Biol 85–86 (2020) 1–14, doi: 10.1016/j.matbio.2019.11.005.

[7] M. Urbanczyk, A. Zbinden, S.L. Layland, G. Duffy, K. Schenke-Layland, Controlled heterotypic pseudo-islet assembly of human β-cells and human umbilical vein endothelial cells using magnetic levitation, Tissue Eng. Part A. 26 (2020) 387–399, doi: 10.1089/ten.tea.2019.0158.

[8] A. Zbinden, M. Urbanczyk, S.L. Layland, L. Becker, J. Marzi, M. Bosch, P. Loskill, G.P. Duffy, K. Schenke-Layland, Collagen and endothelial cell coculture improves β-cell functionality and rescues pancreatic extracellular matrix, Tissue Eng. Part A. (2020) ten.tea.2020.0250, doi: 10.1089/ten.tea.2020.0250.

[9] C. Laporte, E. Tubbs, M. Pierron, A. Gallego, A. Moisan, F. Lamarche, T. Lozano, A. Hernandez, C. Cottet-Rousselle, A.-S. Gauchez, V. Persoons, F. Bottausci, C. Fontelaye, F. Boizot, S. Lablanche, F. Rivera, Improved human islets' viability and functionality with mesenchymal stem cells and arg-gly-asp tripeptides supplementation of alginate micro-encapsulated islets *in vitro*, Biochem. Biophys. Res. Commun. 528 (2020) 650–657, doi: 10.1016/j.bbrc.2020.05.107.

[10] D.M. Salvay, C.B. Rives, X. Zhang, F. Chen, D.B. Kaufman, W.L. Lowe Jr., L.D. Shea, W.L. Lowe, L.D. Shea, Extracellular matrix protein-coated scaffolds promote the reversal of diabetes after extrahepatic islet transplantation, Transplantation 85 (2008) 1456–1464, doi: 10.1097/TP.0b013e31816fc0ea.

[11] T. Linn, K. Schneider, H.P. Hammes, K.T. Preissner, H. Brandhorst, E. Morgenstern, F. Kiefer, R.G. Bretzel, Angiogenic capacity of endothelial cells in islets of Langerhans, FASEB 17 (2003) 1–17, doi: 10.1096/fj.02-0615fje.

[12] A. Gamble, R. Pawlick, A.R. Pepper, A. Bruni, A. Adesida, P.A. Senior, G.S. Korbutt, A.M.J. Shapiro, Improved islet recovery and efficacy through co-culture and co-transplantation of islets with human adipose-derived mesenchymal stem cells, PLoS ONE 13 (2018) e0206449, doi: 10.1371/journal.pone.0206449.

[13] M. Perez-Basterrechea, M.M. Esteban, M. Alvarez-Viejo, T. Fontanil, S. Cal, M.S. Pitiot, J. Otero, A.J. Obaya, M. Sanchez Pitiot, J. Otero, A.J. Obaya, Fibroblasts accelerate islet revascularization and improve long-term graft survival in a mouse model of subcutaneous islet transplantation, PLoS ONE 12 (2017) e0180695, doi: 10.1371/journal.pone.0180695.

[14] A. Zbinden, S.L. Layland, M. Urbanczyk, D.A.C. Berrio, J. Marzi, M. Zauner, A. Hammerschmidt, E.M. Brauchle,

K. Sudrow, S. Fink, M. Templin, S. Liebscher, G. Klein, A. Deb, G.P. Duffy, G.M. Crooks, J.A. Eble, H.K.A. Mikkola, A. Nsair, M. Seifert, Nidogen-1 Mitigates Ischemia and Promotes Tissue Survival and Regeneration, 2002500, 2020, pp. 1–18, doi: 10.1002/advs.202002500.

[15] J. Crisóstomo, A.M. Pereira, S.J. Bidarra, A.C. Gonçalves, P.L. Granja, J.F.J. Coelho, C.C. Barrias, R. Seiça, ECM-enriched alginate hydrogels for bioartificial pancreas: an ideal niche to improve insulin secretion and diabetic glucose profile, J. Appl. Biomater. Funct. Mater. 17 (2019) 2280800019848923, doi: 10.1177/2280800019848923.

[16] J. Cheng, M. Raghunath, J. Whitelock, L. Poole-Warren, Matrix components and scaffolds for sustained islet function, Tissue Eng. Part B, Rev. 17 (2011) 235–247, doi: 10.1089/ten.TEB.2011.0004.

[17] D. Brandhorst, H. Brandhorst, S. Acreman, Y. Kimura, S.L. Layland, K. Schenke-Layland, P.R.V. Johnson, Recombinant nidogen-1 significantly improves survival of hypoxic human islets, J. Nuff. Dep. Surg. Sci. (2020) 1, doi: 10.37707/jnds.v1i2.91.

[18] T.A. Wynn, T.R. Ramalingam, Mechanisms of fibrosis: therapeutic translation for fibrotic disease, Nat. Med. 18 (2012) 1028–1040, doi: 10.1038/nm.2807.

[19] S. Ricard-Blum, G. Baffet, N. Théret, Molecular and tissue alterations of collagens in fibrosis, Matrix Biol. 68–69 (2018) 122–149, doi: 10.1016/j.matbio.2018.02.004.

[20] A. Menke, G. Adler, TGFbeta-induced fibrogenesis of the pancreas, Int. J. Gastrointest. Cancer. 31 (2002) 41–46, doi: 10.1385/IJGC:31:1-3:41.

[21] A. Zbinden, J. Marzi, K. Schlünder, C. Probst, M. Urbanczyk, S. Black, E.M. Brauchle, S.L. Layland, U. Kraushaar, G. Duffy, K. Schenke-Layland, P. Loskill, Non-invasive marker-independent high content analysis of a microphysiological human pancreas-on-a-chip model, Matrix Biol 85–86 (2020) 205–220, doi: 10.1016/j.matbio.2019.06.008.

[22] S. Hinderer, K. Sudrow, M. Schneider, M. Holeiter, S.L. Layland, M. Seifert, K. Schenke-Layland, Surface functionalization of electrospun scaffolds using recombinant human decorin attracts circulating endothelial progenitor cells, Sci. Rep. 8 (2018) 110, doi: 10.1038/s41598-017-18382-y.

[23] R. Daum, D. Visser, C. Wild, L. Kutuzova, M. Schneider, G. Lorenz, M. Weiss, S. Hinderer, U.A. Stock, M. Seifert, K. Schenke-Layland, Fibronectin adsorption on electrospun synthetic vascular grafts attracts endothelial progenitor cells and promotes endothelialization in dynamic in vitro culture, Cells 9 (2020) 778, doi: 10.3390/cells9030778.

[24] X. Xiong, R. Ghosh, E. Hiller, F. Drepper, B. Knapp, H. Brunner, S. Rupp, A new procedure for rapid, high yield purification of type I collagen for tissue engineering, Process. Biochem. 44 (2009) 1200–1212, doi: 10.1016/j.procbio.2009.06.010.

[25] S. Andrew, FastQC. A quality control tool for high throughput sequence data, (2010). https://www.bioinformatics.babraham.ac.uk/projects/fastqc/(accessed January 21, 2021).

[26] F. Krueger, Trim Galore: A wrapper tool around cutadapt and FastQC to consistently apply quality and adapter trimming to FastQ files, with some extra functionality for MspI-digested RRBS-type (reduced representation bisufite-seq) libraries, (2012). https://www.bioinformatics.babraham.ac.uk/projects/trim_galore/(accessed January 21, 2021).

[27] A. Dobin, C.A. Davis, F. Schlesinger, J. Drenkow, C. Zaleski, S. Jha, P. Batut, M. Chaisson, T.R. Gingeras, STAR: ultrafast universal RNA-seq aligner, Bioinformatics 29 (2012) 15–21, doi: 10.1093/bioinformatics/bts635.

[28] L. Wang, S. Wang, W. Li, RSeQC: quality control of RNA-seq experiments, Bioinformatics 28 (2012) 2184–2185, doi: 10.1093/bioinformatics/bts356.

[29] Y. Liao, G.K. Smyth, W. Shi, featureCounts: an efficient general purpose program for assigning sequence reads to genomic features, Bioinformatics 30 (2014) 923–930, doi: 10.1093/bioinformatics/btt656.

[30] P. Ewels, M. Magnusson, S. Lundin, M. Kaeller, Summarize analysis results for multiple tools and samples in a single report, Bioinformatics 32 (2016) 3047–3048, doi: 10.1093/bioinformatics/btw354.

[31] Y. Benjamini, Y. Hochberg, Controlling the false discovery rate: a practical and powerful approach to multiple testing, J. R. Stat. Soc. Ser. B. 57 (1995) 289–300, doi: 10.1111/j.2517-6161.1995.tb02031.x.

[32] M. Kanehisa, S. Goto, KEGG: kyoto encyclopedia of genes and genomes, Nucleic Acids Res. 28 (2000) 27–30, doi: 10.1093/nar/28.1.27.

[33] M. Gillespie, B. Jassal, R. Stephan, M. Milacic, K. Rothfels, A. Senff-Ribeiro, J. Griss, C. Sevilla, L. Matthews, C. Gong, C. Deng, T. Varusai, E. Ragueneau, Y. Haider, B. May, V. Shamovsky, J. Weiser, T. Brunson, N. Sanati, L. Beckman, X. Shao, A. Fabregat, K. Sidiropoulos, J. Murillo, G. Viteri, J. Cook, S. Shorser, G. Bader, E. Demir, C. Sander, R. Haw, G. Wu, L. Stein, H. Hermjakob, P. D'Eustachio, The reactome pathway knowledgebase 2022, Nucleic Acids Res. 50 (2022) D687–D692, doi: 10.1093/nar/gkab1028.

[34] B. Prats Mateu, E. Harreither, M. Schosserer, V. Puxbaum, E. Gludovacz, N. Borth, N. Gierlinger, J. Grillari, Label-free live cell imaging by Confocal Raman Microscopy identifies CHO host and producer cell lines, Biotechnol. J. 12 (2017) 1600037, doi: 10.1002/biot.201600037.

[35] T. Morimoto, L. Da Chiu, H. Kanda, H. Kawagoe, T. Ozawa, M. Nakamura, K. Nishida, K. Fujita, T. Fujikado, Using redox-sensitive mitochondrial cytochrome Raman bands for label-free detection of mitochondrial dysfunction, Analyst 144 (2019) 2531–2540, doi: 10.1039/c8an02213e.

[36] K. Arda, N. Ciledag, E. Aktas, B.K. Aribas, K. Köse, Quantitative assessment of normal soft-tissue elasticity using shear-wave ultrasound elastography, AJR. Am. J. Roentgenol. 197 (2011) 532–536, doi: 10.2214/AJR.10.5449.

[37] Y. Shi, Y. Liu, F. Gao, Y. Liu, S. Tao, Y. Li, K.J. Glaser, R.L. Ehman, Q. Guo, Pancreatic stiffness quantified with MR elastography: relationship to postoperative pancreatic fistula after pancreaticoenteric anastomosis, Radiology 288 (2018) 476–484, doi: 10.1148/radiol.2018170450.

[38] M. Sugimoto, S. Takahashi, M. Kojima, N. Gotohda, Y. Kato, S. Kawano, A. Ochiai, M. Konishi, What is the nature of pancreatic consistency? Assessment of the elastic modulus of the pancreas and comparison with tactile sensation, histology, and occurrence of postoperative pancreatic fistula after pancreaticoduodenectomy, Surgery 156 (2014) 1204–1211, doi: 10.1016/j.surg.2014.05.015.

[39] K. Czamara, K. Majzner, M.Z. Pacia, K. Kochan, A. Kaczor, M. Baranska, Raman spectroscopy of lipids: a review, J. Raman Spectrosc. 46 (2015) 4–20, doi: 10.1002/jrs.4607.

[40] W. Zhang, Y. Ge, Q. Cheng, Q. Zhang, L. Fang, J. Zheng, Decorin is a pivotal effector in the extracellular matrix and

tumour microenvironment, Oncotarget 9 (2018) 5480–5491, doi: 10.18632/oncotarget.23869.
[41] T. Neill, L. Schaefer, R.V. Iozzo, Decorin - A Guardian from the Matrix, Am. J. Pathol. 181 (2012) 380–387, doi: 10.1016/j.ajpath.2012.04.029.
[42] L. Sakhneny, A. Epshtein, L. Landsman, Pericytes contribute to the islet basement membranes to promote beta-cell gene expression, Sci. Rep. 11 (2021) 2378, doi: 10.1038/s41598-021-81774-8.
[43] A. Naba, K.R. Clauser, D.R. Mani, S.A. Carr, R.O. Hynes, Quantitative proteomic profiling of the extracellular matrix of pancreatic islets during the angiogenic switch and insulinoma progression, Sci. Rep. 7 (2017) 40495, doi: 10.1038/srep40495.
[44] J. Svärd, T.H. Røst, C.E.N. Sommervoll, C. Haugen, O.A. Gudbrandsen, A.E. Mellgren, E. Rødahl, J. Fernø, S.N. Dankel, J.V. Sagen, G. Mellgren, Absence of the proteoglycan decorin reduces glucose tolerance in overfed male mice, Sci. Rep. 9 (2019) 4614, doi: 10.1038/s41598-018-37501-x.
[45] R.N. Feng, Y.C. Niu, X.W. Sun, Q. Li, C. Zhao, C. Wang, F.C. Guo, C.H. Sun, Y. Li, Histidine supplementation improves insulin resistance through suppressed inflammation in obese women with the metabolic syndrome: a randomised controlled trial, Diabetologia 56 (2013) 985–994, doi: 10.1007/s00125-013-2839-7.
[46] Y.T. Lee, C.C. Hsu, M.H. Lin, K. Sen Liu, M.C. Yin, Histidine and carnosine delay diabetic deterioration in mice and protect human low density lipoprotein against oxidation and glycation, Eur. J. Pharmacol. 513 (2005) 145–150, doi: 10.1016/j.ejphar.2005.02.010.
[47] X. Sun, R. Feng, Y. Li, S. Lin, W. Zhang, Y. Li, C. Sun, S. Li, Histidine supplementation alleviates inflammation in the adipose tissue of high-fat diet-induced obese rats via the NF-κB-and PPARγ-involved pathways, Br. J. Nutr. 112 (2014) 477–485, doi: 10.1017/S0007114514001056.
[48] B. Rolfe, J. Mooney, B. Zhang, S. Jahnke, S.-J. Le, Y.-Q. Chau, Q. Huang, H. Wang, G. Campbell, J. Campbell, The fibrotic response to implanted biomaterials: implications for tissue engineering, Regen. Med. Tissue Eng. - Cells Biomater., InTech (2011), doi: 10.5772/21790.
[49] T.N. Wight, S. Potter-Perigo, The extracellular matrix: an active or passive player in fibrosis? Am. J. Physiol. Gastrointest. Liver Physiol. 301 (2011) G950–G955, doi: 10.1152/ajpgi.00132.2011.
[50] W.A. Border, N.A. Noble, T. Yamamoto, J.R. Harper, Y. u Yamaguchi, M.D. Pierschbacher, E. Ruoslahti, Natural inhibitor of transforming growth factor-beta protects against scarring in experimental kidney disease, Nature 360 (1992) 361–364, doi: 10.1038/360361a0.
[51] L. Schaefer, K. Macakova, I. Raslik, M. Micegova, H.-J. Gröne, E. Schönherr, H. Robenek, F.G. Echtermeyer, S. Grässel, P. Bruckner, R.M. Schaefer, R.V. Iozzo, H. Kresse, Absence of decorin adversely influences tubulointerstitial fibrosis of the obstructed kidney by enhanced apoptosis and increased inflammatory reaction, Am. J. Pathol. 160 (2002) 1181–1191, doi: 10.1016/S0002-9440(10)64937-1.
[52] T.W.L. Groeneveld, M. Oroszlán, R.T. Owens, M.C. Faber-Krol, A.C. Bakker, G.J. Arlaud, D.J. McQuillan, U. Kishore, M.R. Daha, A. Roos, Interactions of the extracellular matrix proteoglycans decorin and biglycan with C1q and collectins, J. Immunol. 175 (2005) 4715–4723, doi: 10.4049/jimmunol.175.7.4715.
[53] L. Schaefer, R.V. Iozzo, Biological functions of the small leucine-rich proteoglycans: from genetics to signal transduction, J. Biol. Chem. 283 (2008) 21305–21309, doi: 10.1074/jbc.R800020200.
[54] M.V. Nastase, R.V. Iozzo, L. Schaefer, Key roles for the small leucine-rich proteoglycans in renal and pulmonary pathophysiology, Biochim. Biophys. Acta 1840 (2014) 2460–2470, doi: 10.1016/j.bbagen.2014.01.035. Key.
[55] R.V. Iozzo, L. Schaefer, Proteoglycans in health and disease: novel regulatory signaling mechanisms evoked by the small leucine-rich proteoglycans, FEBS J. 277 (2010) 3864–3875, doi: 10.1111/j.1742-4658.2010.07797.x.
[56] S. Chen, D.E. Birk, The regulatory roles of small leucine-rich proteoglycans in extracellular matrix assembly, FEBS J. 280 (2013) 2120–2137, doi: 10.1111/febs.12136.
[57] D. Nolfi-Donegan, A. Braganza, S. Shiva, Mitochondrial electron transport chain: oxidative phosphorylation, oxidant production, and methods of measurement, Redox Biol. 37 (2020) 101674, doi: 10.1016/j.redox.2020.101674.
[58] A. Wiederkehr, C.B. Wollheim, Minireview: implication of mitochondria in insulin secretion and action, Endocrinology 147 (2006) 2643–2649, doi: 10.1210/en.2006-0057.
[59] B.A. Kaufman, C. Li, S.A. Soleimanpour, Mitochondrial regulation of β-cell function: maintaining the momentum for insulin release, Mol Asp. Med. 42 (2015) 91–104, doi: 10.1016/j.mam.2015.01.004.
[60] S. Malmgreh, D.G. Nicholls, J. Taneera, K. Bacos, T. Koeck, A. Tamaddon, R. Wibom, L. Groop, C. Ling, H. Mulder, V.V. Sharoyko, Tight coupling between glucose and mitochondrial metabolism in clonal β-cells is required for robust insulin secretion, J. Biol. Chem. 284 (2009) 32395–32404, doi: 10.1074/jbc.M109.026708.
[61] V.B. Ritov, E.V. Menshikova, J. He, R.E. Ferrell, B.H. Goodpaster, D.E. Kelley, Deficiency of subsarcolemmal mitochondria in obesity and type 2 diabetes, Diabetes 54 (2005) 8–14, doi: 10.2337/diabetes.54.1.8.
[62] S. Buraschi, T. Neill, A. Goyal, C. Poluzzi, J. Smythies, R.T. Owens, L. Schaefer, A. Torres, R.V. Iozzo, Decorin causes autophagy in endothelial cells via Peg3, Proc. Natl. Acad. Sci. U. S. A. (2013) 110, doi: 10.1073/pnas.1305732110.
[63] M.R. Duchen, P.A. Smith, F.M. Ashcroft, Substrate-dependent changes in mitochondrial function, intracellular free calcium concentration and membrane channels in pancreatic β-cells, Biochem. J. 294 (1993) 35–42, doi: 10.1042/bj2940035.
[64] A.A. Gerencser, Metabolic activation-driven mitochondrial hyperpolarization predicts insulin secretion in human pancreatic beta-cells, Biochim Biophys Acta Bioenerg 1859 (2018) 817–828, doi: 10.1016/j.bbabio.2018.06.006.
[65] E. Heart, R.F. Corkey, J.D. Wikstrom, O.S. Shirihai, B.E. Corkey, Glucose-dependent increase in mitochondrial membrane potential, but not cytoplasmic calcium, correlates with insulin secretion in single islet cells, Am. J. Physiol. - Endocrinol. Metab. 290 (2006) 143–148, doi: 10.1152/ajpendo.00216.2005.
[66] J.D. Wikstrom, S.M. Katzman, H. Mohamed, G. Twig, S.A. Graf, E. Heart, A.J.A. Molina, B.E. Corkey, L.M. De Vargas, N.N. Danial, S. Collins, O.S. Shirihai, β-Cell mitochondria exhibit membrane potential heterogeneity that can be altered by stimulatory or toxic fuel levels, Diabetes 56 (2007) 2569–2578, doi: 10.2337/db06-0757.

[67] N. Shrestha, R.B. Reinert, L. Qi, Endoplasmic reticulum protein quality control in β cells, Semin. Cell Dev. Biol. 103 (2020) 59–67, doi: 10.1016/j.semcdb.2020.04.006.
[68] S. Yamaguchi, H. Ishihara, T. Yamada, A. Tamura, M. Usui, R. Tominaga, Y. Munakata, C. Satake, H. Katagiri, F. Tashiro, H. Aburatani, K. Tsukiyama-Kohara, J. Miyazaki, N. Sonenberg, Y. Oka, ATF4-mediated induction of 4E-BP1 contributes to pancreatic β cell survival under endoplasmic reticulum stress, Cell Metab. 7 (2008) 269–276, doi: 10.1016/j.cmet.2008.01.008.
[69] S.G. Fonseca, J. Gromada, F. Urano, Endoplasmic reticulum stress and pancreatic β-cell death, Trends Endocrinol. Metab. 22 (2011) 266–274, doi: 10.1016/j.tem.2011.02.008.
[70] N. Rabhi, E. Salas, P. Froguel, J.S. Annicotte, Role of the unfolded protein response in β cell compensation and failure during diabetes, J. Diabetes Res. (2014) 2014, doi: 10.1155/2014/795171.
[71] A. El Ouaamari, J.-Y. Zhou, C.W. Liew, J. Shirakawa, E. Dirice, N. Gedeon, S. Kahraman, D.F. De Jesus, S. Bhatt, J.-S. Kim, T.R.W. Clauss, D.G. Camp, R.D. Smith, W.-J. Qian, R.N. Kulkarni, Compensatory islet response to insulin resistance revealed by quantitative proteomics, J. Proteome Res. 14 (2015) 3111–3122, doi: 10.1021/acs.jproteome.5b00587.
[72] J. Wang, Y. Chen, Q. Yuan, W. Tang, X. Zhang, K. Osei, Control of precursor maturation and disposal is an early regulative mechanism in the normal insulin production of pancreatic β-cells, PLoS ONE 6 (2011) e19446, doi: 10.1371/journal.pone.0019446.
[73] J. Sun, J. Cui, Q. He, Z. Chen, P. Arvan, M. Liu, Proinsulin misfolding and endoplasmic reticulum stress during the development and progression of diabetes☆, Mol. Aspects Med. 42 (2015) 105–118, doi: 10.1016/j.mam.2015.01.001.
[74] M. Liu, Y. Li, D. Cavener, P. Arvan, Proinsulin disulfide maturation and misfolding in the endoplasmic reticulum, J. Biol. Chem. 280 (2005) 13209–13212, doi: 10.1074/jbc.C400475200.
[75] N. Shrestha, E. De Franco, P. Arvan, M. Cnop, Pathological β-cell endoplasmic reticulum stress in type 2 diabetes: current evidence, Front. Endocrinol. (Lausanne). 12 (2021) 1–7, doi: 10.3389/fendo.2021.650158.
[76] D.L. Eizirik, A.K. Cardozo, M. Cnop, The role for endoplasmic reticulum stress in diabetes mellitus, Endocr. Rev. 29 (2008) 42–61, doi: 10.1210/er.2007-0015.
[77] S.Z. Hasnain, J.B. Prins, M.A. McGuckin, Oxidative and endoplasmic reticulum stress in β-cell dysfunction in diabetes, J. Mol. Endocrinol. 56 (2016) R33–R54, doi: 10.1530/JME-15-0232.
[78] D. Takei, H. Ishihara, S. Yamaguchi, T. Yamada, A. Tamura, H. Katagiri, Y. Maruyama, Y. Oka, WFS1 protein modulates the free Ca 2+ concentration in the endoplasmic reticulum, FEBS Lett 580 (2006) 5635–5640, doi: 10.1016/j.febslet.2006.09.007.
[79] K. Ueda, J. Kawano, K. Takeda, T. Yujiri, K. Tanabe, T. Anno, M. Akiyama, J. Nozaki, T. Yoshinaga, A. Koizumi, K. Shinoda, Y. Oka, Y. Tanizawa, Endoplasmic reticulum stress induces Wfs1 gene expression in pancreatic β-cells via transcriptional activation, Eur. J. Endocrinol. 153 (2005) 167–176, doi: 10.1530/eje.1.01945.
[80] I.X. Zhang, J. Ren, S. Vadrevu, M. Raghavan, L.S. Satin, ER stress increases store-operated Ca2+ entry (SOCE) and augments basal insulin secretion in pancreatic beta cells, J. Biol. Chem. 295 (2020) 5685–5700, doi: 10.1074/jbc.RA120.012721.
[81] L.S. Satin, Localized calcium influx in pancreatic β-cells: its significance for Ca2+-dependent insulin secretion from the islets of Langerhans, Endocrine 13 (2000) 251–262, doi: 10.1385/ENDO:13:3:251.
[82] S.G. Fonseca, M. Fukuma, K.L. Lipson, L.X. Nguyen, J.R. Allen, Y. Oka, F. Urano, WFS1 is a novel component of the unfolded protein response and maintains homeostasis of the endoplasmic reticulum in pancreatic β-cells, J. Biol. Chem. 280 (2005) 39609–39615, doi: 10.1074/jbc.M507426200.
[83] H. Inoue, Y. Tanizawa, J. Wasson, P. Behn, K. Kalidas, E. Bernal-Mizrachi, M. Mueckler, H. Marshall, H. Donis-Keller, P. Crock, D. Rogers, M. Mikuni, H. Kumashiro, K. Higashi, G. Sobue, Y. Oka, M.A. Permutt, A gene encoding a transmembrane protein is mutated in patients with diabetes mellitus and optic atrophy (Wolfram syndrome), Nat. Genet. 20 (1998) 143–148, doi: 10.1038/2441.
[84] H.-Y. Tsai, Y.-F. Yang, A.T. Wu, C.-J. Yang, Y.-P. Liu, Y.-H. Jan, C.-H. Lee, Y.-W. Hsiao, C.-T. Yeh, C.-N. Shen, P.-J. Lu, M.-S. Huang, M. Hsiao, Endoplasmic reticulum ribosome-binding protein 1 (RRBP1) overexpression is frequently found in lung cancer patients and alleviates intracellular stress-induced apoptosis through the enhancement of GRP78, Oncogene 32 (2013) 4921–4931, doi: 10.1038/onc.2012.514.
[85] H. Lu, Y. Yang, E.M. Allister, N. Wijesekara, M.B. Wheeler, The identification of potential factors associated with the development of type 2 diabetes, Mol. Cell. Proteomics. 7 (2008) 1434–1451, doi: 10.1074/mcp.M700478-MCP200.
[86] G.J. Ocaña, L. Pérez, L. Guindon, S.N. Deffit, C. Evans-Molina, D.C. Thurmond, J.S. Blum, Inflammatory stress of pancreatic beta cells drives release of extracellular heat-shock protein 90 α, Immunology 151 (2017) 198–210, doi: 10.1111/imm.12723.
[87] A.S.M. Moin, M. Nandakumar, A. Diane, M. Dehbi, A.E. Butler, The role of heat shock proteins in type 1 diabetes, Front. Immunol. 11 (2021) 1–11, doi: 10.3389/fimmu.2020.612584.
[88] R.C. Wek, T.G. Anthony, EXtENDINg β cell survival by UPRegulating ATF4 translation, Cell Metab 4 (2006) 333–334, doi: 10.1016/j.cmet.2006.10.006.
[89] C. Papadopoulos, P. Kirchner, M. Bug, D. Grum, L. Koerver, N. Schulze, R. Poehler, A. Dressler, S. Fengler, K. Arhzaouy, V. Lux, M. Ehrmann, C.C. Weihl, H. Meyer, VCP /p97 cooperates with YOD 1, UBXD 1 and PLAA to drive clearance of ruptured lysosomes by autophagy, EMBO J 36 (2017) 135–150, doi: 10.15252/embj.201695148.
[90] M. Bensellam, E.L. Maxwell, J.Y. Chan, J. Luzuriaga, P.K. West, J.C. Jonas, J.E. Gunton, D.R. Laybutt, Hypoxia reduces ER-to-Golgi protein trafficking and increases cell death by inhibiting the adaptive unfolded protein response in mouse beta cells, Diabetologia 59 (2016) 1492–1502, doi: 10.1007/s00125-016-3947-y.
[91] N. Hwang, M.Y. Kwon, J.B. Cha, S.W. Chung, J.M. Woo, Tunicamycin-induced endoplasmic reticulum stress upregulates the expression of pentraxin 3 in human retinal pigment epithelial cells, Korean J. Ophthalmol. 30 (2016) 468–478, doi: 10.3341/kjo.2016.30.6.468.
[92] H. Guo, Y. Xiong, P. Witkowski, J. Cui, L.J. Wang, J. Sun, R. Lara-Lemus, L. Haataja, K. Hutchison, S.O. Shan,

P. Arvan, M. Liu, Inefficient translocation of preproinsulin contributes to pancreatic β cell failure and late-onset diabetes, J. Biol. Chem. 289 (2014) 16290–16302, doi: 10.1074/jbc.M114.562355.

[93] Y. ho Lee, J. Kim, K. Park, M.S. Lee, β-cell autophagy: mechanism and role in β-cell dysfunction, Mol. Metab. 27 (2019) S92–S103, doi: 10.1016/j.molmet.2019.06.014.

[94] R. Zhu, X. Li, J. Xu, C. Barrabi, D. Kekulandara, J. Woods, X. Chen, M. Liu, Defective endoplasmic reticulum export causes proinsulin misfolding in pancreatic β cells, Mol. Cell. Endocrinol. 493 (2019) 110470, doi: 10.1016/j.mce.2019.110470.

[95] J. Fang, M. Liu, X. Zhang, T. Sakamoto, D.J. Taatjes, B.P. Jena, F. Sun, J. Woods, T. Bryson, A. Kowluru, K. Zhang, X. Chen, COPII-Dependent ER Export, A Critical Component of Insulin Biogenesis and β-Cell ER Homeostasis., Mol, Endocrinol. 29 (2015) 1156–1169, doi: 10.1210/me.2015-1012.

[96] S. Cockcroft, N. Carvou, Biochemical and biological functions of class I phosphatidylinositol transfer proteins, Biochim. Biophys. Acta - Mol. Cell Biol. Lipids. 1771 (2007) 677–691, doi: 10.1016/j.bbalip.2007.03.009.

[97] N.J. Blunsom, S. Cockcroft, Phosphatidylinositol synthesis at the endoplasmic reticulum, Biochim. Biophys. Acta - Mol. Cell Biol. Lipids. 1865 (2020) 158471, doi: 10.1016/j.bbalip.2019.05.015.

[98] P. Mayinger, Phosphoinositides and vesicular membrane traffic, Biochim. Biophys. Acta - Mol. Cell Biol. Lipids. 1821 (2012) 1104–1113, doi: 10.1016/j.bbalip.2012.01.002.

[99] M.J. MacDonald, L. Ade, J.M. Ntambi, I.U.H. Ansari, S.W. Stoker, Characterization of phospholipids in insulin secretory granules and mitochondria in pancreatic beta cells and their changes with glucose stimulation, J. Biol. Chem. 290 (2015) 11075–11092, doi: 10.1074/jbc.M114.628420.

[100] A.R. Sánchez-Archidona, C. Cruciani-Guglielmacci, C. Roujeau, L. Wigger, J. Lallement, J. Denom, M. Barovic, N. Kassis, F. Mehl, J. Weitz, M. Distler, C. Klose, K. Simons, M. Ibberson, M. Solimena, C. Magnan, B. Thorens, Plasma triacylglycerols are biomarkers of β-cell function in mice and humans, Mol. Metab. 54 (2021) 101355, doi: 10.1016/j.molmet.2021.101355.

[101] K.L. Pappan, Z. Pan, G. Kwon, C.A. Marshall, T. Coleman, I.J. Goldberg, M.L. McDaniel, C.F. Semenkovich, Pancreatic β-cell lipoprotein lipase independently regulates islet glucose metabolism and normal insulin secretion, J. Biol. Chem. 280 (2005) 9023–9029, doi: 10.1074/jbc.M409706200.

[102] C. Muralidharan, A.K. Linnemann, β-cell autophagy in the pathogenesis of type 1 diabetes, Am. J. Physiol. - Endocrinol. Metab. (2021) 321, doi: 10.1152/AJPENDO.00151.2021.

[103] Q. Sheng, X. Xiao, K. Prasadan, C. Chen, Y. Ming, J. Fusco, N.N. Gangopadhyay, D. Ricks, G.K. Gittes, Autophagy protects pancreatic beta cell mass and function in the setting of a high-fat and high-glucose diet, Sci. Rep. 7 (2017) 1–10, doi: 10.1038/s41598-017-16485-0.

[104] C. Muralidharan, A.M. Conteh, M.R. Marasco, J.J. Crowder, J. Kuipers, P. de Boer, A.K. Linnemann, Pancreatic beta cell autophagy is impaired in type 1 diabetes, Diabetologia 64 (2021) 865–877, doi: 10.1007/s00125-021-05387-6.

[105] M. Høyer-Hansen, M. Jäättelä, Connecting endoplasmic reticulum stress to autophagy by unfolded protein response and calcium, Cell Death Differ. 14 (2007) 1576–1582, doi: 10.1038/sj.cdd.4402200.

[106] M. Bugliani, S. Mossuto, F. Grano, M. Suleiman, L. Marselli, U. Boggi, P. De Simone, D.L. Eizirik, M. Cnop, P. Marchetti, V. De Tata, Modulation of autophagy influences the function and survival of human pancreatic beta cells under endoplasmic reticulum stress conditions and in type 2 diabetes, Front. Endocrinol. (Lausanne). 10 (2019) 1–10, doi: 10.3389/fendo.2019.00052.

[107] Y. Riahi, J.D. Wikstrom, E. Bachar-Wikstrom, N. Polin, H. Zucker, M.S. Lee, W. Quan, L. Haataja, M. Liu, P. Arvan, E. Cerasi, G. Leibowitz, Autophagy is a major regulator of beta cell insulin homeostasis, Diabetologia 59 (2016) 1480–1491, doi: 10.1007/s00125-016-3868-9.

[108] S. Buraschi, T. Neill, R.V. Iozzo, Decorin is a devouring proteoglycan: remodeling of intracellular catabolism via autophagy and mitophagy, Matrix Biol 75–76 (2019) 260–270, doi: 10.1016/j.matbio.2017.10.005.

[109] J.X. Zhu, S. Goldoni, G. Bix, R.T. Owens, D.J. McQuillan, C. Reed, R.V. Iozzo, Decorin evokes protracted internalization and degradation of the epidermal growth factor receptor via caveolar endocytosis, J. Biol. Chem. 280 (2005) 32468–32479, doi: 10.1074/jbc.M503833200.

[110] G. Csordas, M. Santra, C.C. Reed, I. Eichstetter, D.J. McQuillan, D. Gross, M.A. Nugent, G. Hajnoczky, R.V. Iozzo, Sustained down-regulation of the epidermal growth factor receptor by decorin. A mechanism for controlling tumor growth *in vivo*, J. Biol. Chem. 275 (2000) 32879–32887, doi: 10.1074/jbc.M005609200.

[111] A. Goyal, T. Neill, R.T. Owens, L. Schaefer, R.V. Iozzo, Decorin activates AMPK, an energy sensor kinase, to induce autophagy in endothelial cells, Matrix Biol. 34 (2014) 46–54, doi: 10.1016/j.matbio.2013.12.011.

[112] M.A. Gubbiotti, T. Neill, H. Frey, L. Schaefer, R.V. Iozzo, Decorin is an autophagy-inducible proteoglycan and is required for proper *in vivo* autophagy, Matrix Biol 48 (2015) 14–25, doi: 10.1016/j.matbio.2015.09.001.Decorin.

[113] A.M. Salicioni, K.S. Mizelle, E. Loukinova, I. Mikhailenko, D.K. Strickland, S.L. Gonias, The low density lipoprotein receptor-related protein mediates fibronectin catabolism and inhibits fibronectin accumulation on cell surfaces, J. Biol. Chem. 277 (2002) 16160–16166, doi: 10.1074/jbc.M201401200.

[114] E. Brandan, C. Retamal, C. Cabello-Verrugio, M.-.P. Marzolo, The low density lipoprotein receptor-related protein functions as an endocytic receptor for decorin, J. Biol. Chem. 281 (2006) 31562–31571, doi: 10.1016/s0021-9258(19)84070-x.

[115] E. Loukinova, S. Ranganathan, S. Kuznetsov, N. Gorlatova, M.M. Migliorini, D. Loukinov, P.G. Ulery, I. Mikhailenko, D.A. Lawrence, D.K. Strickland, Platelet-derived growth factor (PDGF)-induced tyrosine phosphorylation of the low density lipoprotein receptor-related protein (LRP). Evidence for integrated co-receptor function between LRP and the PDGF, J. Biol. Chem. 277 (2002) 15499–15506, doi: 10.1074/jbc.M200427200.

[116] S. Shian Huang, S.M. Leal, C.-.L. Chen, I.-.H. Liu, J. San Huang, Identification of insulin receptor substrate proteins as key molecules for the TβR-V/LRP-1-mediated growth inhibitory signaling cascade in epithelial and myeloid cells, FASEB J. 18 (2004) 1719–1721, doi: 10.1096/fj.04-1872fje.

[117] S.M. Hofmann, L. Zhou, D. Perez-Tilve, T. Greer, E. Grant, L. Wancata, A. Thomas, P.T. Pfluger, J.E. Basford, D. Gilham, J. Herz, M.H. Tschöp, D.Y. Hui, Adipocyte LDL receptor-related protein-1 expression modulates postprandial lipid transport and glucose homeostasis in mice, J. Clin. Invest. 117 (2007) 3271–3282, doi: 10.1172/JCI31929.

[118] R. Ye, R. Gordillo, M. Shao, T. Onodera, Z. Chen, S. Chen, X. Lin, J.A. SoRelle, X. Li, M. Tang, M.P. Keller, R. Kuliawat, A.D. Attie, R.K. Gupta, W.L. Holland, B. Beutler, J. Herz, P.E. Scherer, Intracellular lipid metabolism impairs β cell compensation during diet-induced obesity, J. Clin. Invest. 128 (2018) 1178–1189, doi: 10.1172/JCI97702.

[119] C. Cabello-Verrugio, E. Brandan, A novel modulatory mechanism of transforming growth factor-β signaling through decorin and LRP-1, J. Biol. Chem. 282 (2007) 18842–18850, doi: 10.1074/jbc.M700243200.

[120] A. Sjoholm, C. Hellerstrom, TGF-β stimulates insulin secretion and blocks mitogenic response of pancreatic β-cells to glucose, Am. J. Physiol. - Cell Physiol. 260 (1991), doi: 10.1152/ajpcell.1991.260.5.c1046.

[121] J.H. Lee, J.H. Lee, S.G. Rane, TGF-β signaling in pancreatic islet β cell development and function, Endocrinol. (United States) 162 (2021) 1–10, doi: 10.1210/endocr/bqaa233.

[122] K. Yahiro, M. Satoh, M. Nakano, J. Hisatsune, H. Isomoto, J. Sap, H. Suzuki, F. Nomura, M. Noda, J. Moss, T. Hirayama, Low-density lipoprotein receptor-related protein-1 (LRP1) mediates autophagy and apoptosis caused by Helicobacter pylori VacA, J. Biol. Chem. 287 (2012) 31104–31115, doi: 10.1074/jbc.M112.387498.

[123] R.A. Grosso, P.V.S. Caldarone, M.C. Sánchez, G.A. Chiabrando, M.I. Colombo, C.M. Fader, Hemin induces autophagy in a leukemic erythroblast cell line through the LRP1 receptor, Biosci. Rep. 39 (2019) 1–17, doi: 10.1042/BSR20181156.

Appendix III

Received: 16 September 2020 | Revised: 3 October 2020 | Accepted: 4 October 2020

DOI: 10.1002/jbio.202000375

FULL ARTICLE

JOURNAL OF BIOPHOTONICS

Fluorescence lifetime metabolic mapping of hypoxia-induced damage in pancreatic pseudo-islets

Aline Zbinden[1] | Daniel A. Carvajal Berrio[1,2] | Max Urbanczyk[1] | Shannon L. Layland[1] | Mariella Bosch[1] | Sandro Fliri[1] | Chuan-en Lu[1] | Abiramy Jeyagaran[1] | Peter Loskill[1,3] | Garry P. Duffy[4] | Katja Schenke-Layland[1,2,5,6*]

[1]Department of Women's Health, Research Institute for Women's Health, Eberhard Karls University Tübingen, Tübingen, Germany

[2]Cluster of Excellence iFIT (EXC 2180) "Image-Guided and Functionally Instructed Tumor Therapies", Eberhard Karls University Tübingen, Tübingen, Germany

[3]Fraunhofer IGB, Stuttgart, Germany

[4]Anatomy and Regenerative Medicine Institute, School of Medicine, College of Medicine Nursing and Health Sciences, National University of Ireland, Galway, Ireland

[5]NMI Natural and Medical Sciences Institute at the University of Tübingen, Reutlingen, Germany

[6]Department of Medicine/Cardiology, Cardiovascular Research Laboratories, David Geffen School of Medicine at UCLA, Los Angeles, California

***Correspondence**
Katja Schenke-Layland, NMI Natural and Medical Sciences Institute at the University of Tübingen, Markwiesenstr. 55, Reutlingen 72770, Germany.
Email: katja.schenke-layland@nmi.de, katja.schenke-layland@uni-tuebingen.de

Funding information
Deutsche Forschungsgemeinschaft, Grant/Award Number: INST 2388/33-1; Horizon 2020 Framework Programme, Grant/Award Numbers: H2020-ITN 766181, H2020-NMP10-2014-645991-2; International Foundation for Ethical Research; Ministry of Science, Research and the Arts of Baden-Württemberg, Grant/Award Numbers: 33-729.55-3/214, SI-BW 01222-91

Abstract

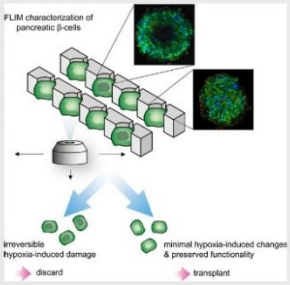

Pancreatic islet isolation from donor pancreases is an essential step for the transplantation of insulin-secreting β-cells as a therapy to treat type 1 diabetes mellitus. This process however damages islet basement membranes, which can lead to islet dysfunction or death. Posttransplantation, islets are further stressed by a hypoxic environment and immune reactions that cause poor engraftment and graft failure. The current standards to assess islet quality before transplantation are destructive procedures, performed on a small islet population that does not reflect the heterogeneity of large isolated islet batches. In this study, we incorporated

Abbreviations: BMIR, blood-mediated inflammatory reaction; ER, endoplasmic reticulum; FAD, flavin adenine dinucleotide; FDA, federal drug administration; FLIM, fluorescence lifetime imaging microscopy; GaAsP, gallium arsenide phosphide; GLUT, glucose transporter; GSIS, glucose-stimulated insulin secretion; HIF-1α, hypoxia-inducible factor 1α; MP, multiphoton; NA, numerical aperture; NADH, nicotinamide adenine dinucleotide; NADPH, nicotinamide adenine dinucleotide phosphate; NDD, nondescanned detection; PMT, photomultiplier tube; ROI, region of interest; ROS, reactive oxygen species; TCA, tricarboxylic acid; TCSPC, time-correlated single photon counting; VEGF, vascular endothelial growth factors.

Aline Zbinden and Daniel A. Carvajal Berrio contributed equally to this study.

fluorescence lifetime imaging microscopy (FLIM) into a pancreas-on-chip system to establish a protocol to noninvasively assess the viability and functionality of pancreatic β-cells in a three-dimensional in vitro model (= pseudo-islets). We demonstrate how (pre-) hypoxic β-cell-composed pseudo-islets can be discriminated from healthy functional pseudo-islets according to their FLIM-based metabolic profiles. The use of FLIM during the pretransplantation pancreatic islet selection process has the potential to improve the outcome of β-cell islet transplantation.

KEYWORDS

FLIM, hypoxia, insulin, pancreatic islet, type 1 diabetes

1 | INTRODUCTION

Islet transplantation is a promising therapy for type 1 diabetes [1]. However, insulin independency declines over time due to significant β-cell death posttransplantation [2]. Islet loss is due to multiple factors occurring pretransplantation and posttransplantation. Blood-mediated inflammatory reaction and hypoxia-associated damage are responsible for the majority of islet loss during intraportal transplantation [3, 4]. During the isolation of pancreatic islets, the pancreas is enzymatically and mechanically digested, resulting in the separation of exocrine and endocrine tissues [5, 6]. The damaged exocrine cells, including mainly acinar cells, can release proteolytic enzymes that further impair endocrine cells [7]. Moreover, the isolation process leads to the destruction of the vascular network and ultimately to the loss of oxygen supply posttransplantation. Exposure to severe hypoxia (1% oxygen) leads to β-cell dysfunction that can compromise glucose-stimulated insulin secretion (GSIS) [8]. The lack of oxygen forces β-cells to transition to anaerobic glycolysis, reducing their ability to respond to high glucose. Prolonged hypoxia permanently impacts β-cells via the hypoxia-inducible factor 1α (HIF-1α) dependent and independent pathways, resulting in ER stress and followed by apoptosis via the mitochondrial cell death pathway [9].

Regulatory bodies, such as the FDA, specify that isolated islets must meet specific standards prior to transplantation such as purity, viability, functionality and sterility [10]. Islet batch sampling may identify unsuitable batches for transplantation; however, approved batches may still contain islets that are damaged, hypoxic, or in a preapoptotic state. Moreover, the standard procedures to assess islet quality are destructive, such as immunofluorescence staining, which requires the addition of exogenous dyes [11]. Therefore, there is a need to develop noninvasive tools, which are able to rapidly assess the viability and functionality of a large batch of single islets prior to transplantation.

Fluorescence lifetime imaging microscopy (FLIM) is a powerful optical method that can probe changes in metabolic state in vitro and in vivo in real time, and can serve as diagnostic tools of pathological tissues in situ [12–14]. The time-dimensional characteristic of FLIM combined with multiphoton (MP) microscopy enables the visualization of endogenous nicotinamide adenine dinucleotide (NADH) and flavin adenine dinucleotide (FAD), and the discrimination between free and protein-bound forms based on their respective lifetimes [15]. Free NADH has a short fluorescence lifetime τ_1 (300-800 ps), while τ_2 of the protein-bound NADH is longer (1000-6500 ps). Similarly, free FAD has a longer fluorescence lifetime τ_2 (2300-2900 ps), and the lifetime of bound FAD τ_1 is shorter (300-455 ps). Based on the respective contribution of τ_1 (α_1) and the optical oxidative ratio (FAD/FAD + NADH), the metabolic equilibrium between glycolysis and oxidative phosphorylation can be evaluated in living cells. FLIM has been used to differentiate metabolic processes including proliferation, differentiation, metabolic switching in tumors, and apoptosis in various cell types [16–19]. The metabolic machineries of pancreatic β-cells are designed to sense blood glucose fluctuations and respond accordingly by the secretion of insulin [20]. β-cells uptake glucose via their transporters of the GLUT family, which is further processed by glycolysis and oxidative phosphorylation, producing NADH and FAD [21]. The increase in ATP leads to the closing of K^+ATP channels and is followed by Ca^{2+} influx, necessary for the exocytosis of insulin granules.

Here, we demonstrate that FLIM can be utilized to monitor the dynamic metabolic changes in β-cells upon glucose stimulation. By combining the detection of (pre-) hypoxic cellular response and the identification of a profile for glucose-stimulated islets, we introduce FLIM as a tool for the screening of single pancreatic pseudo-islets. Identification and exclusion of damaged and glucose nonresponsive isolated islets prior to transplantation has the potential to improve the clinical outcomes for type 1 diabetic patients receiving an islets transplant.

2 | EXPERIMENTAL SECTION

2.1 | Cell culture and pseudo-islet assembly

The EndoC-βH3 (Univercell Biosolutions, Toulouse, France) cell line was cultured as previously described [22]. We modified the protocol by seeding 2000 cells that aggregated into pseudo-islets using nonadherent 96 well U-bottom plates (Thermo Fisher Scientific, Waltham, Massachusetts). Pseudo-islets were cultured under normoxic conditions (37°C, 5% CO_2, 20% O_2) for a total period of 5 days. Hypoxic conditions were defined as 37°C, 5% CO_2 and 1% O_2. Before being subjected to hypoxia, cells were seeded and cultured for 48 hours under normoxic conditions to allow the assembly of cells into pseudo-islets. Pseudo-islets were in hypoxia for periods ranging from 3 to 48 hours. To track the pseudo-islet size over time, brightfield images were taken every 24 hours using a brightfield microscope (Zeiss, Jena, Germany). Diameters were analyzed using the software ImageJ V 1.52p.

2.2 | GSIS assay

Prior to any GSIS assay, pseudo-islets were incubated for 24 hours in starvation medium (Optiβ2, Univercell Biosolutions).

2.2.1 | Standard GSIS

Pseudo-islets were grouped by six per well and washed twice with Krebs buffer (Univercell Biosolutions), supplemented with 1% BSA (Krebs-BSA) (Thermo Fisher Scientific). Pseudo-islets were synchronized for 1 hour in Krebs-BSA and washed twice afterwards. Pseudo-islets were subsequently incubated for 1 hour with Krebs-BSA, Krebs-BSA supplemented with 20 mM glucose (Gibco, Waltham, Massachusetts), and Krebs-BSA for a second time. After each incubation, supernatants were collected and stored at −20°C until further detection of insulin with an ELISA assay (Ultrasensitive Insulin ELISA, Mercodia, Uppsala, Sweden).

2.2.2 | On-FLIM GSIS procedure

Pseudo-islets were loaded into a microfluidic chip as previously described [22]. A low-pressure four-port switching valve (IDEX Health & Science, Oak Harbor, Washington) was used to allow the switch between Krebs-BSA and Krebs-BSA supplemented with 20 mM glucose. Pseudo-islets were incubated for a total of 135 minutes with Krebs-BSA (corresponding to the synchronization phase and 1 hour under Krebs-BSA) before switching to 20 mM glucose for 327 minutes. For nonstimulated GSIS (control), the pseudo-islets were subjected to a total of 459 minutes in Krebs-BSA. The synchronization phase in Krebs-BSA was not measured. Each islet was monitored at the same focus level by acquiring FLIM images every 27 minutes continuously for the duration of the experiments.

2.3 | Immunohistological analyses

Pseudo-islets were washed with PBS (Gibco), embedded in Histogel (Thermo Fisher Scientific), fixed with 4% PFA, and subjected to paraffin-embedding using a Shandon Citadel 1000 (Thermo Fisher Scientific) according to the manufacturer's instructions. Then, 3-µm-thick sections were prepared using the microtome RM2145 (Leica, Wetzlar, Germany). Sections were deparaffinized using xylene and rehydrated by graded ethanol (100%-50%). Then, 1% Triton-X permeabilization and antigen retrieval were performed as described before utilising the following antibodies: anti-insulin: guinea-pig IgG, 1:200 dilution, A0564 (DAKO, Santa Clara, California); anti-vascular endothelial growth factor (VEGF): Rabbit IgG, 1:400 dilution, RB-9031-P (Thermo Fisher Scientific); anti-HIF-1α: rabbit IgG, 1:500 dilution, ab51608 (Abcam, Cambridge, UK) and anti-caspase-3: rabbit IgG, 1:100 dilution, ab13847 (Abcam) [23]. To visualize nuclei, sections were incubated with 4′,6-daimidin-2-phenylindol (DAPI) solution with a concentration of 2 µg/mL (Sigma-Aldrich, St. Louis, Missouri) for 10 minutes. Mounting was performed with Molecular Probes Prolong Gold Anti Fade solution (Invitrogen, Carlsbad, California). Immunofluorescence images were obtained using a Zeiss LSM 880 (Zeiss) and analyzed using Zeiss Zen Blue software and ImageJ V1.52p. Staining intensities (VEGF and caspase-3) were evaluated via the mean gray value per pixel within a region of interest (ROI) defined as $DAPI^+$ areas. HIF-1α-stained images were quantified by three independent unbiased observers. Cells were counted as HIF-1α $^+$ when nuclei were exhibiting a double staining with DAPI and HIF-1α. The ratios of HIF-1α^+ cells were calculated by dividing the number of HIF-1α^+ cells by the number of total $DAPI^+$ cells per pseudo-islets.

2.4 | Multiphoton imaging and FLIM data acquisition

TCSPC-based fluorescence decay measurements were performed with a Zeiss LSM 880 (Zeiss) coupled with a

Ti:Sapphire femtosecond laser (MaiTai HP Spectra Physics, Santa Clara, California) and a two-channel NDD BIG2.0 GaAsP PMT detector (Becker & Hickl GmbH, Berlin, Germany). NADH and FAD autofluorescence was induced with a two-photon excitation at a wavelength of 700 nm and 5% laser power through a ×63/1.4 NA C-plan apochromat objective (Zeiss). Emission light was filtered in the range of 450 to 490 nm for NADH, and 500 to 550 nm for FAD. Total image acquisition time was 161 seconds at a resolution of 512×512 pixels (524.8 µs/pixel). Instrument response function was recorded at 900 nm from crystalline urea (Sigma-Aldrich). Normoxic and hypoxic pseudo-islets were transferred either into µ-slides Angiogenesis (ibidi GmbH, Gräfelfing, Germany), or into a microfluidic chip for FLIM measurements as previously described [22]. All FLIM measurements were performed at 37°C using a microscope stage top incubation system (ibidi heating system, ibidi GmbH).

2.5 | FLIM data analysis

SPICImage (Becker & Hickl GmbH) was used to perform biexponential decay fittings with a 30% threshold of maximum photon count to remove the background. The quality of fit was decided based on a mean χ^2 value smaller than 1.1 per image. ASCII images for α, τ and χ^2 were exported for further analysis. Concentric ROI segmentation based on the outline of the islet was performed on each FLIM image using MATLAB R2020a (The MathWorks Inc., Waltham, Massachusetts). The ROIs were equally spaced at 10 µm in order to calculate mean values for cells at similar depths (MATLAB code available upon request).

2.5.1 | Optical oxidative ratio calculation

The optical oxidative ratio was defined as the total photon counts of FAD divided by the sum of FAD and NADH photon counts [24]. The calculation of the optical oxidative ratio was performed after the image processing by SPICImage and MATLAB software, which includes suppressing the background.

2.5.2 | Lumen ratio calculation

The lumen size was evaluated using an additional threshold of 25% of the total photon count images after background removal by the SPCImage software (MATLAB code available upon request).

2.6 | Statistical analyses

Statistical analyses were performed using GraphPad Prism version 6.00 for Windows (GraphPad Software, San Diego, California). Results are shown throughout the entire manuscript as mean ± standard deviation. Outliers were removed using Grubb's test with a confidence interval of 0.05. Normality was assessed using Shapiro-Wilk tests. Normal distribution was assumed for low n-number samples ($n < 8$). All n-numbers, applied tests, and corresponding significances for each result are listed in the figure legends.

3 | RESULTS AND DISCUSSION

3.1 | Human pancreatic β-cells engineered to form glucose-responsive pseudo-islets in vitro

To mimic the insulin-secretory function of endocrine pancreas, we modified a previously described protocol using human pancreatic β-cells, aggregated at 2000 cells per pseudo-islet [22]. After 5 days of culture, pseudo-islets had properly aggregated into clinically relevant spheres with a mean diameter of 101 ± 5.4 µm (Figure 1A), which were similar in size to previous studies demonstrating a relationship between islet size and functionality in vitro and in vivo in terms of survival rate after transplantation [25, 26]. Smaller rat islets (<125 µm) were superior than larger islets (>150 µm) in terms of insulin release in vitro and restoring glycemic control in a diabetic rat model [26].

The main function of pancreatic β-cells is to secrete insulin in response to glucose stimulation. Pseudo-islets were stimulated with 20 mM glucose and showed a significant increase in insulin secretion upon stimulation (0 mM: 0.63 ± 0.1 mU/L insulin/pseudo-islet vs 1.66 ± 0.6 mU/L insulin/pseudo-islets at 20 mM) (Figure 1B). After stimulation, pseudo-islets returned to their basal insulin secretion level. Immunofluorescence staining showed a homogeneous distribution of insulin throughout the pseudo-islets (Figure 1C). Altogether, these data show the dynamic response of human pseudo-islets to glucose, and their potential to mimic the functional unit of the islets of Langerhans that produce insulin.

3.2 | FLIM enables the noninvasive monitoring of hypoxia-induced cell death in vitro

Hypoxia leads to β-cell dysfunction, which is a major factor contributing to the overall poor efficiency of the Langerhans islet isolation and transplantation procedures

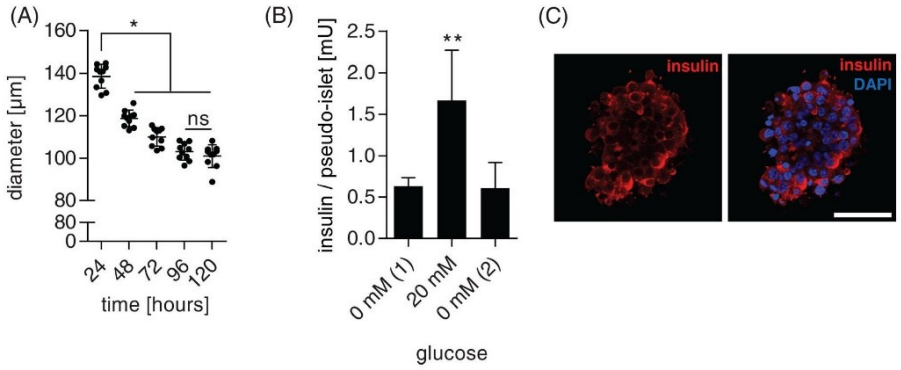

FIGURE 1 Formation of human glucose-responsive pseudo-islets to mimic the insulin-producing endocrine function of the pancreas. A, β-cell aggregation monitored by assessing the mean diameter of pseudo-islets over time. One-way analysis of variance (ANOVA) with Tukey's multiple comparisons test. n = 10. B, Standard glucose-stimulated insulin secretion (GSIS) of pseudo-islets subjected sequentially to 0, 20 and 0 mM glucose. n ≥ 4. C, Immunofluorescence staining of insulin in pseudo-islets (red) and nuclei (DAPI, blue). Scale bar equals 50 µm. *$P < .05$; **$P < .01$

[27]. Severe and prolonged hypoxia (<1% oxygen) induces nonreversible cellular changes resulting in programmed cellular death. To evaluate the impact of severe hypoxia on our pseudo-islet in vitro system, key hypoxic expression markers were evaluated over time, including vascular endothelial growth factor (VEGF), HIF-1α and cleaved caspase-3 (Figure 2).

Adult pancreatic islets continuously secrete VEGF to maintain blood vessel density and proper fenestration [28]. In response to decreased oxygen tension, pancreatic β-cells secrete VEGF as part of an adaptive response to hypoxia [29]. Here, we showed a significant increase in VEGF after 1 hour under hypoxia (Figure 2A).

Our results showed that HIF-1α, which is induced by a decrease in oxygen in the cytoplasm, significantly increased after 6 hours under hypoxia (Figure 2B). The HIF-1α protein, which is stabilized by hypoxic conditions, has a large number of target genes, including HIF-1 and VEGF [30]. Here, we observed a potentially coordinated and significant increase of HIF-1α and VEGF after 1 hour under hypoxic conditions. After 6 hours under hypoxic conditions, HIF-1α expression increased further and reached a plateau, while VEGF expression slowly decreased.

HIF-1α exerts both pro- and anti-apoptotic effects, depending on the severity of hypoxia [31]. Under severe hypoxic conditions, HIF-1α can trigger hypoxia-induced apoptosis, which can be measured by the expression of cleaved caspase-3 [32]. Here, cleaved caspase-3 was significantly upregulated from 12 to 24 hours under hypoxia (Figure 2C). These results suggest that pseudo-islets under hypoxic conditions initiate an adaptive response from 1 to 4 hours, seen by a rapid increase in VEGF. HIF-1α may exert a pro-apoptotic effect via HIF-1α between 4 and 6 hours that leads to the activation of programmed cell death via cleaved caspase-3 between 6 and 12 hours under hypoxia. Identification of dead cells (i.e. after completion of apoptosis) is possible using MP images of the endogenous NADH. The appearance of a hypoxic core, which was depicted by the loss of NADH autofluorescence intensity, can be observed in pseudo-islets at 12 hours under hypoxia (Figure 2D).

FLIM can identify metabolic changes in living cell cultures and in vivo [33]. Here, we were interested in whether FLIM has the fidelity to identify metabolic changes arising from the early adaptive response to hypoxia before the activation of cleaved caspase-3 and following nonreversible cellular changes. Therefore, FLIM images were acquired from the endogenous NADH and FAD autofluorescence of pseudo-islets under normoxia and hypoxia for 3, 6 and 12 hours. Each metabolic profile was characterized by the FLIM parameters τ_1, τ_2 and α_1 from the respective coenzymes NADH and FAD, as well as the optical oxidative ratio (FAD/FAD + NADH) (Figure 2E-J). NADH τ_1 represents the fluorescence lifetime of free NADH, whose major contribution arises from cytosolic NADH in opposition to bound NADH found in the oxidative phosphorylation chain and characterized by τ_2 [34]. NADH and FAD lifetimes are highly sensitive to changes within their microenvironment, such as pH, solvent polarity or viscosity [33]. We showed that hypoxia induced an increase in NADH τ_1 at 3 and 6 hours, while NADH τ_2 was most affected after 3 hours (Figure 2E,F). Hypoxia is known to trigger a switch from aerobic to anaerobic glycolysis, which is a protective strategy against the production of reactive oxygen species (ROS) [35]. It is also the means with which NAD^+ is recovered

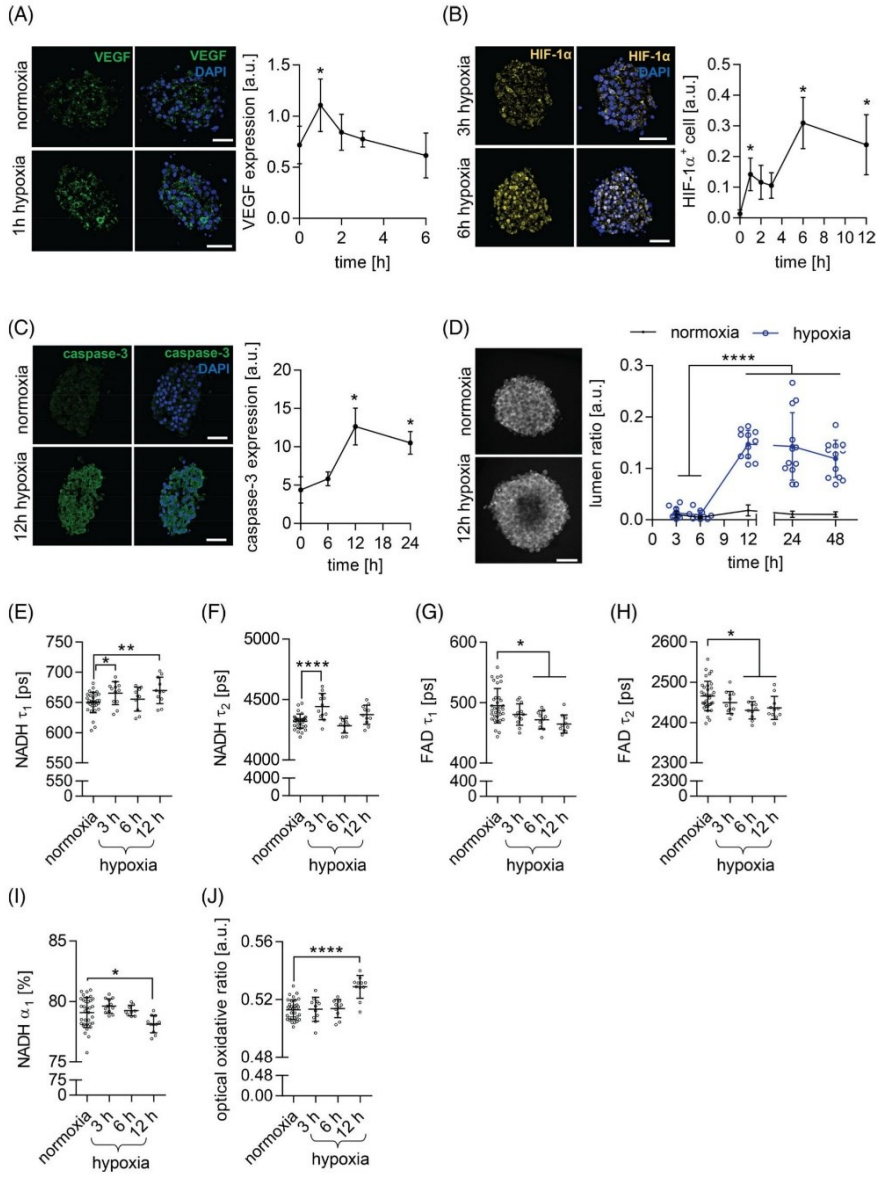

FIGURE 2 Hypoxia-induced cellular response in human pseudo-islets is detectable with fluorescence lifetime imaging microscopy (FLIM). Immunofluorescence staining of, A, vascular endothelial growth factor (VEGF), B, hypoxia-inducible factor 1α (HIF-1α) and, C, cleaved capase-3 in pseudo-islets under normoxic and hypoxic conditions and the corresponding quantification (right). n ≥ 3. D, Multiphoton (MP) imaging and quantification of the lumen size of hypoxic pseudo-islets over a time period of 12 hours. n ≥ 10. E-J, Time lapse FLIM analysis of hypoxic pseudo-islets showing, E, nicotinamide adenine dinucleotide (NADH) τ_1, F, NADH τ_2, G, flavin adenine dinucleotide (FAD) τ_1, H, FAD τ_2, I, NADH α_1 and, J, the optical oxidative ratio based on endogenous fluorescence of FAD/FAD + NADH. n ≥ 10. Scale bars equal 50 μm. One-way analysis of variance (ANOVA) with Tukey's multiple comparisons test. *$P < .05$; **$P < .01$ and ****$P < .0001$

from NADH, which is required to produce ATP. This process produces a large amount of lactic acid. The following acidification of the cytosol may be responsible for the significant change in NADH τ_1. The mitochondria produce ROS via the complexes I and III of the electron chain transporters, whose production levels increase when oxygen levels drop in a range of 5% to 0.5% [35]. Interestingly, oxidative stress arising from ROS has been shown to increase NADH τ_2, which is observed here after 3 hours under hypoxia (Figure 2F) [36]. The recovery of NADH τ_2 at 6 and 12 hours under hypoxia may reflect the activation of antioxidant pathways [37].

Under hypoxia, FAD τ_1 and τ_2 significantly decreased after 6 and 12 hours (Figure 2G,H). The majority of the endogenous fluorescence from FAD arises from the mitochondria when FAD is in a complex with lipoamide dehydrogenases and the electron transfer flavoproteins, whose contributions represent ~50% and ~25% of the total intensity, respectively [38]. The contribution from the electron change transporter is considered negligible, and the remaining 25% of the FAD intensity is not associated with metabolism. Therefore, change in FAD τ_1 and τ_2 are strongly associated with the mitochondrial microenvironment.

NADH α_1, which is the contribution of the free NADH over the total amount of photons collected, significantly decreased in pseudo-islets after 12 hours under hypoxia when compared with the normoxic controls (Figure 2I). This describes a redistribution from free to bound NADH forms to facilitate more efficient ATP production in the mitochondria. The nucleus increases its energy demands, as it prepares the cells for apoptosis [39]. Decrease in NADH α_1 has been reported in vivo in murine keratinocytes undergoing apoptosis [19]. These data are corroborated with a significant increase in optical oxidative ratio at 12 hours under hypoxia, implying that the relative amount of mitochondrial FAD (free and bound) increased when compared to NADH (free and bound) (Figure 2J).

We showed that FLIM can detect metabolic changes that are induced by the hypoxic environment in a nondestructive manner in pancreatic β-cells. Moreover, our data reveals that the NADH lifetimes τ_1 and τ_2 can be used as indicators of the early adaptive hypoxia-induced cellular response, occurring before the appearance of the major peak in HIF-1α or cleaved caspase-3.

3.3 | Spatial distribution of FLIM outputs allow the detection of early adaptive hypoxia-induced cellular response in pseudo-islets

During the isolation process, pancreatic islets are severed from their vasculature and rely on diffusive properties from the surrounding media for their oxygen and nutrient supply. The diffusion gradient is depending partially on the islet size, which is highly heterogenous in the native pancreas [40]. In addition, each islet has a different degree of vascularization and composition of α-, β-, δ-, γ- and PP-cells [41]. FLIM can be used to assess the metabolic state of single cells, which can reveal the heterogeneity within single islets or pseudo-islets. We hypothesize that FLIM can discriminate subregions within one pseudo-islet that differentially react to hypoxic conditions, either by an adaptive response to hypoxia or by initiating a programmed cell death. Therefore, we segmented FLIM acquisitions to create ROIs based on their spatial distribution (see Section 2) within the pseudo-islets as illustrated in Figure 3a. For each ROI representing a 10 μm increment in depth, NADH and FAD lifetimes τ_1 and τ_2, NADH α_1, and optical oxidative ratio were assessed (Figure 3B-G).

Under normoxic conditions, the first ROI (0-10 μm) is metabolically different than all other ROIs: a significantly higher optical oxidative ratio and lower NADH α_1 indicate that cells within the first ROI rely on higher oxidative phosphorylation rates. This is likely due to the direct contact between nutrients/oxygen and β-cells.

Under hypoxia, FLIM parameters NADH τ_1, FAD τ_2, NADH α_1 and optical oxidative ratio were significantly affected by the spatial distribution of the corresponding ROIs. Hypoxia severely impacted FLIM parameters in the central region of the pseudo-islets (30-80 μm), starting from 3 hours under hypoxia, characterized by a steady increase of NADH τ_1, decrease in FAD τ_2, decrease in NADH α_1, and increase in optical oxidative ratio (Figure 3B,E-G). In the pseudo-islet core, hypoxia is most likely <1% oxygen due to the oxygen consumption of the outer cells. Under such conditions, cellular mechanisms concentrate on antioxidant-producing pathways that come at the expense of glycolytic ATP production [37]. After a prolonged time under those severe conditions, the apoptotic cascade is activated, which may be responsible for the further increase in oxidative phosphorylation [42].

In contrast, in the outermost ROI (0-30 μm), a significant decrease in NADH α_1 was observed after 12 hours under hypoxia, while no changes were noted in either NADH τ_1 or optical oxidative ratio. FAD τ_1 and τ_2 decreased after 6 hours only in the first ROI (0-10 μm). This suggests that the cells in the first ROI may have initiated an adaptive response to hypoxia and are able to maintain their glycolytic rate for a longer period.

NADH τ_2 and FAD τ_1 were not affected by the spatial distribution within the pseudo-islets (Figure 3C,D). While NADH τ_2 oscillated during hypoxia, FAD τ_1 was only affected in the first ROI (0-10 μm). Interestingly, both

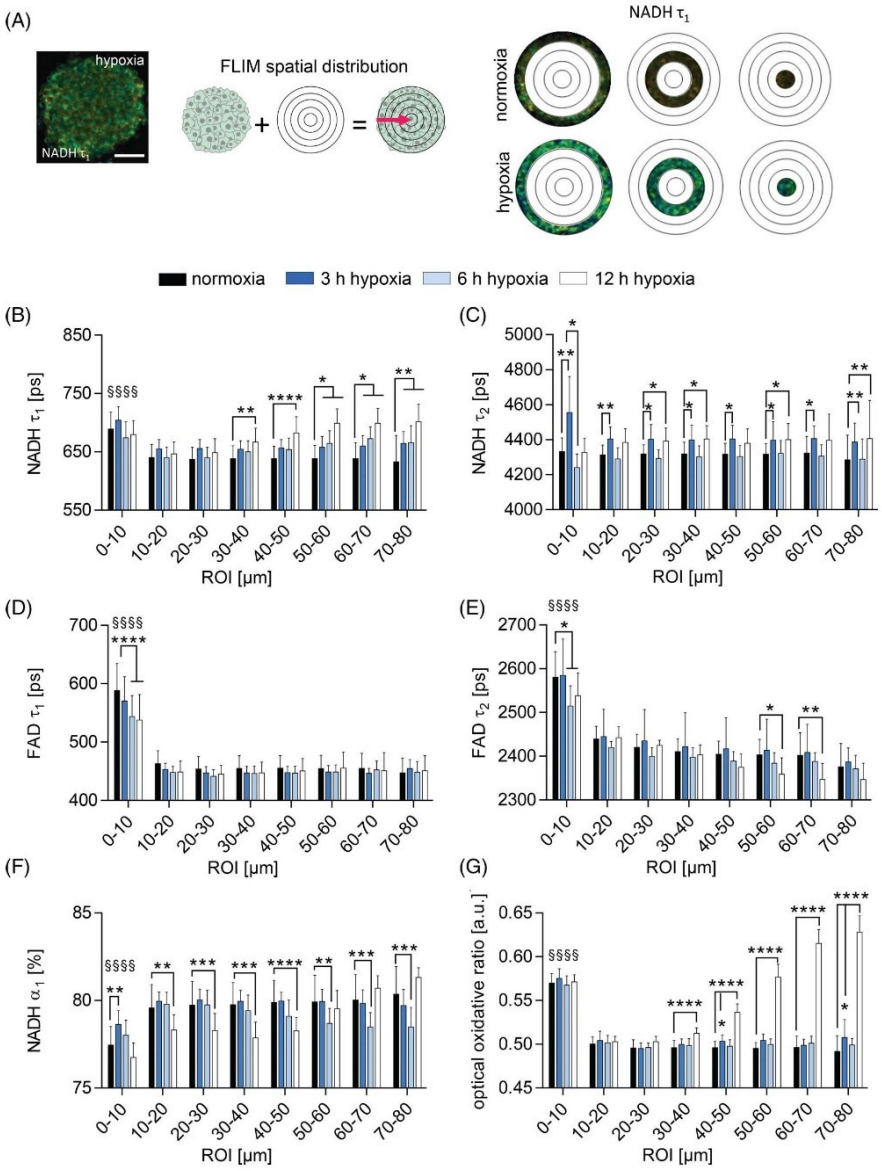

FIGURE 3 Segmentation of fluorescence lifetime imaging microscopy (FLIM) images reveal the heterogeneity of hypoxic pseudo-islets in vitro. A, Schematic illustration of the segmentation of FLIM images creating 10 µm-deep incremented regions of interest (ROIs). B-G, FLIM analysis of hypoxic pseudo-islets over time, and segmented per ROI, showing, B, nicotinamide adenine dinucleotide (NADH) τ_1, C, NADH τ_2, D, flavin adenine dinucleotide (FAD) τ_1, E, FAD τ_2, F, NADH α_1 and, G, the optical oxidative ratio based on endogenous fluorescence of FAD/FAD + NADH. n ≥ 10. Scale bar equals 50 µm. Two-way analysis of variance (ANOVA) with Dunnett's multiple comparisons test. §§§§: significant difference between ROIs $P < .0001$. *: Significant difference between groups within one ROI. *$P < .05$; **$P < .01$, ***$P < .001$ and ****$P < .0001$

NADH τ_2 and FAD τ_1 are protein-bound lifetimes within the mitochondria, which may reduce their sensitivity to microenvironmental changes.

The segmentation of FLIM outputs allowed the discrimination of surviving and apoptotic cells within a single pseudo-islet. As expected, the innermost ROIs are

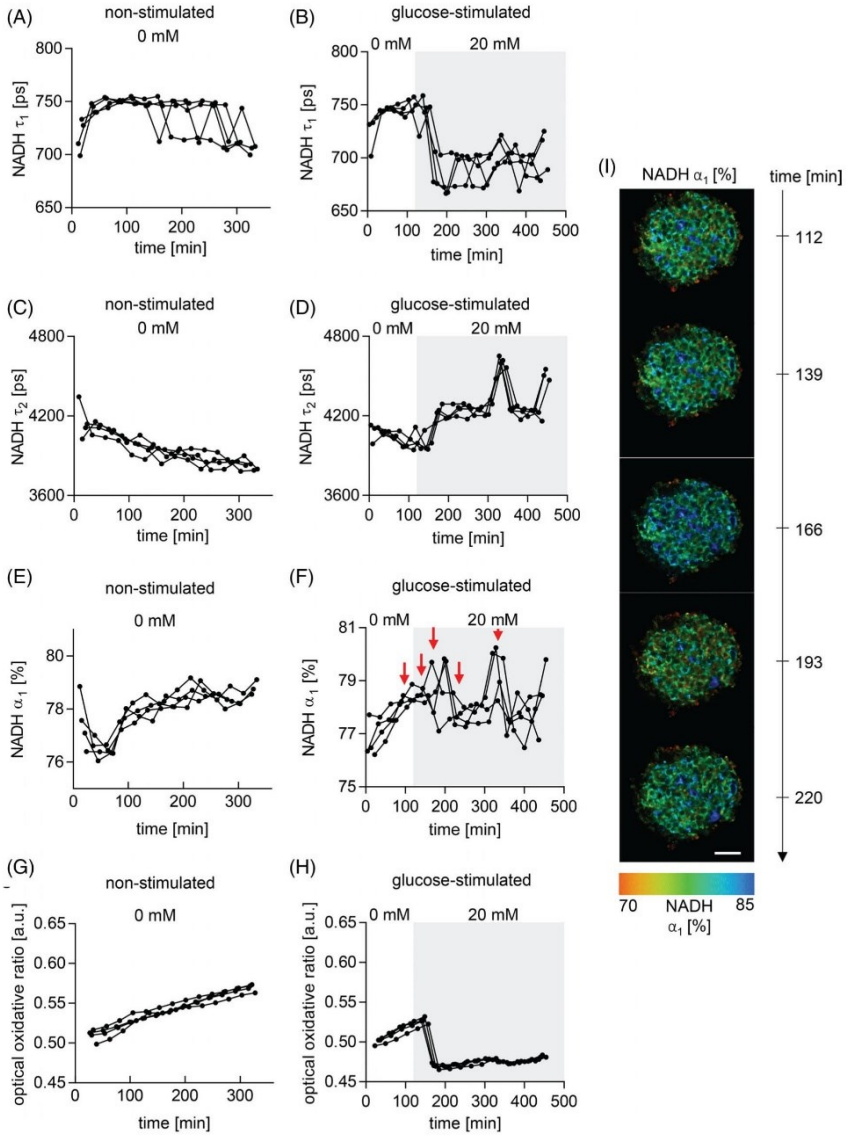

FIGURE 4 In situ fluorescence lifetime imaging microscopy (FLIM) probes glucose-responsiveness of normoxic pseudo-islets in vitro. FLIM analysis over time of nonstimulated pseudo-islets and glucose stimulation with 20 mM shows, A,B, nicotinamide adenine dinucleotide (NADH) τ_1, C,D, NADH τ_2, E,F, NADH α_1 and, G,H, the optical oxidative ratio based on endogenous fluorescence of flavin adenine dinucleotide (FAD)/FAD + NADH. I, Representative images of NADH α_1 over time during glucose stimulation. Corresponding time points are shown with red arrows in F. n = 4. Scale bar equals 50 μm

strongly affected by hypoxia, as indicated by a change in NADH lifetimes, NADH α_1, and oxidative ratio. These changes will likely lead to the nonreversible initiation of apoptosis [19, 42]. The β-cells located in the outer ROIs were characterized by a lower NADH α_1 and stable values for NADH τ_1, FAD τ_2 and optical oxidative ratio. These metabolic changes suggest that the β-cells were affected by hypoxia by redistributing free to bound NADH. However, the stable values of NADH and FAD lifetimes suggest that these β-cells have reached a metabolic equilibrium under hypoxia via an adaptive response.

3.4 | FLIM can noninvasively identify metabolic oscillations of glucose-responsive pseudo-islets

The major prerequisite of transplanted pancreatic islets is the regulation of glucose homeostasis by sensing glucose and secreting appropriate amounts of insulin [1]. Hypoxia decreases aerobic glycolysis, thus reducing the β-cell capacity to secrete insulin upon glucose stimulation [43]. Depending on the severity of the hypoxia-induced cell damage, the downstream effects of HIF-1α activation in β-cells can be transient and reversible. Therefore, assessing the metabolic changes due to glucose stimulation is essential to identify functional islets. Here, we characterized the glucose-response of functional pseudo-islets using FLIM. Normoxic pseudo-islets were stimulated with 20 mM glucose as previously described [22]. FLIM images were acquired during the glucose stimulation of single pseudo-islets over time and compared to nonstimulated pseudo-islets (Figure 4).

In the first 60 minutes of analysis without glucose, NADH τ_1 steadily increased overtime, while NADH α_1 decreased, which reflects the known metabolic changes due to glucose starvation (Figure 4A,E) [44]. Prolonged starvation resulted in NADH τ_1, FAD τ_1 and FAD τ_2 oscillations, steady decrease in NADH τ_2, and an increase in NADH α_1 and optical oxidative ratio (Figures 4A,C,E, G and S1). The absence of glucose diminishes the glycolytic flux and forces mitochondrial adaptation. Carbon sources can be provided, for instance by glutamine, which can fuel the TCA cycle and maintain ATP levels [45]. Additional pathways can be initiated to provide energy, such as the β-oxidation of fatty acids or the pentose phosphate pathway [37]. The pentose phosphate pathway produces nicotinamide adenine dinucleotide phosphate (NADPH), which may be responsible for the increase of free NADH after 60 minutes, as NADPH endogenous fluorescence is included in the NADH signals [46].

Stimulation of β-cells with glucose impacted NADH and FAD lifetimes, oscillations of NADH α_1 and led to a drop of the oxidative ratio (Figures 4B,D,F,H,I and S1). Glycolytic flux abruptly increases as glucose is transported into the cells, which was seen in our data by the immediate changes in NADH and FAD lifetimes and spiking of NADH α_1. Similarly, aerobic glycolysis produces large amounts of NADH, correlating with the decrease in oxidative ratio.

Hypoxia-induced cellular changes can be reversible depending on their severity. For instance, 6 hours under hypoxia altered the mitochondrial lifetimes of NADH and FAD, while NADH α_1 and optical oxidative ratio were stable, suggesting a moderate impact of hypoxia. To investigate the glucose-response of pseudo-islets cultured under hypoxia for 6 hours, FLIM metabolic profiles were assessed during stimulation with 20 mM glucose (Figure 5). We detected large fluctuations in NADH τ_1 and NADH α_1, which did not resemble the metabolic response of stimulated normoxic pseudo-islets (Figure 5A,C). Nevertheless, the value of NADH τ_2 before glucose stimulation under hypoxia was similar to normoxia (Figure 5B,E). Upon stimulation, NADH τ_2 under hypoxia spiked and plateaued at higher values compared with normoxia (Figure 5B). The optical oxidative ratio of hypoxic pseudo-islets, which was overall higher than in normoxia, dropped upon glucose stimulation similarly to normoxic pseudo-islets (Figure 5D). The profile of FAD lifetimes was similar to normoxia as well (Figure S2). Stimulation of pancreatic β-cells with glucose and following insulin secretion requires both glycolysis and oxidative phosphorylation [47]. After 6 hours under hypoxia, pseudo-islets were still glucose-responsive, as indicated by NADH τ_2, FAD τ_1, FAD τ_2 and the optical oxidative ratio. The stimulation lead to an increase in the total NADH compared to FAD, which most likely is produced by an increase in glycolysis. However, the high value of NADH τ_2 indicated an important change within the mitochondrial microenvironment. This change may have arisen from the increasing levels of ROS due to hypoxia and the loss of the metabolic rescue mechanisms of a functional cell, which further increased as the TCA cycle and oxidative phosphorylation are enforced during insulin secretion. Prolongated hypoxia is known to lead to β-cell dysfunction, characterized, in part, by a loss of glucose-response [43]. Here, we showed that pseudo-islets after 6 hours under hypoxia still respond to glucose based on FLIM, which was validated by a standard GSIS assay (Figure S3). However, important changes in the metabolic response of the coenzymes NADH and FAD were detected suggesting cellular

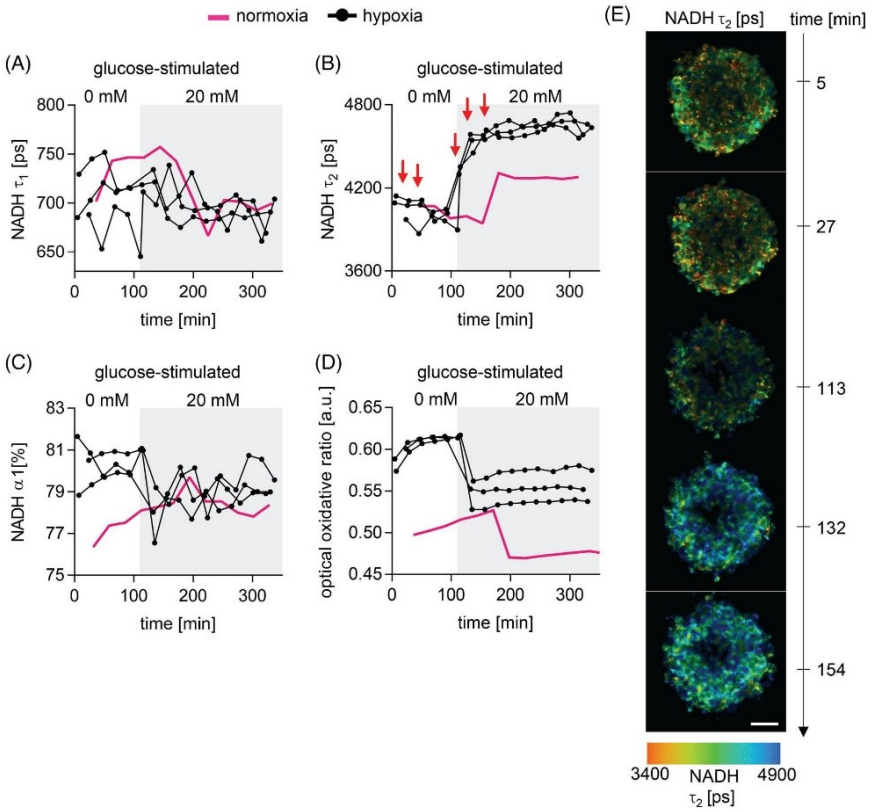

FIGURE 5 In situ fluorescence lifetime imaging microscopy (FLIM) monitors individual pseudo-islet glucose responses under hypoxic conditions for 6 hours. FLIM analysis over time during glucose stimulation with 20 mM reveals, A, nicotinamide adenine dinucleotide (NADH) τ_1, B, NADH τ_2, C, NADH α_1 and, D, the optical oxidative ratio based on endogenous fluorescence of flavin adenine dinucleotide (FAD)/FAD + NADH. Hypoxic pseudo-islets are shown in black and normoxic controls (averaged, n = 4) are shown in pink. E, Representative images of NADH τ_2 over time during glucose stimulation. Corresponding time points are highlighted with red arrows in B. n = 3. Scale bar equals 50 μm

stress. Our data demonstrates how FLIM can detect metabolic impairment in hypoxic pseudo-islets in comparison with standard methods such as GSIS assays.

4 | CONCLUSION

Developing noninvasive tools to assess the quality of isolated pancreatic islets prior implantation has the potential to improve the outcomes of Langerhans islet transplantation to treat type 1 diabetes. In this study, we used an in vitro system mimicking the insulin-producing and glucose-responsive characteristics of the islets of Langerhans and combined it with FLIM to assess pseudo-islet quality and their glucose-response under standard and hypoxic conditions. FLIM identified and discriminated between minor and severe hypoxia-induced cellular damages in β-cells. FLIM further allowed the marker-free and noninvasive detection of a metabolic response due to glucose stimulation in functional living pseudo-islets, which can be used to assess the severity of hypoxia-induced damages during insulin secretion.

ACKNOWLEDGMENTS

A. Z. and D. A. C. B. contributed equally to this work. The authors thank Katharina U. Schlünder (University of Tübingen) for her support with the pancreas-on-chip system. This work was financially supported by the European

Union (H2020-NMP10-2014-645991-2, DRIVE; H2020-ITN 766181, DELIVER to G. P. D and K. S.-L.), the International Foundation for Ethical Research (to A. Z.), as well as the Ministry of Science, Research and the Arts of Baden-Württemberg (33-729.55-3/214 and SI-BW 01222-91 to K. S.-L.) and the Deutsche Forschungsgemeinschaft (INST 2388/33-1 to K. S.-L.). Open access funding enabled and organized by Projekt DEAL.

CONFLICT OF INTEREST

The authors declare no conflict of interest.

AUTHOR CONTRIBUTIONS

Aline Zbinden, **Daniel A. Carvajal Berrio**, **Max Urbanczyk**, **Shannon L. Layland** and **Katja Schenke-Layland**: Designed the experiments and wrote the manuscript. **Aline Zbinden**, **Daniel A. Carvajal Berrio**, **Max Urbanczyk**, **Mariella Bosch**, **Sandro Fliri**, **Chuan-en Lu** and **Abiramy Jeyagaran**: Performed experiments, collected and analyzed data. **Peter Loskill** and **Garry P. Duffy**: Gave conceptual advice.

DATA AVAILABILITY STATEMENT

The main data supporting the findings of this study are available within the article and its supplementary information. The raw data generated in this study are available from the corresponding author upon reasonable request.

ORCID

Katja Schenke-Layland https://orcid.org/0000-0001-8066-5157

REFERENCES

[1] M. R. Rickels, R. P. Robertson, *Endocr. Rev.* **2019**, *40*, 631.
[2] E. A. Ryan, B. W. Paty, P. A. Senior, D. Bigam, E. Alfadhli, N. M. Kneteman, J. R. T. Lakey, A. M. J. Shapiro, *Diabetes* **2005**, *54*, 2060.
[3] Q. Zhou, D. A. Melton, *Nature* **2018**, *557*, 351.
[4] W. Bennet, C. G. Groth, R. Larsson, B. Nilsson, O. Korsgren, *Ups. J. Med. Sci.* **2000**, *105*, 125. https://doi.org/10.1517/03009734000000059.
[5] M. Giuliani, W. Moritz, E. Bodmer, D. Dindo, P. Kugelmeier, R. Lehmann, M. Gassmann, P. Groscurth, M. Weber, *Cell Transplant.* **2005**, *14*, 67.
[6] R. M. Spiers, J. Marzi, E. M. Brauchle, S. E. Cross, R. H. Vaughan, P. A. Bateman, S. J. Hughes, K. Schenke-Layland, P. R. V. Johnson, *Acta Biomater.* **2019**, *99*, 269.
[7] G. Loganathan, R. K. Dawra, S. Pugazhenthi, Z. Guo, S. M. Soltani, A. Wiseman, M. A. Sanders, K. K. Papas, K. Velayutham, A. K. Saluja, D. E. R. Sutherland, B. J. Hering, A. N. Balamurugan, *Transplantation* **2011**, *92*, 1222.
[8] M. Garcia-Contreras, A. Tamayo-Garcia, K. L. Pappan, G. A. Michelotti, C. L. Stabler, C. Ricordi, P. Buchwald, *J. Proteome Res.* **2017**, *16*, 2294. https://doi.org/10.1021/acs.jproteome.7b00160.
[9] X. Zheng, X. Zheng, X. Wang, Z. Ma, V. Gupta Sunkari, I. Botusan, T. Takeda, A. Björklund, M. Inoue, S. B. Catrina, K. Brismar, L. Poellinger, T. S. Pereira, *Cell Death Dis.* **2012**, *3*, e322.
[10] E. Linetsky, C. Ricordi, *Transplant. Proc.* **2008**, *40*, 424.
[11] J. D. Carter, S. B. Dula, K. L. Corbin, R. Wu, C. S. Nunemaker, *Biol. Proced. Online* **2009**, *11*, 3.
[12] P. H. Lakner, M. G. Monaghan, Y. Möller, M. A. Olayioye, K. Schenke-Layland, *Sci. Rep.* **2017**, *7*, 1.
[13] J. Li, A. J. Bower, Z. Arp, E. J. Olson, C. Holland, E. J. Chaney, M. Marjanovic, P. Pande, A. Alex, S. A. Boppart, *J. Biophotonics* **2018**, *11*, e201700195.
[14] A. J. Walsh, R. S. Cook, M. E. Sanders, L. Aurisicchio, G. Ciliberto, C. L. Arteaga, M. C. Skala, *Cancer Res.* **2014**, *74*, 5184. https://doi.org/10.1158/0008-5472.CAN-14-0663.
[15] J. R. Lakowicz, H. Szmacinski, K. Nowaczyk, M. L. Johnson, *Proc. Natl. Acad. Sci. U. S. A.* **1992**, *89*, 1271.
[16] I. A. Okkelman, R. I. Dmitriev, T. Foley, D. B. Papkovsky, *PLoS One* **2016**, *11*, e0167385. https://doi.org/10.1371/journal.pone.0167385.
[17] A. V. Meleshina, V. V. Dudenkova, A. S. Bystrova, D. S. Kuznetsova, M. V. Shirmanova, E. V. Zagaynova, *Stem Cell Res. Ther.* **2017**, *8*, 15.
[18] M. Wang, F. Tang, X. Pan, L. Yao, X. Wang, Y. Jing, J. Ma, G. Wang, L. Mi, *BBA Clin.* **2017**, *8*, 7.
[19] A. J. Bower, M. Marjanovic, Y. Zhao, J. Li, E. J. Chaney, S. A. Boppart, *J. Biophotonics* **2017**, *10*, 143.
[20] P. E. MacDonald, J. W. Joseph, P. Rorsman, *Philos. Trans. R. Soc. B: Biol. Sci.* **2005**, *360*, 2211.
[21] L. J. McCulloch, M. van de Bunt, M. Braun, K. N. Frayn, A. Clark, A. L. Gloyn, *Mol. Genet. Metab.* **2011**, *104*, 648. https://doi.org/10.1016/j.ymgme.2011.08.026.
[22] A. Zbinden, J. Marzi, K. Schlünder, C. Probst, M. Urbanczyk, S. Black, E. M. Brauchle, S. L. Layland, U. Kraushaar, G. Duffy, K. Schenke-Layland, P. Loskill, *Matrix Biol.* **2020**, *85–86*, 205.
[23] K. Schenke-Layland, J. Xie, E. Angelis, B. Starcher, K. Wu, I. Riemann, W. R. MacLellan, S. F. Hamm-Alvarez, *Matrix Biol.* **2008**, *27*, 53.
[24] O. I. Kolenc, K. P. Quinn, *Antioxidants Redox Signal.* **2019**, *30*, 875.
[25] R. Lehmann, R. A. Zuellig, P. Kugelmeier, P. B. Baenninger, W. Moritz, A. Perren, P. A. Clavien, M. Weber, G. A. Spinas, *Diabetes* **2007**, *56*, 594. https://doi.org/10.2337/db06-0779.
[26] W. Li, R. Zhao, J. Liu, M. Tian, Y. Lu, T. He, M. Cheng, K. Liang, X. Li, X. Wang, et al., *J. Diabetes Res.* **2014**, *2014*, 192093. https://doi.org/10.1155/2014/192093.
[27] K. E. Dionne, C. K. Colton, M. L. Yarmush, *Diabetes* **1993**, *42*, 12.
[28] J. D'Hoker, N. de Leu, Y. Heremans, L. Baeyens, K. Minami, C. Ying, A. Lavens, M. Chintinne, G. Stangé, J. Magenheim, et al., *Diabetes* **2013**, *62*, 4165. https://doi.org/10.2337/db12-1827.
[29] K. S. Sankar, S. M. Altamentova, J. V. Rocheleau, *PLoS One* **2019**, *14*, e0222424.
[30] G. L. Semenza, *Biochem. Pharmacol.* **2002**, *64*, 993.
[31] J. P. Piret, D. Mottet, M. Raes, C. Michiels, *Biochem. Pharmacol.* **2002**, *64*, 889.
[32] A. E. Greijer, E. van der Wall, *J. Clin. Pathol.* **2004**, *57*, 1009.
[33] J. V. Chacko, K. W. Eliceiri, *Cytom. Part A* **2019**, *95*, 56.

[34] K. Suhling, L. M. Hirvonen, J. A. Levitt, P. H. Chung, C. Tregidgo, A. Le Marois, D. A. Rusakov, K. Zheng, S. Ameer-Beg, S. Poland, et al., *Med. Photonics* **2015**, *27*, 3.
[35] G. Solaini, A. Baracca, G. Lenaz, G. Sgarbi, *Biochim. Biophys. Acta - Bioenerg.* **2010**, *1797*, 1171.
[36] A. Chorvatova, S. Aneba, A. Mateasik, D. Chorvat, B. Comte, *J. Biomed. Opt.* **2013**, *18*, 067009.
[37] E. Mullarky, L. C. Cantley, *Innovative Medicine*, Springer, Tokyo, Japan **2015**, p. 3.
[38] W. S. Kunz, W. Kunz, *BBA - Gen. Subj.* **1985**, *841*, 237. https://doi.org/10.1016/0304-4165(85)90064-9.
[39] J. M. Levitt, A. Baldwin, A. Papadakis, S. Puri, J. Xylas, K. Münger, I. Georgakoudi, *J. Biomed. Opt.* **2006**, *11*, 064012.
[40] A. A. Elayat, M. M. El-Naggar, M. Tahir, *J. Anat.* **1995**, *186*(Pt 3), 629.
[41] G. da Silva Xavier, *J. Clin. Med.* **2018**, *7*, 54. https://doi.org/10.3390/jcm7030054.
[42] K. L. Eales, K. E. R. Hollinshead, D. A. Tennant, *Oncogenesis* **2016**, *5*, e190.
[43] J. Cantley, S. T. Grey, P. H. Maxwell, D. J. Withers, *Diabetes Obes. Metab.* **2010**, *12*, 159.
[44] Z. Liu, D. Pouli, C. A. Alonzo, A. Varone, S. Karaliota, K. P. Quinn, K. Mönger, K. P. Karalis, I. Georgakoudi, *Sci. Adv.* **2018**, *4*, eaap9302. https://doi.org/10.1126/sciadv.aap9302.
[45] A. Varone, J. Xylas, K. P. Quinn, D. Pouli, G. Sridharan, M. E. McLaughlin-Drubin, C. Alonzo, K. Lee, K. Münger, I. Georgakoudi, *Cancer Res.* **2014**, *74*, 3067. https://doi.org/10.1158/0008-5472.CAN-13-2713.
[46] P. M. Schaefer, S. Kalinina, A. Rueck, C. A. F. von Arnim, B. von Einem, *Cytom. Part A* **2019**, *95*, 34.
[47] S. Jitrapakdee, A. Wutthisathapornchai, J. C. Wallace, M. J. MacDonald, *Diabetologia* **2010**, *53*, 1019.

SUPPORTING INFORMATION

Additional supporting information may be found online in the Supporting Information section at the end of this article.

How to cite this article: Zbinden A, Carvajal Berrio DA, Urbanczyk M, et al. Fluorescence lifetime metabolic mapping of hypoxia-induced damage in pancreatic pseudo-islets. *J. Biophotonics*. 2020;13:e202000375. https://doi.org/10.1002/jbio.202000375

Appendix IV

RESEARCH ARTICLE

ADVANCED HEALTHCARE MATERIALS
www.advhealthmat.de

ECM Proteins Nidogen-1 and Decorin Restore Functionality of Human Islets of Langerhans upon Hypoxic Conditions

Abiramy Jeyagaran, Max Urbanczyk, Daniel Carvajal-Berrio, Teresa Baldissera, Philipp D. Kaiser, Laurence Kuhlburger, Stefan Czemmel, Sven Nahnsen, Garry P. Duffy, Sara Y. Brucker, Shannon L. Layland, and Katja Schenke-Layland**

Transplantation of donor islets of Langerhans is a potential therapeutic approach for patients with diabetes mellitus; however, its success is limited by islet death and dysfunction during the initial hypoxic conditions at the transplantation site. This highlights the need to support the donor islets in the days post-transplantation until the site is vascularized. It was previously demonstrated that the extracellular matrix (ECM) proteins nidogen-1 (NID1) and decorin (DCN) improve the functionality and survival of the β-cell line, EndoC-βH3, and the viability of human islets post-isolation. To advance the use of these ECM proteins toward a clinical application and elucidate the mechanisms of action in primary islets, the study assesses the effects of ECM proteins NID1 and DCN on isolated human donor islets cultured in normoxic and hypoxic conditions. NID1- and DCN-treatment restore β-cell functionality of human donor islets in a hypoxic environment through upregulation of genes involved in glycolytic pathways and reducing DNA fragmentation in hypoxic conditions comparable to normoxic control islets. The results demonstrate that the utilization of NID1 or DCN with islets of Langerhans may have the potential to overcome the hypoxia-induced cell death observed post-transplantation and improve transplant outcomes.

1. Introduction

Islet transplantation for the treatment of type one diabetes mellitus could offer patients autonomous blood glucose homeostasis and insulin independence; however, it is not a common treatment option due to the high demand for the number of donor islets needed for each transplant.[1–3] To ensure sufficient islets survive the initial hypoxic transplant environment, inflammation, fibrotic capsule formation, and immune rejection, at least two donor's worth of islets are needed for a transplant. Through recent advances in stem cell derived-β-cells, alternate cell sources for implantation have been generated; however, the procedural obstacles still exist.[4] Multiple approaches including culture and transplantation of β-cells with extracellular matrix (ECM) proteins,[5] supporting cells (endothelial cells,[6] fibroblasts,[7] mesenchymal stromal cells,[8] etc.),

A. Jeyagaran, M. Urbanczyk, D. Carvajal-Berrio, T. Baldissera, S. L. Layland, K. Schenke-Layland
Institute of Biomedical Engineering
Department for Medical Technologies and Regenerative Medicine
Eberhard Karls University Tübingen
72076 Tübingen, Germany
E-mail: shannon-lee.layland@uni-tuebingen.de; katja.schenke-layland@uni-tuebingen.de

P. D. Kaiser, K. Schenke-Layland
NMI Natural and Medical Sciences Institute at the University of Tübingen
72770 Reutlingen, Germany

L. Kuhlburger, S. Czemmel, S. Nahnsen
Quantitative Biology Center (QBiC)
Eberhard Karls University of Tübingen
72076 Tübingen, Germany

L. Kuhlburger, S. Nahnsen
Biomedical Data Science
Department of Computer Science
Eberhard Karls University
Tübingen
72076 Arkansas, Germany

G. P. Duffy
Discipline of Anatomy and the Regenerative Medicine Institute
School of Medicine
College of Medicine Nursing and Health Sciences
National University of Ireland Galway
Galway H91 TK33, Ireland

G. P. Duffy
Science Foundation Ireland (SFI) Centre for Research in Advanced Materials for Biomedical Engineering (AMBER)
Trinity College Dublin & National University of Ireland Galway
Galway H91 TK33, Ireland

S. Y. Brucker, S. L. Layland
Department of Women's Health Tübingen
University of Tübingen
72076 Tübingen, Germany

The ORCID identification number(s) for the author(s) of this article can be found under https://doi.org/10.1002/adhm.202403017

DOI: 10.1002/adhm.202403017

ADVANCED SCIENCE NEWS
www.advancedsciencenews.com

ADVANCED HEALTHCARE MATERIALS
www.advhealthmat.de

and encapsulation devices have improved cell viability and function.[4] In the body, cell survival and function are greatly supported by the surrounding ECM which acts as both a biophysical and biochemical signaling hub, protecting cells, sequestering growth factors, and activating signaling pathways. As the native ECM is disrupted during islet isolation, many research groups have studied islet ECM to support β-cell survival and function.[4]

Pancreatic islet ECM plays a key role in maintaining the function of multiple cell types including neural, endothelial, and immune cells to ensure there is constant and rapid exchange of nutrients, growth factors, oxygen, glucose, and pancreatic hormones such as insulin and glucagon. Islets are surrounded by both a basement membrane between the islets and the exocrine pancreas and an interstitial matrix between the islet cells themselves. These ECM regions are composed largely of fibrous ECM proteins including collagen types I (COL1) and IV (COL4),[9] laminins (LN),[10,11] fibronectin (FN), and various proteoglycans.[12–14] Many studies using murine and rat β-cells have shown that culturing the cells with these ECM proteins (either as a coating or supplemented in the medium) can support their survival,[15–18] function,[15,17,19–23,18,24–30] and proliferation.[17,27] Furthermore, co-transplantation of ECM proteins with β-cells can improve angiogenesis and integration into the recipient's tissue, allowing for the restoration of blood glucose homeostasis.[31–35] Similar studies culturing human adult and fetal islets with pancreatic ECM proteins also showed increased survival[10,32,36,37] and functionality.[30,23,37–40] Interestingly, combining ECM proteins such as COL4 and LN further improved human islet survival compared to when they are supplied alone;[39,41,42] however, these effects on β-cells were dose-dependent,[41] and at certain doses, it can even disrupt insulin gene transcription and secretion.[43] Interestingly, increased ECM presence can be pathogenic and result in fibrotic capsule formation and dysfunction of the cells. Fibrotic capsule formation is a common obstacle of islet transplantation due to the isolation of the transplant from the recipient's vasculature rendering the transplant ineffective,[4] suggesting a need for ECM regulation to support cell survival and function.

The investigation of adult pancreases for proteins capable of regulating the ECM composition surrounding the islets of Langerhans identified the basement membrane protein nidogen-1 (NID1)[44] and the interstitial matrix protein decorin (DCN)[45] to be highly co-localized with the insulin-producing β-cells. NID1 is a linker protein between COL4 and LN known for its role in stabilizing the basement membrane.[46] DCN is known as the "guardian from the matrix"[47] due to its regulation of collagen fibrillogenesis and sequestering of growth factors important for cell survival and growth.[47] We previously showed that supplementation of these proteins to a human β-cell line improved the cells' functionality.[44,45] Furthermore, NID1 supplementation during the islet isolation process has been shown to increase the viability and number of islets successfully isolated.[2] NID1 and DCN could support human β-cells while also regulating surrounding ECM organization, suggesting a role in improving overall transplant outcomes. In this study, we deepen our understanding of the role of these two ECM proteins in human islet transplant survival and whether they specifically support β-cell function, in a hypoxic, post-transplantation setting. We cultured adult donor islets in a hypoxic environment for three days with and without NID1 or DCN and assessed cell survival and function. We identified that the two ECM proteins restored function of the β-cells in hypoxia. Further analysis using fluorescence lifetime imaging microscopy (FLIM) and next-generation sequencing (NGS) identified glycolytic activity and DNA repair as potential mechanisms of action through which NID1 and DCN support β-cell functionality in hypoxic conditions. Taken together, we demonstrate that the use of NID1 or DCN with islets may overcome the hypoxia-induced cell death observed post-transplantation to improve β-cell function and transplant outcomes.

2. Results

2.1. Protein Treatment and Oxygen Concentration do not Affect Donor Islet Size

Dithizone-staining of donor islets (Figure S2A, Supporting Information) as well as their characterization and quantifications regarding islet particle index (IPI), trapped acinar tissue, and purity of the isolated human islets were performed by the MacDonald Laboratory (Alberta, Canada; Table S3, Supporting Information). The male-to-female ratio was 50%:50%, and 33% of donors were human leukocyte antigen (HLA) A2 positive while 67% were HLA A2 negative (Figure S3, Supporting Information). Brightfield images of donor islets obtained at the start (0 h) and end (72 h) of the experiments for each condition were obtained (Figure S2B,C, Supporting Information), and size tracking showed that there was a significant decrease in islet size from the beginning of the experiment (0 h) compared to the endpoint (72 h). This reduction in size can be attributed to detachment of acinar tissue from the donor islets, leaving the donor islets intact. Protein treatment and oxygen concentration did not have an impact on islet size (Figure S2B—D, Supporting Information, 3-way ANOVA, $N \geq 8$, $^{*}p \leq 0.05$).

To validate that the supplemented ECM proteins interact with the donor islets, we performed IF staining of NID1, insulin (INS), and glucagon (GCG) on CTL and NID1-treated donor islets under normoxia and hypoxia (Figure S4A,B, Supporting Information). Quantification of NID1 integrated density per DAPI count showed a significant increase in NID1 content in NID1-treated samples (Figure S4C, Supporting Information), while insulin and glucagon integrated density per DAPI count were not significantly affected (Figure S4D,E, Supporting Information). Comparable IF staining was performed of DCN, INS, and GCG on CTL and DCN-treated donor islets under normoxia and hypoxia (Figure S5A,B, Supporting Information). Similar results to the NID1 quantification were found after quantification of DCN integrated density per DAPI, where DCN levels were significantly higher in DCN-treated donor islets (Figure S5C, Supporting Information), while insulin and glucagon integrated density per DAPI were not affected (Figure S5D,E, Supporting Information).

2.2. Protein Supplementation Restores Glucose-Responsiveness under Hypoxic Conditions

GSIS and GSGS assays were performed at the 72 h timepoint to determine the functionality of the β-cells within the donor islets

ADVANCED SCIENCE NEWS
www.advancedsciencenews.com

ADVANCED HEALTHCARE MATERIALS
www.advhealthmat.de

upon exposure to hypoxia and NID1- or DCN-treatment. A functional response of the β-cells would demonstrate increased insulin secretion upon increased glucose challenge at 20 mM glucose concentration. Under normoxia, all three groups secreted significantly higher levels of insulin at 20 mM glucose compared to 2 mM glucose (**Figure 1** A, CTL: 0.056 ± 0.04 (2 mM) versus 0.111 ± 0.09 (20 mM), unpaired t-test, $^{****}p \leq 0.0001$; NID1: 0.062 ± 0.04 (2 mM) versus 0.106 ± 0.08 (20 mM), unpaired t-test, $^{****}p \leq 0.0001$; DCN: 0.064 ± 0.04 (2 mM) versus 0.10 ± 0.07 (20 mM), unpaired t-test, $^{***}p \leq 0.001$). Furthermore, there was a significant influence of the glucose concentration on the insulin secretion; however, no significant differences were identified between the treatment groups (Figure S6A, Supporting Information). All protein treatment groups showed a functional GSIS index of above 1 (Figure 1B), where the GSIS index of DCN-treated donor islets was significantly lower compared to NID1-treated donor islets (CTL: 2.00 ± 0.55, NID1: 1.70 ± 0.60, DCN: 1.49 ± 0.62; unpaired t-test, $^{*}p \leq 0.05$, $^{**}p \leq 0.01$, $^{****}p \leq 0.0001$). The responsiveness of each donor is depicted in Figure 1E. The glucose responsiveness of the donors was categorized in two different groups: unresponsive (GSIS index ≤ 1) and responsive (GSIS index above 1) (Figure 1G). In normoxia, 75% of CTL donors' islets showed functionality, while 83% of NID1- and DCN-treated donors' islets were functional.

Under hypoxic conditions, the CTL group did not show any glucose-responsive insulin secretion, while both NID1- and DCN-treated donor islets showed significantly higher insulin secretion upon glucose stimulation (Figure 1C, CTL: 0.15 ± 0.17 (2 mM) versus 0.09 ± 0.07 (20 mM), unpaired t-test, $^{**}p \leq 0.01$; NID1: 0.08 ± 0.06 (2 mM) versus 0.12 ± 0.12 (20 mM), unpaired t-test, $^{****}p \leq 0.0001$; DCN: 0.08 ± 0.06 (2 mM) versus 0.13 ± 0.11 (20 mM), unpaired t-test, $^{****}p \leq 0.001$). Consequently, the GSIS index of the CTL group is below 1 and is significantly lower compared to both NID-1 and DCN-treated donor islets (Figure 1D, CTL: 0.57 ± 2.45, NID1: 1.64 ± 0.77, DCN: 1.74 ± 0.68; unpaired t-test, $^{***}p \leq 0.001$, $^{****}p \leq 0.0001$). Glucose-response under hypoxic conditions for each donor is depicted in Figure 1F. Categorization of responsiveness under hypoxic conditions showed that in the CTL group, only 45% of the donors' islets showed functionality. In contrast, 92% of NID1-treated donors' islets and 100% of DCN-treated donors' islets were functional in hypoxic conditions (Figure 1H). Under hypoxic conditions, there were no significant differences in insulin secretion between the treatment groups (Figure S6B, Supporting Information).

GSGS assays were performed to determine the functionality of the α-cells within the donor islets upon exposure to hypoxia and NID1- or DCN-treatment. A functional α-cell would respond with decreased glucagon secretion upon increased glucose challenge at 20 mM glucose concentration. No significant differences were observed between low and high glucose concentrations within the CTL and protein-treated donor islets in normoxia, while also neither the glucose concentration nor protein supplementation had a significant impact on the glucagon secretion (Figure S7A,B, Supporting Information). A GSGS index below 1 indicates a functional α-cell response. Interestingly, both NID1- and DCN-treated donor islets were responsive compared to the CTL; however, there were no significant differences between the groups (Figure S7C, Supporting Information). In hypoxia, neither glucose concentration nor treatment conditions showed significant impact on glucagon secretion (Figure S7D,E, Supporting Information); however, NID1-treated samples, had a significantly higher GSGS index compared to CTL and DCN-treated samples (Figure S7F, Supporting Information).

2.3. ECM Protein Treatment Reduces DNA Fragmentation in Hypoxic Conditions

The effect of the ECM proteins on donor islet viability was assessed using analysis of DNA fragmentation through TUNEL staining, and apoptotic pathway activation through cleaved caspase-3 staining. Under normoxic conditions, there were no significant differences in TUNEL$^+$ cells between CTL and NID1- or DCN-treated groups (**Figure 2**A). Hypoxic conditions significantly increased the number of TUNEL$^+$ cells compared to normoxia; however, in hypoxia, NID1- and DCN-treated donor islets had significantly reduced TUNEL$^+$ cells compared to the hypoxic CTL donor islets (Figure 2B, normoxia CTL: 4.22% ±2.48, normoxia NID1: 7.23% ± 0.18, normoxia DCN: 7.25% ±0.81 versus hypoxia CTL: 27.6% ± 7.00, hypoxia NID1: 13.4% ± 3.31, hypoxia DCN: 18.5% ± 6.15; 2-way ANOVA, $^{**}p \leq 0.01$, $^{****}p \leq 0.0001$). IF staining for the analysis of apoptosis pathways[48] showed no significant impact of hypoxia or ECM protein treatment on the expression patterns of cleaved caspase-3 (Figure 2C,D, 2-way ANOVA) or p21 (Figure S8, Supporting Information).

2.4. FLIM Indicates ECM Protein Treatment of Human Donor Islets Shifts Metabolic Activity toward Glycolysis in Hypoxia

Donor islets showed a significant decrease in DNA fragmentation in hypoxic conditions after protein treatment; however, this difference is not sufficient to fully explain the restored functionality of ECM protein-treated donor islets compared to the CTL. We performed FLIM to investigate the metabolic activity of CTL and protein-treated donor islets under normoxic and hypoxic conditions (**Figure 3**; Figures S9 and S10, Supporting Information). Prior to the analysis of NADH and FAD, we established a macro to objectively remove lipofuscin signal from our images (Figure 3A,B), as suggested by Azzarello, F., et al. (2022),[49] which significantly decreased the χ^2 value toward a more reliable fitting (Figure 3C, before lipofuscin removal: 1.24 ± 0.11 versus after lipofuscin removal: 1.19 ± 0.07; unpaired *t*-test, $^{****}p \leq 0.0001$). FLIM analysis of NADH demonstrated that the percentage of unbound NADH was influenced by both oxygen conditions, and ECM protein treatment. The contribution of unbound NADH was significantly increased in hypoxia, particularly by NID1- and DCN-treatment, compared to the normoxic conditions or the CTL donor islets (Figure 3D), indicative of increased glycolysis. Interestingly, NID1-treated donor islets had significantly reduced contribution of bound FAD compared to the CTL or DCN-treated donor islets (Figure 3E). NID1-treated donor islets had reduced bound FAD compared to the CTL or DCN-treated donor islets (Figure S9K, Supporting Information), while there were no differences observed in hypoxia (Figure S9L, Supporting Information). Both NID1- and DCN-treatment had an overall significantly greater optical redox ratios compared to the CTL donor islets independent of

ADVANCED SCIENCE NEWS
www.advancedsciencenews.com

ADVANCED HEALTHCARE MATERIALS
www.advhealthmat.de

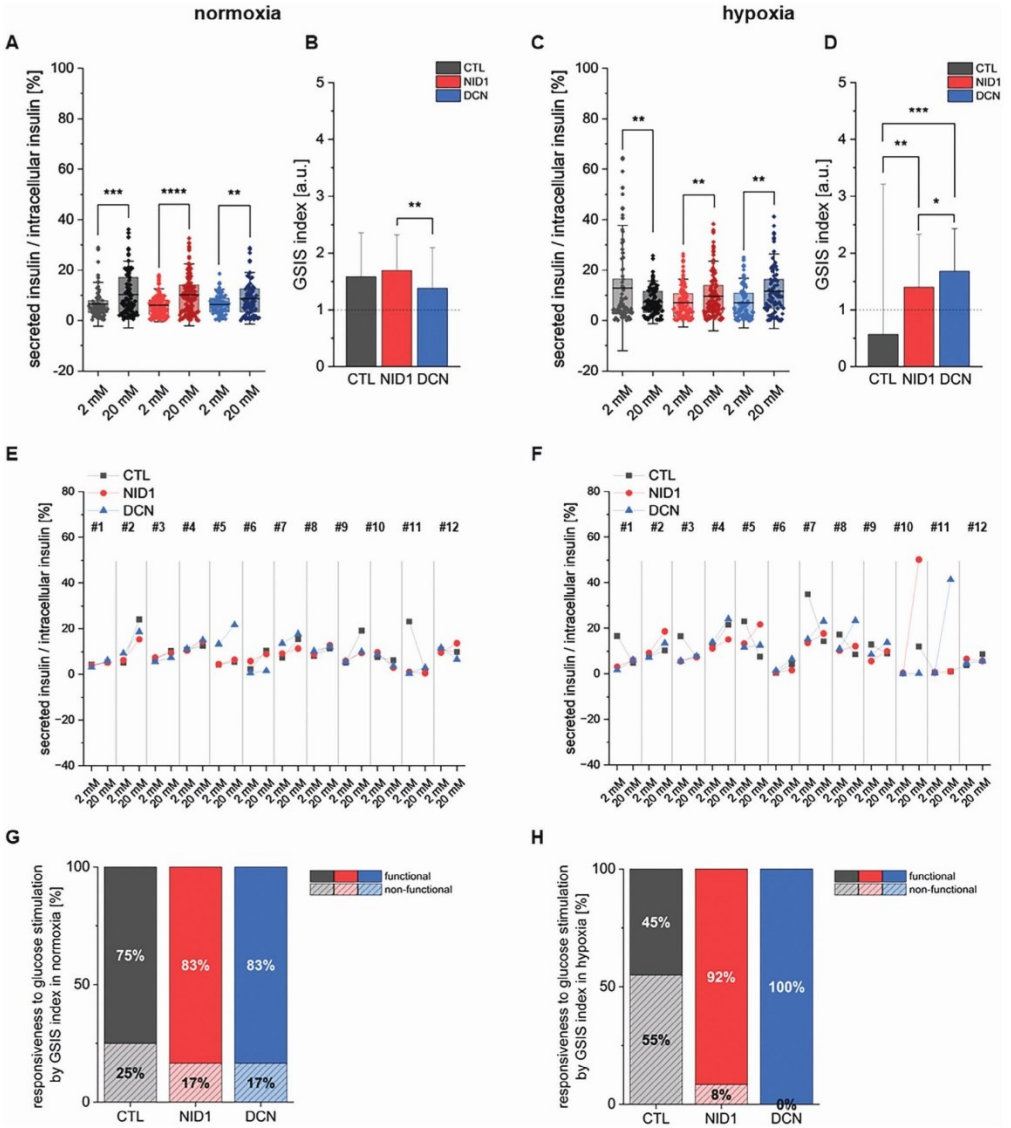

Figure 1. ECM protein treatment improves donor islet functionality in hypoxic conditions. Glucose-stimulated insulin secretion (GSIS) assay results of donor islets treated with either DPBS as control (CTL), NID1, or DCN in A) normoxic and D) hypoxic conditions. Insulin secretion normalized by insulin content of the donor islets. Unpaired *t*-test (N = 12, n ≥ 76), $^{**}p \leq 0.01$, $^{***}p \leq 0.001$, $^{****}p \leq 0.0001$. GSIS index as determined by the fold change in insulin secretion between the 2 and 20 mM glucose challenges in C) normoxic and E) hypoxic conditions. Unpaired *t*-test (N = 12, n ≥ 76), $^{*}p \leq 0.05$, $^{**}p \leq 0.01$, $^{***}p \leq 0.001$. GSIS assay results represented per donor in E) normoxic and F) hypoxic conditions. Percentage of donors showing functional GSIS responses in G) normoxic and H) hypoxic conditions. A GSIS index ≤ 1 is considered unresponsive and dysfunctional, a GSIS index >1 is considered responsive and functional.

ADVANCED SCIENCE NEWS
www.advancedsciencenews.com

ADVANCED HEALTHCARE MATERIALS
www.advhealthmat.de

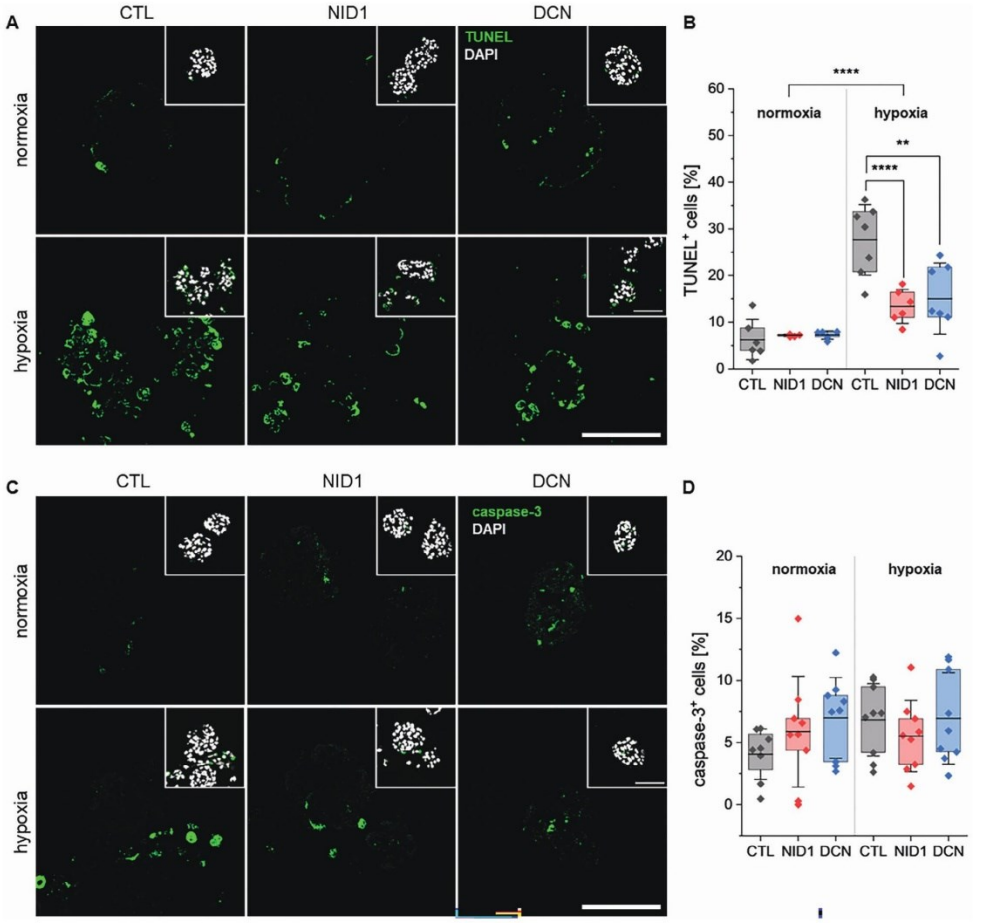

Figure 2. ECM protein treatment reduces DNA fragmentation events in hypoxic conditions. A) Representative images and B) quantification of TUNEL$^+$ cells to identify DNA fragmentation in donor islets under normoxic and hypoxic conditions. 2-way ANOVA (N ≥ 5), ** $p \leq 0.01$, **** $p \leq 0.0001$. C) Representative images and D) quantification of caspase-3$^+$ cells to identify cells undergoing apoptosis in donor islets under normoxic and hypoxic. 2-way ANOVA (N ≥ 6). Scale bars equal 50 µm.

glucose and oxygen concentrations (Figure 3F) suggestive of increased oxidative phosphorylation. Interestingly, while these metabolic parameters were impacted by oxygen conditions and / or the protein-treatments, glucose concentrations did not have a general effect on the donor islets' metabolism (Figure 3D–F; Figure S10, Supporting Information).

2.5. NGS Results Suggest a Pro-Survival and Functional Effect of NID1- and DCN-treatment upon Hypoxic Conditions

NGS of islets from four donors was performed to determine how treatment with NID1- or DCN- supports β-cell functionality under hypoxic conditions. Upon supplementation with the ECM proteins in hypoxic conditions, we observed a rescue/restoration of cell survival and function to levels similar to the normoxic control. To determine how the proteins influenced cell behavior under hypoxic conditions, we assessed significantly differentially expressed genes in pairwise comparisons between the normoxic control and each of our conditions. As there were no significant differences in cell behavior between the protein treatments, we then focused on the differentially expressed genes observed in both NID1 and DCN treatments in hypoxia. Further, as these positive effects on cell survival and function were only observed under hypoxia, we excluded genes influenced by the protein treatments under normoxia. The presented data is significantly

ADVANCED SCIENCE NEWS
www.advancedsciencenews.com

ADVANCED HEALTHCARE MATERIALS
www.advhealthmat.de

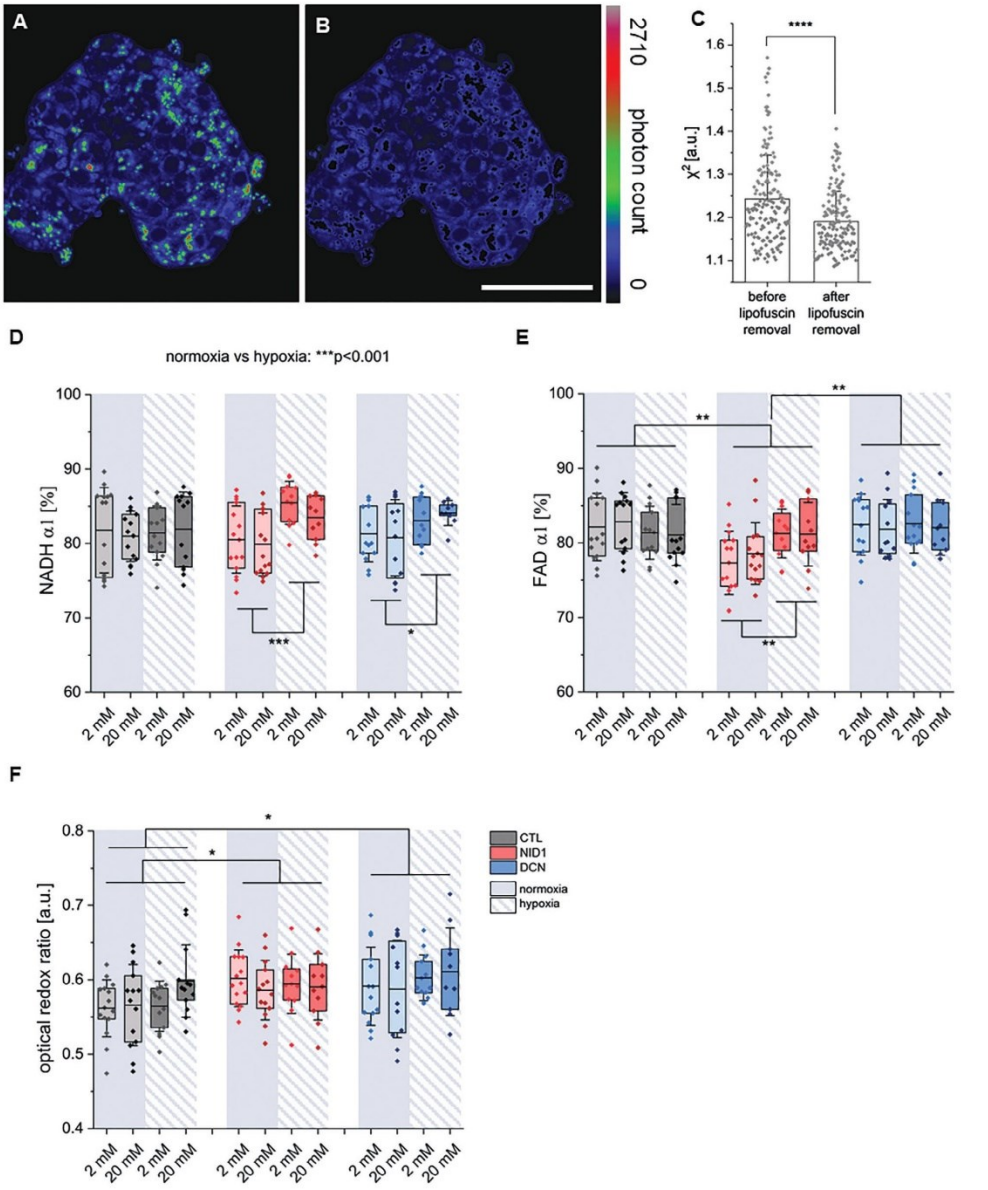

Figure 3. FLIM results before and after lipofuscin removal of NADH component during low and high glucose incubation of normoxic and hypoxic donor islets. NADH readout A) before and B) after quartile outlier removal. Scale bar equals 50 µm. C) Lipofuscin outlier removal significanlty decreases χ^2 fitting value. Unpaired t-test (N = 3, n ≥ 155), $^{****}p < 0.0001$. FLIM image analysis of D) NADH α1, E) FAD α1, and F) the optical redox ratio based on endogenous photon count of FAD / FAD+NADH in normoxia and hypoxia. Error bars represent standard deviation. Statistical significance above graphs: 3-way ANOVA (N = 3, n ≥ 10), $^{*}p \leq 0.05$, $^{**}p \leq 0.01$. Statistical significance below graphs: 2-way ANOVA (N = 3, n ≥ 10), $^{*}p \leq 0.05$, $^{**}p \leq 0.01$, $^{***}p \leq 0.001$.

ADVANCED SCIENCE NEWS
www.advancedsciencenews.com

ADVANCED HEALTHCARE MATERIALS
www.advhealthmat.de

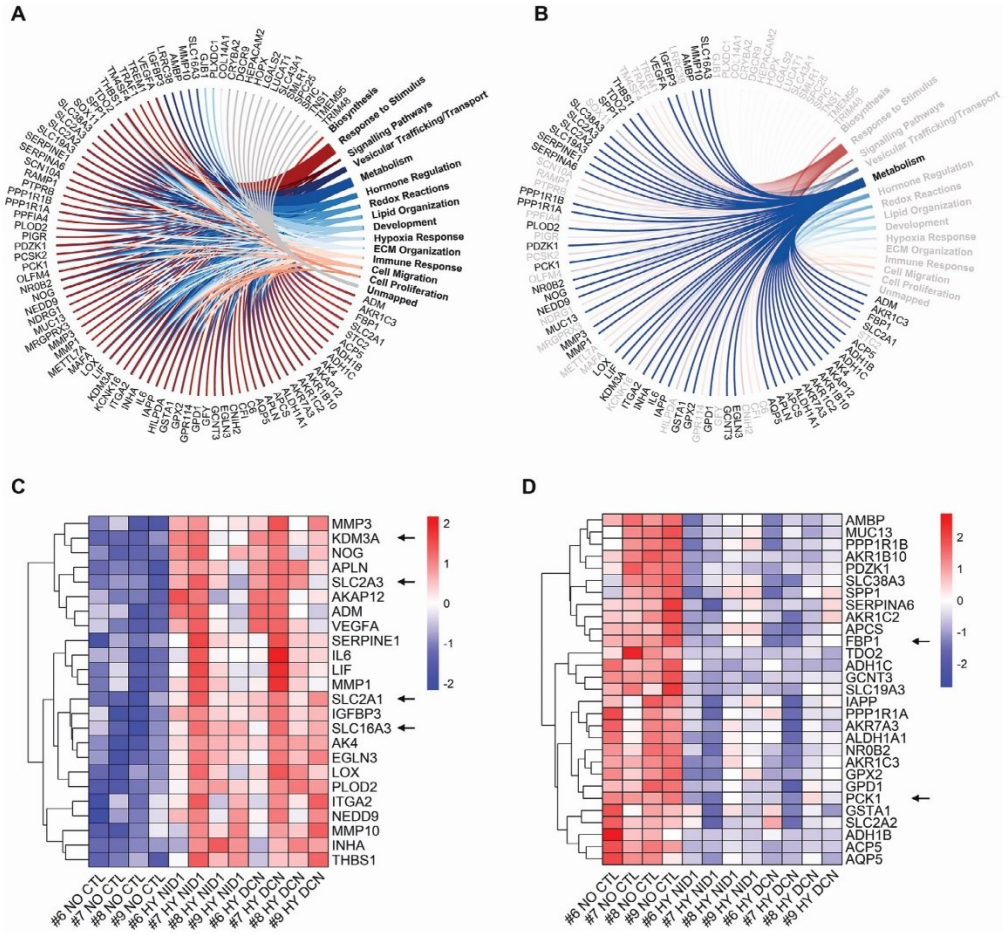

Figure 4. Next-generation sequencing (NGS) identifies significant upregulation of genes involved in metabolic pathways upon protein treatment under hypoxic conditions. Differentially expressed genes of donor islets treated with the ECM proteins in hypoxia were compared to the normoxic control. A) 93 protein-coding genes differentially expressed only in the NID1- and DCN-treated hypoxic donor islets compared to normoxia were identified. B) GO term enrichment analysis mapped 53 of these genes to metabolic pathways, C) 24 of which were upregulated and D) 29 of which were downregulated. All genes are considered as significantly differentially expressed with a $p_{adjusted} \leq 0.05$.

differentially expressed genes only found in the ECM protein-treated donor islets under hypoxia compared to the normoxic control. 93 protein-coding genes were identified, 80 of which were mapped using GO enrichment analysis (**Figure 4A**). To determine how β-cell functionality was maintained in the hypoxic islets upon protein supplementation, differentially expressed genes mapped to the GO term metabolism were further investigated (Figure 4B). Of particular interest was the significant upregulation of solute carrier family 2 members 1 and 3 (*SLC2A1* and *SLC2A3*, respectively), solute carrier family 16 member 3 (*SLC16A3*), and lysine demethylase 3A (*KDM3A*) (Figure 4C, marked with arrows), as well as the significant downregulation of gluconeogenic enzymes fructose-1,6-bisphosphatase 1 (*FBP1*) and phosphoenolpyruvate carboxykinase 1 (*PCK1*) (Figure 4D, marked with arrows). *SLC2A1*, *SLC2A3*, and *SLC16A3* encode glucose transporters 1 (GLUT1), GLUT3, and monocarboxylate transporter 4 (MCT4), respectively. These transporters are involved in the transport of glucose and the glycolysis product pyruvate/lactate into and out of the cell. Interestingly, FBP1 and PCK1 are rate-limiting enzymes key for gluconeogenic events

ADVANCED SCIENCE NEWS
www.advancedsciencenews.com

ADVANCED HEALTHCARE MATERIALS
www.advhealthmat.de

within cells at the reversible steps of glycolysis. These genes play key roles in the regulation of maintaining cellular homeostasis through modulation of glycolysis/gluconeogenesis and cell cycle progression.

3. Discussion

Islet transplantation is a promising therapy for patients suffering from type one diabetes mellitus; however, its success is limited by poor transplant survival. The hypoxic environment post-transplantation and the host's foreign body response create unfavorable conditions for the transplanted islets. This is exacerbated by the loss of native ECM and supportive cells during the pre-operative islet isolation procedure that deprives them of essential signaling cues for survival and function. Much research is done on supporting islet survival and β-cell function through co-transplantation of or encapsulation with ECM proteins. To restore the islet's ECM, we focused on proteins involved in the stabilization of the ECM that also have been shown to support β-cells.[44,45] Here, we demonstrated that NID1 and DCN are capable of restoring β-cell function in isolated human donor islets following exposure to hypoxia. Furthermore, the protein treatments significantly reduced DNA fragmentation events upon hypoxic culture, improving islet viability, increasing glycolysis, and improving overall β-cell functionality to levels comparable to the normoxic control islets.

Under hypoxic conditions, donor islets displayed dysfunctional β-cells and increased DNA fragmentation events which were restored upon NID1- or DCN-treatment. Low oxygen conditions have been shown to induce DNA fragmentation to activate cell apoptotic machinery,[50–52] and inhibiting DNA repair mechanisms.[53] Hypoxia resulted in the reduction of transcription and/or translation of key factors in multiple DNA repair mechanisms including homology-directed repair,[54] non-homologous end joining,[55–57] and mismatch repair.[58–60] Interestingly, many of these inhibitions are mediated through microRNA-155.[53,61–65] Hypoxia-induced cell death is often regulated through the activation of caspase-3 pathways;[66,67] however, our results did not show any significant changes in the caspase-3 expression between our treatment groups. The NID1- and DCN-mediated reduction in DNA fragmentation suggests these proteins promote DNA repair and cell survival mechanisms. It has been shown that NID1 expression can induce p21[44] or p53 activity,[68] known activators of cell-cycle arrest to allow for DNA-repair,[69–71] which could explain the downregulation of DNA fragmentation observed. Interestingly, DCN-treatment also influences the expression of proteins involved in the regulating cell cycle progression including p21,[72] p53,[73] and p27,[74] through which DCN could have supported DNA repair resulting in reduced DNA fragmentation. As differences in p21 expression were not observed in this study, the effects of NID1- and DCN-treatment on DNA fragmentation could be mediated via other cell cycle regulators. Interestingly, NGS analysis identified *KDM3A* to be upregulated in the protein-treated donor islets only under hypoxic conditions. KDM3A is known to regulate cell cycle progression with key roles in DNA repair and preventing apoptosis.[75] Further, it has been shown that KDM3A supports cell survival of myeloma cells in hypoxic environments through promoting glycolysis.[76] This suggests that NID1 and DCN treatments upregulate KDM3A, supporting survival and function in the donor islets under hypoxic conditions.

FLIM analysis of the donor islet metabolism indicated NID1- and DCN-treatment increased the presence of unbound NADH upon hypoxic conditions. The increased unbound NADH is suggestive of increased glycolysis similar to the Warburg effect observed in cancer cells.[77] It has been shown that cancer cells increase their glycolytic activity to meet high-energy demands. This switch to increased glycolytic activity can be induced by hypoxia-inducible factor-1a (HIF1a) to accommodate for the decreased oxygen-dependent mitochondrial oxidative phosphorylation in hypoxic environments.[78,79] Through increasing the glycolytic activity in hypoxia, NID1- and DCN-treatment aid in meeting the donor islets' energy requirements and functionality, particularly for secreting insulin in response to glucose. There was also an overall increase in the optical redox ratio upon protein treatment, suggesting a general shift in metabolic activity toward oxidative phosphorylation. This is in line with our previous work with the human β-cell line that also identified increased oxidative phosphorylation activity upon DCN-treatment in normoxic conditions.[45] Interestingly, this upregulation of oxidative phosphorylation appears to be mediated through different genetic pathways as different genes related to oxidative phosphorylation were identified in the previous study. We were unable to discriminate metabolic differences upon glucose stimulation in contrast to previous work using the human β-cell line[80] which could be attributed to the heterogeneity of the cell types in the donor islets. There could have been contradictory signals arising from the β-cells and α-cells in response to glucose that could not be separated using our FLIM analysis. Wang, Z., et al. (2021)[81] and Azzarello, F., et al. (2022)[49] were able to demonstrate different metabolic profiles between α- and β-cells in islets and successfully distinguish between each cell type using immunofluorescence staining following the measurement. Future FLIM measurements with corresponding cell composition analysis of the islets post-measurement would be beneficial to determine changes in the metabolic activity of the cells.

NGS identified significant differentially expressed genes upon NID1- and DCN-treatment in hypoxia that support the metabolic functionality and viability results observed. Of particular interest for β-cell function was the downregulation of genes *FBP1* and *PCK1* encoding gluconeogenic enzymes. *FBP1* encodes a rate-limiting gluconeogenic enzyme that dephosphorylates fructose-1,6-bisphosphate into fructose-1-phosphate.[82] During glycolysis, fructose-1,6-bisphosphate has been shown to support the biphasic insulin secretion of pancreatic β-cells,[83,84] highlighting the importance of maintaining/generating fructose-1,6-bisphosphate for glycolysis. Further, FBP1 inhibition in murine β-cells improved GSIS results with increased insulin secretion upon glucose stimulation,[85] while its overexpression reduced both cell proliferation and insulin secretion.[86] PCK1 is a tightly regulated enzyme responsible for the reversible conversion of the Krebs Cycle intermediate product oxaloacetate into phosphoenolpyruvate and carbon dioxide in the cytoplasm.[87] PCK1 activity has been shown to be a rate-limiting step in energy-consuming gluconeogenic, glyceroneogenic, and glyconeogenic pathways.[87,88] In hepatic cancers, PCK1 overexpression supported the production of glucose through gluconeogenesis,

suppressing glycolysis.[89–91] In our donor islets, both NID1- and DCN-treatment downregulated the expression of *FBP1* and *PCK1* in hypoxic conditions, potentially as an energy-saving mechanism to maintain their ATP levels and support glycolysis to ensure insulin secretion. There was also increased expression of genes encoding GLUT1 and GLUT3. They are well-studied glucose transporters in β-cells for their role in β-cell maturation and glucose-responsive insulin secretion due to their high affinity for glucose compared to GLUT2.[92–94] Further, GLUT1 was identified as the prominent glucose transporter in human pancreatic islets, in contrast to rodent islets which predominantly use GLUT2,[92,95,96] as well as upregulated by HIF1a in stress conditions such as hypoxia to meet the increased energy demands.[97] *SLC2A1* and *SLC2A3* were upregulated in our hypoxic donor islets upon either NID1- or DCN-treatment, allowing for greater transport of glucose into the cells, increasing the glucose available to go through glycolysis and generate ATP. Furthermore, the upregulation of *SLC16A3*, encoding MCT4 for the transport of lactate and pyruvate, supports increased glycolytic activity through the removal of lactate and remaining pyruvate from the intracellular space in the absence of the Krebs cycle and oxidative phosphorylation.[98] The downregulation of *FBP1* and *PCK1*, and upregulation of *SLC2A1, SLC2A3, SLC16A3*, and *KDM3A* in the protein-treated donor islets under hypoxia further supports the shift toward glycolysis, functional GSIS, and reduced DNA fragmentation observed. β-cell function is known to be impaired upon stress conditions possibly as a trade-off between cell survival and cell function.[99] Together, these results demonstrate that in hypoxia, NID1 and DCN-treatment of donor islets influence cell cycle regulators to support DNA repair mechanisms while also promoting glycolytic activity at multiple steps in the pathway promoting both β-cell viability and functionality.

Together, these results demonstrate the potential of NID1- and/or DCN-treatment on supporting donor islet survival and function in a post-transplantation setting; however, donor variability and differences in islet preparation/shipment durations may influence the outcomes. Donor islets were cultured post-isolation for ≈ 17 to 78 h, while shipping time ranged from 48 h to 120 h (Table S3, Supporting Information), though there were no significant differences in durations between the donors. It must be noted that the 25% of donors (Donors #10-12) that did not demonstrate glucose-responsive insulin secretory function in the normoxic control did not have extended pre-shipment culture or shipment times. Furthermore, necrotic core formation was not observed in the donor islets upon arrival, which was also supported by the lack of TUNEL+ cells under normoxic conditions compared to hypoxic conditions. To improve the effectiveness of the NID1- and DCN-treatments, future studies will work on optimizing the timing of the ECM protein treatment as well as elucidating protein-binding partners. Previous work has demonstrated that NID1 supports donor islet viability in hypoxia, allowing for increased yield and therefore, availability of donor islets for transplantation.[2] Future work identifying the timepoint in donor islet isolation and/or transplantation in which the NID1- and DCN-treatments best support donor islet survival could be beneficial in improving the availability of donor islets and their survival for transplantation purposes. Further elucidation of the exact mechanism of action through protein-binding studies would be valuable in understanding how NID1 and DCN, proteins well-known for ECM-binding and regulation, directly interact with cells of the islets of Langerhans. Further, in vivo experiments will allow for validation of the NID1 and DCN supporting donor islets in a post-transplantation setting, while also allowing for the study of their ECM-regulating capabilities and how they can influence fibrotic capsule formation, improving transplant survival.

4. Conclusion

In summary, the results presented in our study showed that NID1 and DCN support the functionality and survival of cells in donor islets under hypoxic conditions, rescuing glucose responsiveness compared to control islets. DNA fragmentation analysis revealed that both ECM proteins significantly reduce hypoxia-induced fragmentation. FLIM analysis suggests that the protein supplementation increases glycolytic activity in hypoxic conditions within the donor islets. Further, NGS analysis identified that the ECM protein treatment of donor islets in hypoxia regulates cell cycle and glycolysis progression at multiple checkpoints to support cell survival and β-cell function. Taken together, this study demonstrates that NID1 and DCN are strong candidates to be used during the transplantation of donor islets or the implantation of stem cell-derived insulin-producing cells to support the functionality and survival of the cells in a hypoxic post-transplantation environment. The use of NID1 or DCN could allow for increased efficacy and success of cell therapies for the treatment of type one diabetes mellitus.

5. Experimental Section

Human Donor Islet Culture: Human islets from non-diabetic donors were purchased from the MacDonald Laboratory (Alberta, Canada). The human islets were shipped in CMRL1066 supplemented with 0.05% BSA (Equitech Bio Inc., BAL62), 1X insulin-transferrin-selenium (Corning, 25800CR), 2X GlutaMAX (Gibco, 35050061) and 0.5% Pen/Strep (Lonza, 09–757F), and packaged at a maximum concentration of 40 000 IEQ per 50 mL aliquot in a sealed falcon tube. Tubes were packaged laying on the side to prevent pellet formation at the bottom. A temperature sensor was included, which is triggered upon high (above 37 °C) or low (below 2 °C) temperature exposure. Following arrival, donor islets of similar size were handpicked into individual wells of 96-well U-bottom non-adherent well plates (Greiner Bio-One, 650101) to be used for glucose-stimulated insulin secretion (GSIS) and glucose-stimulated glucagon secretion (GSGS) assays. Donor islets to be used for histological analyses and RNA isolation were cultured in 12-well tissue culture-treated plates. Donor islets were cultured in the recommended culture medium: CMRL1066 without Glutamine (Gibco, 21530-027), 0.5% FAF-BSA (Sigma Aldrich, A9576), 1 g L^{-1} glucose (Gibco, A24940-01), 4 mM Glutamax (Gibco, 35050–061), 1% Pen/Strep (Gibco, 15070-063), and 100 µg mL^{-1} Normocin (InvivoGen, ant-nr-1). The medium was exchanged the next day and supplemented with recombinantly-produced NID1[44] at 30 µg mL^{-1}, or recombinantly-produced DCN[100] at 50 µg mL^{-1}. As DPBS was used to solubilize the ECM proteins, DPBS alone was used as the control (CTL). The islets were cultured for 72 hours (h) either under normoxic conditions with 20% oxygen levels or hypoxic conditions with 1% oxygen levels.

Recombinant NID1 Production: NID1 production was optimized from the previous publication[44] using the EXPI293 Expression System (Thermo Fisher Scientific, A14524) in the second batch. For transient transfection of the cells, an expression plasmid was generated based on pcDNA3.4, which contains the cDNA of NID1 (UniProtKB P14543) extended by a coding sequence for a C-terminal His-tag. Cells were

ADVANCED SCIENCE NEWS
www.advancedsciencenews.com

ADVANCED HEALTHCARE MATERIALS
www.advhealthmat.de

cultivated and transfected according to manufacturer´s instructions. Following seven days of expression, expressed NID1 with molecular weight of 134 kDa was purified from the cell-free culture supernatant on an ÄKTA protein purification system by immobilized metal affinity chromatography followed by size exclusion chromatography using a Superdex 200 matrix. The protein solution was concentrated using centrifuge filter units with 30K MWCO. Protein integrity was confirmed via standard SDS-PAGE followed by Coomassie staining (Figure S1A, Supporting Information). The functional effects of the two batches of NID1 on the human donor islets was confirmed to be similar before proceeding with the second batch of NID1 for the experiments (Figure S1B, Supporting Information).

Sample Preparation for Histological Analysis: At the end of the 72 h culture period, donor islets were prepared for histological analysis as previously described.[6] Briefly, donor islets were fixed in 4% paraformaldehyde for 1 h at room temperature (RT), and then embedded in paraffin with a Shandon Citadel 1000 (Thermo Fisher Scientific) according to the manufacturer's protocol. Donor islets were sectioned as 3 µm sections (Leica, Microtom RM2145), deparaffinized with xylene and graded ethanol (96%-50%) and VE-water.

Immunofluorescence (IF) Staining: Antigen retrieval was performed for sections using both TRIS-EDTA (pH 9.0) and citrate (pH 6.0) buffers. The slides were permeabilized for 20 min at RT and blocked with goat serum for 30 min at RT. They were then incubated with the primary antibodies overnight at 4 °C. The antibodies used can be found in Table S1 (Supporting Information). Following secondary antibody staining, the sections were also incubated with 2 µg ml^{-1} 4′,6-Daimidin-2-phenylindol solution (DAPI) solution for 10 min at RT, and then mounted with Prolong Gold Antifade Mountant (Thermo Fisher Scientific, P36930). Images were obtained using a laser scanning microscope (LSM) 880 (Carl Zeiss GmbH). Semi-quantitative analysis using the integrated density of immunofluorescence (IF) stained sections was performed using ImageJ's FIJI. The obtained integrated density of each channel, subtracted by the negative control, was normalized by the DAPI count. For DNA fragmentation analysis, dUTP nick-end labeling (TUNEL) staining (Thermo Fisher Scientific, C10245) was performed on deparaffinized sections as described earlier[101] according to the manufacturer's protocol. TUNEL$^+$ cell count was normalized by the DAPI count.

Functionality Assays: Glucose-stimulated insulin secretion (GSIS) and glucose-stimulated glucagon secretion (GSGS) assays were performed as earlier described.[101,102] Briefly, donor islets were incubated for one hour in β-Krebs buffer (see Table S2, Supporting Information for recipe) with 2 mM glucose. Donor islets were then challenged in either β-Krebs buffer with 2 mM (low) glucose or β-Krebs buffer with 20 mM (high) glucose for another hour. At the end of the incubation, the supernatant was collected and stored at -20 °C for further analysis. The donor islets were then lysed with acid ethanol overnight at 4 °C, collected, and stored at −20 °C for further analysis. The levels of insulin and glucagon secreted by the donor islets as well as the insulin and glucagon contents within the donor islets were analyzed using an ultrasensitive human insulin ELISA kit (Mercodia, 10-1132-01) and glucagon ELISA kit (Mercodia, 100-1271-01). The GSIS index or GSGS was calculated by dividing each samples' insulin or glucagon secretion during 20 mM glucose by 2 mM glucose.

Fluorescence Lifetime Imaging Microscopy (FLIM) and Image Analysis: Donor islets were measured using fluorescence lifetime imaging microscopy (FLIM) during the glucose challenge hour of the GSIS as previously described.[80] Briefly, a Zeiss LSM 880 (Carl Zeiss GmbH) coupled with a Ti:Sapphire femtosecond laser (MaiTai HP Spectra Physics) and a two-channel NDD BIG2.0 GaAsP PMT detector (Becker & Hickl GmbH) was used to obtain TCSPC-based fluorescence decay measurements. The autofluorescence of nicotinamide adenine dinucleotide (NADH) and flavin adenine dinucleotide (FAD) was induced using two-photon excitation with a wavelength of 700 nm at 5% laser power. The NADH emission light was filtered between 450–490 nm and FAD was filtered between 500–550 nm, and images were acquired at a resolution of 512 × 512 pixels with an acquisition time of 161 seconds. For image acquisition, donor islets were transferred into 15-well 3D µ-Slides (ibidi, 81506) and maintained at 37 °C using a stage top heating system (ibidi, 12110) during the measurements.

FLIM image analysis was performed using SPCImage (Becker & Hickl GmbH) to perform biexponential decay fittings. A threshold of 30% of maximum photon counts was used to remove the background. ASCII images for α, τ, and χ^2 were exported for further analysis. Donor islets' images present bright spots that could be attributed to lipofuscin accumulation with age.[103] To remove the effects of the lipofuscin on the fitting model, an automatic algorithm was employed via an Excel macro to set an upper threshold using the formula below to remove the outliers as previously described (see Equation (1)).[49] Briefly, the calculated threshold, where Q represents the quartile, was used to create a binary mask that was applied on the FLIM image to (1)(1)remove the lipofuscin signal defined as outliers, which also improved the mean χ^2 value.

$$Threshold = Q3 + 1.5 * (Q3 - Q1) \quad (1)$$

The optical redox ratio based on endogenous FAD and NADH expression was calculated as previously described (see Equation (2)).[80]

$$Optical\ Redox\ Ratio = \frac{FAD}{FAD + NADH} \quad (2)$$

RNA Isolation and Next-Generation Sequencing (NGS): Following the 72 h incubation in either normoxic or hypoxic conditions, RNA isolation was performed using the RNEasy Micro kit protocol (Qiagen, 74004). Briefly, donor islets were lysed in RPE buffer containing 1% β-mercaptoethanol (Sigma-Aldrich, M7522), and treated with 70% ethanol. Samples were vacuum filtered, and then washed with RW1, twice with RPE, and twice with 80% ethanol with vacuum filtration steps in between each wash. The samples were incubated in the filter Eppendorf tubes with 15 µl RNAse-free water for 5 min before being centrifuged for 3 min at 1000xg to elute the RNA. RNase-free DNase I treatment was done for half hour at 37 °C and then stopped at 65 °C for ten minutes (Promega, M6101). The RNA was stored at −80 °C until NGS was performed.

The concentration of RNA was measured using the Qubit Fluorometric Quantitation and RNA Broad-Range Assay (Thermo Fisher Scientific). RNA integrity number was determined using the Fragment Analyzer 5300 and the Fragment Analyzer RNA kit (Agilent Technologies) and presented a good integrity value of greater than eight. For library preparation, the mRNA fraction was enriched using polyA capture from 30 to 100 ng of total RNA using the NEBNext Poly(A) mRNA Magnetic Isolation Module (NEB). Subsequently, libraries were prepared using the NEB Next Ultra II Directional RNA Library Prep Kit for Illumina and NEBNext UDI UMI (NEB) following the manufacturer's instructions. To minimize technical batch effects, library preparations were performed using the liquid handler Biomek i7 (Beckman). The library molarity was determined by measuring the library size (≈300 bp) using the Fragment Analyzer 5300 and the Fragment Analyzer DNA HS NGS fragment kit (Agilent Technologies) and the library concentration using Qubit Fluorometric Quantitation and dsDNA High sensitivity assay (Thermo Fisher Scientific). The libraries were denaturated according to the manufacturer's instructions, diluted to 210 pM, and sequenced as paired-end 100 bp reads on an Illumina NovaSeq 6000 (Illumina). The sequencing aimed to achieve a depth of ≈ >25 million clusters per sample.

Quality control, read mapping and counting was performed using the Nextflow-based nf-core/rnaseq (version 1.4.2) pipeline (https://nf-co.re/rnaseq).[104] As part of this workflow, quality control assessment of the RNA-seq data was conducted with FASTQC[105] and RSeQC (version 3.0.1),[106] respectively. The mapping of reads to the human reference genome GRCh37 was performed using the STAR (version 2.6.1d) aligner.[107] Raw gene expression was quantified with featureCounts (version 1.6.4).[108] Differential expression and pathway analysis were performed with the nextflow-based rnadeseq (version 2.2) pipeline (https://github.com/qbic-pipelines/rnadeseq), which integrates the R package DESeq2 (version 1.34.0)[109] for DE analysis and gprofiler2 (version 0.2.1) for KEGG and reactome pathway enrichment analysis, used in the R language (version 4.1.2). Genes were considered differentially expressed if p-adjusted value ≤0.05. As part of this pipeline, DEG lists were obtained from simple pairwise comparisons extracted from a linear model using the

design formula: ~ batch + condition_oxygen_levels_and_treatment in DESeq2, in which the fixed effect condition oxygen levels and treatment is the experimental combined factor of treatment with the factor levels decorin treated and nidogen-1 treated and oxygen level with the factor levels Normoxia and Hypoxia and batch the patient condition, and together with their associated log2FC fed into gprofiler2 for pathway enrichment analysis. Final reports were produced using the R package rmarkdown (version 2.1) with the knitr (version 1.28) and DT (version 0.13) R packages. Gene Ontology (GO) term enrichment analysis was performed, and all differentially expressed genes were included, and enrichment was calculated using Fisher's exact test ($p \leq 0.05$). Genes were considered as differentially expressed when the p-adjusted value was ≤ 0.05, the log2FoldChange was $\leq$ -2.0 or $\geq$ 2.0 with a standard error $\leq$20% of the log2FoldChange, and a standard error $\leq$20% of the r_{log} values between donors within a condition. The heatmaps were generated using the r_{log} values of the gene counts and the R package pheatmap (version 1.0.12).[110]

Statistical Analysis: Origin (Version 2023b, OriginLab) was used to perform statistical analysis. Results throughout the manuscript are presented as mean ± standard deviation. All data sets have been tested for normality, and outliers have been detected and removed using Grubb's test with $p \leq 0.05$. Statistically significant difference was defined if $p \leq 0.05$. The performed tests with relevant significances are described in the results part and figure legends. All experiments were performed with donor islets from at least three donors (N) with at least three biological repeats per donor (n).

Supporting Information

Supporting Information is available from the Wiley Online Library or from the author.

Acknowledgements

Human islets for research were provided by the Alberta Diabetes Institute IsletCore at the University of Alberta in Edmonton (http://www.bcell.org/adi-isletcore.html) with the assistance of the Human Organ Procurement and Exchange (HOPE) program, Trillium Gift of Life Network (TGLN), and other Canadian organ procurement organizations. Islet isolation was approved by the Human Research Ethics Board at the University of Alberta (Pro00013094). All donors' families gave informed consent for the use of pancreatic tissue in research. The authors would like to acknowledge Janne Michael and Sven Poths for their assistance in organizing the RNA sequencing experiment, and Michaela Pogoda and Nicolas Casadei for providing technical guidance. The RNA sequencing and analysis. This work was financially supported by the European Union (H2020-NMP10-2014-645991-2, DRIVE; H2020-ITN 766181, DELIVER to G.P.D. and K.S.-L.), as well as the Ministry of Science, Research and the Arts of Baden-Württemberg (33-729.55-3/214 and SI-BW 01222–91 to K.S.-L.), the Wilhelm Schuler Stiftung (D30.31918 to K.S.-L. and M.U.) and the Deutsche Forschungsgemeinschaft (INST 2388/33-1 to K.S.-L). NGS sequencing methods were performed with the support of the DFG-funded NGS Competence Center Tübingen (INST 37/1049-1).

Open access funding enabled and organized by Projekt DEAL.

Conflict of Interest

The authors declare no conflict of interest.

Author Contributions

A.J., M.U., S.L.L., and K.S.-L. contributed equally to this work. A.J., M.U., S.L.L., and K.S-L. designed the experiments and wrote the manuscript. A.J., M.U., D.C-B., and T.B. performed experiments. A.J. and M.U. analyzed data. L.K. and S.C. performed the bioinformatics and statistical analysis. S.N. supervised the statistical and bioinformatics analysis. G.P.D. and S.Y.B. gave conceptual advice. P.D.K. produced the NID protein.

Data Availability Statement

The data that support the findings of this study are available on request from the corresponding author. The data are not publicly available due to privacy or ethical restrictions.

Keywords

decorin, diabetes mellitus, hypoxia, nidogen-1, transplantation, β-cells

Received: August 13, 2024
Revised: October 22, 2024
Published online:

[1] H. Komatsu, F. Kandeel, Y. Mullen, *Pancreas* **2018**, *47*, 533.
[2] D. Brandhorst, H. Brandhorst, S. L. Layland, S. Acreman, K. Schenke-Layland, P. R. V. Johnson, *Acta Biomater.* **2022**, *137*, 92.
[3] R. P. Robertson, I. B. Hirsch, J. E. Mulder, **2021**, 1767.
[4] A. Jeyagaran, C. en Lu, A. Zbinden, A. L. Birkenfeld, S. Y. Brucker, S. L. Layland, *Adv. Drug Delivery Rev.* **2022**, *189*, 114481.
[5] F. C. Wieland, C. A. van Blitterswijk, A. van Apeldoorn, V. L. S. LaPointe, *J. Immunol. Regen. Med.* **2021**, *13*, 100048.
[6] A. Zbinden, M. Urbanczyk, S. L. Layland, L. Becker, J. Marzi, M. Bosch, P. Loskill, G. P. Duffy, K. Schenke-Layland, *Tissue Eng., Part A* **2020**, *27*, 977.
[7] M. Perez-Basterrechea, M. M. Esteban, M. Alvarez-Viejo, T. Fontanil, S. Cal, M. Sanchez Pitiot, J. Otero, A. J. Obaya, *PLoS One* **2017**, *12*, e0180695.
[8] A. Gamble, R. Pawlick, A. R. Pepper, A. Bruni, A. Adesida, P. A. Senior, G. S. Korbutt, A. M. J. Shapiro, *PLoS One* **2018**, *13*, e0206449.
[9] N. Sakata, G. Yoshimatsu, S. Koadma, *OBM Trans.* **2020**, *4*, https://doi.org/10.21926/obm.transplant.2004127.
[10] M. Armanet, A. Wojtusciszyn, P. Morel, G. Parnaud, P. Rousselle, C. Sinigaglia, D. B. Thierry Berney, *FASEB J.* **2009**, *23*, 4046.
[11] I. Virtanen, M. Banerjee, J. Palgi, O. Korsgren, A. Lukinius, L.-E. Thornell, Y. Kikkawa, K. Sekiguchi, M. Hukkanen, Y. T. Konttinen, T. Otonkoski, *Diabetologia* **2008**, *51*, 1.
[12] A. M. Smink, P. de Vos, *Curr. Diab. Rep.* **2018**, *18*, 39.
[13] J. C. Stendahl, D. B. Kaufman, S. I. Stupp, *Cell Transplant.* **2009**, *18*, 1.
[14] S. E. Cross, R. H. Vaughan, A. J. Willcox, A. J. McBride, A. A. Abraham, B. Han, J. D. Johnson, E. Maillard, P. A. Bateman, R. D. Ramracheya, P. Rorsman, K. E. Kadler, M. J. Dunne, S. J. Hughes, P. R. V. Johnson, *Am. J. Transplant.* **2017**, *17*, 451.
[15] L. M. Weber, K. N. Hayda, K. S. Anseth, *Tissue Eng. – Part A* **2008**, *14*, 1959.
[16] G. G. M. Pinkse, W. P. Bouwman, R. Jiawan-lalai, O. T. Terpstra, J. A. Bruijn, E. De Heer, *Diabetes* **2006**, *55*, 312.
[17] M. Krishnamurthy, J. Li, M. Al-Masri, R. Wang, *J. Cell Commun. Signal.* **2008**, *2*, 67.
[18] L. M. Weber, K. N. Hayda, K. Haskins, K. S. Anseth, *Biomaterials* **2007**, *28*, 3004.
[19] L. Sakhneny, A. Epshtein, L. Landsman, *Sci. Rep.* **2021**, *11*, 2378.
[20] G. Parnaud, E. Hammar, D. G. Rouiller, M. Armanet, P. A. Halban, D. Bosco, *Diabetes* **2006**, *55*, 1413.
[21] F. S. Sarvestani, A.-M. Tamaddon, R. Yaghoobi, B. Geramizadeh, S. S. Abolmaali, M. Kaviani, S. Keshtkar, S. Pakbaz, N. Azarpira, *Cell Biochem. Funct.* **2023**, *41*, 296.
[22] C. Kuehn, E. A. Dubiel, G. Sabra, P. Vermette, *Acta Biomater.* **2012**, *8*, 619.
[23] R. D. Fernández-Montes, J. Blasi, J. Busquets, E. Montanya, M. Nacher, *Pancreas* **2011**, *40*, 1153.

[24] M. Barillaro, M. Schuurman, R. Wang, *Front. Cell Dev. Biol.* **2022**, *10*, 1.
[25] N. Nagata, Y. Gu, H. Hori, A. N. Balamurugan, M. Touma, Y. Kawakami, W. Wang, T. T. Baba, A. Satake, M. Nozawa, Y. Tabata, K. Inoue, *Cell Transplant.* **2001**, *10*, 447.
[26] L. M. Weber, K. S. Anseth, *Matrix Biol.* **2008**, *27*, 667.
[27] J. Liu, S. Liu, Y. Chen, X. Zhao, Y. Lu, J. Cheng, *Int. J. Nanomed.* **2015**, *10*, 3519.
[28] M. Sojoodi, A. Farrokhi, A. Moradmand, H. Baharvand, *Cell Biol. Int.* **2013**, *37*, 370.
[29] N. Davis, L. Beenken-Rothkopf, A. Mirsoian, N. Kojic, D. Kaplan, A. Barron, M. Fontaine, *Biomaterials* **2012**, *33*, 6691.
[30] V. Pal, Y. Wang, R. Regeenes, D. M. Kilkenny, J. V. Rocheleau, *Sci. Rep.* **2022**, *12*, 1.
[31] D. M. Salvay, C. B. Rives, X. Zhang, F. Chen, D. B. Kaufman, W. L. Lowe, L. D. Shea, *Transplantation* **2008**, *85*, 1456.
[32] K. Sigmundsson, J. R. M. Ojala, M. K. Öhman, A.-M. Österholm, A. Moreno-Moral, A. Domogatskaya, L. Y. Chong, Y. Sun, X. Chai, J. A. M. Steele, B. George, M. Patarroyo, A.-S. Nilsson, S. Rodin, S. Ghosh, M. M. Stevens, E. Petretto, K. Tryggvason, *Matrix Biol.* **2018**, *70*, 5.
[33] C. H. Stephens, K. S. Orr, A. J. Acton, S. A. Tersey, R. G. Mirmira, R. V. Considine, S. L. Voytik-Harbin, *Am. J. Physiol. – Endocrinol. Metab.* **2018**, *315*, E650.
[34] R. B. Jalili, A. M. Rezakhanlou, A. Hosseini-Tabatbaei, Z. Ao, G. L. Warnock, A. Ghahary, A. Hosseini-Tabatabaei, Z. Ao, G. L. Warnock, A. Ghahary, *J. Cell. Physiol.* **2011**, *226*, 1813.
[35] Y. Hamamoto, S. Fujimoto, A. Inada, M. Takehiro, K. Nabe, D. Shimono, M. Kajikawa, J. Fujita, Y. Yamada, Y. Seino, *Horm. Metab. Res.* **2003**, *35*, 460.
[36] M. Banerjee, I. Virtanen, J. Palgi, O. Korsgren, T. Otonkoski, *Mol. Cell. Endocrinol.* **2012**, *355*, 78.
[37] H. Matsushima, T. Kuroki, T. Adachi, A. Kitasato, S. Ono, T. Tanaka, M. Hirabaru, N. Kuroshima, T. Hirayama, Y. Sakai, A. Soyama, M. Hidaka, M. Takatsuki, T. Kin, J. Shapiro, S. Eguchi, *Cell Transplant.* **2016**, *25*, 1525.
[38] T. Kaido, M. Yebra, V. Cirulli, A. M. Montgomery, *J. Biol. Chem.* **2004**, *279*, 53762.
[39] L. A. Llacua, B. J. de Haan, P. de Vos, *J. Tissue Eng. Regener. Med.* **2018**, *12*, 460.
[40] Y. Nakashima, H. Iguchi, K. Takakura, Y. Nakamura, K. Izumi, N. Koba, S. Haneda, M. Tsukahara, *Cell Transplant.* **2022**, *31*, https://doi.org/10.1177/09636897221120500.
[41] A. Llacua, B. J. de Haan, S. A. Smink, P. de Vos, *J. Biomed. Mater. Res.* **2016**, *104*, 1788.
[42] E. Hadavi, J. Leijten, M. Engelse, E. De Koning, P. Jonkheijm, M. Karperien, A. Van Apeldoorn, *Tissue Eng. – Part C Methods* **2019**, *25*, 1.
[43] T. Kaido, M. Yebra, V. Cirulli, C. Rhodes, G. Diaferia, A. M. Montgomery, *Diabetes* **2006**, *55*, 2723.
[44] A. Zbinden, S. L. Layland, M. Urbanczyk, D. A. Carvajal Berrio, J. Marzi, M. Zauner, A. Hammerschmidt, E. M. Brauchle, K. Sudrow, S. Fink, M. Templin, S. Liebscher, G. Klein, A. Deb, G. P. Duffy, G. M. Crooks, J. A. Eble, H. K. A. Mikkola, A. Nsair, M. Seifert, K. Schenke-Layland, *Adv. Sci.* **2021**, *8*, 2002500.
[45] M. Urbanczyk, A. Jeyagaran, A. Zbinden, C. en Lu, J. Marzi, L. Kuhlburger, S. Nahnsen, S. L. Layland, G. Duffy, K. Schenke-Layland, *Matrix Biol.* **2023**, *115*, 160.
[46] M. S. P. Ho, K. Böse, S. Mokkapati, R. Nischt, N. Smyth, *Microsc. Res. Tech.* **2008**, *71*, 387.
[47] T. Neill, L. Schaefer, R. V. Iozzo, *Am. J. Pathol.* **2012**, *181*, 380.
[48] A. G. Porter, R. U. Jänicke, *Cell Death Differ.* **1999**, *6*, 99.
[49] F. Azzarello, L. Pesce, V. De Lorenzi, G. Ferri, M. Tesi, S. Del Guerra, P. Marchetti, F. Cardarelli, *Commun. Biol.* **2022**, *5*, 1232.
[50] R. Beeri, Z. Symon, M. Brezis, S. A. Ben-Sasson, P. H. Baehr, S. Rosen, R. A. Zager, *Kidney Int.* **1995**, *47*, 1806.
[51] D. M. Rosenbaum, M. Michaelson, D. K. Batter, P. Doshi, J. A. Kessler, *Ann. Neurol.* **1994**, *36*, 864.
[52] W. Akhter, Q. M. Ashraf, S. A. Zanelli, O. P. Mishra, M. Delivoria-Papadopoulos, *Neonatology* **2001**, *79*, 187.
[53] A. R. Kaplan, P. M. Glazer, *Mutagenesis* **2021**, *35*, 61.
[54] N. Chan, M. Koritzinsky, H. Zhao, R. Bindra, P. M. Glazer, S. Powell, A. Belmaaza, B. Wouters, R. G. Bristow, *Cancer Res.* **2008**, *68*, 605.
[55] D. Fanale, V. Bazan, S. Caruso, M. Castiglia, G. Bronte, C. Rolfo, G. Cicero, A. Russo, *Biomed Res. Int.* **2013**, *2013*, https://doi.org/10.1155/2013/746858.
[56] J. M. J. Jongen, L. M. van der Waals, K. Trumpi, J. Laoukili, N. A. Peters, S. J. S. van Schelven, K. M. Govaert, I. H. M. B. Rinkes, O. Kranenburg, *Oncotarget* **2017**, *8*, 86296.
[57] A. X. Meng, F. Jalali, A. Cuddihy, N. Chan, R. S. Bindra, P. M. Glazer, R. G. Bristow, *Radiother. Oncol.* **2005**, *76*, 168.
[58] V. T. Mihaylova, R. S. Bindra, J. Yuan, D. Campisi, L. Narayanan, R. Jensen, F. Giordano, R. S. Johnson, S. Rockwell, P. M. Glazer, *Mol. Cell. Biol.* **2003**, *23*, 3265.
[59] M. Koshiji, K. K. W. To, S. Hammer, K. Kumamoto, A. L. Harris, P. Modrich, L. E. Huang, *Mol. Cell* **2005**, *17*, 793.
[60] H. Nakamura, K. Tanimoto, K. Hiyama, M. Yunokawa, T. Kawamoto, Y. Kato, K. Yoshiga, L. Poellinger, E. Hiyama, M. Nishiyama, *Oncogene* **2008**, *27*, 4200.
[61] M. E. Crosby, R. Kulshreshtha, M. Ivan, P. M. Glazer, *Cancer Res.* **2009**, *69*, 1221.
[62] U. Bruning, L. Cerone, Z. Neufeld, S. F. Fitzpatrick, A. Cheong, C. C. Scholz, D. A. Simpson, M. O. Leonard, M. M. Tambuwala, E. P. Cummins, C. T. Taylor, *Mol. Cell. Biol.* **2011**, *31*, 4087.
[63] I. A. Babar, J. Czochor, A. Steinmetz, J. B. Weidhaas, P. M. Glazer, F. J. Slack, *Cancer Biol. Ther.* **2011**, *12*, 908.
[64] J. R. Czochor, P. Sulkowski, P. M. Glazer, *Mol. Cancer Res.* **2016**, *14*, 363.
[65] P. Gasparini, F. Lovat, M. Fassan, L. Casadei, L. Cascione, N. K. Jacob, S. Carasi, D. Palmieri, S. Costinean, C. L. Shapiro, K. Huebner, C. M. Croce, *Proc. Natl. Acad. Sci. USA* **2014**, *111*, 4536.
[66] M. C. Chiang, Q. M. Ashraf, O. P. Mishra, M. Delivoria-Papadopoulos, *Neurochem. Res.* **2008**, *33*, 1232.
[67] G. Cao, W. Pei, J. Lan, R. A. Stetler, Y. Luo, T. Nagayama, S. H. Graham, X. M. Yin, R. P. Simon, J. Chen, *J. Neurosci.* **2001**, *21*, 1.
[68] M. Rokavec, N. Bouznad, H. Hermeking, *Cell. Mol. Gastroenterol. Hepatol.* **2019**, *7*, 783.
[69] T. Abbas, A. Dutta, *Nat. Rev. Cancer* **2009**, *9*, 400.
[70] K. H. Vousden, C. Prives, *Cell* **2009**, *137*, 413.
[71] D. P. Lane, *Nature* **1992**, *358*, 15.
[72] A. De Luca, M. Santra, A. Baldi, A. Giordano, R. V. Iozzo, *J. Biol. Chem.* **1996**, *271*, 18961.
[73] A. R. Yoon, J. W. Hong, C. O. Yun, *Oncotarget* **2017**, *8*, 76666.
[74] A. S. Hamid, Y. W. Jinran Li, X. Wu, H. A. A. Ali, Z. Du, L. Bo, Y. Zhang, G. Zhang, *Mol. Med. Rep.* **2013**, *8*, 511.
[75] M. Baker, M. Petasny, N. Taqatqa, M. Bentata, G. Kay, E. Engal, Y. Nevo, A. Siam, S. Dahan, M. Salton, *RNA* **2021**, *27*, 1353.
[76] S. Ikeda, A. Kitadate, F. Abe, N. Takahashi, H. Tagawa, *Blood Adv.* **2018**, *2*, 323.
[77] H. C. D. Medeiros, S. Y. Lunt, *Mol. Cell* **2022**, *82*, 3119.
[78] R. Courtnay, D. C. Ngo, N. Malik, K. Ververis, S. M. Tortorella, T. C. Karagiannis, *Mol. Biol. Rep.* **2015**, *42*, 841.
[79] P. Vaupel, G. Multhoff, *J. Physiol.* **2021**, *599*, 1745.
[80] A. Zbinden, D. A. Carvajal Berrio, M. Urbanczyk, S. L. Layland, M. Bosch, S. Fliri, C.-E. Lu, A. Jeyagaran, P. Loskill, G. P. Duffy, K. Schenke-Layland, *J. Biophotonics* **2020**, *13*, 202000375.

[81] Z. Wang, T. Gurlo, A. V. Matveyenko, D. Elashoff, P. Wang, M. Rosenberger, J. A. Junge, R. C. Stevens, K. L. White, S. E. Fraser, P. C. Butler, *Commun. Biol.* **2021**, *4*, 594.
[82] F. Westermeier, T. Holyoak, J. L. Asenjo, R. Gatica, F. Nualart, I. Burbulis, R. Bertinat, *Trends Endocrinol. Metab.* **2019**, *30*, 520.
[83] M. J. Merrins, A. R. Van Dyke, A. K. Mapp, M. A. Rizzo, L. S. Satin, *J. Biol. Chem.* **2013**, *288*, 33312.
[84] A. J. Yáñez, R. Bertinat, C. Spichiger, J. G. Carcamo, M. de los Angeles García, I. I. Concha, F. Nualart, J. C. Slebe, *J. Cell. Physiol.* **2005**, *205*, 19.
[85] Y. Zhang, Z. Xie, G. Zhou, H. Zhang, J. Lu, W. J. Zhang, *Endocrinology* **2010**, *151*, 4688.
[86] M. Kebede, J. Favaloro, J. E. Gunton, D. R. Laybutt, M. Shaw, N. Wong, B. C. Fam, K. Aston-Mourney, C. Rantzau, A. Zulli, J. Proietto, S. Andrikopoulos, *Diabetes* **2008**, *57*, 1887.
[87] S. Yu, S. Meng, M. Xiang, H. Ma, *Mol. Metab.* **2021**, *53*, 101257.
[88] J. Yang, S. C. Kalhan, R. W. Hanson, *J. Biol. Chem.* **2009**, *284*, 27025.
[89] J. Xiang, K. Wang, N. Tang, *Genes Dis.* **2023**, *10*, 101.
[90] J. Xiang, Y. Zhang, L. Tuo, R. Liu, D. Gou, L. Liang, C. Chen, J. Xia, N. Tang, K. Wang, *Genes Dis.* **2020**, *7*, 150.
[91] Y. Tang, Y. Zhang, C. Wang, Z. Sun, L. Li, S. Cheng, W. Zhou, *Cell. Physiol. Biochem.* **2018**, *47*, 344.
[92] C. Berger, D. Zdzieblo, *Pflugers Arch.* **2020**, *472*, 1249.
[93] A. Pingitore, I. Ruz-Maldonado, B. Liu, G. C. Huang, P. Choudhary, S. J. Persaud, *Cell. Physiol. Biochem.* **2017**, *44*, 1352.
[94] J.-Q. Chen, J. Russo, *Biochim. Biophys. Acta – Rev. Cancer* **2012**, *1826*, 370.
[95] L. J. McCulloch, M. van de Bunt, M. Braun, K. N. Frayn, A. Clark, A. L. Gloyn, *Mol. Genet. Metab.* **2011**, *104*, 648.
[96] A. De Vos, H. Heimberg, E. Quartier, P. Huypens, L. Bouwens, D. Pipeleers, F. A. Schuit, K. F. Schuit, *J. Clin. Invest.* **1995**, *96*, 2489.
[97] J. Zehetner, C. Danzer, S. Collins, K. Eckhardt, P. A. Gerber, P. Ballschmieter, J. Galvanovskis, K. Shimomura, F. M. Ashcroft, B. Thorens, P. Rorsman, W. Krek, *Genes Dev.* **2008**, *22*, 3135.
[98] S. Puri, D. A. Cano, M. Hebrok, *Diabetes* **2009**, *58*, 433.
[99] J. Cantley, S. T. Grey, P. H. Maxwell, D. J. Withers, *Diabetes, Obes. Metab.* **2010**, *12*, 159.
[100] S. Hinderer, K. Sudrow, M. Schneider, M. Holeiter, S. L. Layland, M. Seifert, K. Schenke-Layland, *Sci. Rep.* **2018**, *8*, 110.
[101] M. Urbanczyk, A. Zbinden, S. L. Layland, G. Duffy, K. Schenke-Layland, *Tissue Eng., Part A* **2020**, *26*, 387.
[102] A. Zbinden, J. Marzi, K. Schlünder, C. Probst, M. Urbanczyk, S. Black, E. M. Brauchle, S. L. Layland, U. Kraushaar, G. Duffy, K. Schenke-Layland, P. Loskill, *Matrix Biol.* **2020**, *85–86*, 205.
[103] M. Cnop, S. J. Hughes, M. Igoillo-Esteve, M. B. Hoppa, F. Sayyed, L. van de Laar, J. H. Gunter, E. J. P. de Koning, G. V. Walls, D. W. G. Gray, P. R. V. Johnson, B. C. Hansen, J. F. Morris, M. Pipeleers-Marichal, I. Cnop, A. Clark, *Diabetologia* **2010**, *53*, 321.
[104] P. A. Ewels, A. Peltzer, S. Fillinger, H. Patel, J. Alneberg, A. Wilm, M. U. Garcia, P. Di Tommaso, S. Nahnsen, *Nat. Biotechnol.* **2020**, *38*, 276.
[105] S. Andrews, S. Andrew, "FastQC. A Quality Control Tool for High Throughput Sequence Data," can be found under https://www.bioinformatics.babraham.ac.uk/projects/fastqc/, (accessed: Dec 2023).
[106] L. Wang, S. Wang, W. Li, *Bioinformatics* **2012**, *28*, 2184.
[107] A. Dobin, C. A. Davis, F. Schlesinger, J. Drenkow, C. Zaleski, S. Jha, P. Batut, M. Chaisson, T. R. Gingeras, *Bioinformatics* **2012**, *29*, 15.
[108] Y. Liao, G. K. Smyth, W. Shi, *Bioinformatics* **2014**, *30*, 923.
[109] M. I. Love, W. Huber, S. Anders, *Genome Biol.* **2014**, *15*, 550.
[110] R. Kolde, **2019** https://cran.r-project.org/web/packages/pheatmap/index.html, (accessed: Mar 2024).

